

DEVELOPMENT OF A METHOD FOR EVALUATING
CARBON DIOXIDE MISCIBLE FLOODING PROSPECTS--FINAL REPORT

Principal Investigators
Don W. Green and George W. Swift
University of Kansas
Lawrence, Kansas 66045

The results reported are in large measure based on the research done by John Ezekwe, Harlan Cramer, Kevin Belden, Mehrdad Azadeh, Edward Daub and Carlos Rocha. These persons were all graduate students in chemical engineering at the University of Kansas, Lawrence, Kansas.

Fred W. Burtch, Technical Project Officer
Bartlesville Project Office
Department of Energy
P.O. Box 1398
Bartlesville, Oklahoma 74005

Work Performed for the Department of Energy
Under Contract No. DE-AC19-79BC10122

BARTLESVILLE PROJECT
DEPARTMENT OF ENERGY
BARTLESVILLE, OKLAHOMA

Date Published--March 1985

DEVELOPMENT OF A METHOD FOR EVALUATING CARBON DIOXIDE
MISCIBLE FLOODING PROSPECTS

ABSTRACT

Research was undertaken to develop a method of evaluating reservoirs as prospects for carbon dioxide flooding. Evaluation was to be based on a determination of miscibility pressure and displacement efficiency under idealized conditions. To reach the objective, project work was divided into five areas.

i) Conducting of phase-equilibrium studies of carbon dioxide with synthetic oils.

ii) Application of an equation of state to simulate the phase behavior of carbon dioxide - oil systems.

iii) Conducting of linear displacements of crude oils and synthetic oils by carbon dioxide in a slim-tube apparatus.

iv) Application of the equation of state, the phase-behavior data and slim-tube data to develop a method of screening reservoirs for carbon dioxide flooding based on determination of minimum miscibility pressure and displacement efficiency.

v) Development of a one-dimensional mathematical model, based on the equation of state, for application in conjunction with the results of parts i to iv.

Bubble point phase-behavior data were taken for binary and ternary systems containing carbon dioxide. The phase behavior was adequately simulated with the Soave-Redlich-Kwong (SRK) equation of state when suitable interaction coefficients were used. Addition of water to the CO₂-hydrocarbon system reduced the bubble point due to absorption of CO₂ into the water phase. However, when absorption of CO₂ was accounted for, phase behavior on a water-free basis was essentially unchanged from the case when no water was in the system.

Several displacements were conducted in a slim-tube apparatus. For ternary systems (CO₂ plus two hydrocarbon components), measured MMP values were in good agreement with values predicted based on known phase behavior. The presence of immobile water in these displacements had negligible affect on MMP. Miscibility pressures were measured for a number of Kansas crude oils and were found to be a function of API gravity, decreasing as API gravity increased. MMP also increased with temperature and decreased when lower molecular weight hydrocarbons (C₄-C₆) were added to the crude.

The proposed screening method is based on the generation of pseudo-ternary phase-behavior diagrams for carbon dioxide-crude oil systems. The diagrams are used for estimation of MMP and for estimation of

displacement efficiency when applied with an appropriate mathematical model.

To test the method, the SRK equation of state was used to generate pseudo-ternary diagrams for two oils described in the literature and three Kansas crudes studied in this project. For the literature oils, calculations were based on reported compositions. The Kansas oil compositions were estimated from ASTM D-86 and true boiling point distillation curves. Literature sources were used in conjunction with the estimated compositions to calculate required physical properties for generation of the ternary diagrams.

The pseudo-ternary diagrams were applied to predict MMP values for the five crude oil systems and a comparison was made to values obtained from slim-tube displacements for the same oils. The best agreement was obtained when a linear range of interaction coefficients was used in the SRK equation of state. The smallest coefficient value was assigned to C_5 and the largest to C_{25} . When a suitable set of interaction coefficients was used in the equation of state, the MMP was correctly predicted for a given crude. The dependence of MMP on temperature was also described satisfactorily. It was not, however, possible to model adequately all of the oils studied with a single set of interaction coefficients. The value of the smallest coefficient (assigned to C_5) had to be adjusted to produce a satisfactory prediction of MMP.

The method was relatively insensitive to the specifications of the pseudo components in the pseudo-ternary representation. Also, the method was not very sensitive to the interaction coefficient value assigned to the heavy component (C_{25}).

Finally, the slim-tube displacement results were simulated mathematically using a modification of a model reported in the literature. The model was based on the use of the pseudo-ternary diagrams to describe phase behavior. The model, in general, did a good job of describing displacement performance in a slim-tube apparatus, however history matching was required.

TABLE OF CONTENTS

		PAGE
ACKNOWLEDGEMENTS.....		i
ABSTRACT.....		ii
TABLE OF CONTENTS.....		iv
LIST OF TABLES.....		vii
LIST OF FIGURES.....		x
CHAPTER 1	INTRODUCTION.....	1
1.1	Objective.....	1
1.2	Project Organization.....	1
1.3	Background.....	1
1.4	Approach and Scope of Work.....	7
CHAPTER 2	PHASE BEHAVIOR OF MEASUREMENTS AND CALCULA- TIONS.....	8
2.1	Introduction.....	8
2.2	Apparatus, Procedure and Materials.....	9
2.3	Experimental Results.....	13
2.4	Application of the Soave-Redlick-Kwong (SRK) Equation of State.....	14
CHAPTER 3	SLIM-TUBE DISPLACEMENT EXPERIMENTS.....	24
3.1	Introduction.....	24
3.2	Experimental Apparatus and Procedure.....	26
3.3	Calibration and Checking of the Apparatus.....	28
3.4	Results of Displacements with Carbon Dioxide and Binary Hydrocarbon Systems.....	30
3.5	Results of Displacements in the Presence of an Immobile Water Phase.....	33

TABLE OF CONTENTS
(Continued)

		PAGE
3.6	Results of Displacements with Carbon Dioxide and Crude Oils.....	38
CHAPTER 4	APPLICATION OF PSEUDO-TERNARY DIAGRAMS FOR THE PREDICTION OF DISPLACEMENT PERFORMANCE.....	47
4.1	Introduction.....	47
4.2	Application of Ternary Diagrams to Ternary Systems.....	48
4.3	Application of Pseudo-Ternary Diagrams to Crude Oil Systems - Literature Data.....	53
4.4	Application of Pseudo-Ternary Diagrams to Crude Oil Systems - Kansas Crude Oils.....	76
4.5	Prediction of Miscibility Pressures Using Literature Correlations.....	90
CHAPTER 5	APPLICATION OF MATHEMATICAL MODELING TO PREDICT DISPLACEMENT PERFORMANCE.....	92
5.1	Introduction.....	92
5.2	Description of the Mathematical Model.....	92
5.3	Application of the Model to Describe Linear Displacements in Slim-Tube Apparatus.....	102
CHAPTER 6	SUMMARY OF MAJOR CONCLUSIONS.....	121
REFERENCES	123
APPENDIXES		
Appendix A:	Additional Phase Behavior Data.....	127
Appendix B:	Additional Slim-Tube Miscibility Pressure Measurements.....	138

TABLE OF CONTENTS
(Continued)

	PAGE
Appendix C: Supplemental Tables and Figures for Chapter 4.....	147
Appendix D: Supplemental Figures For Chapter 5.....	168

LIST OF TABLES

TABLES	PAGE
2-1	Interaction Coefficients for Various Aromatic and Naphthentic Components with Carbon Dioxide.....15
2-2	Interaction Parameters for Various CO ₂ -Paraffinic Components Regressed from Literature Data.....15
2-3	Comparisons of Interaction Parameters from Correlations.....16
2-4	Regression of Carbon Dioxide, n-Butane and n-Decane Data at 160°F.....21
2-5	Interaction Coefficients Obtained From Regression 4 Through 11 From Carbon Dioxide (1), n-Butane (2), n-Decane (3), n-Butylcyclohexane (4) and n-Butylbenzene (50).....21
2-6	Maximum Miscibility Composition (MMC) for Mixtures of Carbon Dioxide and n-Butane with n-Decane, n-Butylcyclohexane or n-Butylbenzene, (MMC is Reported as Mole Fraction of Heavy Hydrocarbon on A Carbon Dioxide-Free Basis).....23
3-1	Measured Miscibility Pressures, Crude Oils - State of Kansas.....42
4-1	Reported Composition of Maljamar Crude Oil.....55
4-2	Predicted Interaction Coefficients.....56
4-3	Interaction Coefficient (IP) Ranges Utilized to Match Maljamar Crude Bubble-Point Pressure Curve.....60
4-4	Reported Composition of West Texas Stock Tank Oil of Yellig and Metcalfe.....71
4-5	Adjusted Composition of West Texas Stock Tank Oil of Yellig and Metcalfe.....72
4-6	Comparison of Calculated and Measured Miscibility Pressures, West Texas Oil of Metcalfe and Yarborough.....75
4-7	Abernathy-Collins Crude Compositional Summary, Based on ASTM D-86 Distillation.....77

LIST OF TABLES
(Continued)

		PAGE
4-8	Johanning B Crude Compositional Summary, Based on ASTM D-86 Distillation.....	78
4-9	Single Carbon Number Analysis, Based on the Empirical True Bubble-Point Curve, Abernathy-Collins Crude.....	80
4-10	Single Carbon Number Analysis Based on Empirical True Boiling-Point Curve, Johanning B Crude.....	81
4-11	Comparison of the Albertson Crude Compositional Analyses.....	82
4-12	Slim-Tube Miscibility Pressure Measurements.....	83
4-13	Comparison of Calculated and Measured Miscibility Pressures.....	89
4-14	Summary of Literature MMP Correlation Results.....	91
5-1	Summary of Truncation Error Expressions.....	101
5-2	Systems Simulated With the Carbon Dioxide Displacement Model.....	104
A-1	Bubble-Point Pressures for CO ₂ -Toluene at 140, 170, 200°F.....	127
A-2	Bubble-Point Pressures for CO ₂ -Ethylbenzene at 140, 170, 200°F.....	128
A-3	Bubble-Point Pressures for CO ₂ -Propylbenzene at 140, 170, 200°F.....	129
A-4	Bubble-Point Pressures for CO ₂ -Cyclopentane at 140, 170, 200°F.....	130
A-5	Bubble-Point Pressures for CO ₂ -Cyclopentane at 140, 170, 200°F.....	131
A-6	Bubble-Point Pressures for CO ₂ -Methylcyclohexane at 140, 170, 200°F.....	132
A-7	Bubble-Point Pressure Reduction Due to the Presence of Water, CO ₂ -n-Butane at 160°F.....	133

LIST OF TABLES
(Continued)

TABLES	PAGE
A-8	Bubble-Point Pressure Reduction Due to the Presence of Water, CO ₂ -n-Decane at 160°F.....134
A-9	Bubble-Point Pressure Due to the Presence of Water, CO ₂ -Toluene at 160°F.....135
A-10	Bubble-Point Pressure Reduction Due to the Presence of Water, CO ₂ -n-Butane at 100°F.....136
A-11	Bubble-Point Pressures at 160°F.....137
C-1	Summary of Generalized Katz-Firoozabadi-Whitson Properties.....148
C-2	Summary of TC, PC, and W Calculations with Lee-Kesler Equations for KFW Properties.....149
C-3	ASTM D-86 Distillation of Stock Tank Oil in 50°F Cut Steps to 700°F.....150
C-4	ASTM D-86 Distillation of Stock Tank Oil in 50°F Cut Steps to 700°F.....151
C-5	ASTM D-86 Distillation of Stock Tank Oil in 50°F Cut Steps to 700°F.....152
C-6	True Boiling Point Distillation of Stock Tank Oil153
C-7	Comparison of Distillation Curves For the Abernathy-Collins Crude.....154
C-9	Summary of Additional IP Ranges Utilized in Ternary Analyses.....155

LIST OF FIGURES

FIGURES	PAGE
1-1	Pseudo Ternary Diagram Showing Phase Behavior of a CO ₂ -Crude Oil System.....3
1-2	Typical Results From Slim-Tube Displacements.....5
2-1	Schematic Diagram of Equilibrium Cell and Associated Flow Lines.....11
2-2	Schematic Diagram of the Metering System.....12
2-3	Interaction Coefficients as A Function of Pressure, CO ₂ -n-Butane.....17
2-4	Interaction Coefficients as A Function of Pressure, CO ₂ -n-Decane.....18
2-5	Bubble-Point Pressure Displacement Due to the Presence of Water.....19
3-1	Typical Results From Slim-Tube Displacements.....25
3-2	Slim-Tube Apparatus.....27
3-3	Slim-Tube Results, CO ₂ -n-Hexane Binary System.....29
3-4	Phase Envelopes for the CO ₂ : C ₆ : C ₁₀ Ternary System at 100°F and Various Pressures.....31
3-5	Slim-Tube Results, CO ₂ : n-Decane Ternary System (Hydrocarbon is 50% Hexane, 50% Decane).....32
3-6	Slim-Tube Results, CO ₂ : n-Butane: n-Decane Ternary System (Hydrocarbon is 40% Butane, 60% Decane).....34
3-7	Slim-Tube Results, CO ₂ : n-Butane: n-Decane Ternary System (Hydrocarbon is 82% Butane, 18% Decane).....35
3-8	Slim-Tube Results, CO ₂ : n-Butane: n-Butylbenzene Ternary System (Hydrocarbon is 82% Butane, 18% Butylbenzene).....36
3-9	Effect of Immobile Water on Slim-Tube Results (Hydrocarbon is 50% Hexane, 50% Decane).....37
3-10	Slim-Tube Recovery Curves, With and Without the Presence of Immobile Water.....39

LIST OF FIGURES
(Continued)

FIGURES	PAGE
3-11	Slim-Tube Results, Johanning Crude Oil.....40
3-12	Slim-Tube Results, Abernathy Crude Oil.....41
3-13	Effect of Temperature on Slim-Tube Miscibility Pressure, Johanning Crude Oil.....43
3-14	Effect of Hydrocarbon Composition on Slim-Tube Miscibility Pressure (Hexane Added to Crude Oil).....45
3-15	Effect of Hydrocarbon Composition on Slim-Tube Miscibility Pressure (Butane Added to Crude Oil).....46
4-1	Calculated Ternary Diagram for CO ₂ -Butane-Decane (P = 1300 psia, T = 160°F).....49
4-2	Calculated Ternary Diagram for CO ₂ -Butane-Decane (P = 1400 psia, T = 160°F).....50
4-3	Calculated Ternary Diagram for CO ₂ -Butane- Butylbenzene (P = 1300 psia, T = 160°F).....51
4-4	Calculated Ternary Diagram for CO ₂ -Butane- Butylbenzene (P = 1400 psia, T = 160°F).....52
4-5	Comparison of Experimental and Calculated Bubble- Point Pressures, Maljamar Oil, 90°F: Use of Correlations for Interaction Coefficients (IP).....57
4-6	Comparison of Experimental and Calculated Bubble- Point Pressures, Maljamar Oil, 90°F: Use of Constant Interaction Coefficients (IP).....58
4-7	Comparison of Experimental and Calculated Bubble- Point Pressures, Maljamar Oil, 90°F: Use of Linear Range of Interaction Coefficients (IP).....61
4-8	Calculated Ternary Phase Diagram for Maljamar Oil (IP Range 7-13, P = 800 psia).....62
4-9	Calculated Ternary Phase Diagram for Maljamar Oil (IP Range 7-13, P = 1050 psia).....63
4-10	Calculated Ternary Phase Diagram for Maljamar Oil (IP Range 7-13, P = 1100 psia).....64

LIST OF FIGURES
(Continued)

FIGURES	PAGE
4-11	Calculated Ternary Phase Diagram for Maljamar Oil (IP Range 7-13, P = 1400 psia).....65
4-12	Calculated Ternary Phase Diagram for Maljamar Oil: Effect of Pseudo Component Composition - Heavy Component C ₁₆ ⁺ (IP Range 7-13, P = 1100 psia).....67
4-13	Calculated Ternary Phase Diagram for Maljamar Oil: Effect of Pseudo Component Composition - Heavy Component C ₁₁ ⁺ (IP Range 7-13, P = 1100 psia).....68
4-14	Calculated Ternary Phase Diagram for Maljamar Oil: Effect of Pseudo Component Composition - Heavy Component C ₉ ⁺ (IP Range 7-13, P = 1100 psia).....69
4-15	Calculated Ternary Phase Diagram for Yellig and Metcalf Oil (IP Range 7-13, P = 1150 psia).....73
4-16	Calculated Ternary Phase Diagram for Abernathy- Collins Crude Oil (IP Range 4-13, P = 1450 psia).....85
4-17	Calculated Ternary Phase Diagram for Abernathy- Collins Crude Oil (IP Range 4-13, P = 1850 psia).....86
4-18	Calculated Ternary Phase Diagram for Albertson Crude Oil (IP Range 5-13, P = 1200 psia).....87
4-19	Calculated Ternary Phase Diagram for Albertson Crude Oil (IP Range 5-13, P = 1250 psia).....88
5-1	Phase Behavior Representation on a Ternary Diagram - Types of Phase Behavior Considered.....97
5-2	Representation of Phase Behavior in the Mathematical Model.....98
5-3	CO ₂ Displacing Butane and Decane (P = 1200 psia; T = 160°F).....105
5-4	CO ₂ Displacing Butane and Decane (P = 1400 psia; T = 160°F).....106
5-5	CO ₂ Displacing 82% Butane and 18% Decane at 160°F.....108
5-6	CO ₂ Displacing 82% Butane and 18% Butylbenzene at 160°F.....109

LIST OF FIGURES
(Continued)

FIGURES	PAGE
5-7	CO ₂ Displacing 50% Hexane and 50% Decane (T = 100°F).....110
5-8	CO ₂ Displacing Maljamar Separator Oil.....112
5-9	CO ₂ Displacing Yellig and Metcalfe STO (T = 118°F).....113
5-10	CO ₂ Displacing Yellig and Metcalfe STO (T = 150°F).....114
5-11	CO ₂ Displacing Abernathy-Collins #1 (P = 1330 psia; T = 126°F).....115
5-12	CO ₂ Displacing Abernathy-Collins #1 (P = 1670 psia; T = 126°F).....116
5-13	CO ₂ Displacing Abernathy-Collins #1 (T = 126°F).....117
5-14	CO ₂ Displacing Johanning B #1 (T = 102°F).....119
5-15	CO ₂ Displacing Johanning B #1 (T = 125°F).....120
B-1	Slim-Tube Results - Seevers Crude Oil.....138
B-2	Slim-Tube Results - Newcombe Crude Oil.....139
B-3	Slim-Tube Results - Albertson Crude Oil.....140
B-4	Slim-Tube Results - Olson B #6 Crude Oil.....141
B-5	Slim-Tube Results - Newcomer #4 Crude Oil.....142
B-6	Slim-Tube Results - Olive Crude Oil.....143
B-7	Slim-Tube Results - #1 Dieter Crude Oil.....144
B-8	Slim-Tube Results - #1 Lofgren Crude Oil.....145
B-9	Slim-Tube Results - #2 Bishop Crude Oil.....146
C-1	Calculated Ternary Phase Diagram for Yellig and Metcalfe Oil (IP Range 7-13, P = 1250 psia, T = 118°F).....156

LIST OF FIGURES
(Continued)

FIGURES	PAGE
C-2	Calculated Ternary Phase Diagram for Yellig and Metcalfe Oil (IP Range 7-13, P = 1600 psia, T = 118°F).....157
C-3	Calculated Ternary Phase Diagram for Yellig and Metcalfe Oil (IP Range 7-13, P = 1800 psia, T = 150°F).....158
C-4	Calculated Ternary Phase Diagram for Yellig and Metcalfe Oil (IP Range 7-13, P = 2250 psia, T = 150°F).....159
C-5	Calculated Ternary Phase Diagram for Yellig and Metcalfe Oil (IP Range 6-13, P = 1100 psia, T = 95°F).....160
C-6	Calculated Ternary Phase Diagram for Yellig and Metcalfe Oil (IP Range 6-13, P = 1350 psia, T = 118°F).....161
C-7	Calculated Ternary Phase Diagram for Yellig and Metcalfe Oil (IP Range 6-13, P = 1600 psia, T = 150°F).....162
C-8	Calculated Ternary Phase Diagram for Yellig and Metcalfe Oil (IP Range 6-13, P = 1800 psia, T = 150°F).....163
C-9	Calculated Ternary Phase Diagram for Yellig and Metcalfe Oil (IP Range 6-13, P = 2000 psia, T = 150°F).....164
C-10	Calculated Ternary Phase Diagram for Abernathy-Collins Crude Oil (IP Range 7-13, P = 1550 psia, T = 126°F).....165
C-11	Calculated Ternary Phase Diagram for Johanning B Crude Oil (IP Range 3-13, P = 1150 psia, T = 102°F).....166
C-12	Calculated Ternary Phase Diagram for Johanning B Crude Oil (IP Range 3-13, P = 1200 psia, T = 102°F).....167
D-1	CO ₂ Displacing Butane and Butylbenzene (P = psia; T = 160°F).....168

LIST OF FIGURES
(Continued)

FIGURES	PAGE
D-2	CO ₂ Displacing Butane and Butylbenzene (P = 1200 psia; T = 160°F).....169
D-3	CO ₂ Displacing Butane and Butylbenzene (P = 1300 psia; T = 160°F).....170
D-4	CO ₂ Displacing Butane and Butylbenzene (P = 1400 psia; T = 160°F).....171
D-5	CO ₂ Displacing Butane and Butylbenzene (P = 1500 psia; T = 160°F).....172
D-6	CO ₂ Displacing Hexane and Decane (P = 930 psia; T = 100°F).....173
D-7	CO ₂ Displacing Hexane and Decane (P = 1020 psia; T = 100°F).....174
D-8	CO ₂ Displacing Hexane and Decane (P = 1050 psia; T = 100°F).....175
D-9	CO ₂ Displacing Hexane and Decane (P = 1110 psia; T = 100°F).....176
D-10	CO ₂ Displacing Johanning B #1 (P = 1040 psia; T = 102°F).....177
D-11	CO ₂ Displacing Johanning B #1 (P = 1210 psia; T = 102°F).....178
D-12	CO ₂ Displacing Johanning B #1 (P = 1570 psia; T = 125°F).....179
D-13	CO ₂ Displacing Johanning B #1 (P = 2060 psia; T = 125°F).....190

CHAPTER 1

INTRODUCTION

1.1 Objective

The ultimate objective of this project was to develop an effective method for evaluating petroleum reservoirs as prospects for carbon-dioxide miscible flooding. The method was to provide estimates of miscibility pressure plus expected displacement efficiency. Further, the method was to be based on fluid property-reservoir data that are normally available or can be easily obtained.

1.2 Project Organization

The project was organized into areas having the following work goals.

1. Make phase-equilibrium studies of carbon dioxide with synthetic oils. One purpose of the synthetic oil studies was to assess the impact of known paraffinic-naphthenic-aromatic (PNA) components and relative compositions on the phase equilibrium of carbon dioxide-rich systems. A second purpose was to provide data for determination of the constants of an equation-of-state model. Additionally, phase behavior on synthetic oils was to be determined in the presence of fresh water.
2. "Fine-tune" the coefficients of an appropriate equation of state to predict, within engineering precision, the phase behavior of carbon dioxide with hydrocarbons and water as reported in the technical literature, plus that determined in part 1 above.
3. Make linear displacements/extractions of both synthetic and actual reservoir oils with carbon dioxide in slim-tubes packed with porous media.
4. Use the phase-behavior data, equation of state and slim-tube results to develop a method of screening reservoirs as potential prospects for carbon dioxide flooding and to test existing correlations of miscibility pressure.
5. Develop a linear-displacement, compositional mathematical model based on the equation of state. The model was to be used to simulate results from the slim-tube experiments and to complement the development of the screening method.

1.3 Background

Carbon dioxide is most effective in oil-displacement when applied in so-called dynamic miscible or multi-contact miscible (MCM) pro-

cesses. In these processes, displaced and displacing fluids are not miscible upon first contact. Rather, miscibility is developed through composition modification that results from repetitive equilibrium contacts between the phases.

1.3.1 Application of Pseudo-Ternary Diagrams to Describe Miscibility Development

A useful way to visualize the development of miscibility is to employ the pseudo-ternary concept of Benham, et al.⁷ Refer to the ternary system depicted on Figure 1-1 for which phase behavior is shown at constant temperature and pressure. CO₂ is one component and the crude oil is divided into two pseudo components: light and intermediate hydrocarbons (C₅-C₁₂) and the balance of the oil (C₁₃⁺).

The binodal curve is made up of the dew point and bubble point curve which meet at the critical point. The binodal curve encloses a two-phase region wherein vapor-liquid equilibrium tie lines are shown. The convergence of the tie lines at the critical point, i.e., the tangent to the binodal curve at the critical point, is termed the critical tie line. The extension of this critical tie line to the crude-oil baseline forms regions of interest for dynamic miscible displacement.

A crude oil of such composition that it is located to the right of the critical tie-line extension (point OOC for example) would develop dynamic miscibility with injected CO₂. In such a displacement, the gas phase would be enriched by having its composition progress towards the critical point. After a sufficient number of contacts the enriched gas phase would become miscible with the crude oil of composition OOC.

Conversely, if the original crude oil composition were located to the left of the critical tie-line extension, then enrichment of the gas phase by extraction of hydrocarbons would cease before miscibility was achieved.

The development of miscibility under dynamic conditions is clearly dependent on operating pressure, temperature and composition of the resident crude oil and injected fluid. For a given fluid system (crude oil and injected fluid) and temperature, the minimum pressure at which miscibility can be achieved through multiple contacts is referred to as the minimum miscibility pressure (MMP). This is a primary design variable. It is typically measured for a specific fluid system in a slim-tube displacement apparatus¹⁶. The slim-tube equipment used in this study is described in Chapter 3.

Another parameter of interest in this work is the maximum miscibility composition (MMC) defined in Figure 1-1. For a given system, at a specified temperature and pressure, the MMC is defined as the maximum composition of the heavy fraction of the oil for which miscibility can be achieved. In the figure, the MMC is 0.378 mole fraction of the C₁₃⁺ pseudo component.

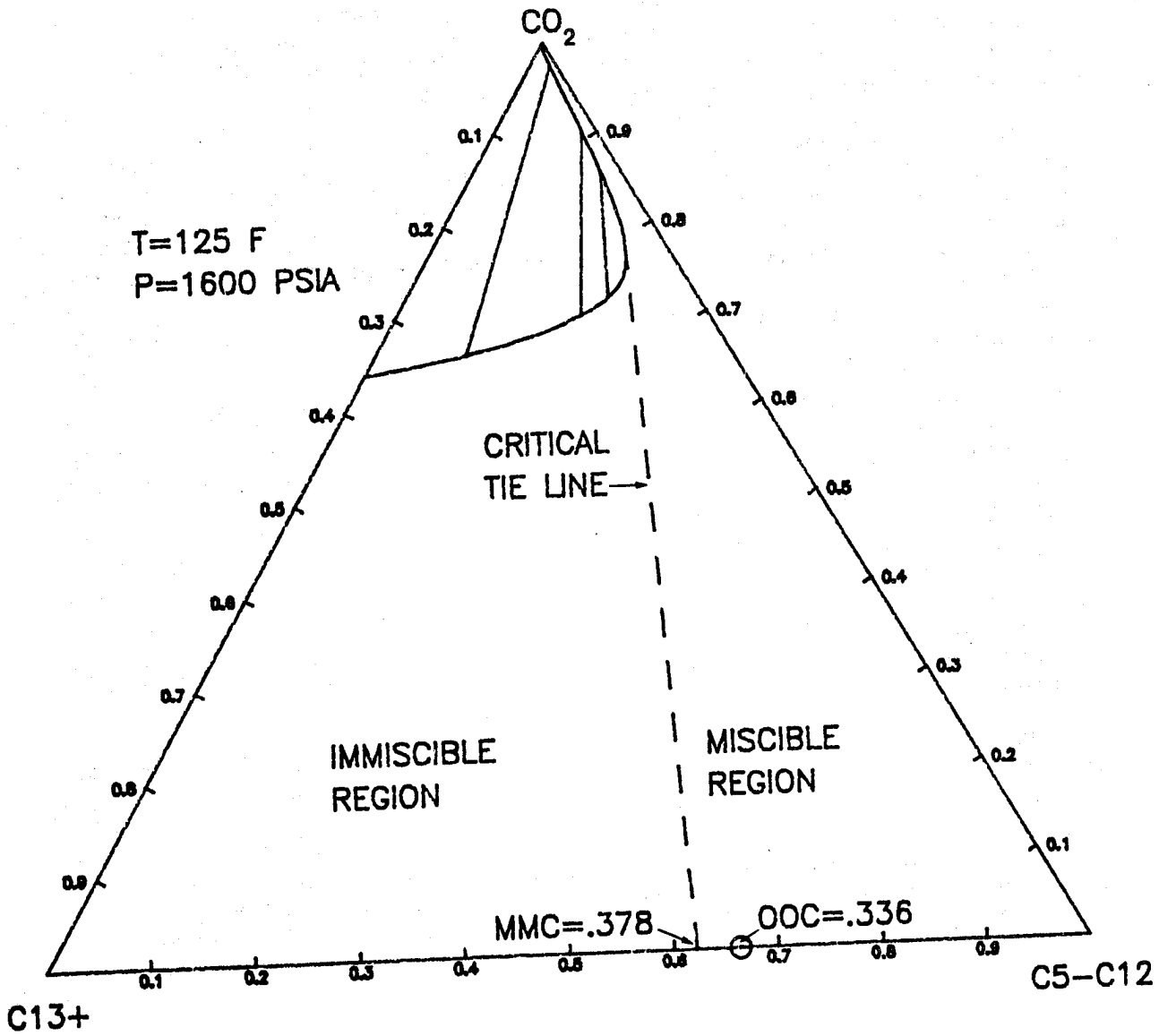


FIGURE 1-1: Pseudo Ternary Diagram Showing Phase Behavior of a CO₂-Crude Oil System.

1.3.2 Existing Correlations for Minimum Miscibility Pressure (MMP)

Several methods for defining the MMP from experimental slim-tube data and for predicting the MMP of CO₂-oil systems have been developed. These correlations are reviewed in chronological order.

In 1974, Holm and Josendal¹⁶ logically reasoned that the achievement of high oil recoveries is evidence of miscible displacement. They defined "miscibility displacement pressure" as "that pressure where more than 80% of oil in place is recovered at CO₂ breakthrough and more than 94% is recovered ultimately from a slim-tube displacement. At this pressure, a sufficient volume of the extracted hydrocarbons is present at the displacement front to maintain the residual oil saturation at a minimum value throughout the flood path".

They developed a correlation to predict MMP as a function of temperature and the C₅+ molecular weight (MW) of the oil. The predicted MMP increases with temperature in a linear fashion. At a set temperature, the MMP increases slightly as the C₅+ MW varies from 180 to 240.

Holm and Josendal¹⁶ determined that the presence of solution gas in the oil had a negligible effect on the MMP. They theorized that the solution gas was initially stripped from the oil by CO₂ and moved ahead of the displacement front. Dynamic miscibility is then developed by the extraction of C₅+ hydrocarbons by the CO₂.

In the 1976 NPC report,¹¹ a MMP prediction method is proposed based on reservoir temperature and the API gravity of the oil. The correlation does a fairly poor job of predicting MMP.

In 1980, Yellig and Metcalfe⁴³ offered a definition for the experimental slim-tube MMP. At a constant temperature, slim-tube displacements were conducted at different pressures, typically five, and the recovery at 1.2 pore volumes (PV) of CO₂ injected was plotted versus pressure. Miscible displacements were defined to have final recoveries which were "equal to or very near the maximum final recovery obtained in a series of tests". This is shown in Figure 1-2 where the MMP is located at the "break point" in the recovery curve and approximately determined by the intersection of the immiscible and miscible recovery slopes. They also studied the appearance of transition-zone fluids and took as an indication of a MCM process color gradations from dark oil to a yellow fluid.

Yellig and Metcalfe⁴³ determined experimental MMP's for a set of four recombined oils over the temperature range of 95° to 192°F. They mixed the same West Texas C₇+ composition (MW = 201) with varying proportions of C₁ and C₂-C₆. They concluded that the recombined oil composition had no effect on MMP at low temperature and little effect at high temperature. They then developed a correlation that predicts the MMP as a function of temperature only and relates MMP linearly with temperature with a slope of 15 psi/°F. Additionally, Yellig and Metcalfe⁴³ reported that for highly volatile recombined reservoir fluids the bubble-point pressure of the oil may be higher than the predicted MMP. In this case, the predicted MMP is set equal to the bubble-point

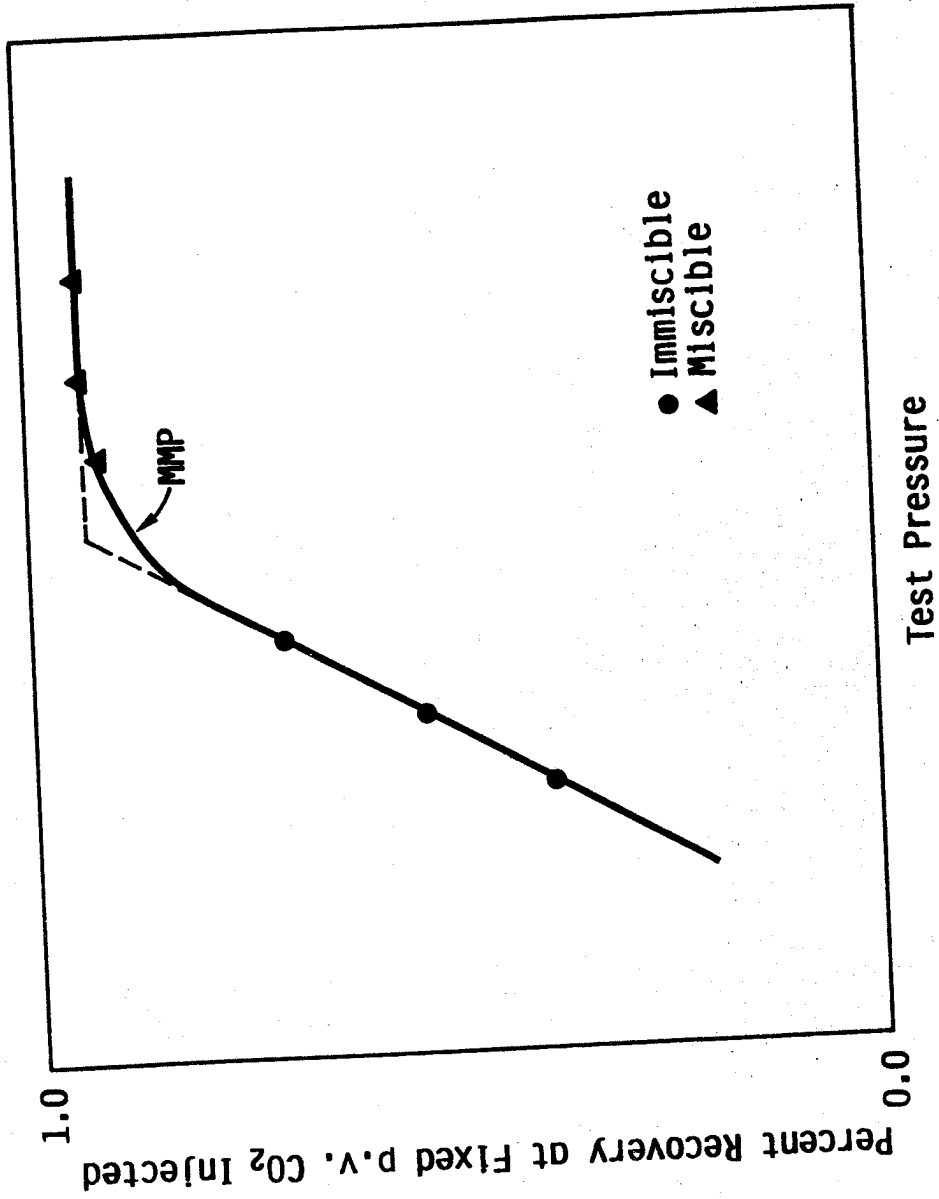


FIGURE 1-2: Typical Results From Slim Tube Displacements.

pressure of the oil. They reasoned that the MMP must be at least as great as the bubble-point pressure of the oil because the oil must be single phase at the slim-tube test pressure.

In 1980, Johnson and Pollin¹⁹ developed a correlation which they claimed predicts the MMP for a wide variety of stock tank oils and recombinant reservoir fluids with pure and diluted CO₂. They studied a total of 25 systems, including 15 stock tank oils, 4 recombinant reservoir fluids and 6 pure and mixed alkanes. They defined the experimental MMP in a fashion similar to that of Yellig and Metcalfe.⁴³ They picked the MMP as the "break point" in the recovery versus pressure curve for a series of slim-tube displacements. However, for recovery they plotted the "effective 1 PV recovery" defined as the average of the breakthrough and ultimate recoveries. In their work on CO₂-alkane (C₁₀-C₂₀) systems, Johnson and Pollin¹⁹ discovered a close correlation between the experimental MMP and the CO₂-alkane critical pressure. For pure CO₂, the correlation indicates that MMP increases with temperature, oil molecular weight and the paraffinic nature of the oil.

In 1982, Holm and Josendal¹⁷ developed a new correlation based on the solvency of CO₂ as indicated by its density, and the weight percent of C₅-C₃₀ hydrocarbons in the C₅+ fraction of the oil. They continued to define MMP as that pressure where 80% of the oil is recovered at breakthrough and 94% is recovered ultimately. They claimed that "the different definitions of MMP have resulted in small but not fundamental differences in the MMP calculated by the different experimentalists".

According to Holm and Josendal,¹⁷ the density of CO₂ has a marked effect on its solvent power. Initial hydrocarbon extraction begins in the density range of 0.25 to 0.35 g/cc. The density required to produce a multi-contact miscible displacement is somewhat higher and a function of oil composition. The authors also stated that the C₅-C₁₂ fraction of the oil affects the MMP, the higher the C₅-C₁₂ content the lower the MMP. In fact, most of their evidence supported the notion that C₅-C₁₂ content is a critical factor.

Holm and Josendal¹⁷ also examined the effect of the type of hydrocarbons on miscible displacement. They replaced the 400-850°F fraction of a paraffinic Farnsworth oil with an equal weight of the 400-850°F fraction of a more aromatic (and naphthenic) Wilmington Ford oil. Both fractions had similar boiling point ranges. The "Hybrid" oil produced a higher recovery. Therefore, Holm and Josendal¹⁷ concluded that more aromatic oils produce lower MMP's than paraffinic oils.

This new method again omits solution gas as a factor. They claimed "this is consistent with the work of Yellig and Metcalfe⁴³ subject to the qualification that if the bubble-point pressure of the oil is greater than the predicted MMP, then the MMP is set equal to the bubble-point pressure."

In 1983, Alston, et al.² presented a new correlation for estimating the MMP for live oils and impure CO₂ streams. Their criterion for slim-tube miscibility was chosen to be 90% recovery at a gas breakthrough,

with no two-phase flow evident in the sight glass. The predicted MMP increases with temperature and C_5^+ molecular weight. Also, the MMP is affected by the molar amounts of constituents such as N_2 and H_2S . They also presented an additional correlation to account for impure CO_2 streams.

1.4 Approach and Scope of Work

The approach and scope of work in this project generally involved the tasks listed under Project Organization (Section 1.2). In this report, work under Tasks 1 and 2 is described in Chapter 2. Work related to Tasks 3, 4 and 5 is described in Chapters 3, 4 and 5, respectively.

The general approach taken in development of a method of evaluation of potential CO_2 miscible displacement candidates focused on phase-behavior and application of pseudo-ternary diagrams. The Soave-Redlich-Kwong (SRK) equation of state was used to make phase-behavior calculations. Some experimental bubble-point pressure data were taken on binary and ternary systems as a means of checking the equation of state and developing information and interaction coefficients required for the calculations (Tasks 1 and 2). The effect of a water phase on phase behavior was also checked experimentally using binary systems (Task 2).

Slim-tube displacements were conducted with simple hydrocarbon systems and with a number of crude oils (Task 3). This was done to provide miscibility pressure data for use in conjunction with phase-behavior calculations.

The approach taken for prediction of ideal performance of a CO_2 miscible displacement (Task 4) was to use the equation of state to generate pseudo-ternary diagrams for a CO_2 -oil system. Generation of pseudo-ternary diagrams provided, first of all, a method of prediction of MMP. Also, when used in conjunction with a mathematical model, the pseudo-ternary information provided a basis for performance calculations at miscibility and near-miscibility conditions (Task 5). This approach was thus thought to yield more information than application of the correlations for MMP. Also, work required was significantly less than that for application of a fully compositional mathematical model of the process. Data required on the crude oil or hydrocarbon systems for the calculations consisted of measured compositions or estimated compositions based on distillation curves.

The approach was tested on five crude oil systems for which compositional or distillation data and slim-tube measurements of MMP were available. The approach was found to be promising although not completely successful. It was possible to predict MMP values for the crude oils. However, to accomplish this, interaction coefficients required in the SRK equation of state had to be modified from crude to crude. That is, it was not possible to predict the behavior for all five crudes using a single set of coefficients.

CHAPTER 2

PHASE BEHAVIOR MEASUREMENTS AND CALCULATIONS

2.1 Introduction

The scope of the project involves the use of an equation of state to model the phase behavior of carbon dioxide-hydrocarbon systems. The Soave-Redlich Kwong (SRK) equation of state was selected for this purpose. To support the application of the model, it was desirable to obtain a limited amount of phase-behavior data with carbon dioxide and relatively simple hydrocarbon systems.

There were three main objectives of the phase-behavior studies. The first was to make bubble-point pressure measurements and then apply these data to "fine tune" the interaction parameters in the SRK equation of state. It was planned that this work would form the basis for application of the model to simulated and real crude oil systems. Since significant literature data existed for CO₂-paraffinic hydrocarbons, experimental measurements in this work focused on CO₂-aromatic and CO₂-naphthenic systems.

A second objective was to evaluate the effect on phase behavior of an immobile water phase. While it is reasonable to assume, based on general knowledge of the phase behavior of carbon dioxide-hydrocarbon systems, that the presence of immobile water would not significantly affect the phase behavior, this had not been verified. Therefore, phase behavior measurements were made in the presence of water.

A third objective was to examine the effect of paraffinic, naphthenic and aromatic hydrocarbon type on the achievement of miscibility in carbon dioxide-hydrocarbon systems. Crude oils are mixtures of these three hydrocarbon types and their distribution varies from crude to crude¹³. On the average, 30 to 50 volume percent of the crude is non-paraffinic. Holm and Josendal¹⁷ reported data from slim-tube displacement experiments indicating that crude oil containing a more aromatic mid-range fraction gave a slightly increased oil recovery when compared to data acquired on crude oil containing less aromatics. This implies a reduction in MMP as the oil is enriched in aromatics. However, the limited results reported in the literature are unclear on this point and it was deemed useful to obtain additional data.

Computer programs for the SRK equation of state were available to the project through the Kurata Low Temperature Thermodynamics Laboratory at the University. New experimental data were taken and these data fall into three general categories:

- 1) Bubble-point pressures of CO₂-hydrocarbon binary mixtures in which aromatic and naphthenic hydrocarbons were used.

- ii) Bubble-point pressure reduction of CO₂-hydrocarbon mixtures in the presence of water.

iii) Bubble-point pressures and densities of CO₂-hydrocarbon ternary mixtures which contain paraffinic, naphthenic, or aromatic components.

This chapter describes the materials, equipment and procedures. Interaction parameters obtained using the SRK equation of state are presented and the effect of an immobile water phase on bubble-point pressure reduction is discussed.

2.2 Apparatus, Procedure and Materials

2.2.1 Materials and Experimental Conditions

To meet Objective 1 as stated earlier, several CO₂-hydrocarbon binary systems were used for the measurement of pressure-composition data at fixed temperatures. The hydrocarbons used were aromatic and naphthenic components. The systems were CO₂-toluene, CO₂-ethylbenzene, CO₂-propylbenzene, CO₂-cyclopentane, CO₂-cyclohexane and CO₂-methylcyclohexane. Temperatures were 140°F, 170°F and 200°F. As indicated earlier, sufficient data for paraffinic hydrocarbons exist in the literature. Data taken in this work, along with literature data, were used to calculate interaction parameters in the SRK equation of state.

To reach Objective 2, pressure-composition data were taken for CO₂-n-butane in the presence of fresh water at 160°F. Finally, for Objective 3, bubble-point pressure data were taken at 160°F and about 1400 psia on ternary systems comprised of carbon dioxide, n-butane and n-decane; carbon dioxide, n-butane and n-butylcyclohexane; and carbon dioxide, n-butane and n-butylbenzene, and on one five-component system comprised of carbon dioxide, n-butane, n-decane, n-butylcyclohexane and n-butylbenzene where the three hydrocarbons of carbon number 10 were combined in the molar ratio of 5:4:1, respectively.

The experimental design procedures of Howat and Swift¹⁸ were used to select a priori the number and compositional locations for the data of the three ternary systems such that the interaction parameters for the SRK equation of state would be adequately defined for the purpose of this work. SRK coefficients and mixing rules were from Graboski and Daubert^{14,15} and critical constants for the chemical compounds of interest were from Reid, et al.³³.

The average uncertainties in results are ±10 psi, ±0.1°F and ±0.004 in mole fraction.

All of the hydrocarbons used in this work were purchased from Phillips Petroleum Company Special Products Division, Borger, Texas, and they were pure grade with a purity of at least 99.0%. The carbon dioxide was bought from Matheson Company, Joliet, Illinois. The specified purity of the carbon dioxide is 99.99% minimum. To avoid rusting and pitting of the equilibration cells and the feed lines, the water used in these experiments was distilled and deionized. It was supplied by the Department of Biochemistry of the University of Kansas, Lawrence, Kansas.

2.2.2 Apparatus

The major items in the experimental equipment were: i) the volumetric metering system, ii) the test system, and iii) the gas chromatograph.

The volumetric metering system was used to introduce known amounts of test materials into the cells of the test system. This equipment has been described by Laurance²⁴. A schematic diagram of the equipment is shown as Figure 2-1.

The test system was used to measure the pressure-volume behavior of known mixtures (schematic diagram in Figure 2-2). It consists of two stainless steel cells of approximately 200 cm³ internal volume each. At one end of each cell is a movable piston driven by hydraulic oil from a Sprague oil pump. By this means, the volume of the cells can be varied. An indicator rod attached to the piston locates the relative position of the piston inside the cells. Through measurement of the height of the indicator rod with a vernier height scale, changes in the volume of the cells can be determined precisely. The movable piston and a stationary plug at the other end of the cells are fitted with Viton O-rings (V709-9, size 2-214).

Both cells are attached to a metal bracket on a horizontal pivot that passes through two self-aligning ball bearings. This enables the cells and their contents to be rotated about a horizontal axis. The rotation helps to mix the contents of the cells and allows sampling of two different phases, if they coexist, depending on the position of the cells.

Two pressure transducers were used to measure the pressures of the contents of the two cells. Each cell has its own transducer. The pressure transducers were supplied by Consolidated Electrodynamics Corporation. They are of types 4-356-0001 and CEC 1000-04 and both have pressure ranges of 0-5000 psi. The transducers were calibrated against a Ruska Dead Weight Gage, serial #14459 with piston #B3-377.

For part of the work, a Paroscientific DigiquartzTM pressure transducer (Model 73K-002, Series 9917) was installed on one of the cells. Its range was 0-3000 psia. Together with its pressure computer (Model 600), this transducer provided the capability of direct pressure output in any chosen unit. It eliminated the procedure of recalibrating the CEC transducers before and after each run. This resulted in at least a one-third savings in time for each experimental run.

An F&M Model 720 dual column programmed gas chromatograph was used for compositional analysis. It was equipped with a thermal conductivity detector and a Honeywell Electronic strip chart recorder with a range of -0.20 to +1.00 millivolts. A digital integrator supplied by Columbia Scientific Industries, Model CSI 38 was also connected to the output of the thermal conductivity detector. The carrier gas was helium.

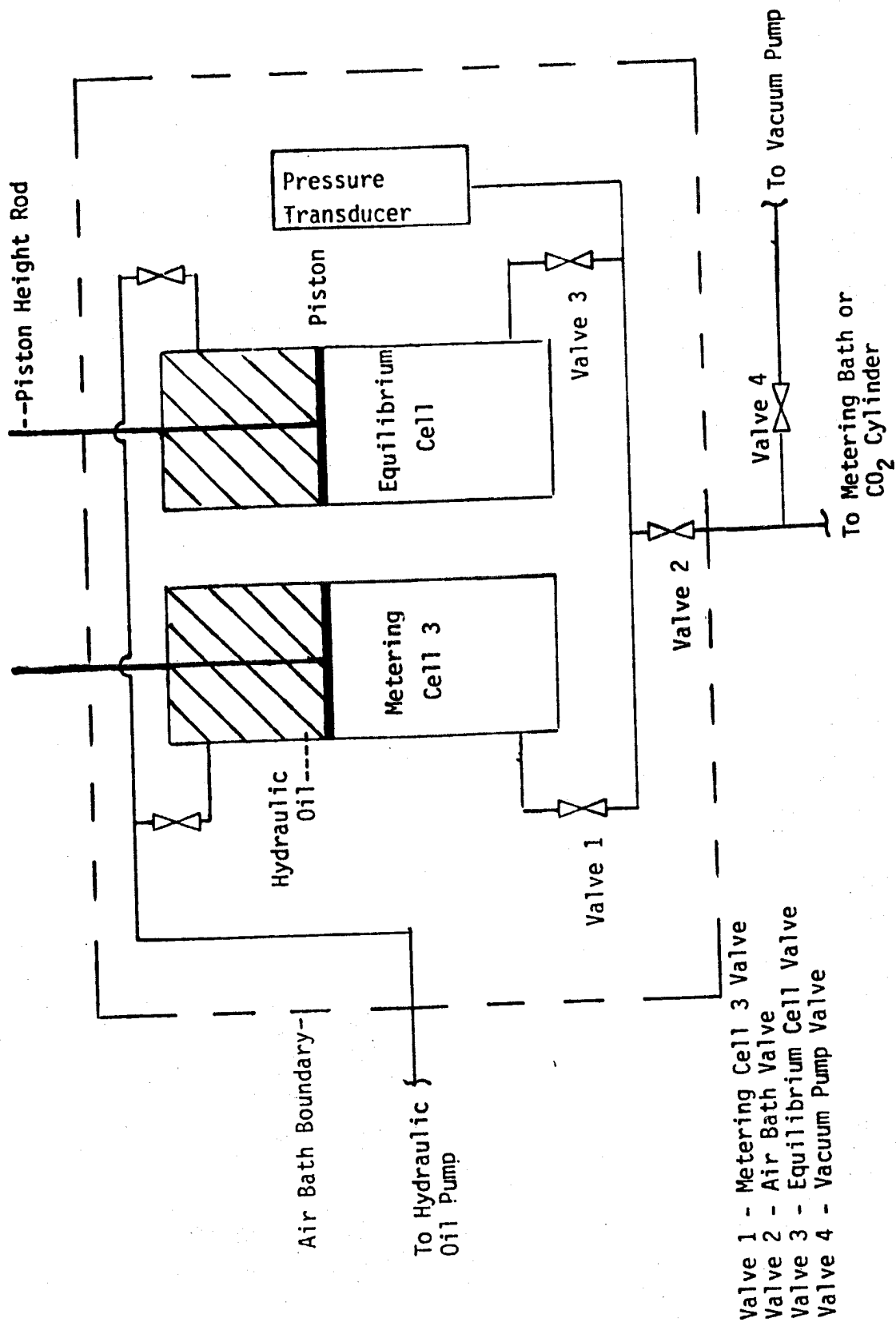


FIGURE 2-1: Schematic Diagram of Equilibrium Cell and Associated Flow Lines

- Valve 1 - Metering Cell 3 Valve
- Valve 2 - Air Bath Valve
- Valve 3 - Equilibrium Cell Valve
- Valve 4 - Vacuum Pump Valve

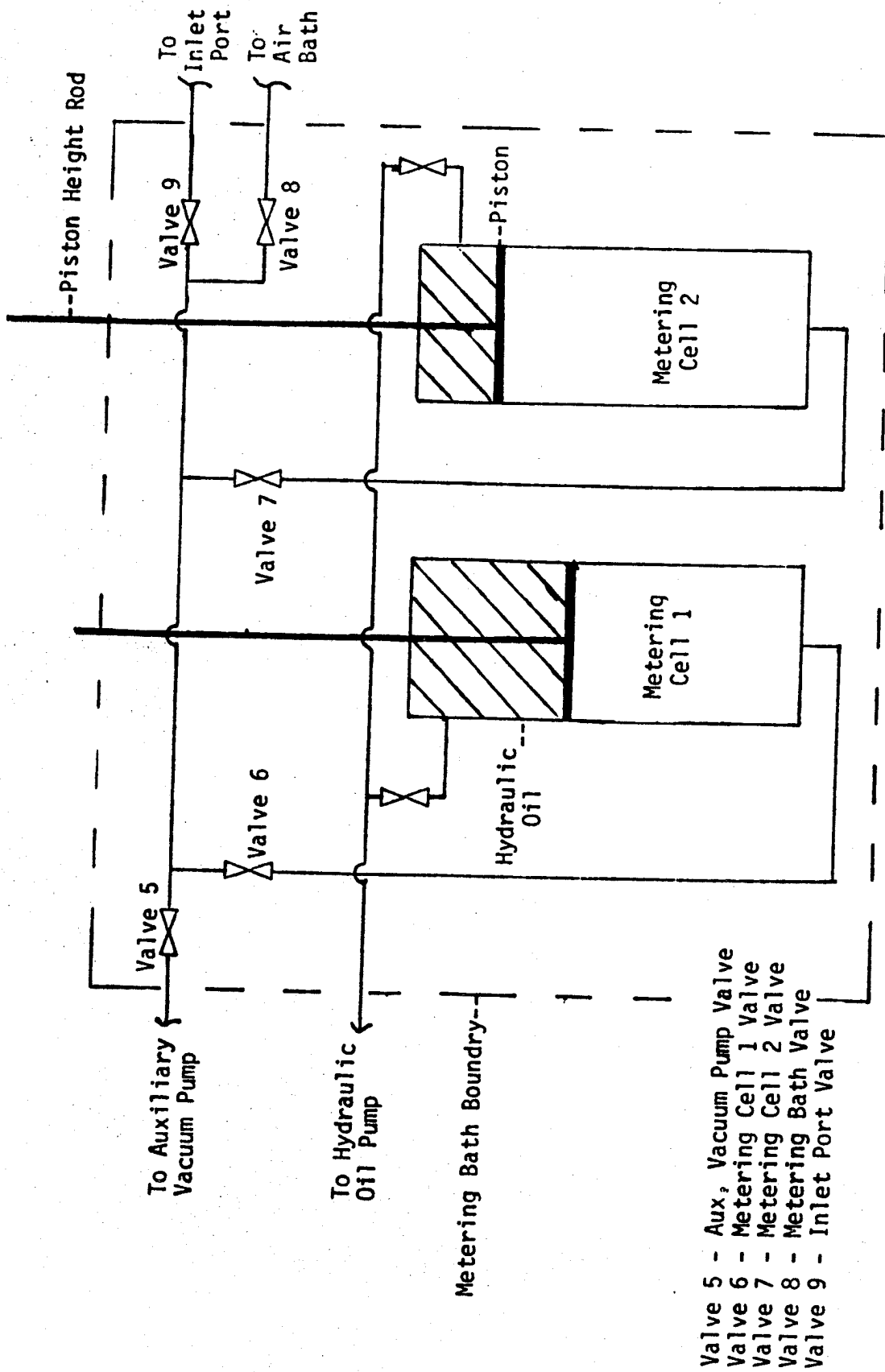


FIGURE 2-2: Schematic Diagram of the Metering System

The chromatographic columns were packed with PORAPAK QS, mesh range 120-150. Each column was two (2) meters long with an internal diameter of 1.5 mm.

A gas sampling valve (Model V-6-UHTaHC) and a liquid sampling valve (Model FSV-4-UTaHC) were used to inject samples of the mixtures into the chromatograph. Both were supplied by Valco Instruments Company and can operate at pressures up to 3000 psia. Direct sampling reduces errors (such as inconsistent sample size, etc.) that may occur by injecting samples into a chromatograph with a syringe.

Additional information about the equipment is given by Ezekwe¹² and Cramer⁸.

2.2.3 Procedure

To prepare a mixture, carbon dioxide was added to the variable volume cell at known temperature, pressure and volume. The data of Angus, et al.⁴ were used to calculate the mass of carbon dioxide present. The prescribed amounts of hydrocarbons were then injected into the cell from high-pressure, variable volume cells housed in a separate, oil-filled thermostat held at a prescribed temperature. These calibrated variable volume cells served as burettes to add known volumes of hydrocarbons displaced at a constant reference pressure. For the n-butylcyclohexane and n-butylbenzene, reference densities to convert from volume to mass were measured at 1250 psia and 100°F: 46.75 lbm/ft³ for n-butylcyclohexane and 53.3 lbm/ft³ for n-butylbenzene. Densities for displacement of other hydrocarbons were obtained from the literature.

Bubble-point pressures for the various mixtures were determined by the pressure-volume intersection method. The cross-sectional area of the variable volume cell was constant, thus the method reduced to measuring pressure as a function of piston position in the cell. The piston position was determined to ±0.001 inch. Cramer⁸ gives details on the procedure used to get bubble point pressures from the pressure versus piston position data.

The experimental procedure used in the determination of the effect of water on the bubble-point pressures of CO₂-hydrocarbon systems was similar to the procedure used in the acquisition of isothermal P-x data. The major difference was that after the bubble-point pressure of the CO₂-hydrocarbon mixture had been measured, incremental amounts of water were injected into the cell. The bubble-point pressure of the composite mixture was then measured again.

Additional details about the experimental procedure are given by Ezekwe¹² and Cramer⁸.

2.3 Experimental Results

The experimental results are reported in Appendix A. The results are grouped as follows:

- 1) Bubble-point pressures for binaries of CO₂-aromatic and CO₂-

naphthenic hydrocarbons are presented in Tables A-1 through A-6. (Ezekwe¹²).

ii) Bubble-point pressure reductions of CO₂-hydrocarbon binaries in the presence of water are given in Tables A-7 through A-10. (Ezekwe¹¹).

iii) Bubble-point pressures and densities for CO₂-hydrocarbon ternary mixtures are shown in Table A-11 (Cramer⁸).

2.4 Application of the Soave-Redlich-Kwong (SRK) Equation of State

2.4.1 Introduction

The SRK equation of state with the coefficients and mixing rules recommended by Graboski and Daubert^{14,15} was used to model all CO₂-hydrocarbon phase equilibria. Critical constants for the chemical compounds of interest used in SRK were taken from Reid et al.³³ A regression program (Ezekwe¹² and Cramer⁸) was used to determine the binary interaction coefficients for the SRK equation of state which best fit bubble-point data.

2.4.2 Interaction Coefficients-Regression of Binary Data

Tables 2-1 and 2-2 present the CO₂-hydrocarbon binary interaction coefficients (K_{ij} 's) determined from data of this work and literature data as reported by Ezekwe¹². Based on these results, Ezekwe attempted to correlate the interaction coefficients with only moderate success as shown in Table 2-3. Ezekwe's work showed that the interaction coefficients were dependent on temperature but the nature of this dependence could not be correlated. Cramer⁸ showed that the K_{ij} 's were also pressure dependent, as seen in Figures 2-3 and 2-4.

2.4.3 Effect of Water on Phase Behavior

The experimental data for CO₂-hydrocarbon water systems are given in Tables A-7 through A-10. The data demonstrate the effect of water on the bubble-point pressures of CO₂-hydrocarbon systems.

To obtain the data, bubble-point pressures of the mixtures were measured in the absence of water in the equilibration cell. After the addition of water, the bubble-point pressure of the mixture was measured again. There was always an appreciable drop in the bubble-point pressure of the latter mixture. To examine the effect of water the bubble-point pressure of the mixture without water in the cell was first plotted. Then, the bubble-point pressure of the mixture with water, was plotted on a water-free basis. The important finding was that the bubble-point pressure of the mixture, after the addition of water, was always located on the bubble-point locus of the system in the absence of water if plotted on the basis of the composition of the hydrocarbon-rich phase (Figure 2-5).

This observation indicated that after the water phase has solubilized the carbon dioxide in the mixture to its saturation condition, the remaining carbon dioxide together with the hydrocarbon (which is essentially insoluble in the water-rich phase) exhibited the

Table 2-1

Interaction Coefficients for Various Aromatic and Naphthenic Components with Carbon Dioxide

Components	Interaction Coefficients (%STD*)			
	140°F	170°F	200°F	All Temp.
CO2-toluene	.1016(5.4%)	.0958(7.8%)	.0999(4.4%)	.0996(5.6%)
CO2-Ethylbenzene	.1057(3.6%)	.1020(2.5%)	.1048(2.6%)	.1042(2.9%)
CO2-Propylbenzene	.1017(2.9%)	.1040(2.9%)	.1040(1.1%)	.1036(2.3%)
CO2-Cyclopentane	.1358(2.2%)	.1348(2.2)	.1338(1.7%)	.1354(2.0%)
CO2-Cyclohexane	.1422(4.5%)	.1423(4.2%)	.1412(4.2%)	.1423(4.3%)
CO2-Methylcycloh.	.1387(3.8%)	.1362(3.9%)	.1369(3.5%)	.1364(3.7%)
CO2-n-Butane**	---	---	---	.1480(3.0%)
CO2-n-Decane**	---	---	---	.1100(3.7%)

$$*\text{STD} = 100 \frac{\sqrt{\frac{\sum (P_{\text{cal}} - P_{\text{exp}})^2}{N}}}{N-1}$$

** 100 and 160°F only

Table 2-2

Interaction Parameters for Various CO₂-Paraffinic Components Regressed from Literature Data

Components	Interaction Coefficients (**)				
Methane	.0979(259.8)	.0972(271.4)	.0979(A)	.1325(293.1)	.1322(A)
Ethane	.1379(243.1)	.1332(263.1)	.1323(283.1)	.1615(A)	
n-Propane	.1608(310.9)	.1617(327.6)	.1625(344.2)	.1475(A)	
n-Butane	.1476(310.9)	.1476(344.2)	.1463(377.6)	.1163(A)	
n-Pentane	.1118(311.0)	.1154(344.1)	.1155(377.6)	.1306(A)	
n-Hexane	.1245(313.1)	.1305(353.1)	.1409(393.1)	.1108(A)	
n-Heptane	.1116(310.60)	.1103(352.6)	.1114(394.2)	.1153(A)	
n-Decane	.1154(310.9)	.1152(344.2)	.1160(377.6)		

** Numbers in Parentheses are temperatures in Kelvin

**A = All Isotherms

Table 2-3

Comparisons of Interaction Parameters from Correlations

<u>Component</u>	<u>$(K_{ij})^*$</u>	<u>Corr. #1</u>	<u>Corr. #2</u>	<u>Corr. #3</u>
Methane	0.0979	0.1310	0.1351	0.1304
Ethane	0.1322	0.1373	0.1307	0.1405
Propane	0.1615	0.1376	0.1260	0.1386
n-Butane	0.1480	0.1355	0.1235	0.1353
n-Pentane	0.1163	0.1319	0.1216	0.1310
n-Hexane	0.1306	0.1276	0.1201	0.1261
n-Heptane	0.1108	0.1235	0.1192	0.1216
n-Decane	0.1100	0.1126	0.1175	0.1097
Benzene	0.0860	0.1051	0.1122	0.1074
Toluene	0.0996	0.1030	0.1128	0.1047
Ethylbenzene	0.1042	0.1014	0.1133	0.1027
Propylbenzene	0.1036	0.1006	0.1138	0.1014
Cyclopentane	0.1354	0.1184	0.1160	0.1176
Cyclohexane	0.1423	0.1164	0.1156	0.1158
Methylcyclohexane	0.1364	0.1200	0.1173	0.1189
RMSE(%)	0.0	1.6	2.0	1.6

Correlation #1: $\text{Log}_{10}K_{ij} = -0.8849 - 0.2145 * \omega_i (\delta_i - \delta_j)$

Correlation #2: $\text{Log}_{10}K_{ij} = -0.9173 - 0.0017 * k_i * (\delta_i - \delta_j)$

Correlation #3: $\text{Log}_{10}K_{ij} = -0.8888 - 0.0189 * \omega_i k_i * (\delta_i - \delta_j)$

K = Interaction Coefficients

ω = Acentric Factor

δ = Hildebrand Solubility Parameter

k = Watson Characterization Parameter

and where subscript i = hydrocarbon, subscript j = CO₂

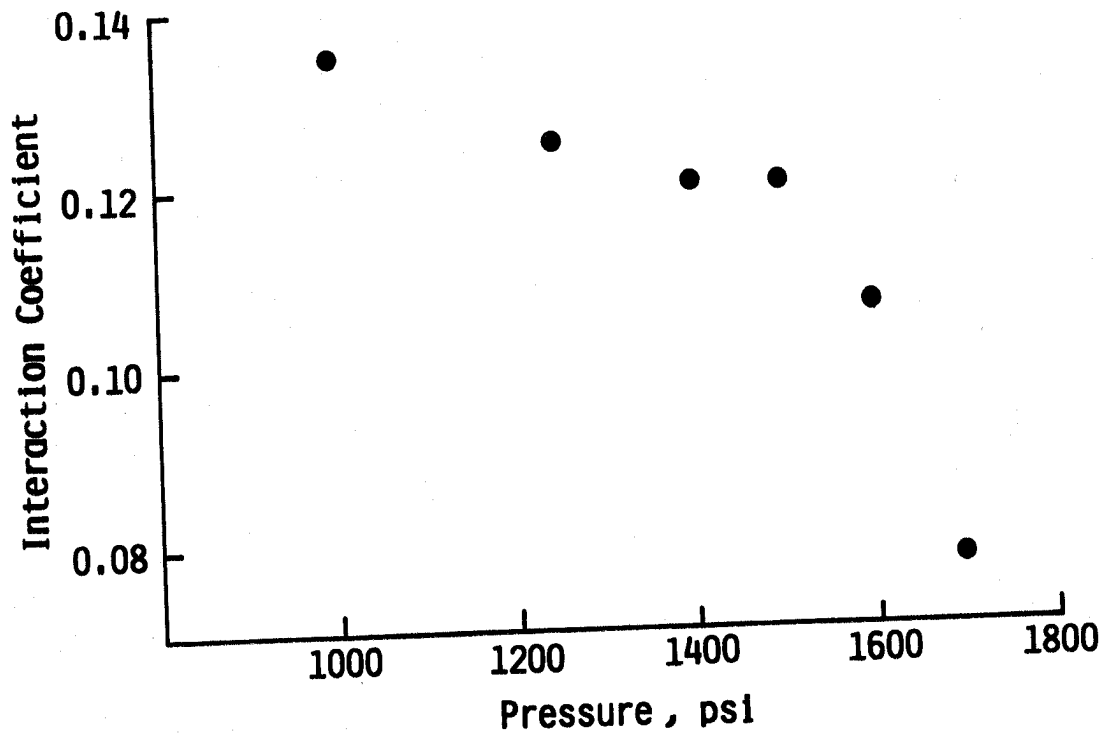


FIGURE 2-3: Interaction Coefficients as a Function of Pressure, CO₂ - n-Butane.

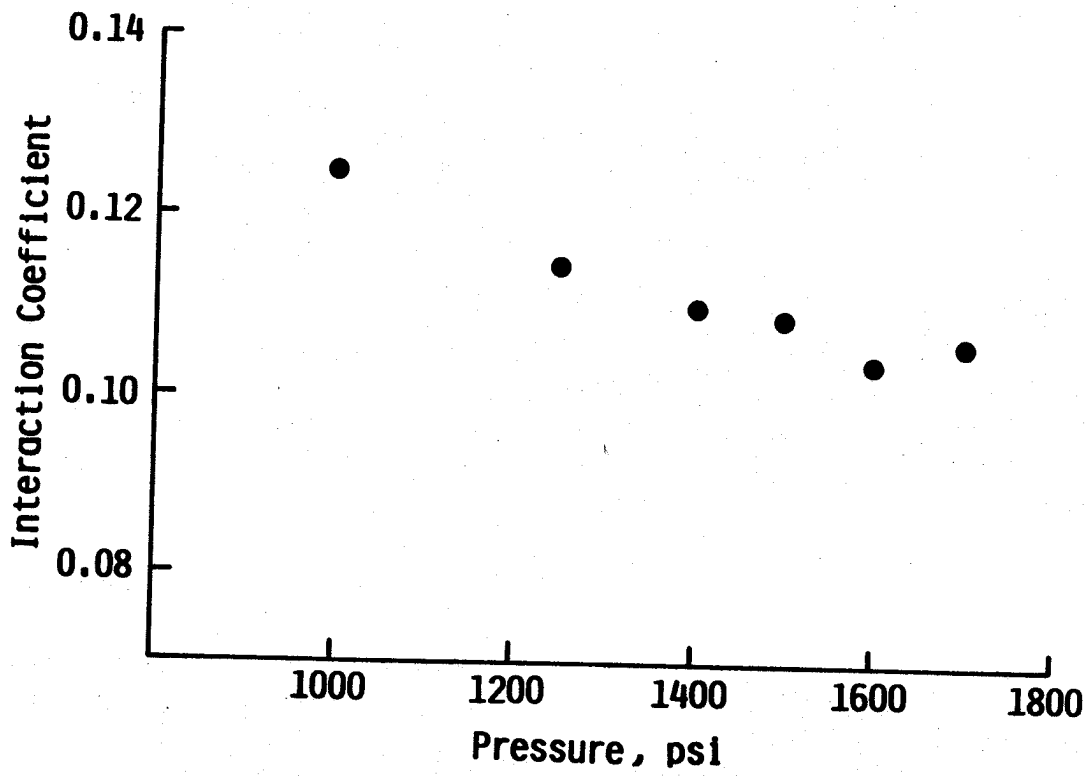


FIGURE 2-4: Interaction Coefficients as a Function of Pressure, CO₂ - n-Decane.

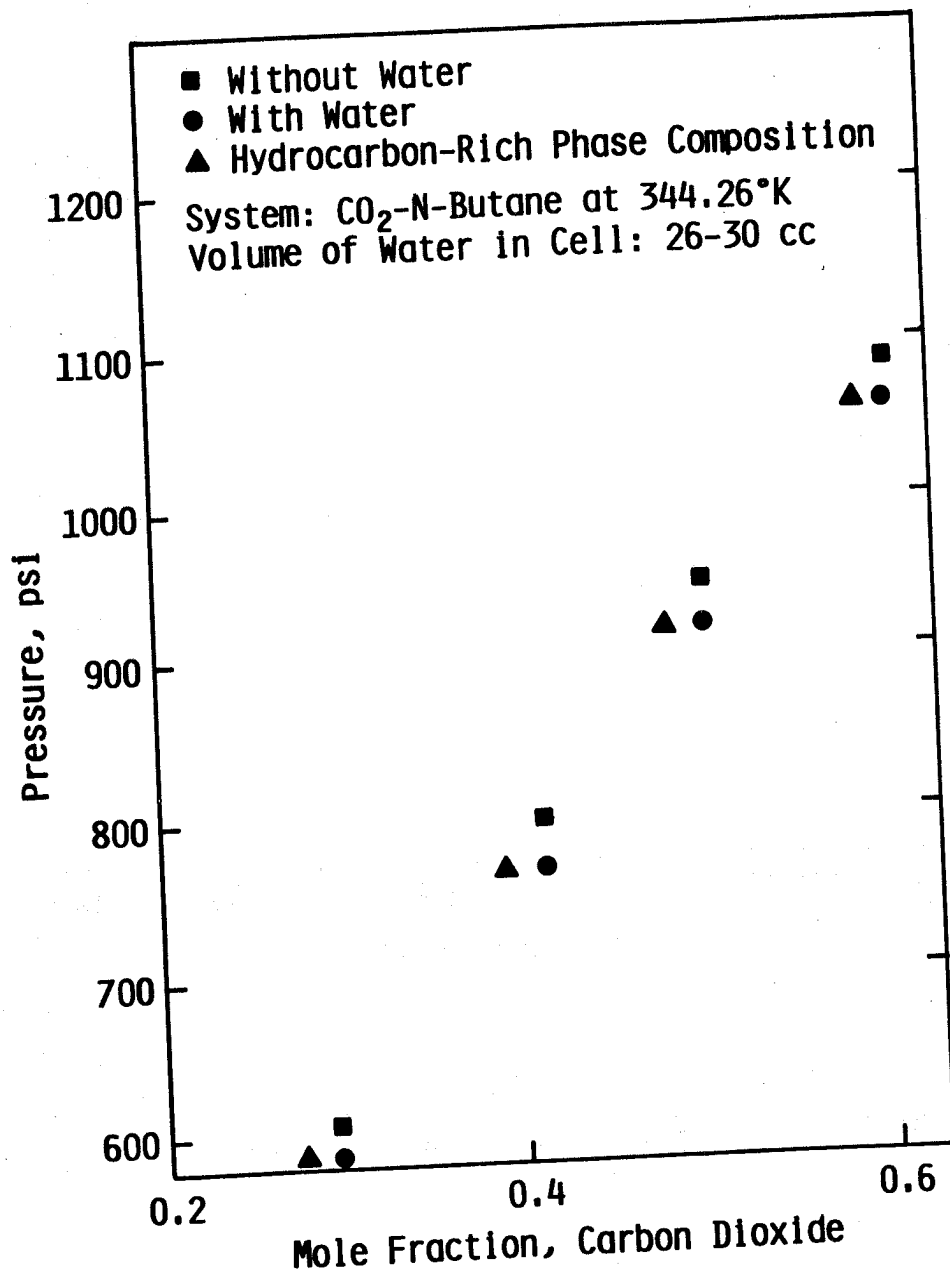


FIGURE 2-5: Bubble-point Pressure Displacement Due to the Presence of Water.

phase behavior of a mixture with similar initial composition in the absence of water. This means that the dominant effect of adding water to these mixtures is the reduction of the amount of carbon dioxide available for the hydrocarbon-rich phase through solubilization. The conclusion is that miscibility pressure for CO₂-hydrocarbon systems as measured in a slim-tube apparatus should be minimally affected by the presence of immobile water.

2.4.4 Interaction Coefficients-Regression of Ternary Data

The measured bubble-point pressures are reported in Table A-11. Uncertainties in temperature and pressure (reported as two standard deviations) are 0.07°F and 5 psia respectively. Uncertainties in composition are shown for each mixture as the last table entry.

A multicomponent least-squares regression program was used to determine the binary interaction coefficients for the SRK equation of state which best fit the ternary system bubble-point data sets of Table A-11.

The only ternary data found in the literature for comparison were the carbon dioxide, n-butane, n-decane data of Metcalfe and Yarborough²⁶. Of their data, only those at 160°F and approximately 1400 psia could be compared directly. Table 2-4 presents the results of three regressions for carbon dioxide, n-butane and n-decane where: 1) the data of this work and those of Metcalfe and Yarborough were combined for regression, 2) data of this work were regressed alone, and 3) the data of Metcalfe and Yarborough were regressed alone.

The results of Table 2-4 show that the calculated pressures, root mean-square errors and interaction coefficients obtained from the three regressions are very similar. This indicates that data of this work and those of Metcalfe and Yarborough agree. Therefore, the other data reported in Table A-11 should be reliable.

In the regression results which follow, only the data of Table A-11, excluding the last data point, were used. The results of eight regressions are reported in Table 2-5 where regressions 4, 5 and 6 are for the n-decane, n-butylcyclohexane and n-butylbenzene data separately with zero hydrocarbon interaction coefficients; 7, 8 and 9 are for the n-decane, n-butylcyclohexane and n-butylbenzene data separately with variable n-butane, heavy hydrocarbon interaction coefficients; 10 is for all data simultaneously with zero hydrocarbon interaction coefficients; and 11 is for all data simultaneously with variable n-butane, heavy hydrocarbon interaction coefficients. There was insufficient information for regression with variable interaction coefficients between the heavy hydrocarbon compounds.

Regressions 4-9 show marked variations in carbon dioxide, n-butane interaction coefficients as the heavy hydrocarbon component changes from paraffinic to naphthenic to aromatic. This is unacceptable within the constraints of the mixing rules being used with the SRK equation of state. Regression 10 does not represent the data within experimental uncertainty while regression 11 does represent the data within experimental uncertainty and with a root-mean-square error which is

Table 2-4

Regression of Carbon Dioxide, n-Butane and n-Decane Data at 160°F

Regr #	Data Ref.	-- mole fraction --			P exp psia	P cal psia	% Diff	K(1,2)	K(1,3)	RMSE %
1	(8)	0.670	0.000	0.330	1386	1396	+0.8	0.1244	0.1087	0.60
		0.674	0.068	0.258	1415	1398	-1.2			
		0.681	0.138	0.180	1395	1393	-0.2			
		0.712	0.200	0.089	1387	1394	+0.6			
		0.754	0.206	0.040	1399	1400	0.0			
		0.753	0.207	0.040	1392	1398	+0.4			
		0.680	0.083	0.237	1402	1409	+0.5			
	(26)	0.685	0.128	0.187	1401	1405	+0.2			
		0.679	0.140	0.182	1399	1387	-0.9			
		0.710	0.179	0.111	1406	1414	+0.6			
		0.763	0.203	0.034	1403	1400	-0.2			
		0.670	0.000	0.330	1386	1397	+0.8	0.1246	0.1089	0.65
		0.674	0.068	0.258	1415	1399	-1.1			
		0.681	0.138	0.180	1395	1393	-0.1			
0.712	0.200	0.089	1387	1395	+0.4					
0.754	0.206	0.040	1399	1400	+0.1					
0.753	0.207	0.040	1392	1398	+0.5					
0.680	0.083	0.237	1402	1412	+0.7	0.1204	0.1099			
3	(26)	0.685	0.128	0.187	1401			1405	+0.3	
		0.679	0.140	0.182	1399			1387	-0.9	
		0.710	0.179	0.111	1406			1411	+0.3	
		0.763	0.203	0.034	1403			1395	-0.6	

1 = carbon dioxide

2 = butane

3 = decane

Table 2-5

Interaction Coefficients Obtained from Regression 4 through 11 for Carbon Dioxide (1), n-Butane (2), n-Decane (3), n-Butylcyclohexane (4) and n-Butylbenzene (5). Data Point Numbers Refer to Those Given in Table A-11.

Regr. #	Data Pt #	K(1,2)	k(1,3)	k(1,4)	k(1,5)	k(2,3)	k(2,4)	k(2,5)	RMSE %
4	1-6	0.125	0.109						0.45
5	7-13	0.087		0.092					0.61
6	14-21	0.078			0.090				0.37
7	1-16	0.070	0.108			-0.089			0.61
8	6-13	0.120		0.092			0.060		0.44
9	14-21	0.113			0.090			0.062	0.28
10	1-21	0.094	0.112	0.091	0.089				1.49
11	1-21	0.105	0.109	0.092	0.090	-0.032	0.032	0.049	0.49

about the same as those of regressions 4 through 9. The bubble-point pressure of the last data point of Table A-11 was measured to be 1404 psia. Using the coefficients from regression 10, the value calculated for this composition was 1384 psia (1.5% low), whereas the value calculated with the coefficients from regression 11 was 1400 psia (only 0.3% low). Based on these observations, the interaction coefficients of regression 11 seem to best represent the experimental data although the use of non-zero n-butane heavy hydrocarbon interaction coefficients is contrary to current practice in equation-of-state prediction of carbon dioxide-hydrocarbon phase behavior. Note that while negative interaction coefficients, e.g., the n-butane, n-decane interaction coefficient of regression 11 (Table 2-5), are excluded in theory, they may be obtained from regression analysis since the SRK equation of state and mixing rules are, at best, semi-theoretical.

Maximum miscibility compositions expressed as mole fractions of the heavy hydrocarbon components on a carbon dioxide-free basis were calculated using the various interaction coefficient sets reported in Table 2-5 in a multicomponent flash program (Cramer⁸). Particular care was taken to obtain convergence in the critical region so that tie line extrapolation by the method of Benham, et al.⁷ would be correct. These maximum miscibility compositions are reported in Table 2-6.

The expected uncertainty in the maximum miscibility composition calculation is 0.008 mole fraction. Therefore, from these results there seems to be no significant difference in maximum miscibility composition as the heavy hydrocarbon compound type changes from paraffinic to naphthenic to aromatic save, perhaps, for calculations made with interaction coefficients from regressions 7, 8 and 9. Those coefficients have already been disallowed because of the variation of the carbon dioxide, n-butane interaction coefficient as the heavy hydrocarbon compound is changed from paraffinic to naphthenic to aromatic type.

Table 2-6

Maximum Miscibility Composition (MMC) for Mixtures of Carbon Dioxide and n-Butane with n-Decane, n-Butylcyclohexane or n-Butylbenzene, (MMC is Reported as Mole Fraction of Heavy Hydrocarbon on a Carbon Dioxide-Free Basis)

T = 160°F, P = 1400 psia

Ternary System with	MMC Using Reg 4,5,6	MMC Using Reg 7,8,9	MMC Using Reg 10	MMC Using Reg 11
n-Decane	0.226	0.197	0.239	0.210
n-Butylcyclohexane	0.216	0.244	0.217	0.231
n-Butylbenzene	0.223	0.239	0.213	0.235

CHAPTER 3

SLIM-TUBE DISPLACEMENT EXPERIMENTS

3.1 Introduction

An accepted method of measuring experimental dynamic miscibility pressure of a displacing fluid-crude oil system involves the application of a slim-tube apparatus such as described by Yellig and Metcalfe⁴³. The apparatus basically consists of a long tube of small diameter packed with sand or glass beads. In an experiment, the tube is saturated with the oil, brought to reservoir temperature, then the oil is displaced at approximately constant pressure with the displacing fluid of interest. Cumulative recovery of the oil is measured as a function of the amount of fluid injected. The experiment is continued until breakthrough of the displacing fluid occurs or until a specified number of pore volumes has been injected. Total oil recovery up to the point of termination is recorded. The experiment is then repeated at different pressures, each experiment yielding an oil recovery as a function of average displacement pressure.

Typically, recovery increases with increasing pressure in a manner shown schematically in Figure 3-1. The point at which the curve breaks over, or at which extrapolations of the two parts of the curve intersect, is termed the miscibility pressure. Slightly different methods of conducting a slim-tube experiment and of measuring miscibility pressure have been proposed and there is no standardized method. However, the different methods, which are variations on the same theme, do appear to yield reasonably consistent results and, at least, to be internally consistent in a particular laboratory.

A slim-tube apparatus was constructed for this project and experiments were run to determine miscibility pressures for several systems. The purpose of conducting slim-tube experiments was to provide data on miscibility pressures and recovery efficiencies that could provide a basis for verification of phase-behavior and mathematical-model calculations to be described later in this report. Four different series of slim-tube experiments were conducted. The first series was done on simple hydrocarbon systems to verify the operation of the apparatus. Next, a series of experiments was done with simple ternary systems consisting of CO₂ plus two hydrocarbon components. The third series was also done with a ternary system, but displacements were conducted with an immobile water phase present. The fourth series of displacements involved measurement of miscibility pressures for a number of crude oils from the State of Kansas.

This chapter contains a description of the apparatus, the procedure and a summary of the experimental results. Additional discussion, which relates the results to the phase-behavior studies and computer simulation, is presented in the following chapters.

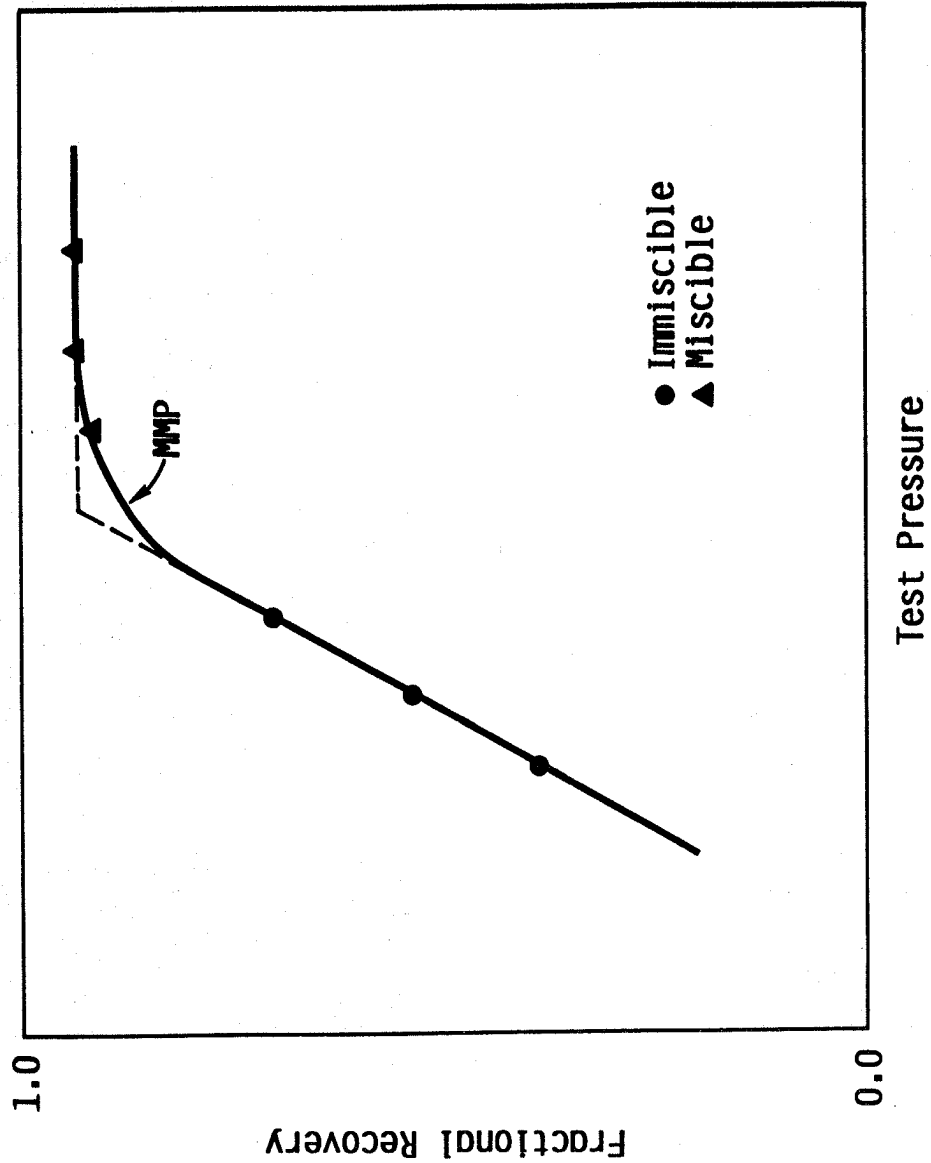


FIGURE 3-1: Typical Results From Slim Tube Displacements.

3.2 Experimental Apparatus and Procedure

3.2.1 Apparatus

A schematic of the apparatus is shown in Figure 3-2. The main element was the slim tube which consisted of a stainless-steel (type 316) tube, 5/16 inch OD by 0.35 inch thick. Individual pieces were used to make up the total length which was either 40 ft or 80 ft for the results reported here. The tubing was formed into a coil approximately 3 feet in length which was mounted horizontally to minimize gravity effects. The tubing was packed with 80-100 mesh glass beads which were washed with water and acetone prior to packing. Porous-media porosity was about 30 percent in all runs.

A positive-displacement pump (ISCO model 314) was used to drive fluids through the slim tube. The pump had a pressure limitation of 3000 psia. It was hydraulically connected to two hydraulic accumulators (Parker Hydraulic Accumulator, Model A2A-0058A1K) which were in turn connected to the slim-tube entrance. These movable piston accumulators were used for fluid storage and as a means of preventing the pump hydraulic oil from contacting the hydrocarbon-CO₂ system. At the slim-tube exit, a dome back-pressure regulator (Grove Model SD-91-WX) was used to maintain a constant specified back pressure on the tube. Pressure gauges (Marsh Instr. Co., Model KH-363) were mounted at the upstream and downstream ends of the slim tube.

The tube and transfer accumulator parts of the apparatus were contained inside a constant temperature air bath. The bath consisted of a wood cabinet (4 ft by 4 ft by 2.5 ft) lined with fiber glass insulation. Temperature was controlled in the bath using a temperature controller (Bayley Inst. Co., Model 252). Two heaters and two squirrel-type blowers were used to provide uniform heating of the bath. The temperature of the bath could be maintained within $\pm 1^\circ\text{F}$ at temperatures between 85°F and 200°F.

The apparatus was designed such that a gas chromatograph (Varian Model 3700) could be connected to the effluent of the slim tube. However, in the results reported here, no gas chromatograph analyses are included since none were made.

3.2.2 Procedure

The slim tube was packed with glass beads and pressure tested for leaks to 2700 psia. Volumetric calculations were made based on weight measurements. The temperature control system was set at the desired level. To saturate the tube with the hydrocarbon for which miscibility pressure was to be measured, several pore volumes of the hydrocarbon were allowed to flow through the coil. The effluent was observed through transparent tubing at the effluent end to determine that no gas was evolving by the end of the saturation procedure. After the tube was saturated, the back-pressure regulator was pressurized to about 20 to 40 psi higher than the back-pressure and the entire system was allowed to stabilize for about 1 1/2 hours to ensure thermal equilibrium.

A displacement was then conducted by injecting CO₂ at a constant rate. Produced hydrocarbon was collected in a graduated cylinder and a

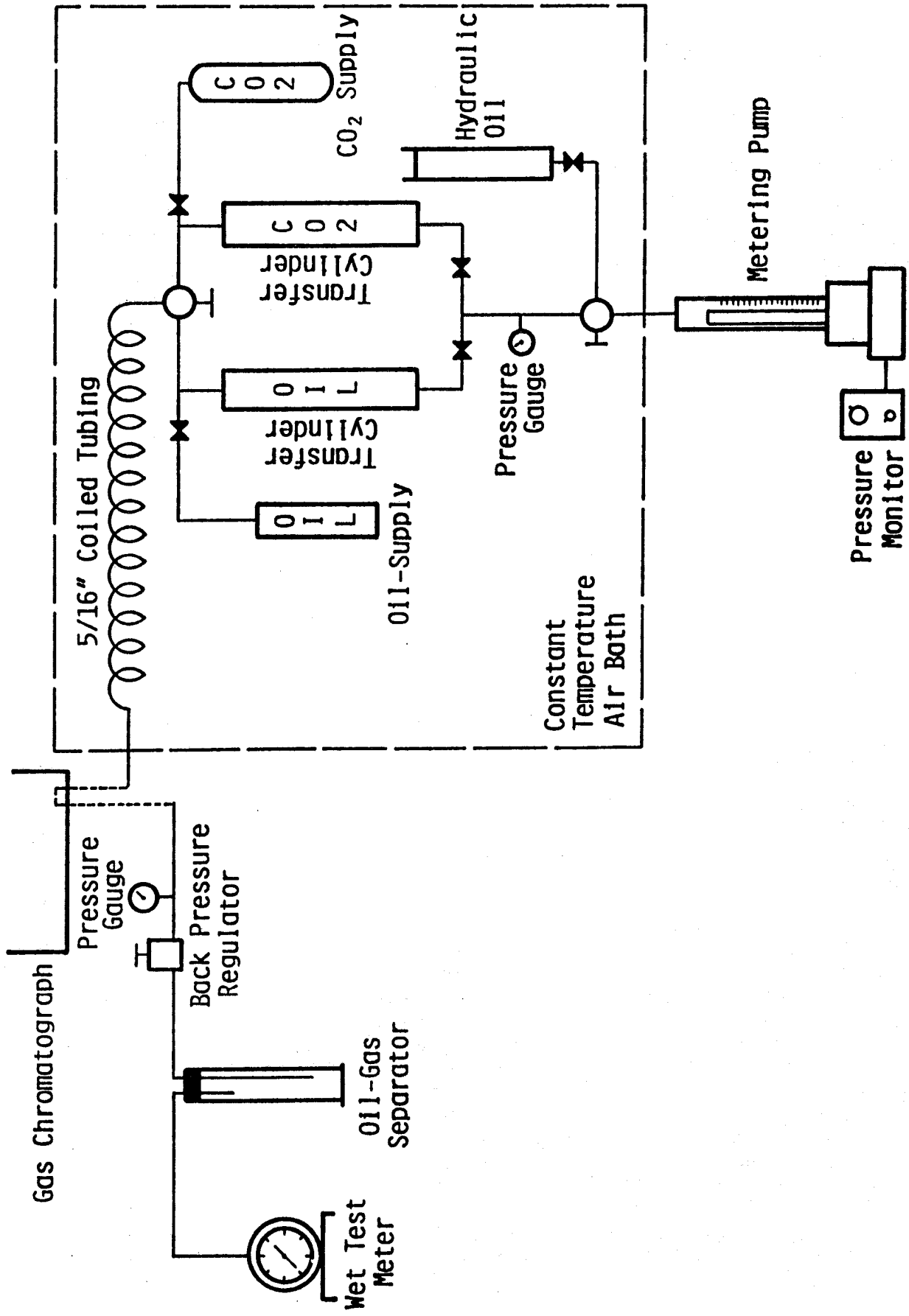


FIGURE 3-2: Slim-Tube Apparatus

time-versus-production record was kept. Temperatures, pressure, and pump settings were monitored throughout a run. A run was continued well beyond the point of a CO₂ gas-phase breakthrough.

After a run was terminated, preparation was made for additional runs by thoroughly flushing the slim tube with a solvent and then displacing the solvent with the hydrocarbon to be tested.

In experiments for which the effect of immobile water was measured, the procedure was essentially the same except that an irreducible water saturation condition was first established. This was done by first saturating the tube with distilled water prior to hydrocarbon injection. The water was then displaced with the test hydrocarbon to drive water saturation to an irreducible minimum. Residual water saturation was typically on the order of 21 percent.

3.3 Calibration and Checking of the Apparatus

Several calibration and check runs were conducted to establish the validity of experimental results. The first of these was a measurement of the miscibility pressure of n-hexane with CO₂ at a temperature of 100°F. The phase equilibrium for the system of carbon dioxide and n-hexane is reported in the literature (Turek, et. al.⁴⁰). In order to determine the miscibility pressure for this binary system at the test temperature, a phase-boundary curve was constructed from experimental data. Carbon dioxide and hexane were predicted to be miscible at pressure levels of 1110 psi and higher.

A series of experiments was carried out in which pure n-hexane was displaced by pure carbon dioxide at a temperature of 100°F and a constant carbon-dioxide injection rate of 80 cc/hr (approximately 400 ft/day). Displacements were conducted at pressures both above and below the predicted miscibility pressure to determine the apparent minimum miscibility pressure in the slim-tube apparatus. In all experiments, CO₂ breakthrough was detected by visual observation. After breakthrough occurred, only slightly more hexane (between 2 and 2.5 percent) was recovered. Injection of carbon dioxide was continued after breakthrough for an additional 0.1 pore volume to make sure that maximum recovery was achieved.

A plot of ultimate recovery versus displacement pressure is given in Figure 3-3. Miscibility pressure was determined as the intersection of the extrapolations of the miscible and immiscible parts of the overall curve. A value of 1125 psia was obtained, in good agreement with the predicted value of 1110 psia.

A few experiments were conducted to check for reproducibility and for the effects of flow rate and tube length. Results from replicate runs indicated that reproducibility was quite good and on the order of 1 recovery percent for simple hydrocarbon systems. Ultimate recovery at an injection rate of 20 cc/hr was within 1 recovery percent of that obtained at 80 cc/hr. There were, however, differences of a few percent in the relationship between recovery and pore volumes of CO₂ injected.

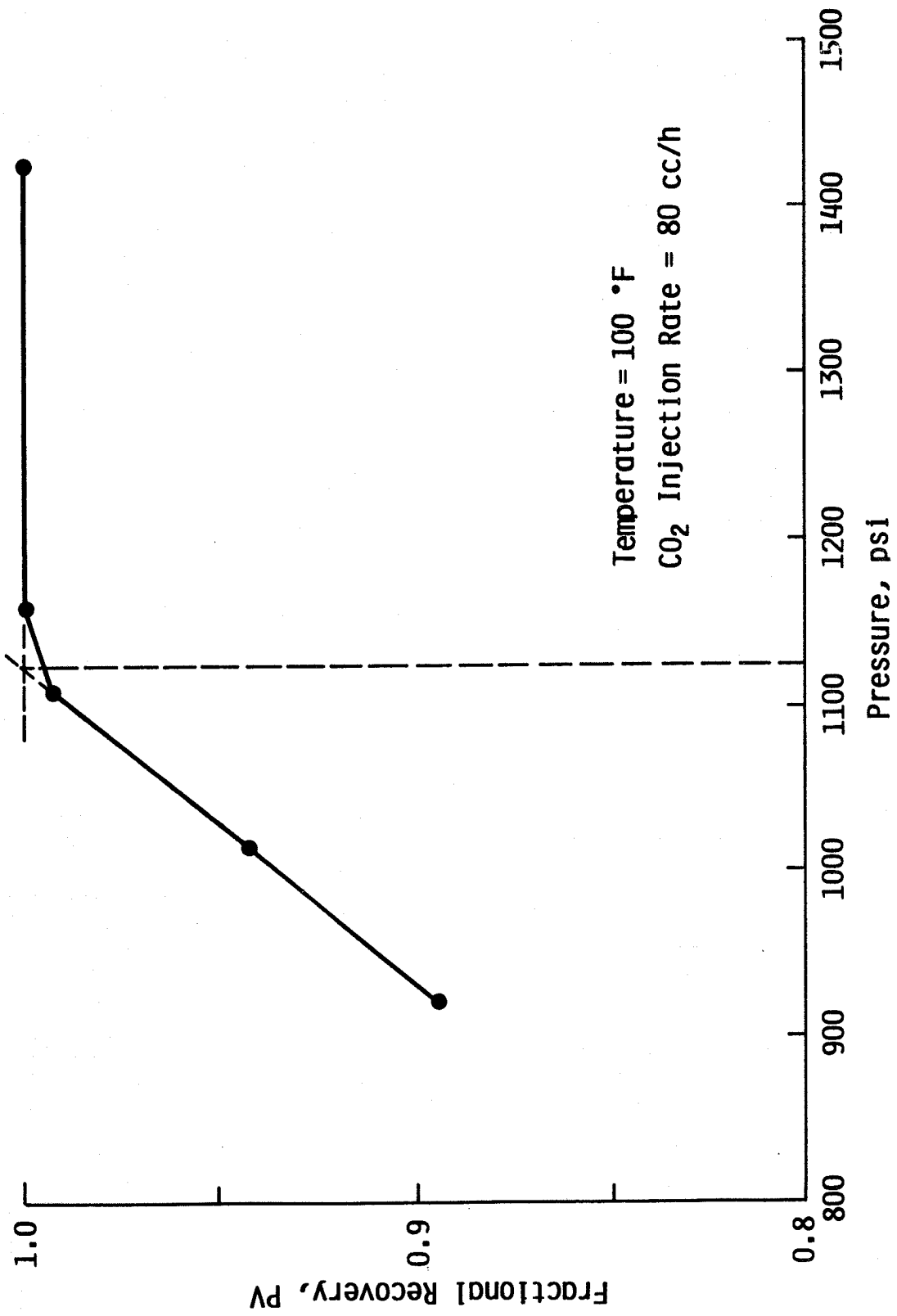


FIGURE 3-3: Slim Tube Results, CO₂ - n-Hexane Binary System.

Johnson and Pollin¹⁹ have reported that velocity does affect the ultimate recovery in slim-tube displacements but that the miscibility pressure as determined from the recovery versus pressure curve is not significantly affected. The effect of length was checked by conducting displacements in 40 ft and 80 ft tubes with all other parameters the same. Recoveries and miscibility pressures were in good agreement. Additional details of the experiments performed to check the apparatus are given by Azadeh⁵.

3.4 Results of Displacements with Carbon Dioxide and Binary Hydrocarbon Systems

In this series of experiments, pure carbon dioxide was the displacing fluid and different binary hydrocarbon mixtures were used as the oil phase. The phase behavior for these experiments could be directly represented on a constant pressure/constant temperature ternary diagram. The systems tested were

CO₂ - C₆ - C₁₀ (n-decane)
CO₂ - C₄ - C₁₀ (n-decane)
CO₂ - C₄ - C₁₀ (n-butylbenzene)

3.4.1 Hexane - Decane System

As a follow-up to the measurements made with pure hexane described earlier, a binary system of hexane-decane was used as the oil phase. No previous studies were found in the literature on the phase equilibrium of the mixture of carbon dioxide, hexane, and decane. In order to predict the miscibility pressure of this binary system with carbon dioxide, a computer phase-behavior model was used to generate the data for construction of a ternary phase diagram (Ezekwe¹²). Ezekwe used the model described in Chapter 2 of this report to calculate the ternary diagrams at 100°F shown in Figure 3-4. From these calculations, a miscibility pressure between 1100 and 1150 psia was predicted for an oil having a composition of 50 mole % hexane and 50% decane. It is realized that a possibility exists for the formation of a second liquid phase at this relatively low temperature. However, it was assumed that the effect of a second phase, if it existed, would be negligible on the measurement of miscibility pressure in the slim tube.

A plot of recovery versus pressure is given in Figure 3-5. A miscibility pressure between 1120 and 1150 psia was determined for the data, in excellent agreement with the prediction from the ternary diagrams.

3.4.2 Butane-Decane System

This system was investigated by Metcalfe and Yarborough²⁶ by conducting CO₂ displacements in Berea cores. They determined from phase behavior studies that, at a temperature of 160°F, an oil phase consisting of 40 mole % butane and 60 mole % decane should be first-contact miscible at 1900 psia, multiple-contact miscible at 1700 psia and not miscible at 1500 psi.

In the present work, slim-tube displacements of this same system

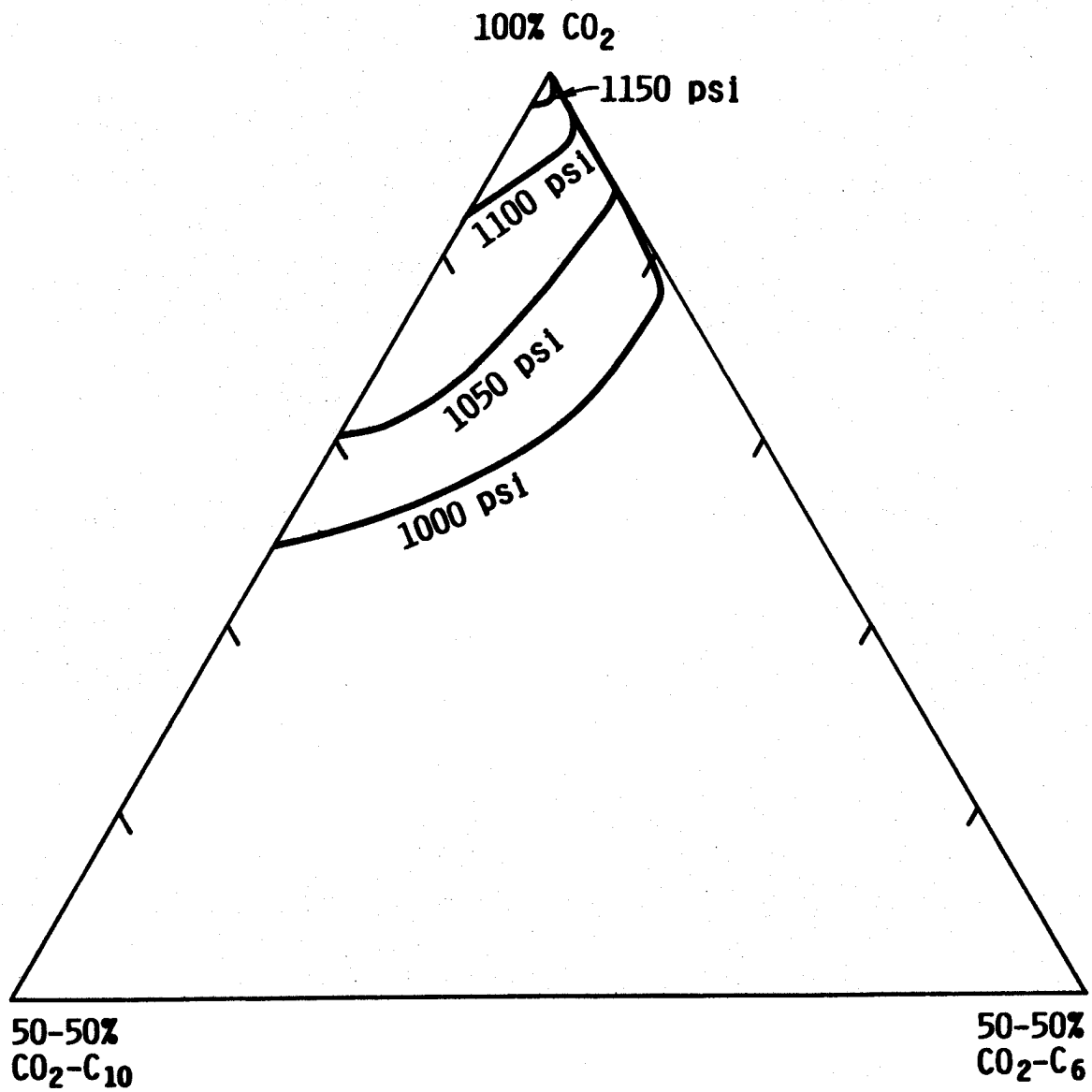


FIGURE 3-4: Phase Envelopes for the $\text{CO}_2 : \text{C}_6 : \text{C}_{10}$ Ternary System at 100°F and Various Pressures.

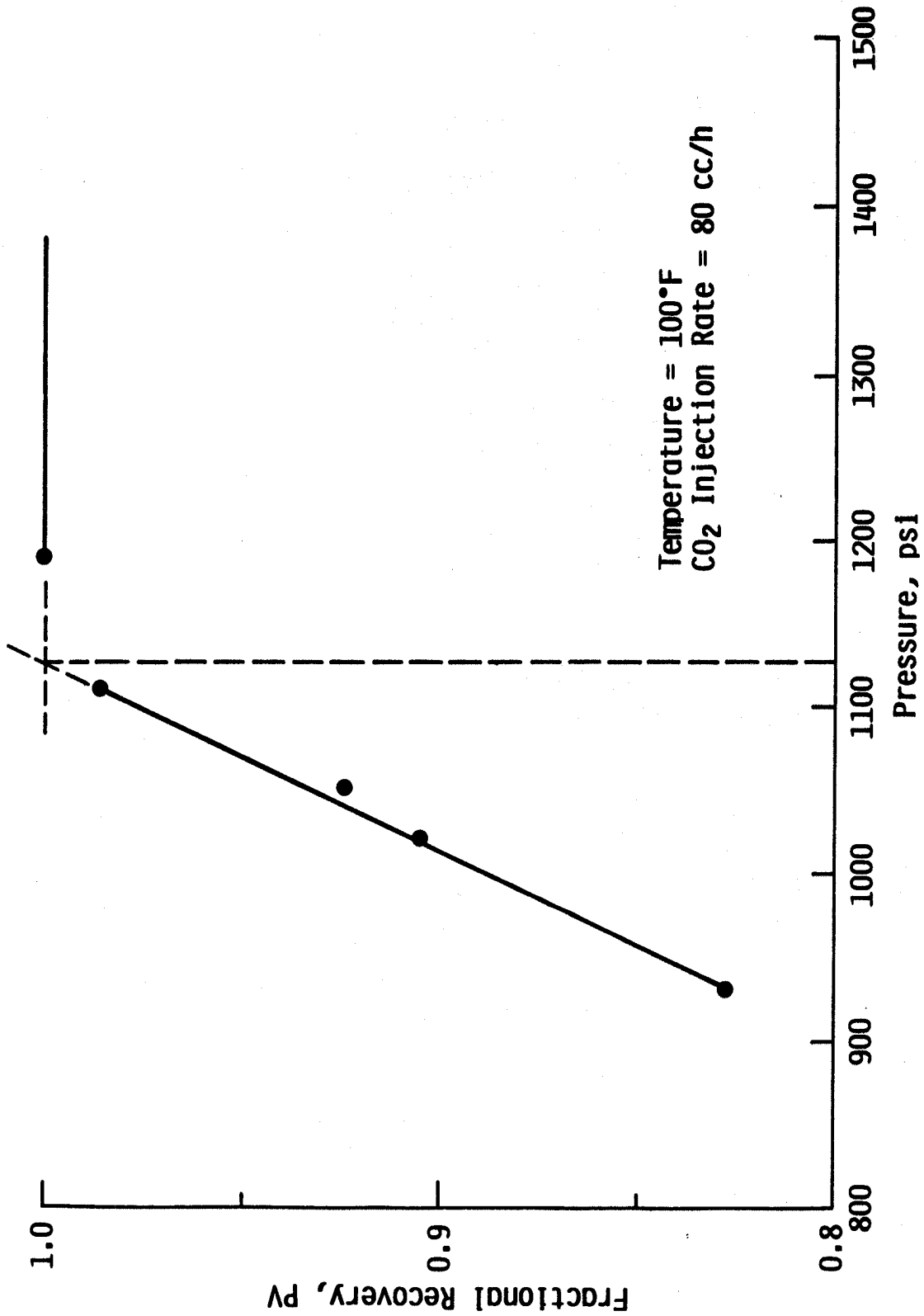


FIGURE 3-5: Slim Tube Results, CO₂ : n-Hexane : n-Decane Ternary System
(Hydrocarbon is 50% Hexane, 50% Decane).

were conducted at a temperature of 160°F and pressures of 1400, 1550 and 1900 psia. The results are compared to those of Metcalfe and Yarborough in Figure 3-6. The results from the study are breakthrough recoveries, i.e., recoveries to the point of CO₂ gas-phase breakthrough. An additional 2 to 3 recovery percent was generally produced after CO₂ breakthrough, but there was some experimental uncertainty in this value and thus the breakthrough recoveries are plotted. Considering that the displacements were conducted in different systems (Berea cores versus slim tube), the results are in reasonable agreement. The high recoveries in the slim tube at the lower pressure (<1700 psia) are intuitively consistent since the slim tube is a more permeable, homogeneous media than Berea sandstone. From the limited data, it is not feasible to estimate the minimum miscibility pressure.

A second butane-decane system was tested in which the temperature was again 160°F, but the hydrocarbon composition was 82 mole % butane and 18 mole % decane. A plot of breakthrough recovery versus displacement pressure is presented in Figure 3-7. As expected, recoveries at corresponding pressures are higher for this hydrocarbon system than for the 60% decane-40% butane system. Based on the change in slope of the recovery curve, the miscibility pressure is estimated to be on the order of 1400 to 1450 psia.

3.4.3 Butane-n-Butylbenzene System

Displacement experiments were made on a system in which the original hydrocarbon phase (oil) was 82 mole % butane and 18% butylbenzene. The composition of the oil was the same as previously run, but the paraffin n-decane was replaced by the aromatic n-butylbenzene. Breakthrough recovery is shown as a function of pressure in Figure 3-8. A miscibility pressure of about 1300 psia is obtained based on the slope change as compared to 1400 to 1450 psia for the butane-decane system.

3.5 Results of Displacements in the Presence of an Immobile Water Phase.

A series of slim-tube displacements was conducted to determine the effect of the presence of an immobile water phase on miscibility pressure. For these runs, a 50:50 (mole %) mixture of hexane and decane was used as the oil. The slim tube was first saturated with fresh water, and the water was then displaced with the oil. Residual water saturation was about 21 percent.

Results from several displacements at different pressures are shown in Figure 3-9 where ultimate recoveries are plotted versus displacement pressure. Also, shown on the plot are results for the same hydrocarbon system in the absence of water. These latter data points are the same as those given in Figure 3-5. As seen, the immobile water phase had negligible effect on fractional recovery, therefore, the miscibility pressure in the presence of water was the same as that previously obtained without water. This is consistent with results discussed in Chapter 2. Ezekwe¹² has shown that the role of water basically is to

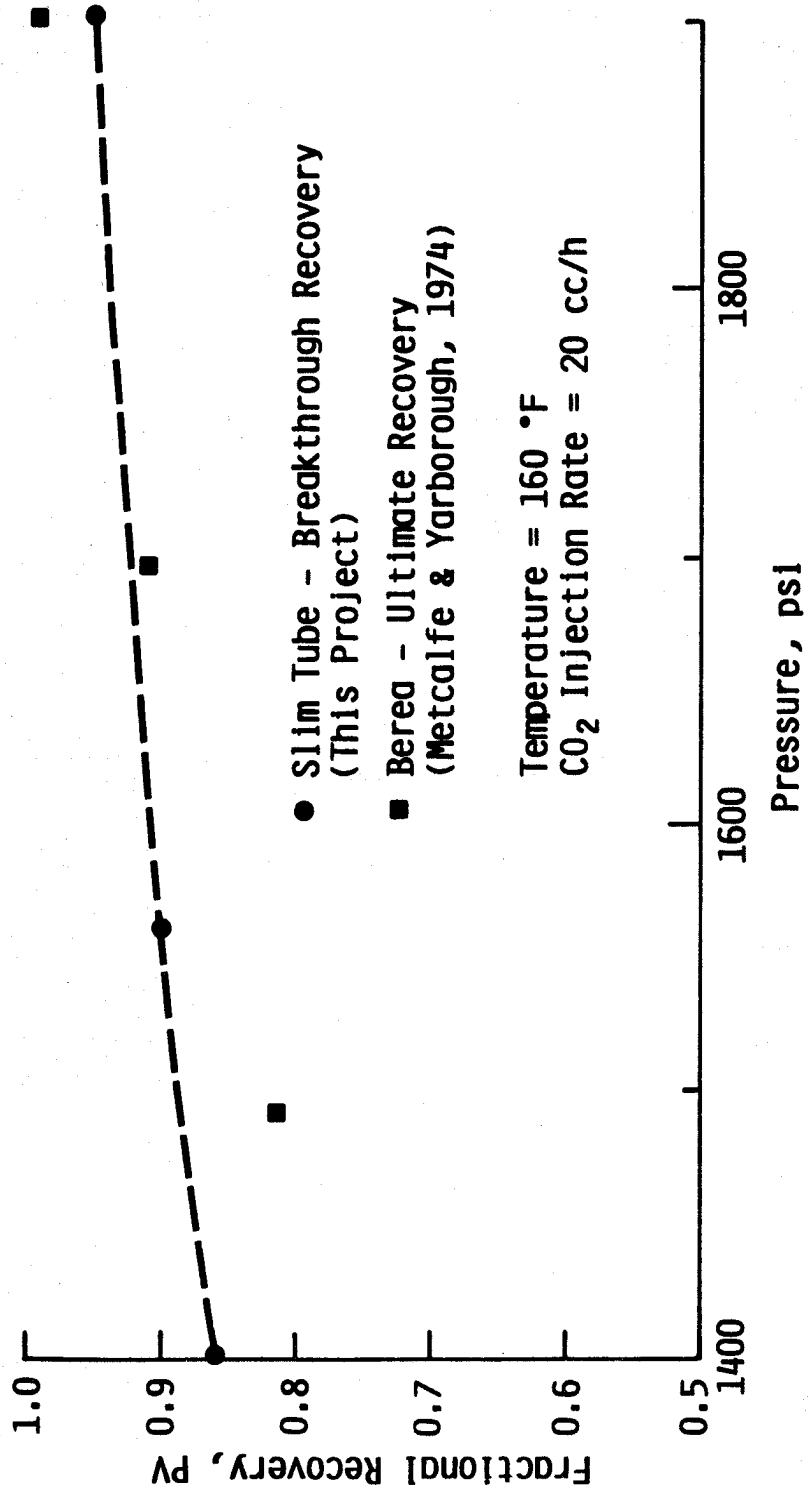


FIGURE 3-6: Slim Tube Results, CO₂ : n-Butane : n-Decane Ternary System
 (Hydrocarbon is 40% Butane, 60% Decane).

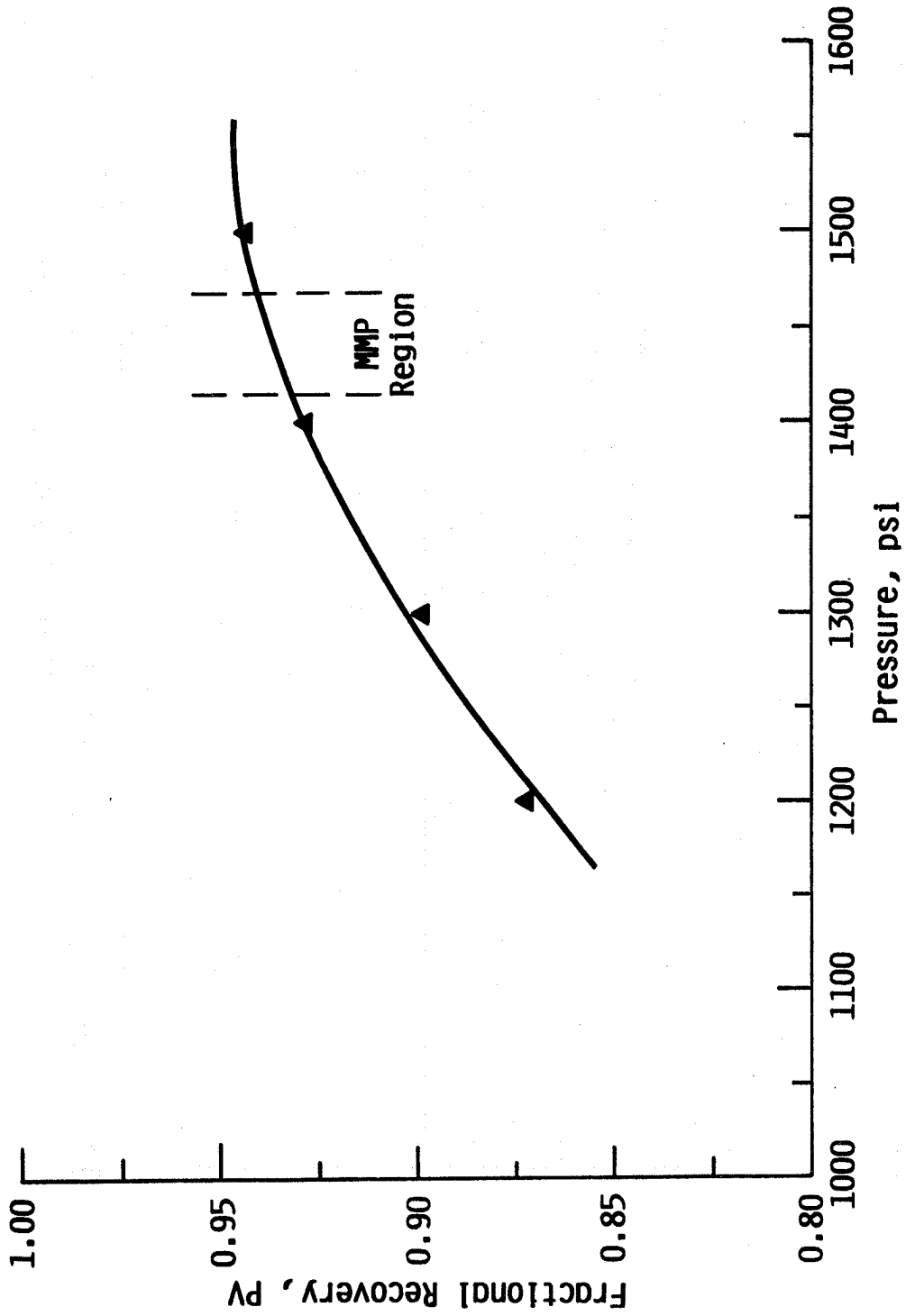


FIGURE 3-7: Slim Tube Results, CO₂ : n-Butane : n-Decane Ternary System
(Hydrocarbon is 82% Butane, 18% Decane).

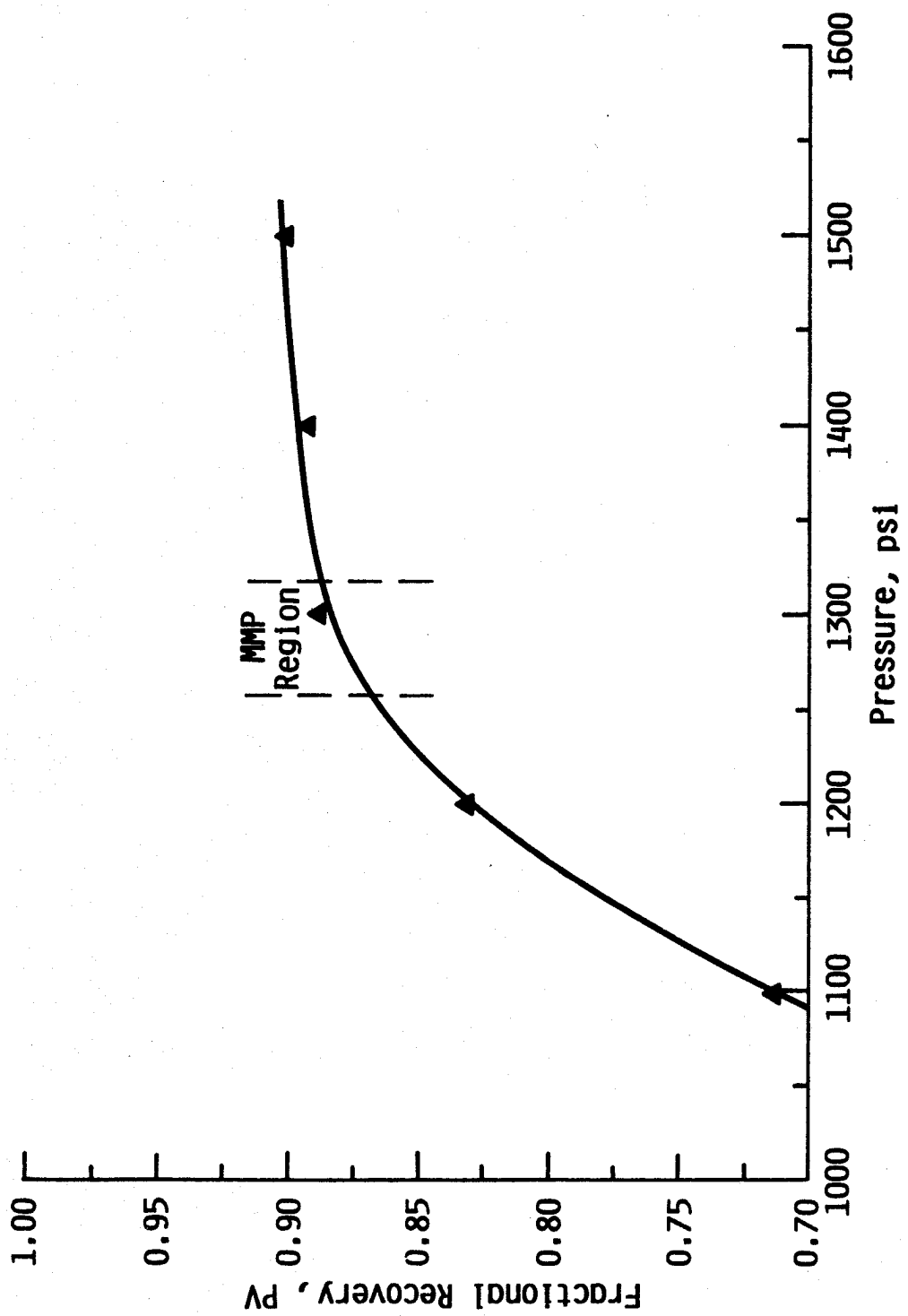


FIGURE 3-8: Slim Tube Results, CO₂ : n-Butane : n-Butylbenzene Ternary System (Hydrocarbon is 82% Butane, 18% Butylbenzene).

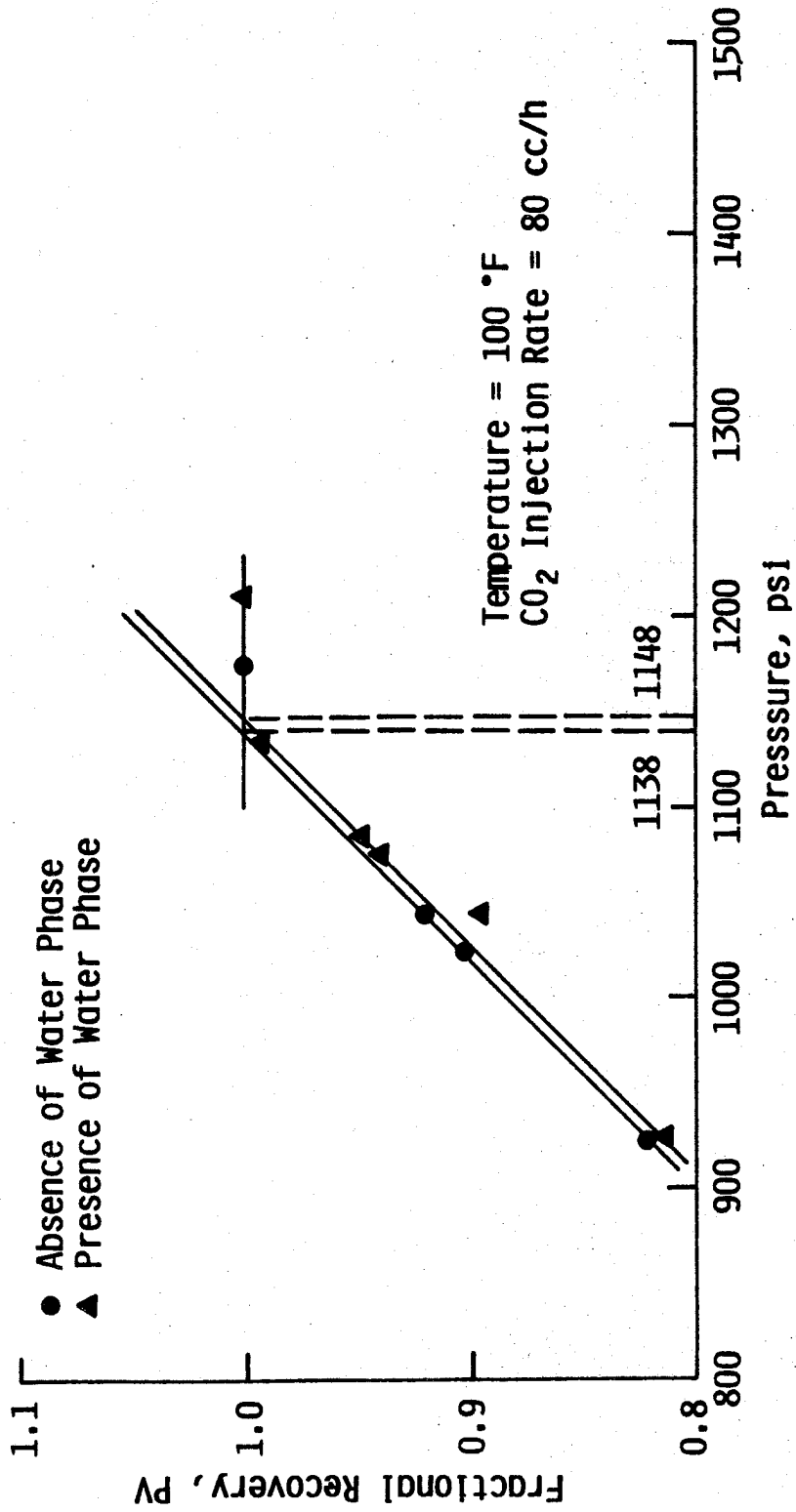


FIGURE 3-9: Effect of Immobile Water on Slim Tube Results (Hydrocarbon is 50% Hexane, 50% Decane).

remove CO₂ from the system and, once this is accounted for, the CO₂-hydrocarbon phase behavior is essentially unchanged.

During the slim-tube experiments, oil recovery was monitored as a function of the amount of CO₂ injected. These recovery curves were affected by the presence of water as shown in Figure 3-10. This figure shows recovery versus CO₂ injection for two displacements conducted at the same pressure, one in the presence of water and the other with no water. Recovery is delayed by the presence of water even though ultimate recoveries are essentially equal. The recovery delay is probably due to absorption of CO₂ into the water with corresponding reduction of CO₂ volume.

3.6 Results of Displacements with Carbon Dioxide and Crude Oils

A number of stock-tank crude-oil samples were obtained from reservoirs located in the Central Kansas uplift area of Kansas. The reservoirs are at a depth of about 3000 ft with temperatures on the order of 105° to 110°F. Crude oils tested had API gravities ranging from about 34° to 39° and viscosities (25°C) from 25 cp to 6 cp. Since the samples were stock-tank samples, they were relatively dead oils. However, the reservoirs are producing at very low gas-oil ratios and the samples are probably reasonably representative of the crude oils at reservoir conditions.

Slim-tube experiments to determine miscibility pressures were conducted with a number of the crude oils at the individual reservoir temperatures. Typical results are presented in what follows. Experiments were also conducted with one crude oil at different temperatures. In another set of displacements, the effect of adding small amounts of low molecular-weight hydrocarbons to the crude oil was examined.

3.6.1 Results of Miscibility Pressure Determinations

Results for crude oils from the Johanning and Abernathy leases are shown in Figures 3-11 and 3-12 where ultimate recovery is plotted as a function of displacement pressure. Johanning oil has a gravity of 36.8°API, and the Abernathy oil gravity is 34.6°API. The miscibility pressures were determined to be approximately 1230 psia and 1600 psia respectively.

The results given in Figures 3-11 and 3-12 are typical. Measured miscibility pressures for several crudes are listed in Table 3-1 and additional slim-tube results are given in Appendix B.

3.6.2 Effect of Temperature on Miscibility Pressure

Slim-tube displacements were run at different temperatures for two of the crude oils. Data for one of these, the Johanning lease crude oil are given in Figure 3-13. As expected, miscibility pressure increases with temperature and for this oil the increase is about 20-25 psi per °F increase in temperature.

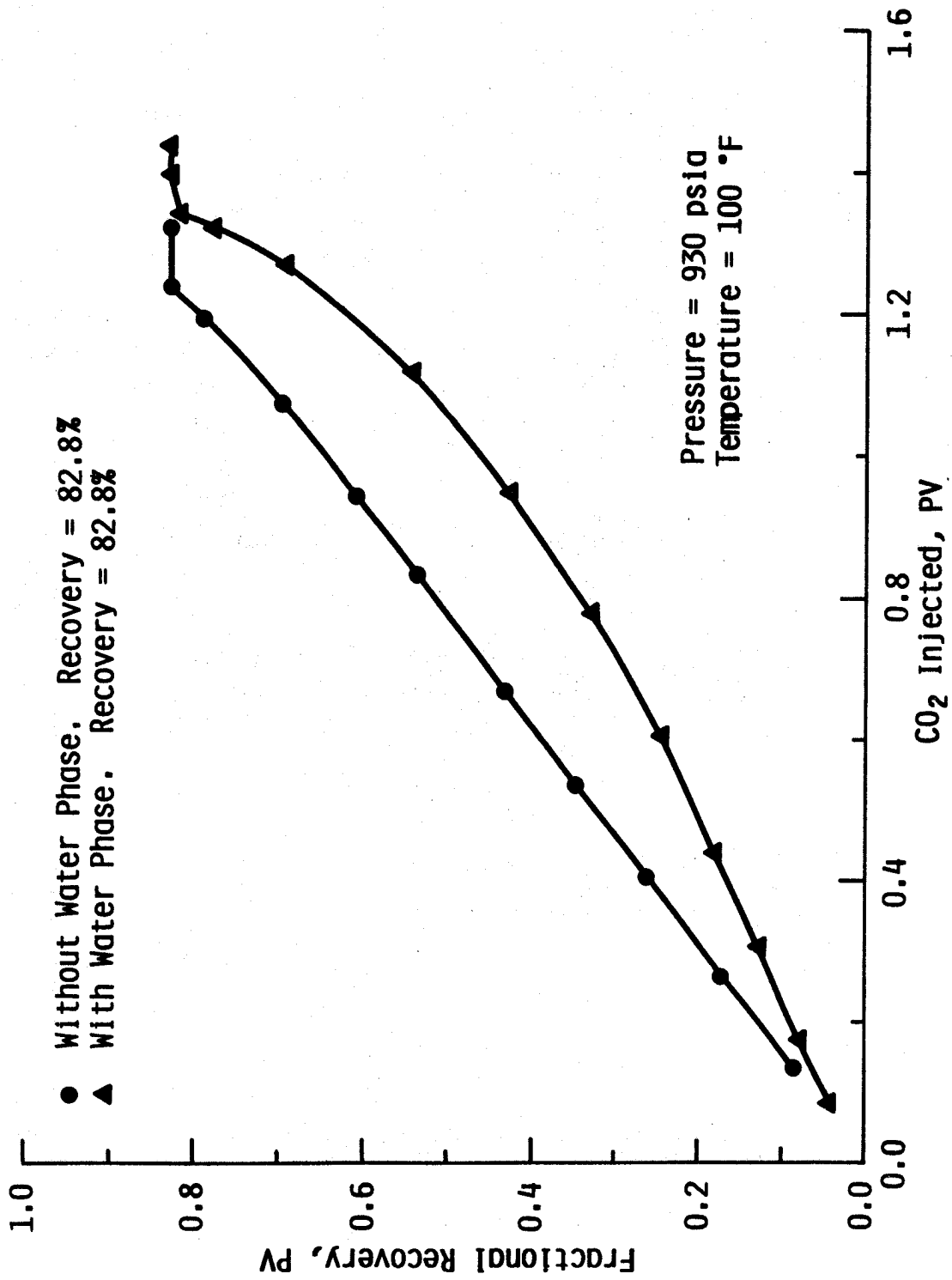


FIGURE 3-10: Slim Tube Recovery Curves, With and Without the Presence of Immobile Water.

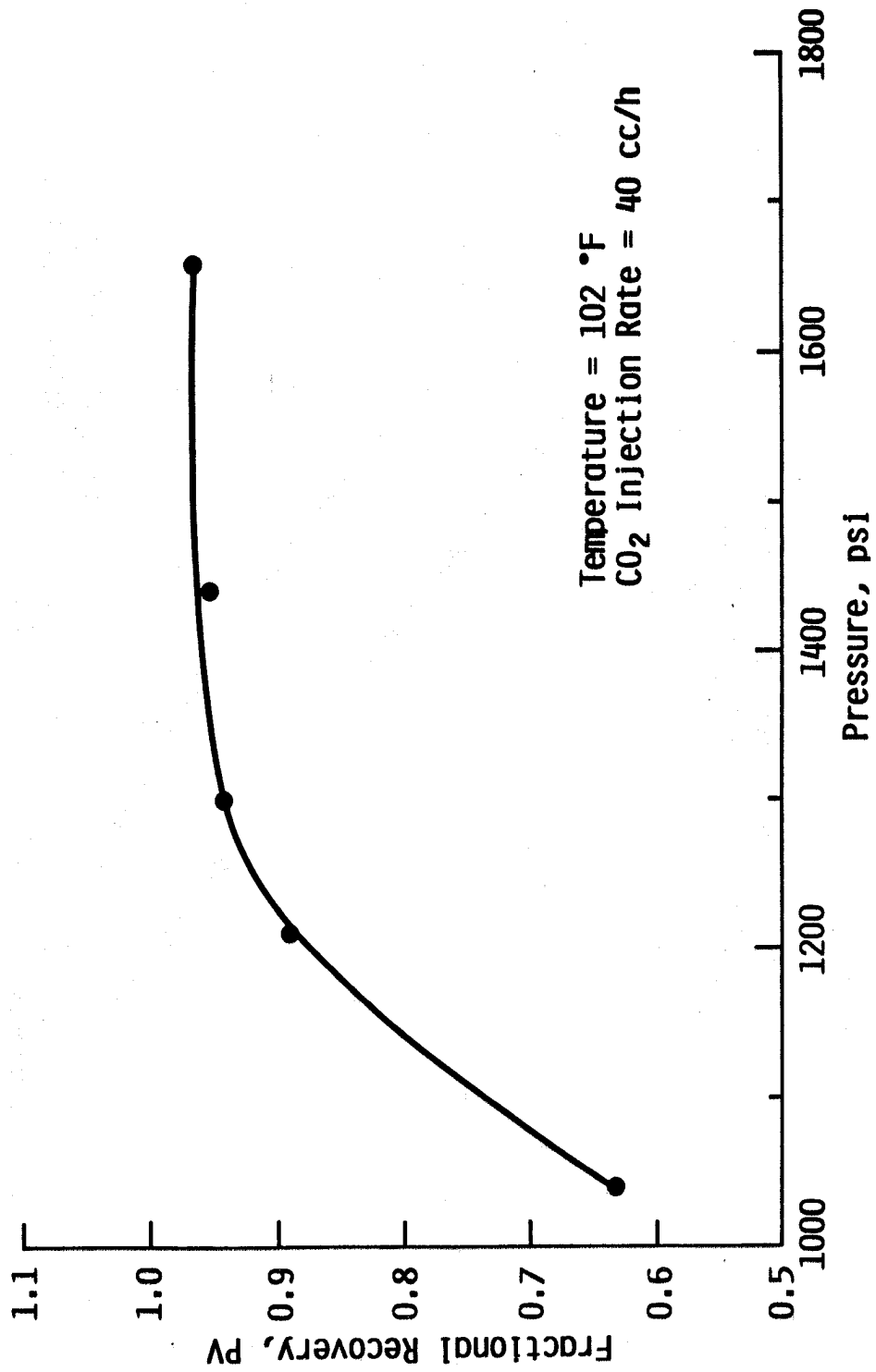


FIGURE 3-11: Slim Tube Results, Johanning Crude Oil.

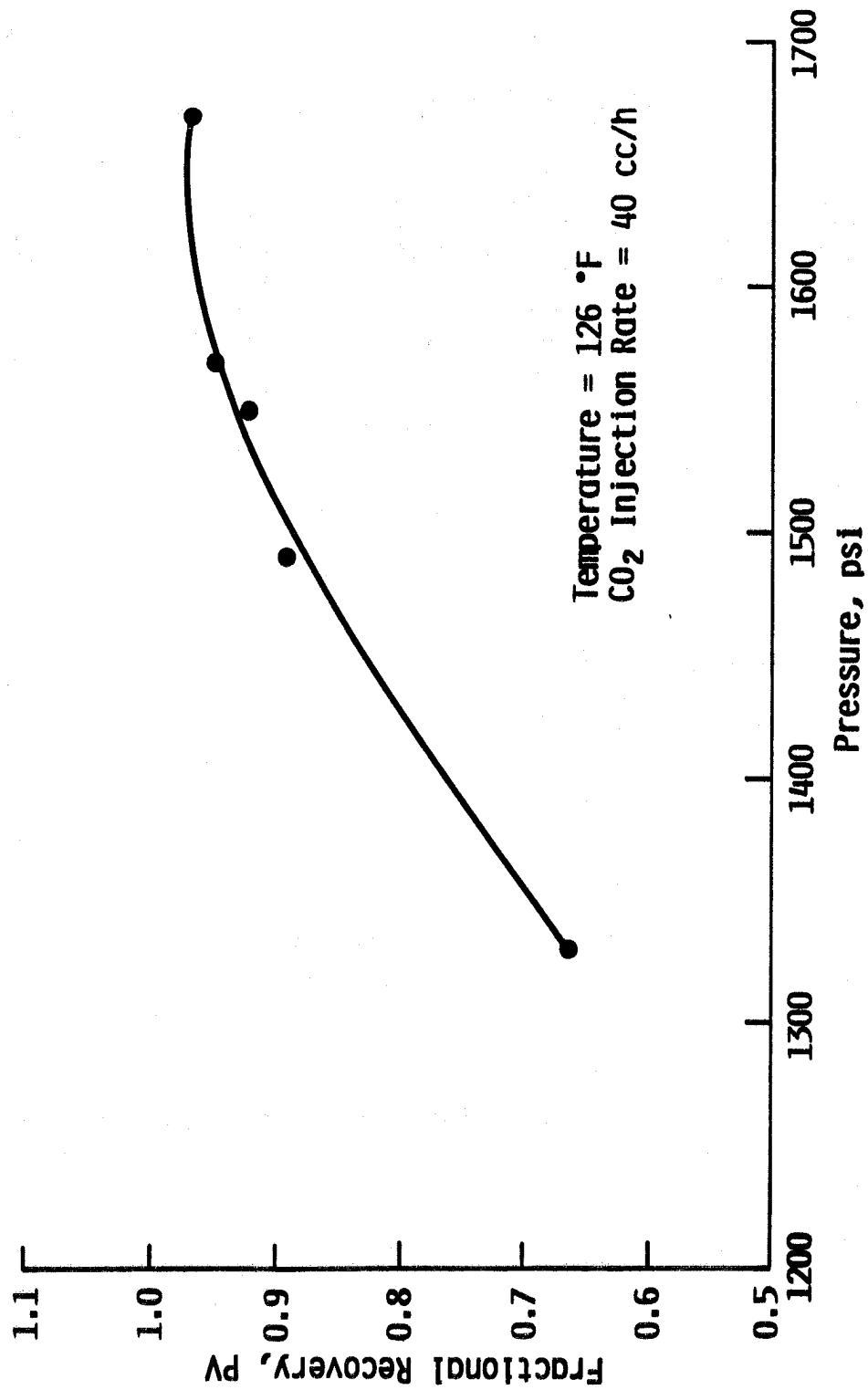


FIGURE 3-12: Slim Tube Results, Abernathy Crude Oil.

Table 3-1

Measured Miscibility Pressures
Crude Oils - State of Kansas

Lease/Well Name	Formation	°API	Temperature °F	Minimum Miscibility Pressure
Johanning B#1	Lansing-KC	36.8	102	1230
Abernathy #1	Marmaton	34.6	126	1600
Seevers #4-2	Lansing-KC	30.1	105	above 2400
Newcombe A#2	Lansing-KC	27.5	105	above 2600
Olson B#4	Lansing-KC	37.8	105	1230
Albertson	Lansing-KC	37.0	110	1260
Olson B#6	Gorham Sand	34.5	105	1500
Newcome #4	Tarkio	36.1	105	1250
Olive Waterflood	Lansing-KC	39.5	105	1160
#1 Dieter*	Maquokata	35.1	105	above 2200
#1 Lofgren*	Maquokata	37.5	105	1260
Bishop #2*	MMSP	34.4	105	above 2200

* Salina Basin

Other samples from Central Kansas Uplift

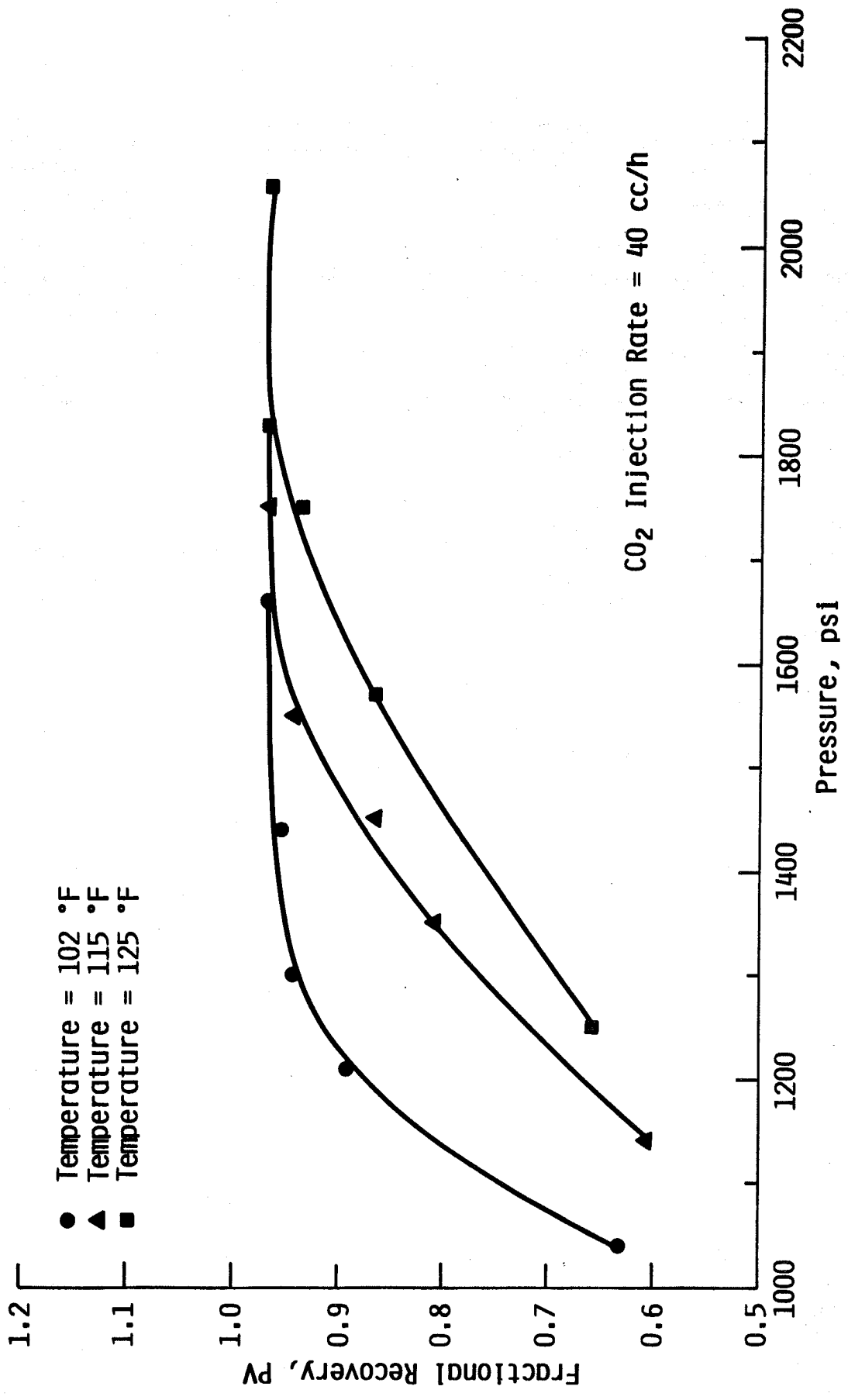


FIGURE 3-13: Effect of Temperature on Slim Tube Miscibility Pressure, Johanning Crude Oil.

3.6.3 Effect of Addition of Light Hydrocarbons to Crude Oil on Miscibility Pressure

Two sets of slim-tube experiments were made in which low molecular weight hydrocarbons were added to the crude oil. The Abernathy lease crude previously discussed (Figure 3-12) was modified in composition by the addition of 10 volume percent hexane. The result was to reduce significantly the miscibility pressure, as presented in Figure 3-14. The miscibility pressure decreased by approximately 200 psi. A similar result was obtained by saturating the Olson lease crude with butane. This is shown in Figure 3-15. The trends in the data are consistent with miscibility pressure correlations which have been presented in the literature (Holm and Josendal¹⁷).

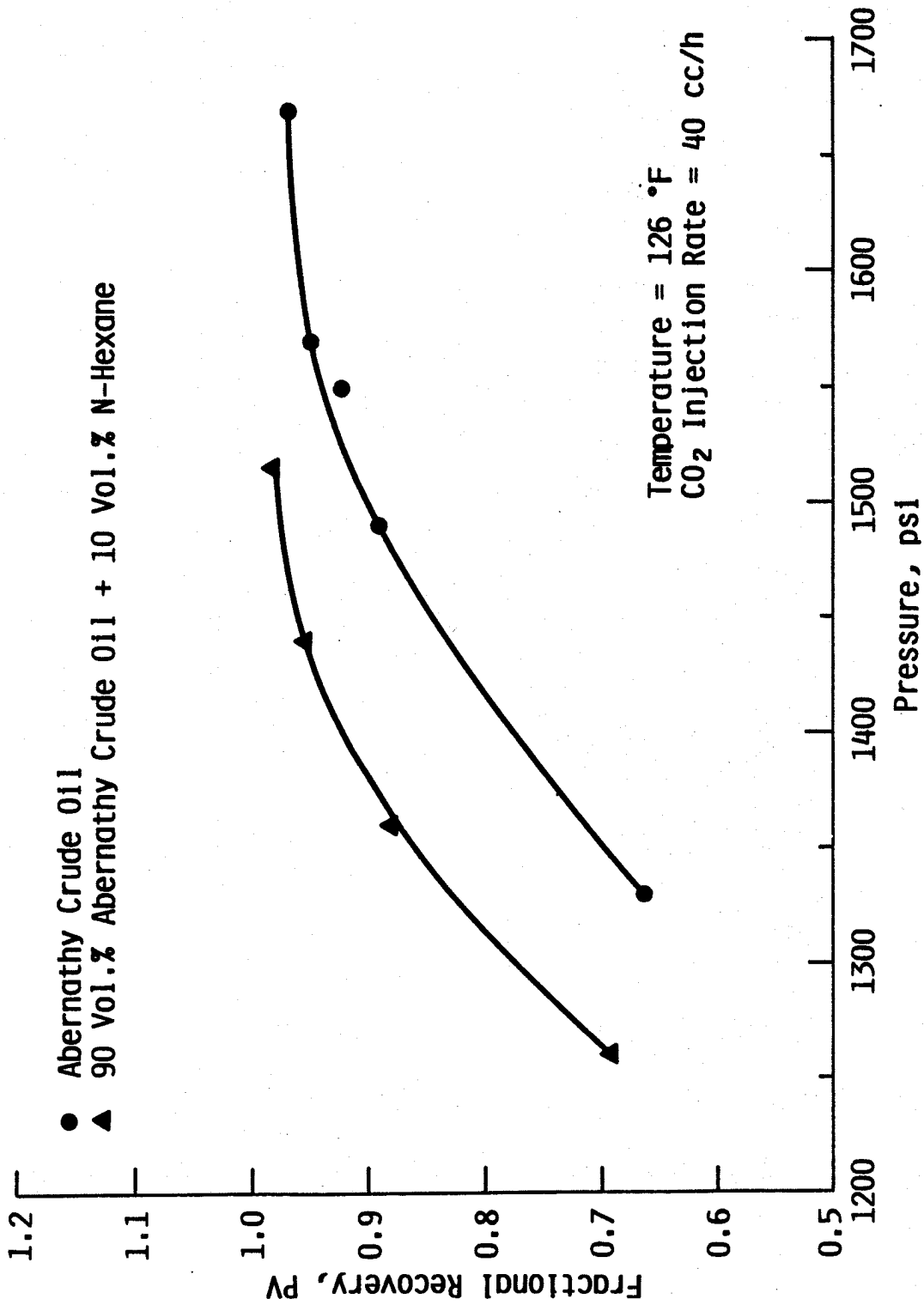


FIGURE 3-14: Effect of Hydrocarbon Composition on Slim Tube Miscibility Pressure (Hexane Added to Crude Oil).

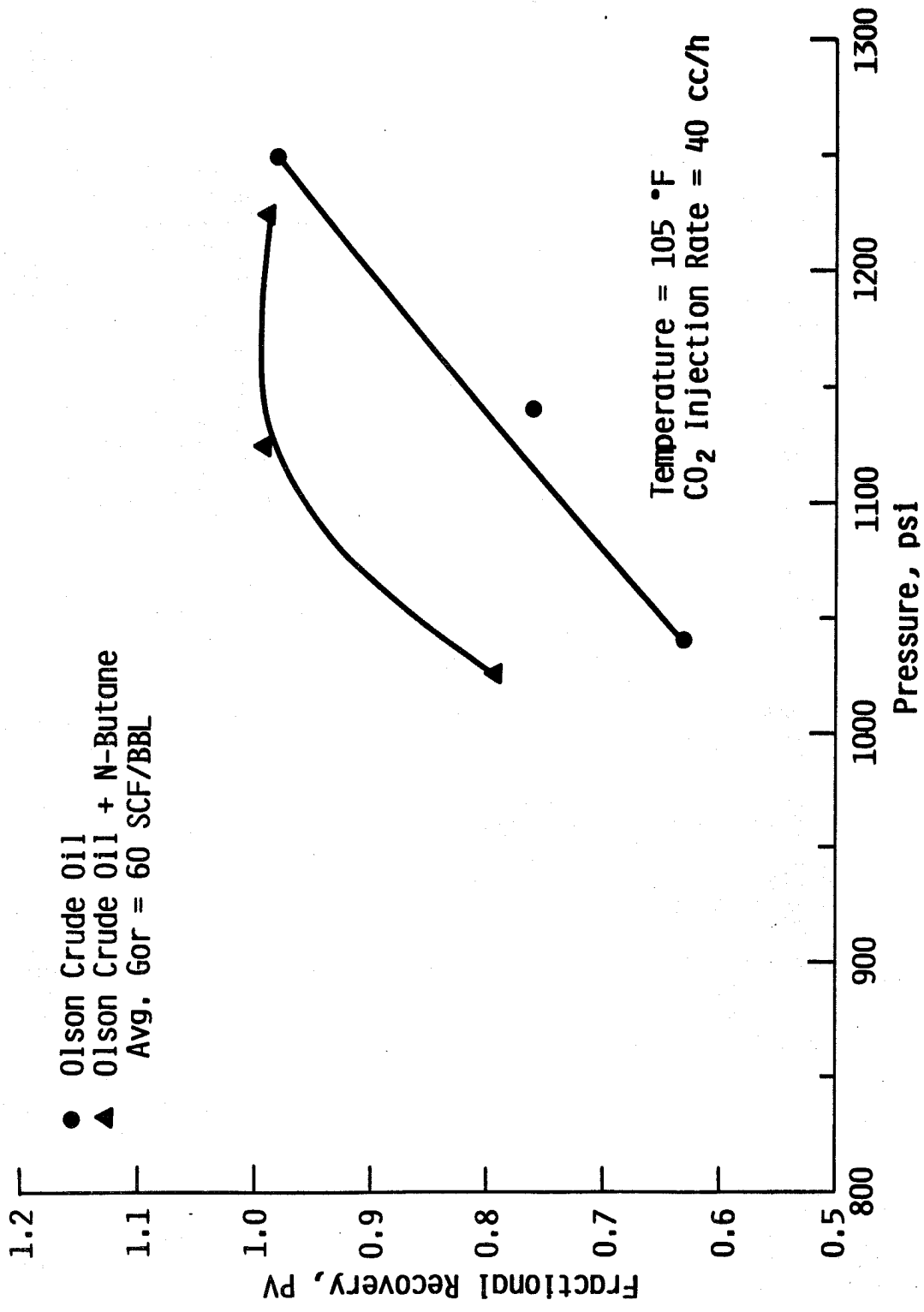


FIGURE 3-15: Effect of Hydrocarbon Composition on Slim Tube Miscibility Pressure (Butane Added to Crude Oil).

CHAPTER 4

APPLICATION OF PSEUDO-TERNARY DIAGRAMS FOR THE PREDICTION OF DISPLACEMENT PERFORMANCE

4.1 Introduction

Ternary and pseudo-ternary diagrams have been used for the purpose of illustrating conceptually the manner in which dynamic miscibility is achieved in a displacement process. For a true ternary system, such as CO₂-butane-decane, phase behavior is described rigorously on a ternary diagram. For a given "oil", consisting of specified mole fractions of butane and decane, the miscibility pressure can be determined from calculated ternary diagrams.

Since crude oils are composed of numerous hydrocarbons, the application of ternary diagrams for phase-behavior description is not rigorous and can be viewed at best as an empirical or semi-empirical approach. Even so, this approach has found utility for phase-behavior calculations (Orr, et al.²⁹) for systems other than true ternary systems.

For the work reported in this chapter, the approach taken was to apply pseudo-ternary diagrams for the purpose of predicting dynamic miscible displacement performance of CO₂-crude oil systems. The steps involved in the calculational procedure were the following:

- a) Characterize the crude oil using ASTM D-86 or true-boiling-point distillation.
- b) Apply empirical correlations to the distillation data to obtain a distribution of pseudo-hydrocarbon components.
- c) Apply empirical correlations to the pseudo-hydrocarbon components to calculate physical properties.
- d) Use the SRK equation of state with the designated components and physical properties to calculate phase behavior. This requires estimation of the interaction coefficients for the SRK equation of state.
- e) Lump the hydrocarbon components together in a specified manner to form two pseudo components. Use these pseudo components as the basis for display of the phase behavior on ternary diagrams at fixed temperatures and pressures.
- f) Use the pseudo-ternary diagrams to determine minimum miscibility pressure (MMP) at fixed oil composition, or maximum miscibility composition (MMC) of fixed pressure.
- g) As a supplement to step (f), apply the pseudo-ternary diagrams in conjunction with the mathematical simulation described in

Chapter 5 to predict displacement performance.

In what follows in this chapter, the utility of ternary diagrams is illustrated by application to two true ternary systems for which phase behavior and slim-tube experimental data were taken in this project. The use of pseudo-ternary diagrams for miscibility prediction is then shown for two crude-oil systems described in the literature. For these systems, crude-oil compositions were specified and estimation from distillation curves was not required. Finally, the complete method, based on distillation curves, is applied to three crude oils from the State of Kansas. Results were compared to miscibility pressures determined from the slim-tube apparatus described in Chapter 3.

The approach is shown to be encouraging but not totally successful. Interaction coefficients for the SRK equation of state that are required to predict correctly the miscibility pressure for crude oils are not consistent with those obtained from the phase-behavior study described in Chapter 2. Further, a single set of interaction coefficients could not be found that would correctly predict the miscibility pressure for the five crude oils tested. That is, some adjustment of interaction coefficients for low carbon number hydrocarbons was necessary between the different crude oils in order to correctly predict miscibility pressure as measured in a slim-tube apparatus.

4.2 Application of Ternary Diagrams to Ternary Systems

4.2.1 Experimental Data

Phase-behavior, bubble-point pressure measurements were made on ternary systems consisting of CO₂-n-butane-n-decane, CO₂-n-butane-n-butylcyclohexane and CO₂-n-butane-n-butylbenzene as described in Chapter 2. A temperature of 160°F and a pressure of about 1400 psia were used. The data were used in regression analyses to calculate interaction coefficients from the SRK equation of state (Table 2-5). This equation was used, in turn, to calculate phase behavior for display on ternary diagrams and to calculate minimum miscibility pressure (MMP) or maximum miscibility composition (MMC).

4.2.2 Prediction of Miscibility Conditions

As shown in Table 2-6, the MMC for ternary systems in which the C₁₀ component is n-decane or n-butylbenzene was determined to be about 21-23% (molar) of the C₁₀ component at 160°F and 1400 psia. Calculated ternary diagrams for these two systems at the specified temperature and pressures of 1300 and 1400 psia are shown as Figures 4-1 through 4-4. These were based on the interaction coefficient set of regression 11 in Table 2-5. The MMC values were determined by extrapolation of the limiting tie line, i.e., the tangent to the binodal curve at the critical point. This is done using a routine in the computer program which calculates the ternary diagram (Daub⁹).

The same two ternary systems were used for measurement of miscibility pressures in the slim-tube apparatus. The data from these runs are shown in Figures 3-7 and 3-8. "Oil" composition for both

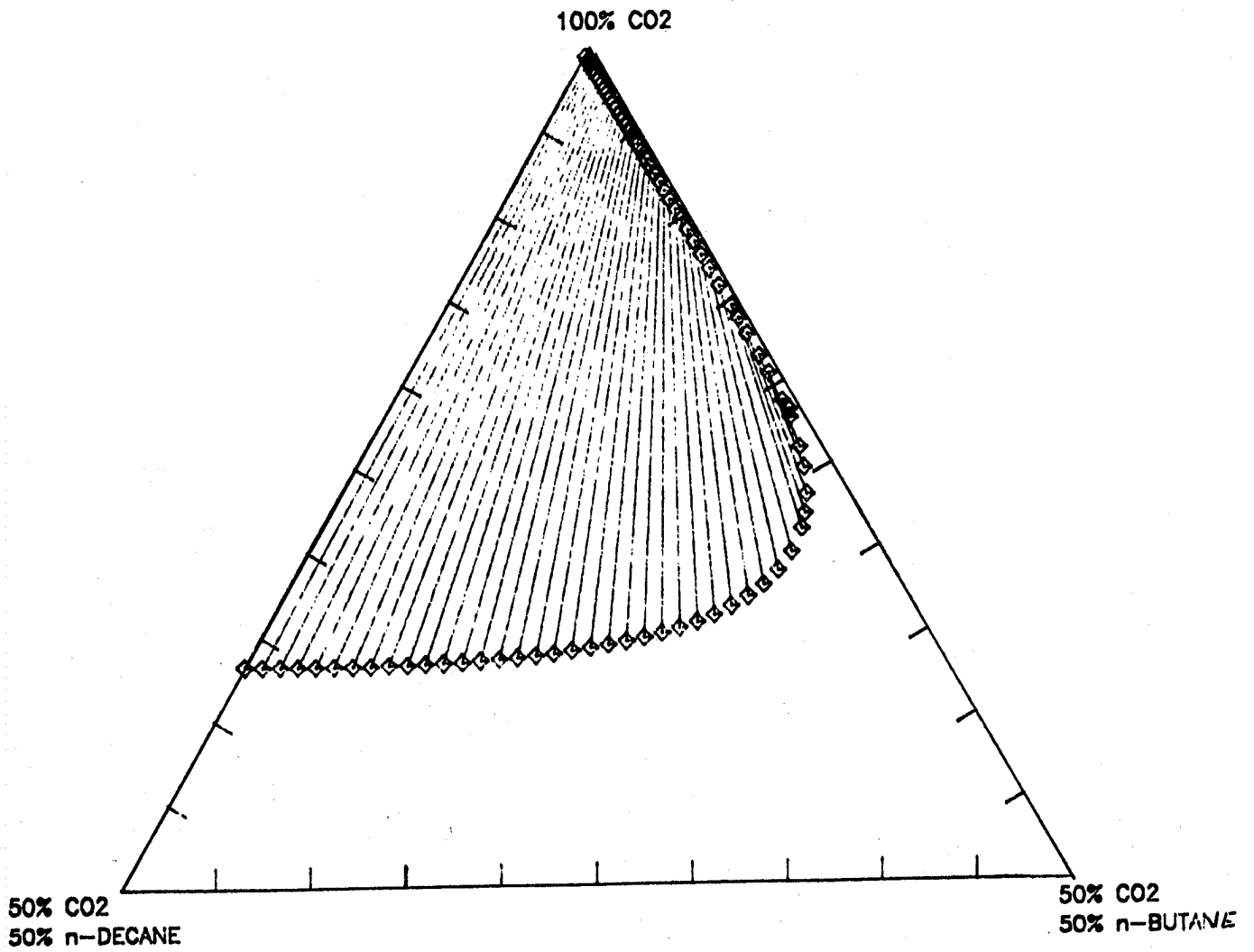


FIGURE 4-1: Calculated Ternary Diagram for CO₂-Butane-Decane (P = 1300 psia, T = 160°F)

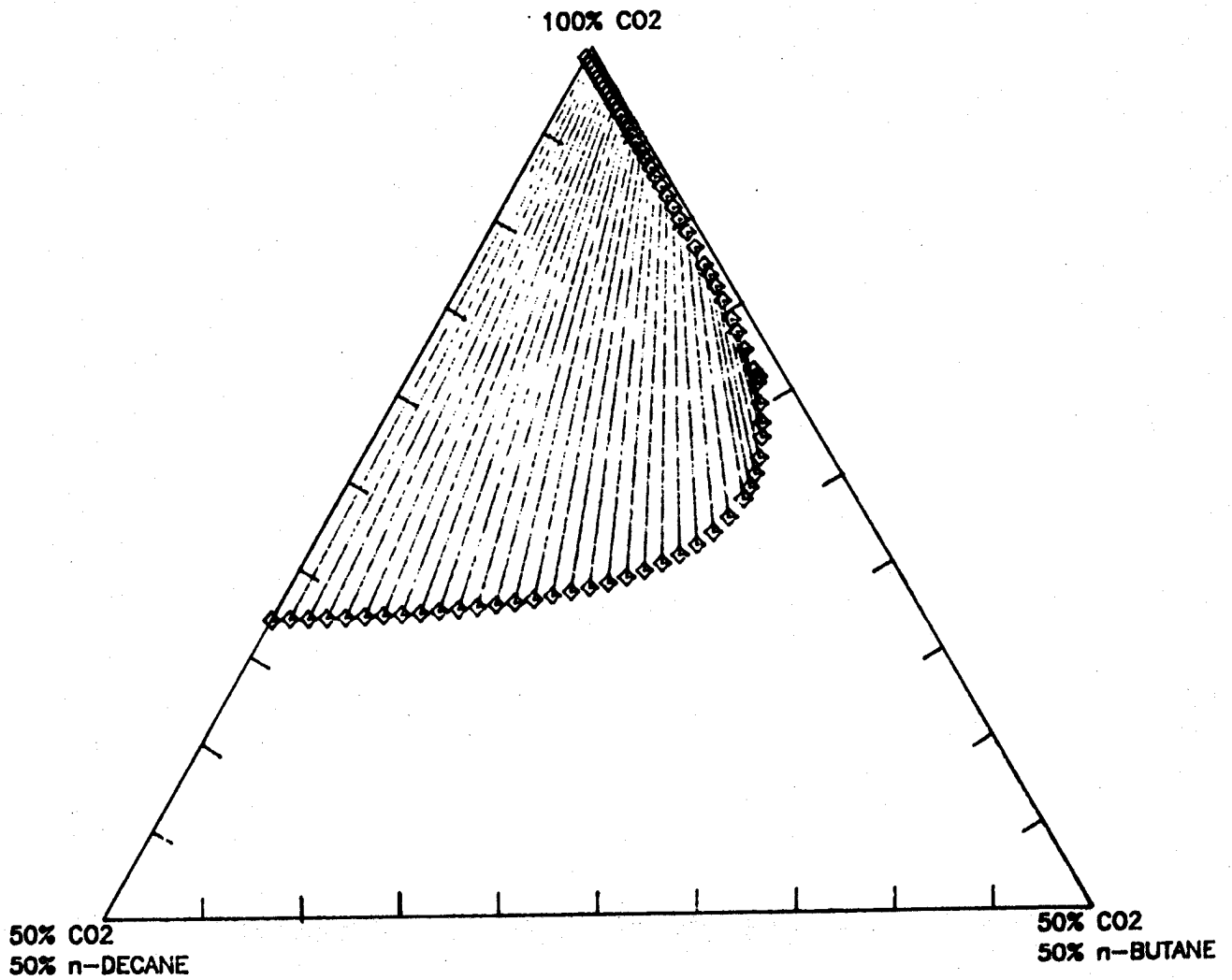


FIGURE 4-2: Calculated Ternary Diagram for CO₂-Butane-Decane
(P = 1400 psia, T = 160°F)

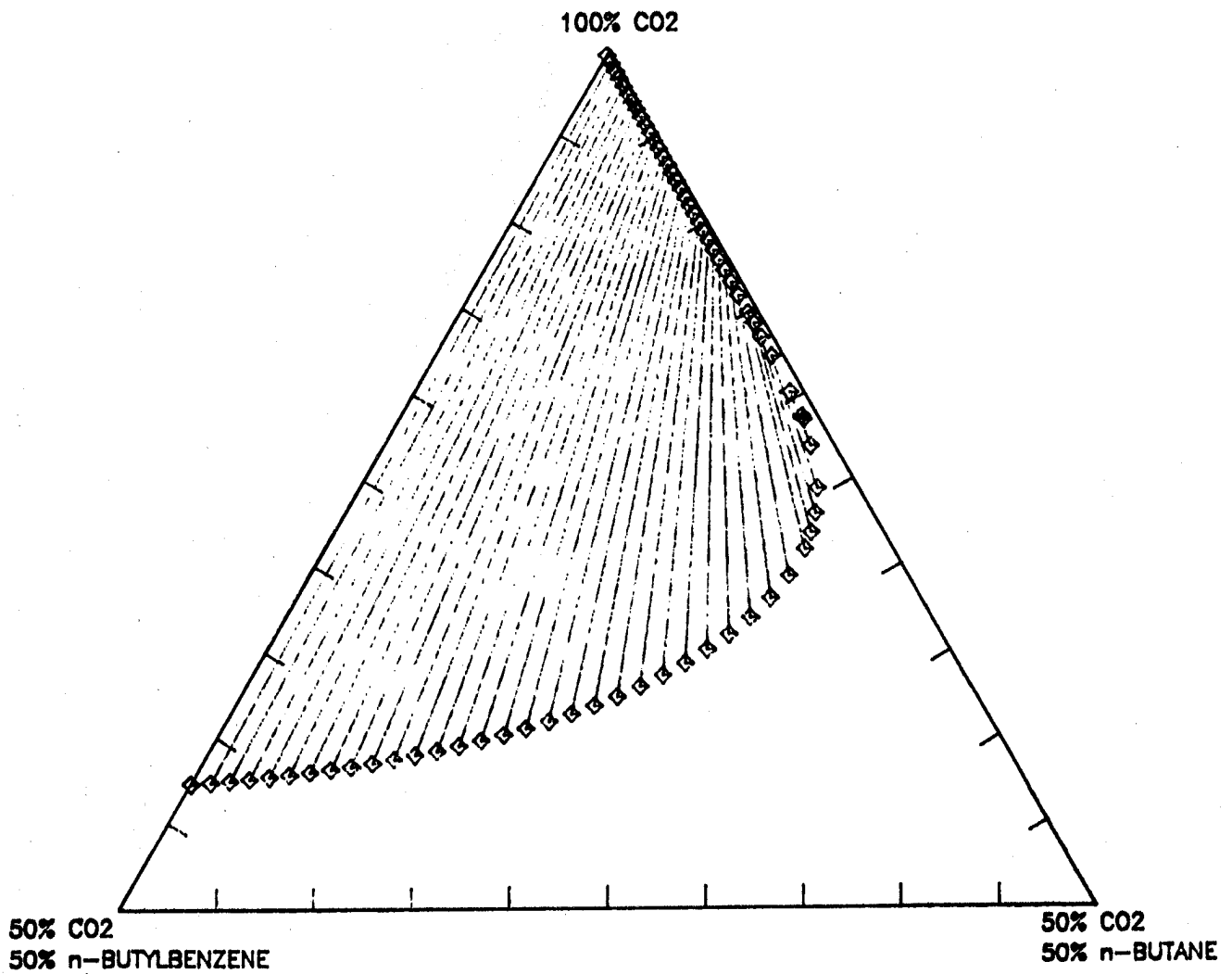


FIGURE 4-3: Calculated Ternary Diagram for CO₂-Butane-Butylbenzene (P = 1300 psia, T = 160°F)

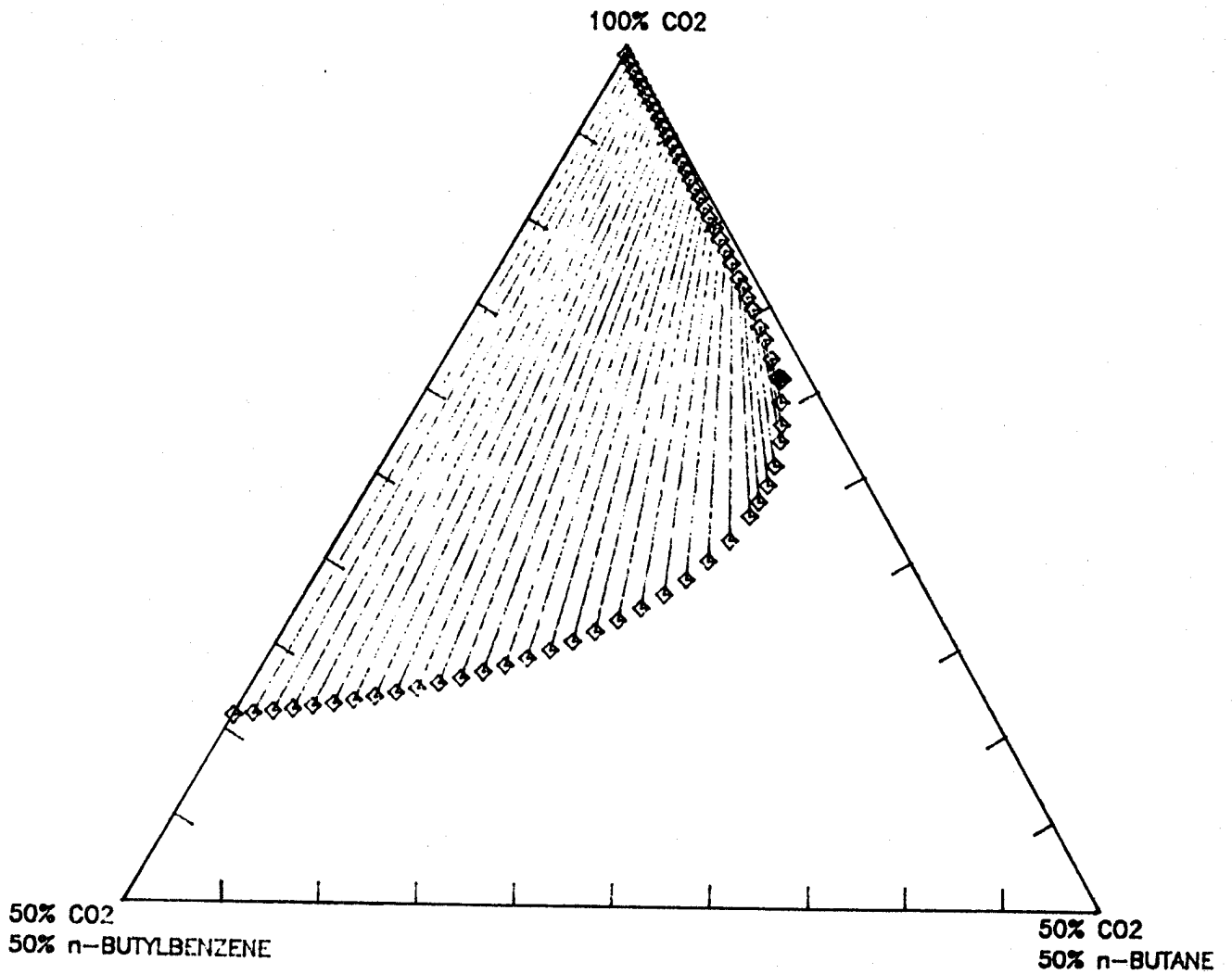


FIGURE 4-4: Calculated Ternary Diagram for CO₂-Butane-Butylbenzene (P = 1400 psia, T = 160°F)

systems was 18 mole percent of the C_{10} component. Fractional recoveries plotted are recoveries at breakthrough of the CO_2 -rich gas phase. The MMP of the n-decane system appears to be approximately 1450 psia while the MMP of the n-butylbenzene system is about 1300 psia.

The agreement between the calculated and measured MMP values for the n-butylbenzene system is quite good. Ternary diagrams for this system at pressures of 1300 psia and 1400 psia are presented as Figures 4-3 and 4-4. From examination of the plots it is seen that the MMP should be between 1300 and 1400 psia. A similar agreement is seen for the n-decane system. Extrapolation of the limiting tie line of Figure 4-2, at 1400 psi, indicates that the MMC (21%) is just slightly higher than the 18 mole percent n-decane and therefore the predicted MMP value is slightly less than 1400 psia. In both cases, predicted MMP values are within 100 psi of those measured with the slim tube.

4.3 Application of Pseudo-Ternary Diagrams to Crude Oil Systems- Literature Data

4.3.1 Literature Data

The literature was searched for crude-oil systems for which both composition data and MMP values were available. Two systems were selected for study. These were the Maljamar stock-tank oil reported by Orr³¹ and the West Texas stock-tank oil described by Yellig and Metcalfe²⁶. For both systems, compositions and MMP values from slim-tube tests were reported. Additionally, the bubble-point pressure curve at reservoir temperature was reported for the Maljamar crude. Since compositions of the oils were reported, steps (i) and (ii) of the calculational procedure outlined in Section 4.1 were omitted.

4.3.2 Characterization of Literature Oils

The compositions of the Maljamar and West Texas stock-tank oils were expressed in mole percent by single carbon number from C_5 - C_{40} . These oils had been analyzed by gas chromatographic distillation. The distillation curves were then converted to single carbon number mole fractions using estimated molecular weights and boiling ranges.

To characterize these oils, C_5 was represented by the properties of n-pentane.³³ Components C_6 - C_{40} were represented by the single carbon number generalized properties of Katz and Firoozabadi,²⁰ subsequently modified by Whitson.⁴² The Watson Characterization Factor, K_w , of the "generalized" oil is approximately 11.9 which is reasonably close to the K_w 's of the literature oils (11.6 - 11.7). Table C-1 (Appendix C) summarizes the Katz-Firoozabadi-Whitson (KFW) properties entered in the phase-behavior calculation. Katz²⁰ provides boiling-point ranges and average boiling point and Whitson⁴² provides the specific gravity and molecular weight.

The Lee-Kesler critical property correlations were selected based on Whitson's⁴² recommendations. The Lee-Kesler equations were utilized to calculate critical temperature, critical pressure and eccentric factor for each single carbon number. These results are given in Table C-2. Additional details are given by Daub⁹.

4.3.3 Application of Phase Behavior Calculations to the Maljamar Crude-Oil

The first system investigated was the Maljamar crude described by Orr, et al.³¹. His single carbon number analysis is listed in Table 4.1. Approximate weight and volume fractions were determined based on the KFW properties. The C₃₇₊ fraction was assigned the properties of C₄₀. The calculated molecular weight of 178.1 is somewhat lower than the experimental value of 183.7. Either the KFW C₄₀ molecular weight is too low or the C₃₇₊ fraction should be assigned a higher carbon number, for example C₄₅. This minor discrepancy was deemed insignificant. The Watson Characterization Factor was estimated at 11.6 based on molecular weight and specific gravity.

Slim-tube recovery data were also available on this system at 90°F and four pressures ranging from 800-1400 psia.³⁰ By defining the MMP as the intersection of the immiscible and miscible recovery slopes, the experimental MMP was estimated to be 1050 psia at 90°F.

Additionally, Orr, et al.³⁰ provided an experimental bubble-point pressure curve at 90°F. Grabowski and Daubert^{14,15} recommended that interaction coefficients for the equation of state be regressed from bubble-point pressure data. Therefore, it seemed reasonable to test the utility of the correlations of Ezekwe¹² and Grabowski and Daubert^{14,15} using the bubble-point pressure data. The correlation of Ezekwe was discussed in Chapter 2. Interaction coefficients from the correlations were extrapolated for carbon numbers C₁₀ to C₂₅. Also C₂₅⁺ components were assigned to C₂₅.

Interaction coefficients predicted with the correlations are shown in Table 4-2 along with solubility parameters. Figure 4.5 shows the calculated bubble-point pressure results with the two correlations compared to the experimental curve. At low CO₂ concentrations, the Grabowski and Daubert correlation^{14,15} provides acceptable results. However, above 40 mole percent CO₂ this correlation consistently underpredicts the CO₂ solubility. Conversely, the Ezekwe correlation¹² consistently overpredicts CO₂ solubility over the entire concentration range. Seemingly, neither correlation is entirely acceptable.

Since neither correlation produced acceptable results, the next step was to estimate a set of interaction coefficients in an attempt to develop a better fit to the experimental bubble-point pressure curve. Initially, the interaction coefficients were assumed to be constant for all carbon numbers. As seen in Figure 4.6, use of a constant interaction parameter of 0.120 bounds the experimental curve on the left. Likewise, a value of 0.100 bounds the experimental curve on the right while a constant value of 0.108 does a good job of matching the bubble-point pressure curve in the region of developing miscibility.

As a second guess, it was assumed that interaction coefficients increase with carbon number. For simplicity, the interaction coefficients were assigned to single carbon numbers in a linear manner. The C₂₅ value was set at 0.130. The C₅ value was then assigned for example, at .070. The other carbon numbers were set at values in between these limits using linear interpolation. The set of interaction coefficients

TABLE 4.1 - Reported Composition of Maljamar Crude Oil³¹

SCN	M/F	CUM.M/F	W/F	CUM.W/F	V/F	CUM.V/F	WT	VOL
5	.0390	.0390	.016	.016	.021	.021	2.82	4.46
6	.0937	.1327	.044	.060	.053	.074	7.87	11.41
7	.1027	.2354	.055	.115	.063	.174	9.86	13.56
8	.1354	.3708	.081	.196	.089	.226	14.49	19.34
9	.1191	.4899	.081	.277	.087	.313	14.41	18.76
10	.0750	.5649	.056	.333	.059	.372	10.05	12.85
11	.0559	.6208	.046	.380	.048	.420	8.22	10.36
12	.0432	.6640	.039	.419	.040	.460	6.96	8.65
13	.0393	.7033	.039	.457	.039	.499	6.88	8.44
14	.0329	.7362	.035	.492	.035	.534	6.25	7.57
15	.0273	.7635	.032	.524	.031	.565	5.62	6.73
16	.0226	.7861	.028	.552	.028	.593	5.02	5.95
17	.0223	.8084	.030	.582	.029	.622	5.29	6.21
18	.0134	.8218	.019	.601	.018	.640	3.36	3.93
19	.0107	.8325	.016	.617	.015	.655	2.81	3.27
20	.0136	.8461	.021	.638	.020	.675	3.74	4.32
21	.0110	.8571	.018	.656	.017	.692	3:20	3.68
22	.0077	.8648	.013	.669	.012	.704	2.31	2.64
23	.0096	.8744	.017	.686	.016	.720	3.00	3.40
24	.00988	.8832	.016	.702	.015	.735	2.85	3.22
25	.0068	.8900	.013	.715	.012	.747	2.29	2.58
26	.0038	.8938	.007	.722	.007	.754	1.33	1.49
27	.0059	.8997	.0121	.734	.011	.765	2.12	2.37
28	.0038	.9035	.008	.742	.007	.772	1.41	1.57
29	.0040	.9075	.009	.751	.008	.780	1.53	1.69
30	.0040	.9115	.009	.760	.008	.788	1.58	1.75
31	.0040	.9155	.009	.769	.008	.796	1.62	1.78
32	.0040	.9195	.009	.778	.008	.804	1.66	1.82
33	.0013	.9208	.003	.781	.003	.807	0.55	0.61
34	.0014	.9222	.003	.784	.003	.810	0.61	0.67
35	.0014	.9236	.004	.788	.003	.813	0.62	0.68
36	.0014	.9250	.004	.792	.003	.816	0./64	0.69
37 ⁺	.0750	1.0000	.208	1.000	.184	1.000	37.13	39.88
							178.1	216.3

MW = 183.7 SG = .835 K_w = 11.6

SCN = Single Carbon number
M/F = Mole fraction
W/F = Weight fraction
V/F = Volume fraction
VOL = Volume

MW = Molecular Weight
SG = Specific Gravity
K_w = Watson Characterization Factor

TABLE 4.2 - Predicted Interaction Coefficients

<u>SCN</u>	<u>δ H/C*</u>	<u>K_{ij}(G & D)</u>	<u>K_{ij}(JE)</u>
5	7.02	.132	.130
6	7.52	.138	.124
7	7.68	.139	.120
8	7.78	.139	.116
9	7.85	.139	.113
10	7.92	.139	.110
11	7.97	.138	.107
12	8.02	.138	.103
13	8.06	.137	.100
14	8.10	.137	.097
15	8.14	.136	.094
16	8.16	.136	.092
17	8.20	.135	.089
18	8.22	.135	.087
19	8.24	.134	.084
20	8.26	.134	.082
21	8.28	.133	.080
22	8.30	.133	.078
23	8.34	.132	.075
24	8.38	.131	.073
25	8.42	.130	.070

* Obtained from Figure 8B1.6 - API DATA BOOK³

G & D Correlation $K_{ij} = .1294 + .0292 | \delta_{HC} - \delta_{CO_2} | - .0222 [\delta_{HC} - \delta_{CO_2}]^2$

JE Correlation $\text{LOG } K_{ij} = -.8849 - .2145 * W_{HC}(\delta_{HC} - \delta_{CO_2})$

δ = Solubility Parameter (cal/cc)^{1/2} ; $\delta_{CO_2} = 7.12$

SCN = Single carbon number

G & D = Grabowski and Daubert correlation^{14,15}

JE = Ezekwe correlation¹²

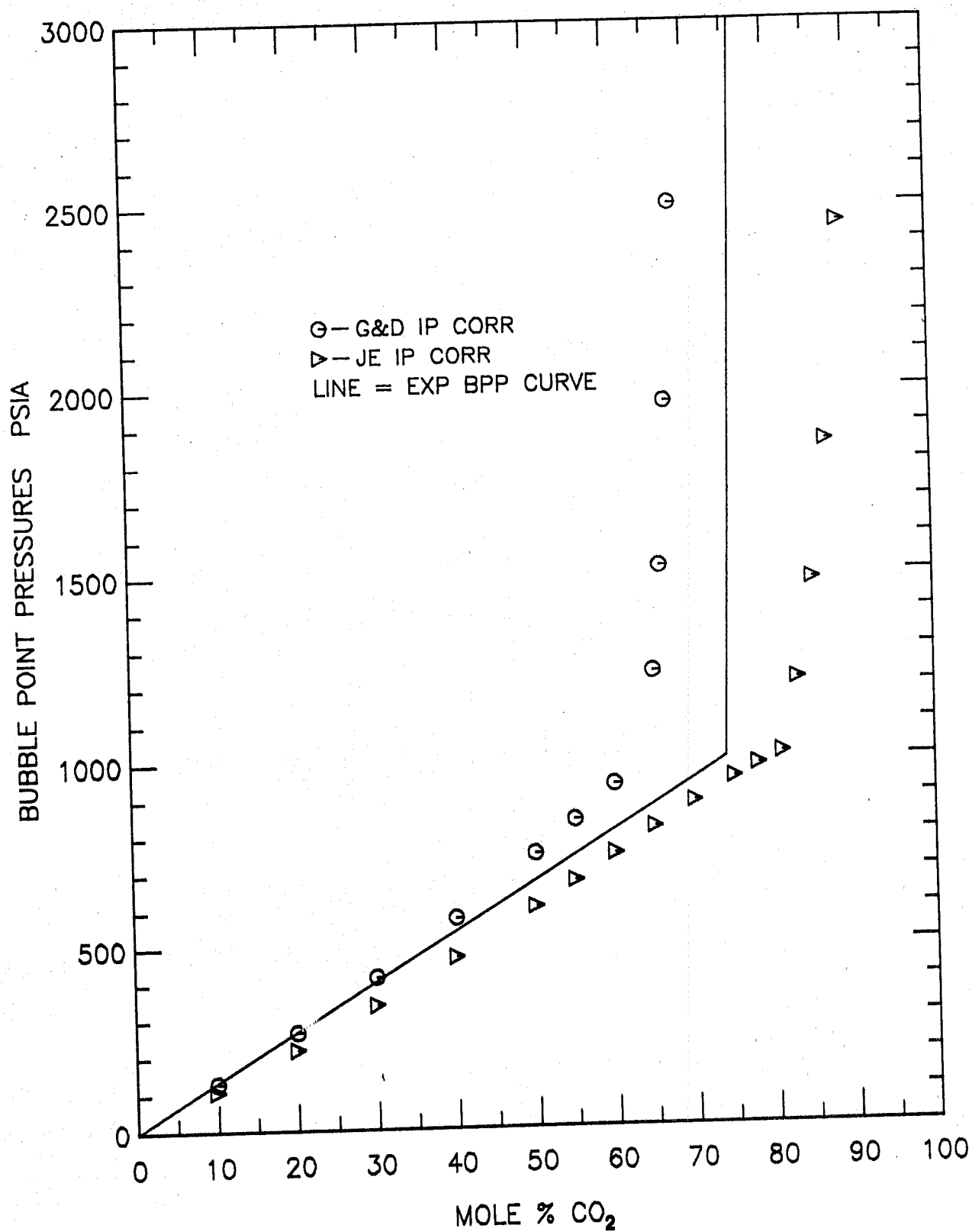


FIGURE 4-5: Comparison of Experimental and Calculated Bubble-Point Pressures, Maljamar Oil, 90°F: Use of Correlations for Interaction Coefficients (IP).

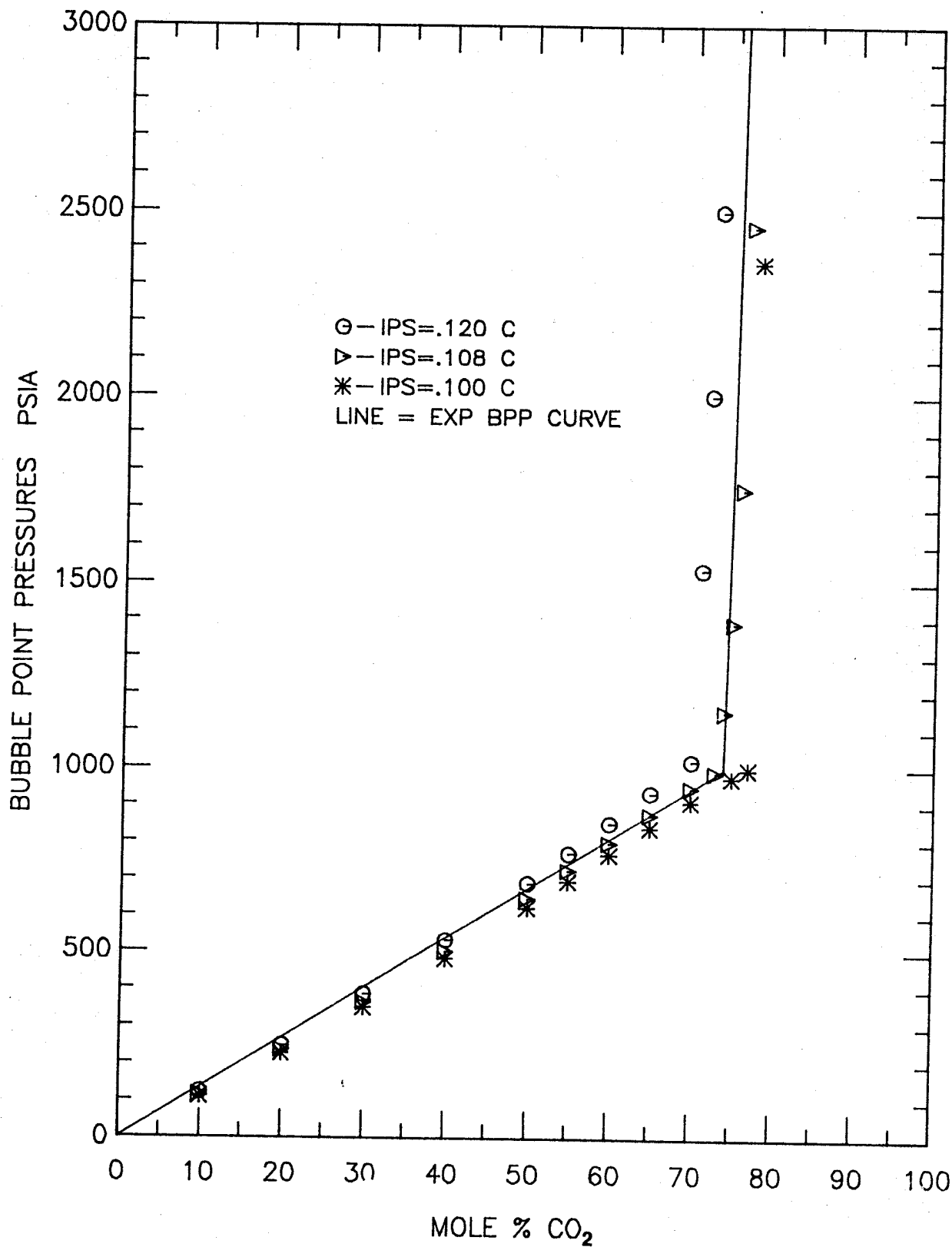


FIGURE 4-6: Comparison of Experimental and Calculated Bubble-Point Pressures, Maljamar Oil, 90°F: Use of Constant Interaction Coefficients (IP).

is referred to as an IP range from .07 to .13, or just 7-13 for short. Table 4.3 lists four IP ranges from 11-13 to 5-13. As before, the C_{26}^+ fraction is assigned the value for C_{25} . The four IP ranges were utilized to calculate bubble-point pressures for the Maljamar crude. Figure 4.7 compares the predicted curves with the experimental curve. The experimental curve is bounded on the left by the 9-13 range and on the right by the 5-13 range, while the 7-13 range fits the curve best in the region of developing miscibility.

Next, the assumed sets of interaction coefficients were used to predict the miscibility pressure at 90°F. The light and heavy fractions of the crude were split at C_5-C_{12} and C_{13}^+ to form two pseudo components. This corresponds to a volume fraction of the heavy pseudo component of 0.54 and a composition of 0.336 mole fraction.

The constant interaction coefficient set of 0.108 was used to generate a pseudo-ternary diagram at a series of pressures from 800 psia to 2200 psia (at a temperature of 90°F). At a pressure of 1100 psia, the extrapolated MMC was 0.183, well below the composition of the heavy pseudo component. At 2200 psia, the pseudo-ternary diagram still did not predict miscibility for the crude oil. The conclusion was that, even though the set of constant values of 0.108 led to prediction of a correct bubble-point pressure curve, the miscibility pressure was not correctly predicted. Therefore, the use of a set of constant interaction parameters was assumed not to be valid.

The 7-13 IP range was next utilized to generate a series of pseudo-ternary diagrams at 90°F and 800, 1000, 1050, 1100, and 1400 psia. Selected plots are shown in Figures, 4-8 to 4-11. At 800 psia, the predicted CO_2 solubility in the light hydrocarbon fraction is 73 mole % (Figure 4-8). At 1000 psia, the light hydrocarbon fraction was close to first contact miscibility with CO_2 . At 1050 psia, the phase-behavior description changes significantly as CO_2 begins to effectively extract hydrocarbons (Figure 4.9). And at 1050 psia, a miscible condition is predicted with a calculated MMC of .370 compared to the original oil composition of 0.336 mole fraction of heavy component. At 1100 psia, the MMC increases only slightly to .378 (Figure 4-10). Finally, the size of the phase envelope at 1400 psia moderately decreases from that at 1100 psia (Figure 4-11). This series of diagrams does qualitatively explain the onset of dynamic miscibility. The 7-13 IP range both matches the bubble-point pressure curve and predicts the experimental MMP of 1050 psia. It was concluded that interaction coefficients which varied linearly with carbon number could be applied to predict correctly the onset of dynamic miscibility.

It was noted that under some conditions a discontinuity appeared in the pseudo-ternary diagram as shown in Figure 4-9. The reason for this discontinuity is not understood. It is known (Orr, et al.²⁹) that the Maljamar oil- CO_2 system forms three phases at temperatures less than about 120°F. It is possible that this tendency is reflected in the calculation, causing the discontinuity. In any event, the discontinuity disappeared at 1100 psia and did not significantly affect the prediction of the MMP. The algorithm did converge in the region of the discontinuity. The effect of the appearance of a third phase on the

TABLE 4.3 - Interaction Coefficient(IP) Ranges
 Utilized to Match Maljamar Crude
 Bubble-Point Pressure Curve

<u>SCN</u>	IP RANGES			
	.11-.13 (11-13)	.09-.13 (9-13)	.07-.13 (7-13)	.05-.13 (5-13)
5	.110	.090	.070	.050
6	.111	.092	.073	.054
7	.112	.094	.076	.058
8	.113	.096	.079	.062
9	.114	.098	.082	.066
10	.115	.100	.085	.070
11	.116	.102	.088	.074
12	.117	.104	.091	.078
13	.118	.106	.094	.082
14	.119	.108	.097	.086
15	.120	.110	.100	.090
16	.121	.112	.103	.094
17	.122	.114	.106	.098
18	.123	.116	.109	.102
19	.124	.118	.112	.106
20	.125	.120	.115	.110
21	.126	.122	.118	.114
22	.127	.124	.121	.118
23	.128	.126	.124	.122
24	.129	.128	.127	.126
25	.130	.130	.130	.130
26 ⁺	.130	.130	.130	.130

SCN = Single carbon number

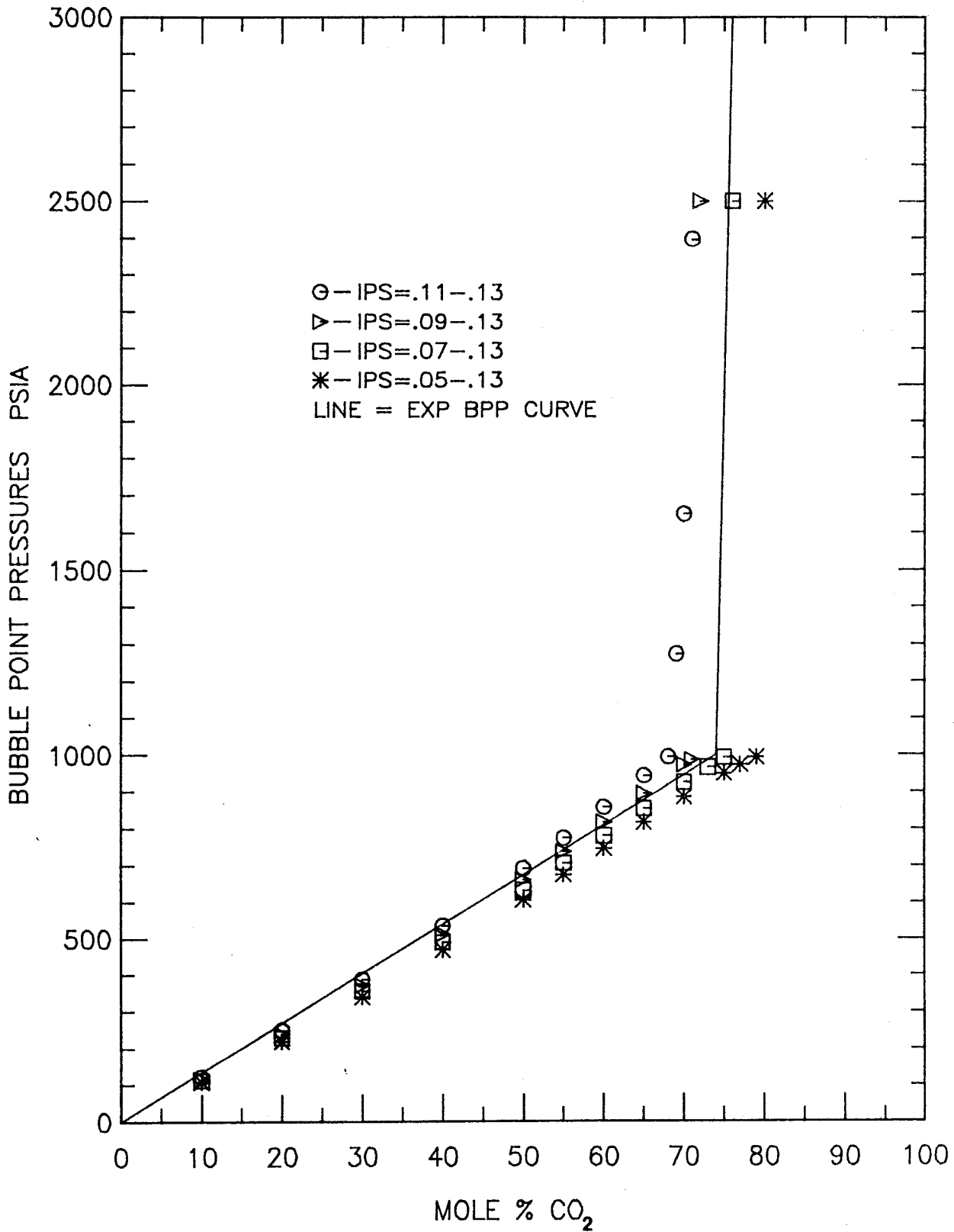


FIGURE 4-7: Comparison of Experimental and Calculated Bubble-Point Pressures, Maljamar Oil, 90°F: Use of Linear Range of Interaction Coefficients (IP).

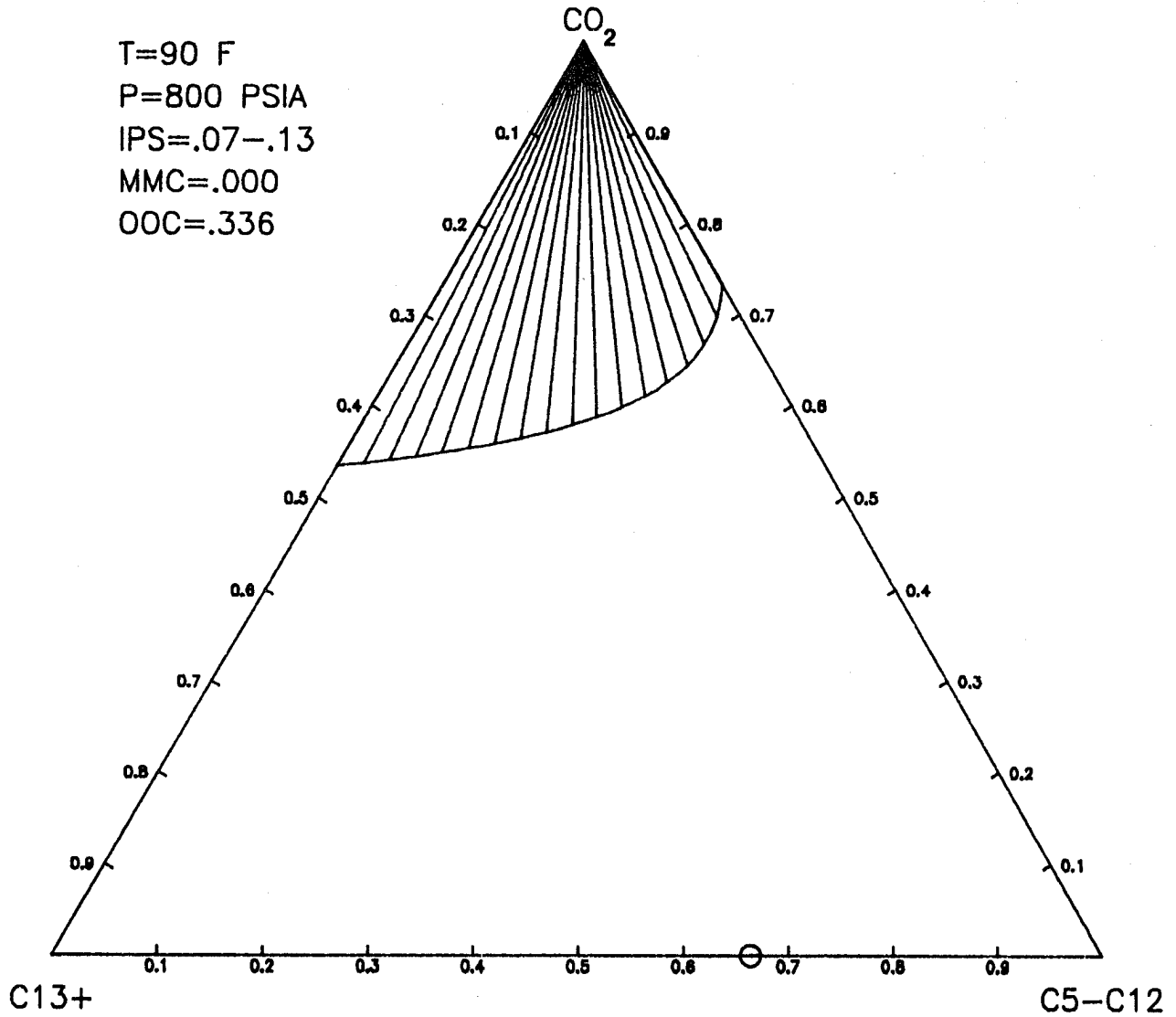


FIGURE 4-8: Calculated Ternary Phase Diagram for Maljamar Oil
 (IP Range 7-13, P = 800 psia).

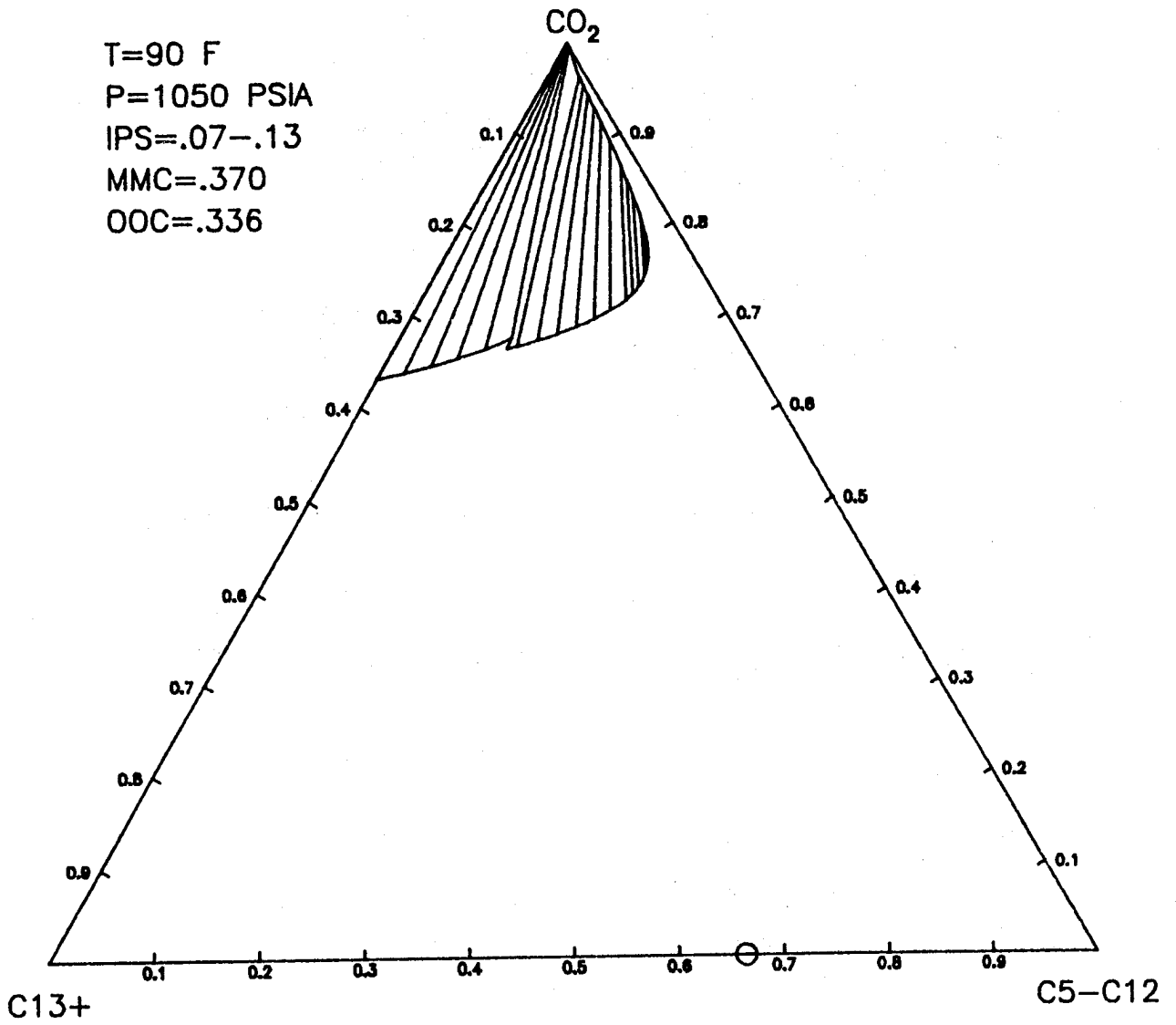


FIGURE 4-9: Calculated Ternary Phase Diagram for Maljamar Oil
 (IP Range 7-13, P = 1050 psia).

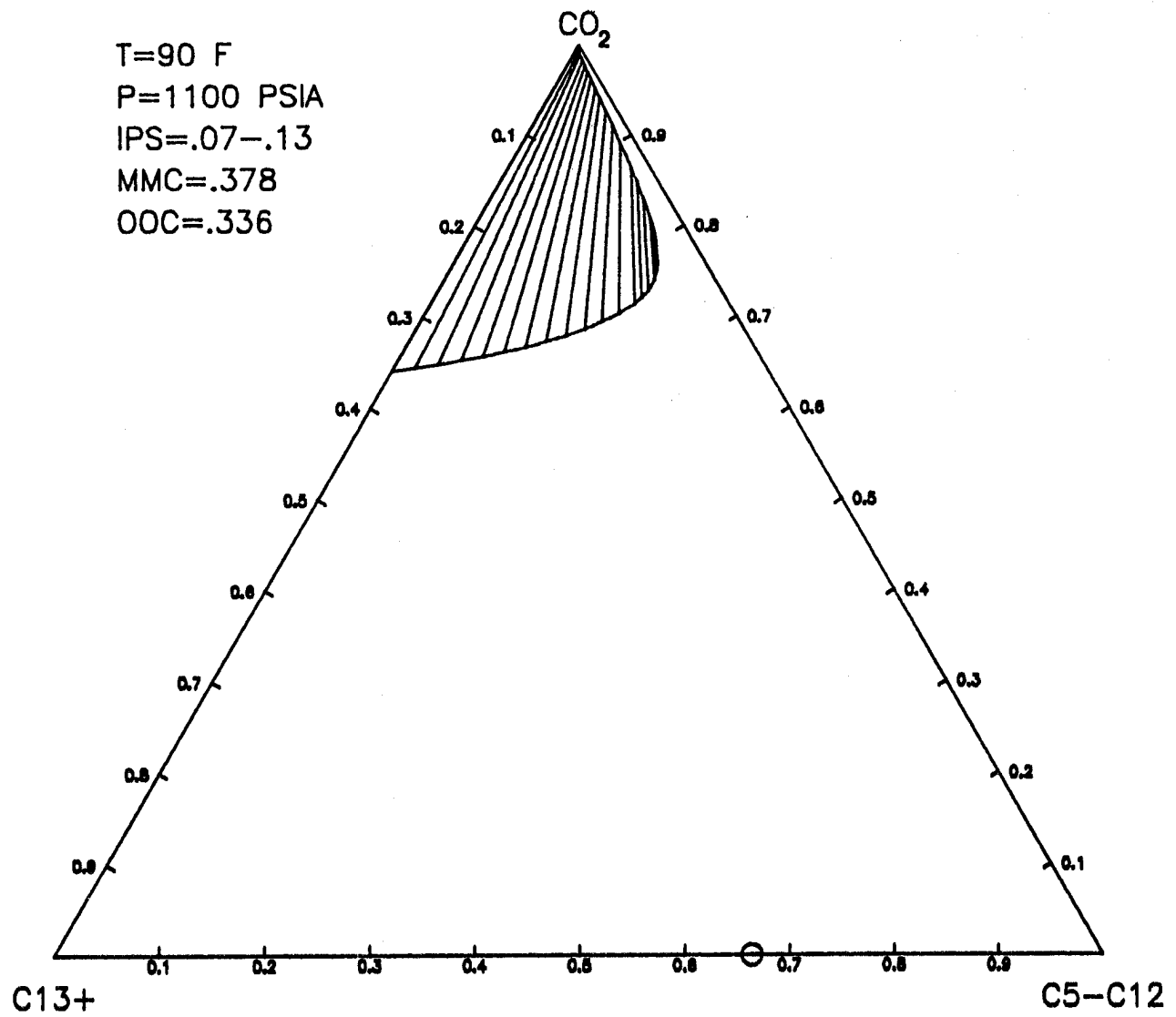


FIGURE 4-10: Calculated Ternary Phase Diagram for Maljamar Oil
 (IP Range 7-13, P = 1100 psia).

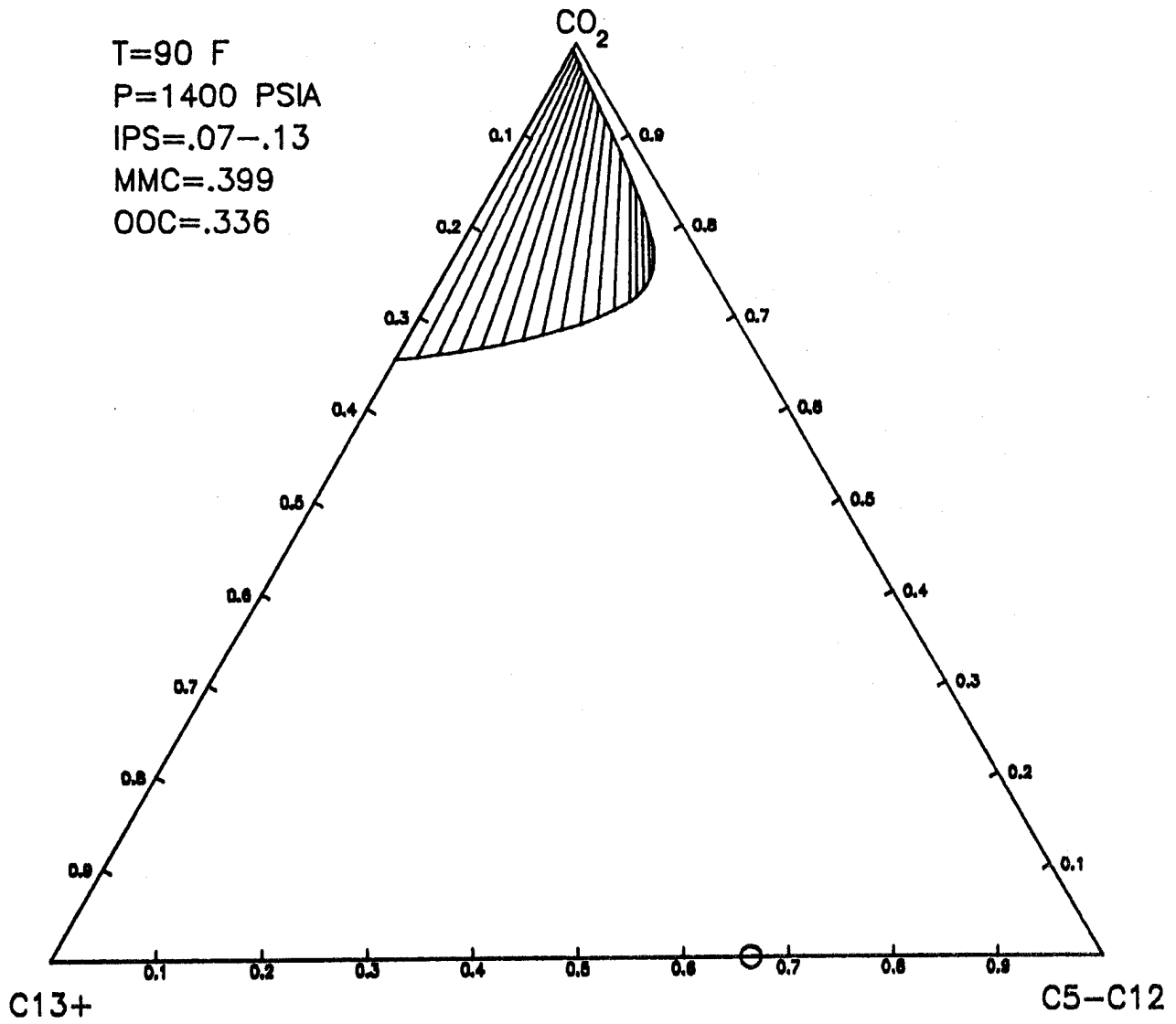


FIGURE 4-11: Calculated Ternary Phase Diagram for Maljamar Oil
 (IP Range 7-13, P = 1400 psia).

miscibility behavior was not considered.

The 5-13 and 9-13 IP ranges were both used to predict miscibility pressure. As expected the 5-13 range predicted a lower miscibility pressure while the 9-13 range gave a MMP value that was much too high.

As a further check on the uniqueness of the 7-13 IP range, the interaction coefficient sets predicted by the Grabowski and Daubert^{14,15} and Ezekwe¹² correlations were used to generate pseudo-ternary diagrams and to predict miscibility pressure. Neither correlation gave satisfactory results. The Grabowski and Daubert correlation yielded a miscibility pressure in excess of 2200 psi, thus it underpredicted CO₂ solubility and overpredicted miscibility pressure. The Ezekwe correlation gave a miscibility pressure of 1550 psia. This correlation thus overpredicted both CO₂ solubility and miscibility pressure, an apparent inconsistent behavior.

Miscibility pressure data were available for this system only at a temperature of 90°F. However, the general effect of temperature on MMP is known. The IP range of 7-13 was used to generate a set of pseudo-ternary diagrams and predict the MMP at 120°F. At the higher temperature, the calculated miscibility pressure was 1500 psia, corresponding to an increase in miscibility pressure of 15 psi per °F increase in temperature. This is consistent with reported literature values.

For the calculation procedure, the question arises as to whether the pseudo-component lumpings can be changed and still produce an equivalent result. To help answer this question, three different light pseudo components were used: C₅-C₁₅, C₅-C₁₀, and C₅-C₈. These fractions correspond to light pseudo component volume fractions of .565, .372, and .226 respectively. For the 7-13 IP range, pseudo-ternary diagrams were generated at 90°F and 1100 psia. The resulting graphs are shown in Figures 4-12 to 4-14. As expected, the shape of the phase envelope changes with the component lumpings. However, the C₅-C₁₅ and C₅-C₁₀ lumpings predict a miscible condition and therefore produce essentially equivalent results to the original choice of a light pseudo component of C₅-C₁₂. The C₅-C₈ lumping gives an MMP value slightly above 1100 psia. (The MMC at 1100 psia is 0.57 compared to an oil composition of 0.63). The calculations appear not to be highly sensitive to specification of the pseudo components at the conditions of this system. However, this result should be tested over a wider range of conditions before it is generalized.

Another assumption tested was the representation of all C₂₅⁺ components as C₂₅ in the specification of physical properties. A calculation was made in which C₂₅⁺ components were represented by C₃₅ rather than C₂₅. Phase behavior or the pseudo-ternary diagrams was essentially unchanged as were predicted values of MMP. The use of C₂₅ to represent C₂₅⁺ components was thus assumed to be valid.

4.3.4 Application of Phase Behavior-Calculations to the Yellig and Metcalfe West Texas Oil

The second literature oil investigated was a West Texas stock-tank oil studied by Yellig and Metcalfe⁴³. Table 4-4 lists the reported oil

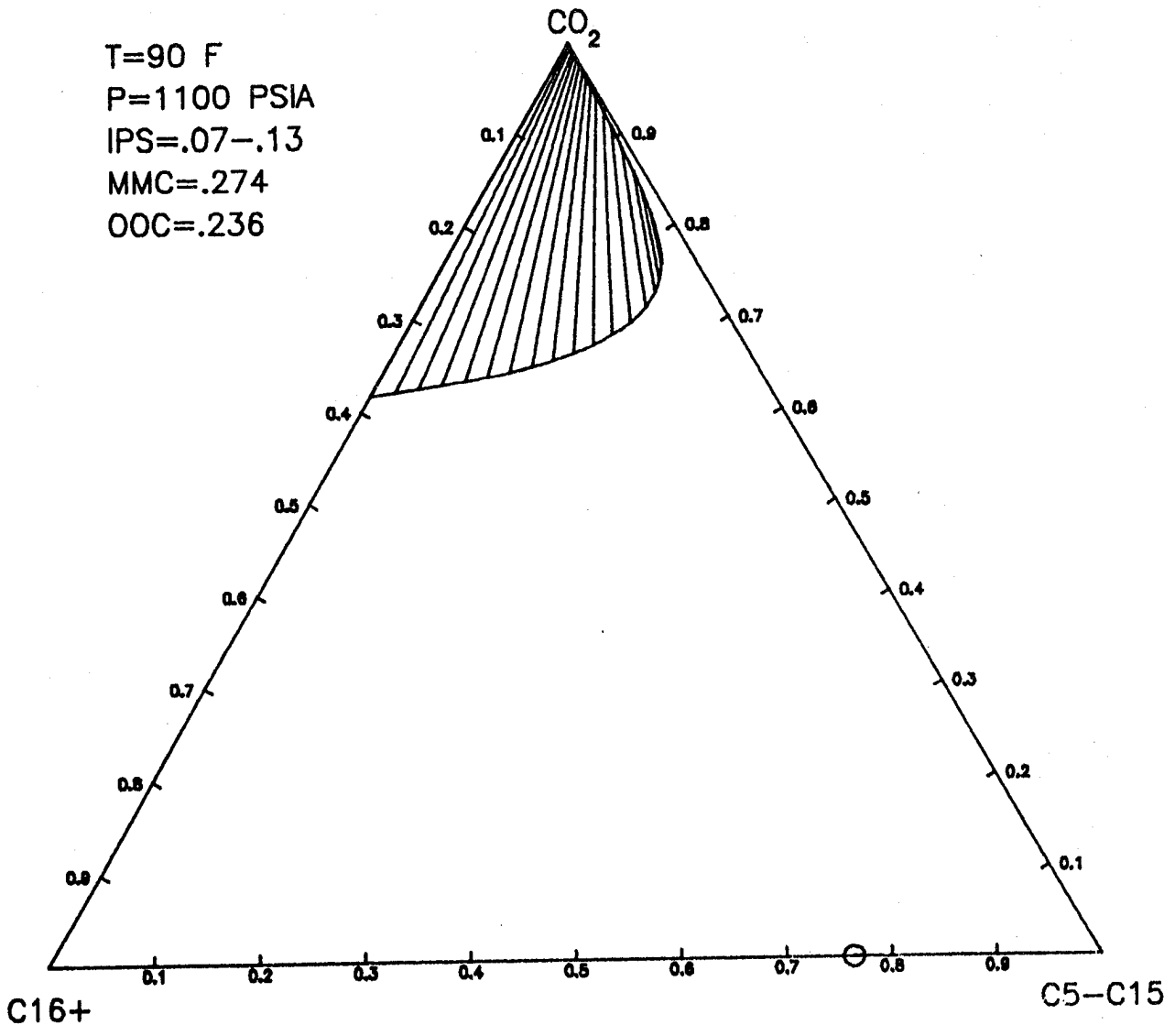


FIGURE 4-12: Calculated Ternary Phase Diagram for Maljamar Oil: Effect of Pseudo Component Composition - Heavy Component C_{16}^+ (IP Range 7-13, P = 1100 psia).

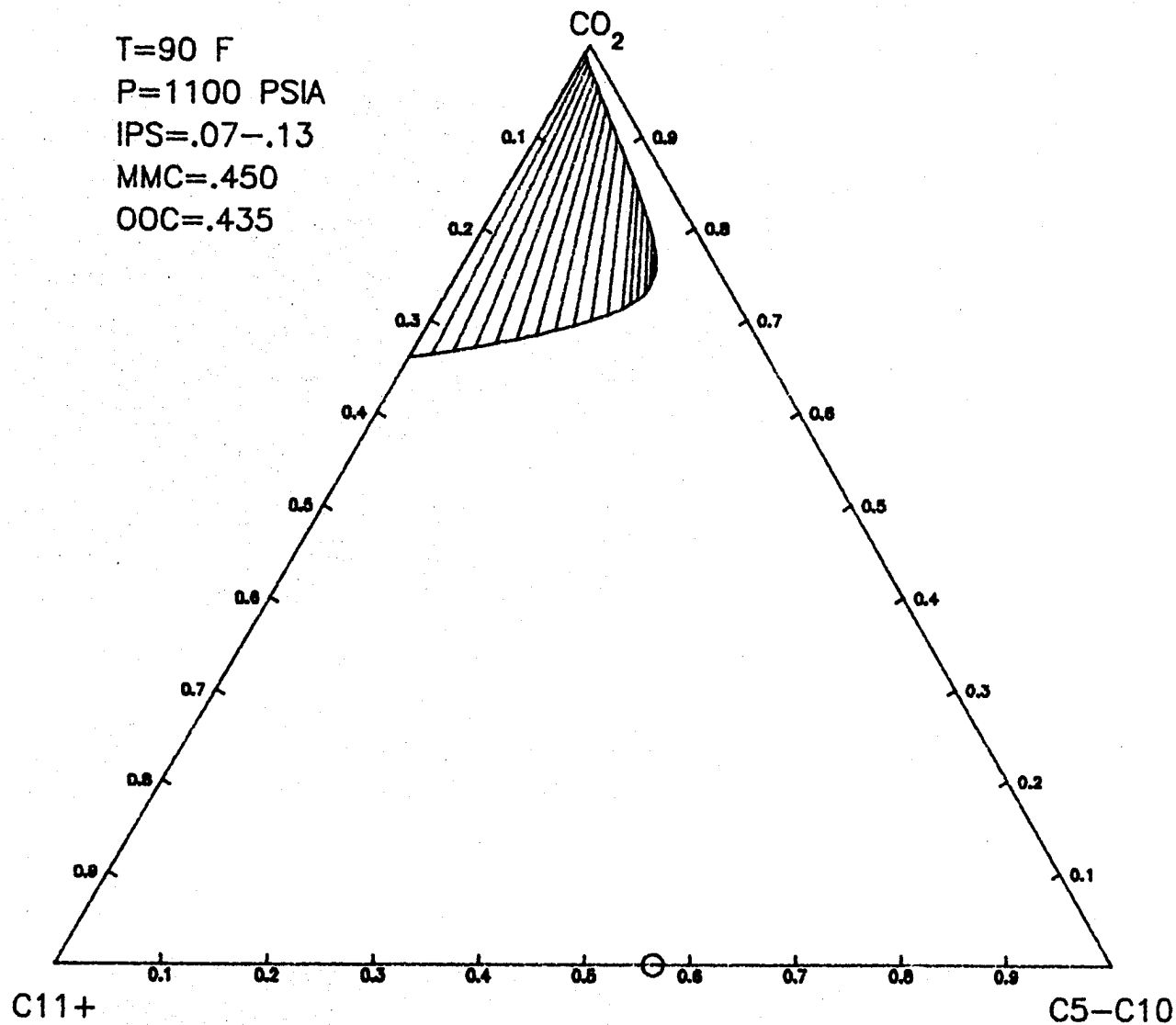


FIGURE 4-13: Calculated Ternary Phase Diagram for Maljamar Oil: Effect of Pseudo Component Composition - Heavy Component C_{11+} (IP Range 7-13, P = 1100 psia).

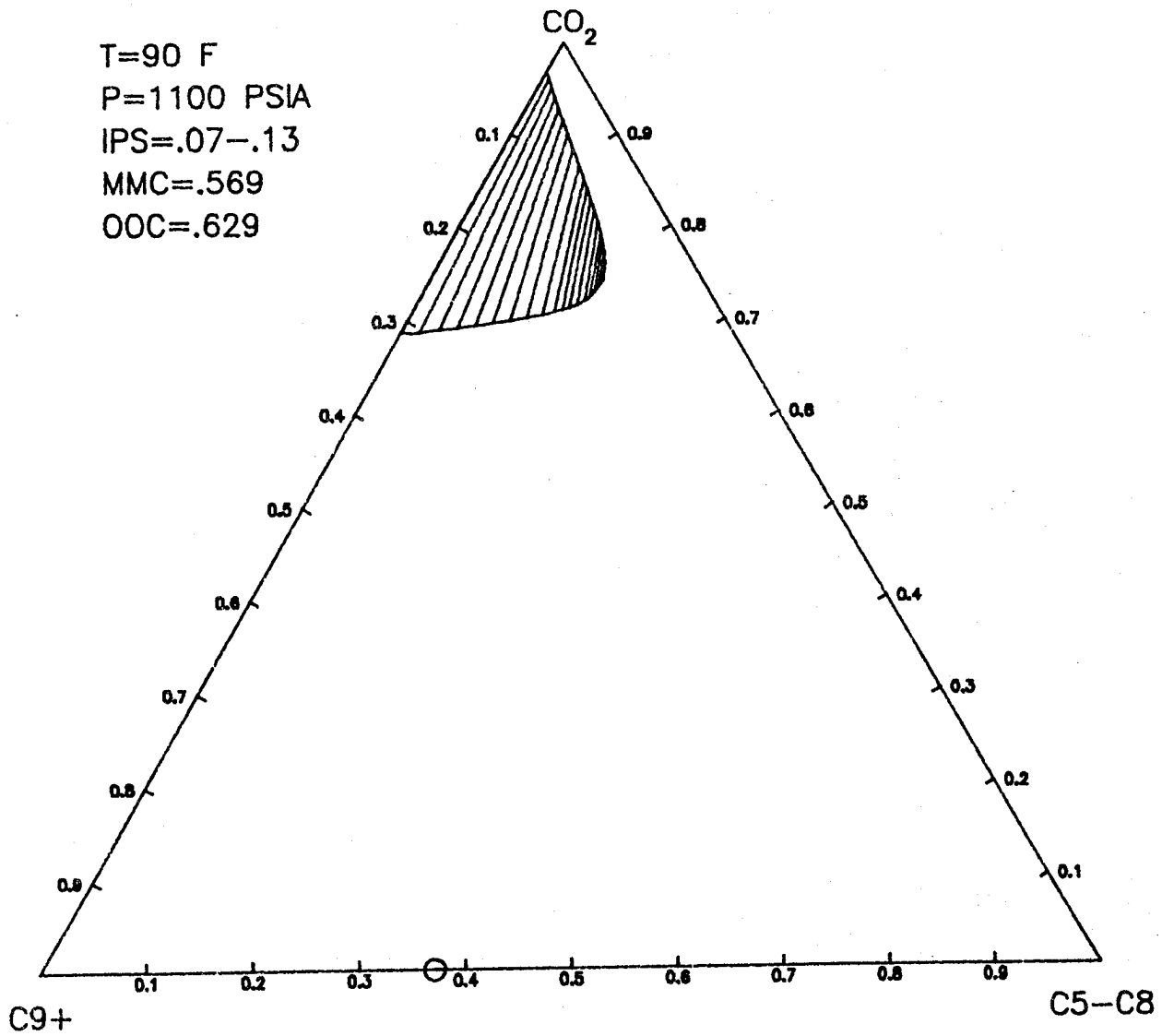


FIGURE 4-14: Calculated Ternary Phase Diagram for Maljamar Oil: Effect of Pseudo Component Composition - Heavy Component C₉+ (IP Range 7-13, P = 1100 psia).

composition. The C_7 composition is relatively high because an unspecified amount of n-heptane was added to the oil. However, there is a problem with the analysis because the calculated molecular weight is 146.9 compared to their reported experimental molecular weight of 201. The C_{25}^+ composition, 0.0285, is much lower than that reported for the Maljamar oil, .1168.

Yellig was contacted and asked about the discrepancy⁴⁴. It was explained that the analysis was obtained by gas chromatographic distillation. The difference was related to the fact that the heavy fraction was not totally eluted from the column and essentially the reported values did not include a compensation for this. Orr, et al.³¹ did compensate for this problem by calculating a C_{37}^+ fraction.

Therefore, it became necessary to estimate the true C_{25}^+ composition by calculating a value that matched the experimental molecular weight. The C_{25}^+ fraction was assigned a molecular weight of 560 and a specific gravity of .979. These are the average values for the three Kansas oil residues analyzed by Core Labs. (To be discussed later.) A revised compositional analysis for the West Texas oil is listed in Table 4-5. Due to the C_7 addition, the oil composition is similar to the Maljamar crude. The estimated C_{25}^+ adjusted mole fraction is .145, considerably higher than the original value. The estimated K_w of the oil is 11.7.

Yellig and Metcalfe experimentally determined the slim-tube MMP for this oil at three different temperatures.⁴³ Their results were as follows:

<u>T(F)</u>	<u>MMP(psia)</u>
95	1115
118	1465
150	1990

The change of MMP with temperature between 95 and 118°F is 15.2 psi/°F and between 118 and 150°F is 16.4 psi/°F.

The objective of the calculations using pseudo-ternary diagrams was to predict the miscibility pressure at the three temperatures. The pseudo components were split at C_6-C_{12} and C_{13}^+ . This corresponds to a volume fraction of the heavy component of 0.58 and a mole fraction of the heavy component of 0.346. For the flash calculations, the C_{25}^+ fraction was assigned the properties of C_{35} .

Pseudo-ternary diagrams were generated for this crude at the three experimental temperatures using the 7-13 IP range. For each temperature, diagrams were calculated at several pressures to determine the MMP. The diagram at the predicted miscibility pressure of 1150 psia at 95°F is shown in Figure 4-15. This compares well with the measured value for the slim-tube of 1115 psia.

At the two higher temperatures of 118°F and 150°F however, the predicted miscibility pressures using the 7-13 IP range were too high. At 118°F the predicted value was 1600 psia compared to an experimental

TABLE 4.4 - Reported Composition of West Texas Stock-Tank Oil
of Yellig and Metcalfe⁴³

<u>SCN</u>	<u>M/F</u>	<u>CUM.M/F</u>	<u>WT</u>	<u>VOL</u>
6	.0160	.0160	1.34	1.95
7	.2914	.3074	27.97	38.48
8	.1422	.4496	15.22	20.31
9	.0959	.5455	11.60	15.11
10	.0785	.6240	10.52	13.45
11	.0678	.6918	9.97	12.57
12	.0523	.7441	8.42	10.47
13	.0422	.7863	7.39	9.05
14	.0350	.8213	6.65	8.05
15	.0379	.8592	7.81	9.34
16	.0294	.8886	6.53	7.74
17	.0208	.9094	4.93	5.79
18	.0153	.9247	3.84	4.49
19	.0124	.9371	3.26	3.79
20	.0093	.9464	2.56	2.95
21	.0079	.9543	2.30	2.64
22	.0071	.9614	2.13	2.43
23	.0058	.9672	1.81	2.05
24	.0043	.9715	1.39	1.57
25	.0037	.9752	1.25	1.40
26	.0032	.9784	1.12	1.25
27	.0027	.9811	0.97	1.08
28	.0028	.9839	1.04	1.16
29	.0023	.9862	0.88	0.97
30	.0020	.9882	0.79	0.87
31	.0017	.9899	0.69	0.76
32	.0016	.9915	0.66	0.73
33	.0014	.9929	0.60	0.65
34	.0014	.9943	0.61	0.67
35	.0013	.9956	0.58	0.63
36	.0012	.9968	0.55	0.59
37	.0011	.9979	0.51	0.55
38	.0010	.9989	0.48	0.51
39	.0007	.9996	0.34	0.36
40	.0004	1.0000	0.20	0.21
			146.91	184.63

MW = 183.7 SG = .835 $K_w = 11.6$

SCN = Single Carbon number MW = Molecular Weight
M/F = Mole fraction SG = Specific Gravity
WT = Weight K_w = Watson Characterization Factor
VOL = Volume

TABLE 4.5 - Adjusted Composition of West Texas Stock Tank Oil
of Yellig and Metcalfe⁴³

<u>SCN</u>	<u>M/F</u>	<u>CUM.M/F</u>	<u>W/F</u>	<u>CUM.W/F</u>	<u>V/F</u>	<u>CUM.V/F</u>	<u>WT</u>	<u>VOL</u>
6	.014	.0214	.006	.006	.007	.007	1.18	1.70
7	.256	.270	.122	.128	.144	.151	24.58	33.80
8	.125	.395	.067	.195	.076	.227	13.38	17.86
9	.084	.479	.051	.246	.056	.283	10.16	13.23
10	.069	.548	.046	.292	.050	.333	9.25	11.82
11	.060	.608	.044	.336	.047	.380	8.82	11.12
12	.046	.654	.037	.373	.039	.419	7.41	9.21
13	.037	.691	.032	.405	.034	.453	6.48	7.94
14	.031	.722	.029	.434	.030	.483	5.89	7.13
15	.033	.755	.034	.468	.035	.518	6.80	8.13
16	.026	.781	.029	.497	.029	.547	5.77	6.85
17	.018	.799	.021	.518	.021	.568	4.27	5.01
18	.014	.813	.017	.535	.018	.586	3.51	4.11
19	.011	.824	.014	.549	.014	.600	2.89	3.36
20	.009	.833	.012	.561	.012	.612	2.48	2.86
21	.006	.839	.009	.570	.009	.621	1.75	2.00
22	.006	.845	.009	.579	.009	.630	1.80	2.05
23	.005	.850	.008	.587	.008	.638	1.56	1.77
24	.005	.855	.008	.595	.008	.646	1.62	1.83
25 ⁺	.145	1.000	.405	1.000	.354	1.000	<u>81.20</u>	<u>82.94</u>
							200.8	234.7

MW = 183.7 SG = .835 $K_w = 11.6$

SCN 25⁺ Properties based on MW = 560 & SG = .979

- SCN = Single Carbon number
- M/F = Mole fraction
- W/F = Weight fraction
- V/F = Volume fraction
- WT = Weight
- VOL = Volume
- SG = Specific Gravity

T=95 F
 P=1150 PSIA
 IPS=.07-.13
 MMC=.346
 OOC=.346

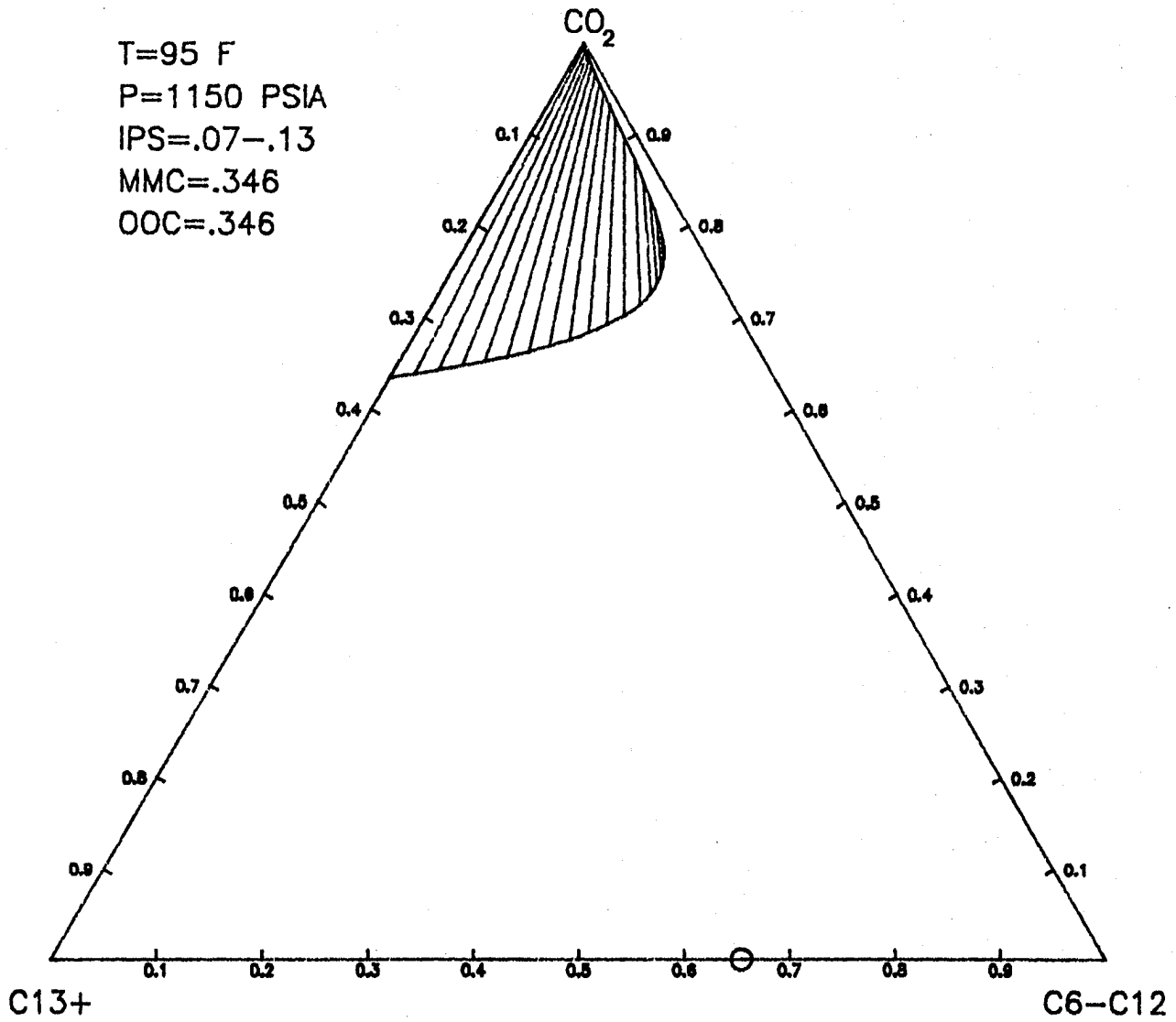


FIGURE 4-15: Calculated Ternary Phase Diagram for Yellig and Metcalfe Oil
 (IP Range 7-13, P = 1150 psia).

value of 1465 psia and at 150°F the predicted value was 2250 psia compared to a slim-tube value of 1990 psia. Example calculated pseudo-ternary diagrams using the 7-13 IP range are shown as Figures C-1 through C-4 in Appendix C.

Since the 7-13 IP range predicted MMP values that were too high at the higher temperatures, the calculations were repeated using an IP range of 6-13. That is, the interaction coefficient assigned to C_5 was reduced by one unit. This did improve the calculated result, yielding a somewhat improved agreement with the measured values. Results for both the 6-13 and 7-13 IP ranges are shown in Table 4-6. Typical calculated pseudo-ternary diagrams for the 6-13 range are shown in Figures C-5 through C-8.

The two IP ranges used, 6-13 and 7-13, yield calculated results that bound the miscibility pressures obtained from the slim-tube at the three temperatures. The West Texas crude of Yellig and Metcalfe is similar in composition to the Maljamar crude reported by Orr, thus the agreement in results is not unexpected. The use of the pseudo-ternary diagrams does do a good job of predicting the dependence of MMP on temperature.

To check the appropriateness of using an interaction coefficient of 0.13 for the heavy component, a solubility calculation was made at several conditions for the West Texas crude and the Maljamar crude. As an example, at 1250 psia and 118°F, the average predicted CO_2 solubility in the heavy fraction is 60.3 mole %. The CO_2 solubility predicted by the Simon and Graue correlation³⁸ is 60 mole %. Therefore, the assignment of an interaction coefficient value of .130 to the C_{25+} fraction is reasonable.

The effect on calculated miscibility pressure of using different lumpings of pseudo components was again checked. The light component was represented by C_6-C_{10} and C_6-C_{15} in different calculations made at 150°F and using the 6-13 IP range. For both of these groupings, calculated MMP values at 150°F increased by about 100 psia. Thus, there was a small but probably insignificant effect of using different pseudo components in the calculation.

4.3.5 Summary - Literature Oils

Two crude oils for which compositions and slim-tube miscibility pressures were reported in the literature were the basis for calculations using pseudo-ternary diagrams. Use of interaction coefficients determined from the Grabowski and Daubert^{14,15} and Ezekwe¹² correlations did not yield acceptable results for calculations of MMP. Similarly, use of a constant interaction coefficient was not acceptable. However, sets of linearly increasing interaction coefficients did produce acceptable agreement between calculated and measured miscibility pressures. The IP range used for the two oils was essentially the same. The calculation of the increase of miscibility pressures with temperature was quite acceptable based on general trends reported in the literature and agreement between calculated and measured miscibility pressures for the West Texas oil.

TABLE 4.6 - Comparison of Calculated and Measured
 Miscibility Pressures
 West Texas Oil of Metcalfe and Yarborough⁴³

<u>Temperature °F</u>	<u>Slim Tube MMP (psi)</u>	<u>Calculated MMP (psi) IP Range 6-13</u>	<u>Calculated MMP (psi) IP Range 7-13</u>
95	1115	1100	1150
118	1465	1350	1600
150	1990	2000	2250

Additional information about the calculations on the literature oils and additional results are given by Daub⁹.

4.4 Application of Pseudo-Ternary Diagrams to Crude Oil System - Kansas Crude Oils

4.4.1 Experimental Data on Kansas Crude Oils

Slim-tube miscibility pressures were measured for several crude oils (stock-tank oils) from the central part of Kansas. These results are reported in Chapter 3 and Appendix B. Miscibility pressures were measured at reservoir temperature for all crudes except the Johanning B lease crude. For that sample, measurements were made at the reservoir temperature of 102°F as well as temperatures of 115 and 126°F.

In addition, three crude oils were analyzed by Core Labs (Dallas, Texas). The Abernathy-Collins (ABC) and Johanning B (JOB) lease crudes were subjected to ASTM D-86 distillation. Copies of the Core Labs reports are shown as Tables C-3 and C-4. Albertson (ALB) lease crude oil was analyzed using ASTM D-86 distillation and a true boiling-point (TBP) distillation. Copies of the Core Labs reports are shown as Tables C-5 and C-6.

4.4.2 Characterization of the Kansas Crude Oils

For the ABC and JOB crudes, the mole fractions, volume fractions and weight fractions of the different cuts were estimated from the ASTM D-86 distillation curve using the API Data Book³. Each cut was then assigned a single carbon number based on the average boiling point of the cut using the Riazi-Daubert equation³⁴. From this procedure, C₇ was the lightest component. Results of these calculations are summarized in Tables 4-7 and 4-8.

The true boiling-point and equilibrium flash-vaporization curves were then estimated from the API Data Book correlations.³ The results for the ABC crude are listed in Table C-7. To check the validity of the crude characterization, binary bubble-point temperatures were calculated with the SRK equation of state and compared with the ASTM D-86 cut temperatures. The results for the ABC crude are given in Table C-8. There is reasonable agreement between the two temperatures throughout the complete range. As a second check on the characterization, atmospheric pressure flashes were calculated with the SRK equation of state from 350 to 650°F. The calculated moles of vapor were converted to volume percent by linear interpolation and the results were compared to the predicted equilibrium flash vaporization curve. Again, the agreement was sufficiently consistent to presume that the original oil characterization was valid.

Next, the true boiling-point information in Table C-7 and the ASTM D-86 residue information were used to determine the single carbon number molar analysis based on the Katz-Firoozabadi-Whitson properties²⁰. The results for the ABC and JOB crudes are given in Tables 4-9 and 4-10. As expected, the true boiling-point characterization yields higher concentrations of the lighter hydrocarbons (C₆-C₁₅) than does the ASTM D-86 characterization.

TABLE 4.7 - Abernathy-Collins Crude Compositional Summary
Based on ASTM D-86 Distillation

<u>SCN</u>	<u>M/F</u>	<u>CUM.M/F</u>	<u>V/F</u>	<u>CUM.V/F</u>	<u>W/F</u>	<u>CUM.W/F</u>
5						
6						
7	.056	.056	.030	.030	.024	.024
8	.122	.178	.070	.100	.059	.083
9	.128	.306	.080	.180	.070	.153
10						
11	.096	.402	.065	.245	.059	.211
12	.054	.456	.040	.285	.037	.248
13	.067	.523	.055	.340	.051	.299
14						
15	.068	.591	.060	.400	.058	.357
16						
17	.057	.648	.055	.455	.054	.411
18						
19	.062	.710	.065	.520	.065	.475
20						
21						
22	.060	.770	.070	.590	.070	.546
23						
24						
25	.094	.864	.120	.710	.121	.667
26 ⁺	.136	1.000	.290	1.000	.333	1.000

SCN = Single carbon number

M/F = Mole fraction

V/F = Volume fraction

W/F = Weight fraction

TABLE 4.8 - Johanning B Crude Compositional Summary
Based on ASTM D-86 Distillation

<u>SCN</u>	<u>M/F</u>	<u>CUM.M/F</u>	<u>V/F</u>	<u>CUM.V/F</u>	<u>W/F</u>	<u>CUM.W/F</u>
5						
6						
7						
8	.052	.052	.030	.030	.026	.026
9	.143	.195	.090	.120	.079	.105
10	.137	.332	.095	.215	.086	.191
11	.087	.419	.065	.280	.061	.251
12						
13	.074	.493	.060	.340	.057	.308
14	.079	.572	.070	.410	.068	.377
15						
16	.072	.644	.070	.480	.069	.446
17						
18	.070	.714	.075	.555	.075	.521
19						
20						
21	.081	.795	.095	.650	.097	.617
22						
23						
24	.095	.890	.125	.775	.127	.745
25						
26 ⁺	.110	1.000	.225	1.000	.255	1.000

SCN = Single carbon number

M/F = Mole fraction

V/F = Volume fraction

W/F = Weight fraction

The ALB oil was analyzed by three different methods. The oil was distilled by the ASTM D-86 and true boiling-point methods by Core Labs. It was also analyzed via GC distillation by Gulf Labs, Kansas City. The purpose was to compare the results provided by the various distillation methods. Using the true boiling-point information, single carbon number compositions were determined based both on average boiling points and the Katz-Firoozabadi-Whitson properties²⁰. The true boiling-point curve was also estimated from the ASTM D-86 distillation as was done for the ABC and JOB crudes. This empirical distillation curve was then used to determine single carbon number compositions, again based on the Katz-Firoozabadi-Whitson²⁰ properties. Single carbon number compositions determined by the above three methods, as well as the GC analysis reported by Gulf, are shown in Table 4-11.

The two calculated compositions of the ALB crude based on the experimental true boiling-point curve are in good agreement. However, the calculation based on the ASTM D-86 distillation and empirical true boiling-point curve yielded compositions that differed somewhat from those determined from the experimental true boiling-point curve. Mole fractions from the ASTM D-86 were higher for C₅ and C₆ and generally lower at higher carbon numbers. The mole fraction of the C⁺₂₀ component, however, was higher for the ASTM D-86 data. The GC data were not in agreement with calculations based on the distillation curves. There was some uncertainty in the GC data and so they were not used in subsequent calculations.

The Lee-Kesler equations²¹ were applied to calculate critical temperature, critical pressure and acentric factor for each single carbon number constituent as was done for the literature oils.

The characterization procedure and computer programs used to make the calculations are described in detail by Daub⁹.

4.4.3 Application of Phase Behavior Calculations to Kansas Crudes

As reported in Chapter 3, slim-tube miscibility pressure measurements were made on the three crude-oil samples that were also analyzed by Core Labs. Results are summarized in Table 4-12.

Initial calculations for the ABC and JOB crudes were done using the single carbon number analyses that were based on the ASTM D-86 distillations. Pseudo components were C₇-C₁₅ and C₁₆⁺ for the ABC crude, and C₈-C₁₄ and C₁₅⁺ for the JOB crude. Application of the 7-13 IP range, which resulted in good predictions for the literature oils, yielded miscibility pressures that were much too large. For example, miscibility was not predicted for the ABC crude at 126°F at a pressure as high as 3100 psia. The pseudo-ternary diagram for this system at 1550 psia is shown as Figure C-10.

The IP range was modified to determine that range which would predict the correct miscibility pressure. It was determined from trial and error that the experimental MMP was bounded by calculations using 3-13 and 4-13 as IP ranges. A summary of additional IP ranges is given in Table C-9.

TABLE 4.9 - Single Carbon Number Analysis Based on the
Empirical True Bubble-Point Curve -
Abernathy-Collins Crude

<u>SCN</u>	<u>M/F</u>	<u>CUM.M/F</u>	<u>V/F</u>	<u>CUM.V/F</u>	<u>W/F</u>	<u>CUM.W/F</u>
6	.088	.088	.0404	.0404	2.789	.0332
7	.078	.166	.0387	.0791	2.813	.0293
8	.078	.244	.0421	.1212	3.157	.0295
9	.080	.325	.0477	.1689	3.666	.0303
10	.069	.393	.0442	.2131	3.457	.0258
11	.059	.452	.0412	.2543	3.263	.0222
12	.051	.503	.0386	.2929	3.107	.0193
13	.039	.543	.0319	.3248	2.608	.0149
14	.034	.576	.0290	.3538	2.394	.0126
15	.030	.606	.0275	.3813	2.307	.0112
16	.024	.630	.0241	.4054	2.042	.0092
17	.026	.656	.0268	.4322	2.275	.0096
18	.021	.677	.0232	.4554	1.983	.0079
19	.019	.696	.0223	.4777	1.920	.0073
20	.018	.714	.0214	.4991	1.843	.0067
21	.029	.744	.0370	.5361	3.230	.0111
22	.027	.770	.0344	.5705	3.030	.0101
23	.026	.796	.0345	.6050	3.026	.0097
24	.024	.820	.0333	.6383	2.948	.0091
25	.022	.842	.0317	.6700	2.797	.0083
26	.021	.864	.0317	.7017	2.827	.0081
27	.006	.869	.0083	.7100	.756	.0021
RESIDUE	.131	1.000	.2900	1.0000	<u>28.282</u>	<u>.0491</u>
					86.520	.3766

$$\text{Calculated Molecular Weight} = 86.520 / .3766 = 229.7$$

SCN = Single carbon number

M/F = Mole fraction

V/F = Volume fraction

WT = Weight

GMOLS = Gram moles

TABLE 4.10 - Single Carbon Number Analysis Based on
Empirical True Boiling-Point Curve
Johanning B Crude

<u>SCN</u>	<u>M/F</u>	<u>CUM.M/F</u>	<u>V/F</u>	<u>CUM.V/F</u>	<u>WT</u>	<u>GMOLS</u>
6	.022	.022	.0105	.0105	.731	.0087
7	.080	.102	.0411	.0516	2.986	.0311
8	.068	.169	.0377	.0893	2.825	.0264
9	.089	.258	.0546	.1439	4.199	.0347
10	.088	.346	.0587	.2026	4.596	.0343
11	.076	.421	.0547	.2573	4.337	.0295
12	.063	.485	.0496	.3069	3.993	.0248
13	.046	.531	.0388	.3457	3.168	.0181
14	.041	.572	.0365	.3822	3.021	.0159
15	.036	.608	.0346	.4168	2.884	.0140
16	.029	.637	.0303	.4471	2.553	.0115
17	.031	.668	.0337	.4808	2.868	.0121
18	.028	.696	.0318	.5126	2.711	.0108
19	.030	.725	.0352	.5478	3.025	.0115
20	.027	.753	.0338	.5816	2.915	.0106
21	.025	.777	.0324	.6140	2.823	.0097
22	.022	.799	.0296	.6436	2.580	.0086
23	.021	.821	.0296	.6732	2.621	.0084
24	.020	.841	.0283	.7015	2.495	.0077
25	.020	.861	.0297	.7312	2.629	.0078
26	.019	.880	.0297	.7609	2.652	.0076
27	.090	.889	.0141	.7750	1.260	.0035
RESIDUE	.111	1.000	.2250	1.0000	<u>21.613</u>	<u>.0434</u>
					85.485	.3907

Calculated Molecular Weight = $85.485 / .3907 = 218.8$

- SCN = Single carbon number
- M/F = Mole fraction
- V/F = Volume fraction
- WT = Weight
- GMOLS = Gram moles

TABLE 4.11 - Comparison of the Albertson Crude Compositional Analyses

TBP(Experimental)* (Core Labs)		TBP(Experimental)** (By SCN)		TBP(Emprical)*** (By SCN)		GC(Experimental) (Gulf Labs)		
SCN	M/F	CUM.M/F	M/F	CUM.M/F	M/F	CUM.M/F	M/F	CUM. M/F
5			.013	.013	.047	.047	.027	.027
6	.087	.087	.079	.092	.088	.135	.030	.057
7	.101	.188	.099	.191	.075	.210	.060	.117
8	.111	.299	.106	.297	.087	.296	.079	.196
9	.090	.389	.091	.388	.073	.369	.079	.275
10	.084	.473	.068	.456	.062	.431	.059	.334
11			.059	.515	.053	.485	.049	.383
12	.067	.540	.051	.566	.045	.529	.058	.441
13	.071	.611	.045	.611	.036	.565	.044	.485
14	.057	.668	.039	.650	.032	.597	.037	.522
15			.034	.684	.028	.626	.039	.561
16	.055	.723	.028	.712	.023	.649	.045	.606
17			.029	.741	.024	.673	.035	.641
18	.052	.775	.024	.765	.020	.693	.040	.681
19			.006	.770	.018	.712	.036	.717
20+	.225	1.000	.230	1.000	.288	1.000	.283	1.000

* Based on Average Boiling Points and Core Labs Experimental TBP Curve

** Based on KFW Properties and Core Labs Experimental TBP Curve

*** Based on KFW Properties and Empirical TBP Curve Derived From ASTM

D-86 Distillation

SCN = single carbon number

M/F = mole fraction

TBP = true bubble-point

KFW = Katz-Firoozabadi-Whitson²⁰

TABLE 4-12 - Slim Tube Miscibility Pressure Measurements

Kansas Crude Oils

<u>Oil</u>	<u>T(°F)</u>	<u>MMP(psia)</u>
Abernathy-Collins (ABC)	126	1540
Johanning B (JOB)	102	1260
	115	1520
	125	1720
Albertson (ALB)	110	1260

Since the single carbon number compositions based on a true boiling-point curve were thought to be more representative of the crudes, these compositions were used in calculations which are subsequently discussed.

For the ABC crude, pseudo components were split into C_6-C_{15} and C^+_{16} . This corresponded to an oil composition of 0.394 mole fraction and 0.38 volume fraction for the heavy component. An IP range of 7-13 still yielded a miscibility pressure at 126°F that was much too large. Again, the IP range was modified to determine that range which would correctly predict miscibility. A range of 4-13 predicted miscibility at 1450 psia while a 5-13 range predicted miscibility at between 1800 - 1850 psia, thus the best range lies somewhere between the two. Example pseudo-ternary diagrams for the 4-13 range are shown as Figures 4-16 and 4-17.

The same procedure was used for the JOB crude. The measured miscibility pressures at the three temperatures were bounded with calculations using IP ranges of 3-13 and 4-13. (Predicted MMP values were more nearly correct using the 3-13 range than the 4-13 range). Example calculations for the 3-13 range are given in Figures C-11 to C-12.

Finally, the calculation was repeated using the ALB crude for which there was an experimental true boiling-point curve. An IP range of 5-13 was found to correctly predict a miscibility pressure of 1250 psia at 110°F. With a range of 6-13, miscibility was predicted not to occur until a pressure of 1700 psia was reached. Phase envelopes are given at pressures of 1200 psia and 1250 psia for the 5-13 IP range in Figures 4-18 and 4-19.

Results for the three oils are summarized in Table 4-13.

As indicated, the predicted MMP is very sensitive to the interaction coefficients assigned to the lighter hydrocarbons. It was felt it would be interesting to check the effect of increasing the interaction coefficient values for the heavier hydrocarbons. For example, an IP range of 3-15 was used and results compared to those obtained using a 3-13 range. There was only a small effect in the calculated miscibility pressure.

Also, since lower interaction coefficient values were required for the Kansas crudes, the CO_2 solubility in the heavy fraction was checked. For the ABC crude, at 1450 psia, the average predicted CO_2 solubility was 62.2 mole %. The Simon and Graue correlation³⁸ predicts a CO_2 solubility of approximately 62.5 mole %. The use of lower interaction coefficients for the light hydrocarbons did not adversely affect the CO_2 solubility prediction in the heavy pseudo component.

4.4.4 Summary - Kansas Oils

Miscibility pressures were calculated for the three Kansas oils for which distillation curves had been obtained. Data for all three of the oils could not be matched using a single set of interaction coefficients. Ranges from 3-13 to 5-13 were necessary to correctly

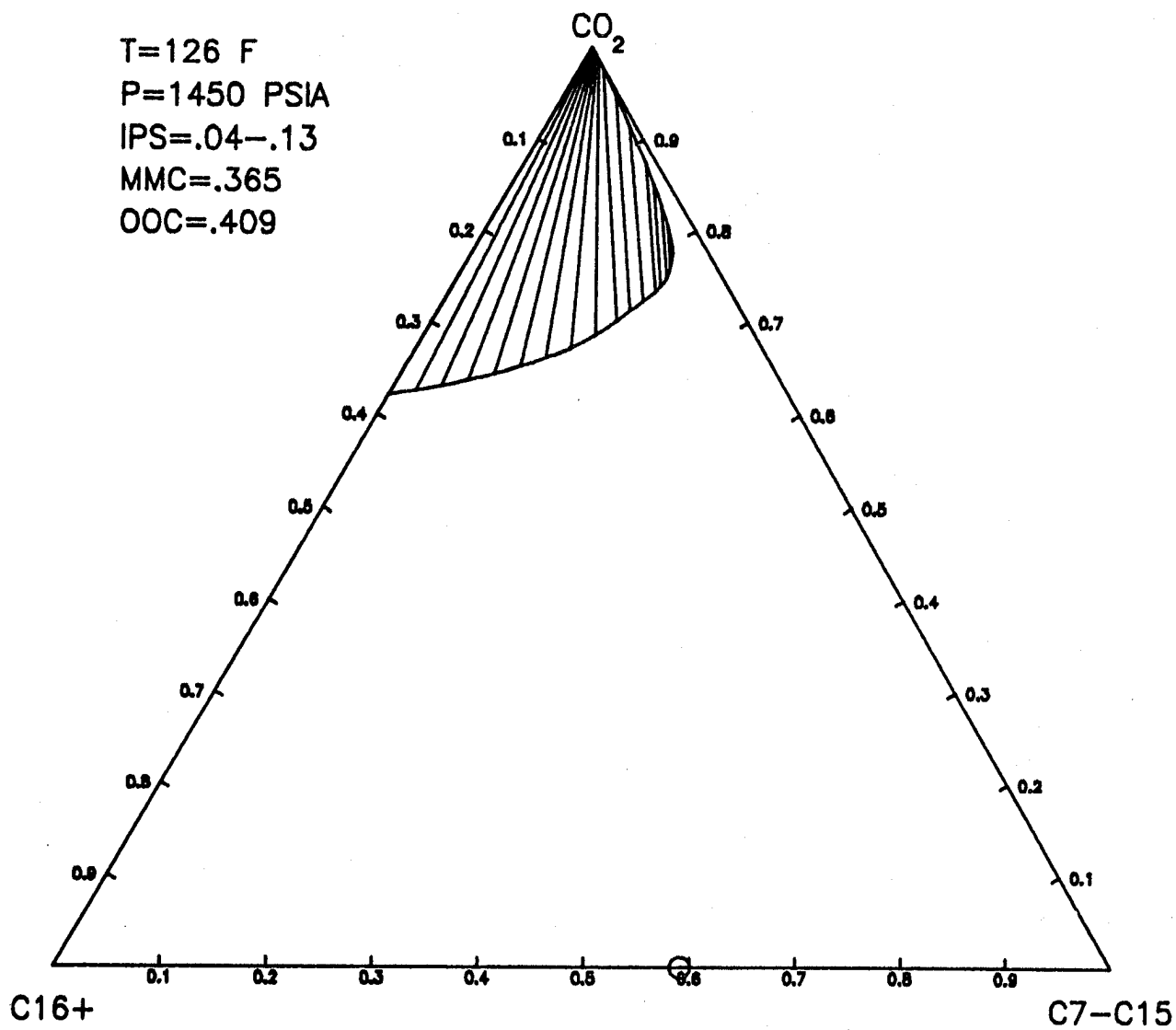


FIGURE 4-16: Calculated Ternary Phase Diagram for Abernathy Collins Crude Oil
 (IP Range 4-13, P = 1450 psia).

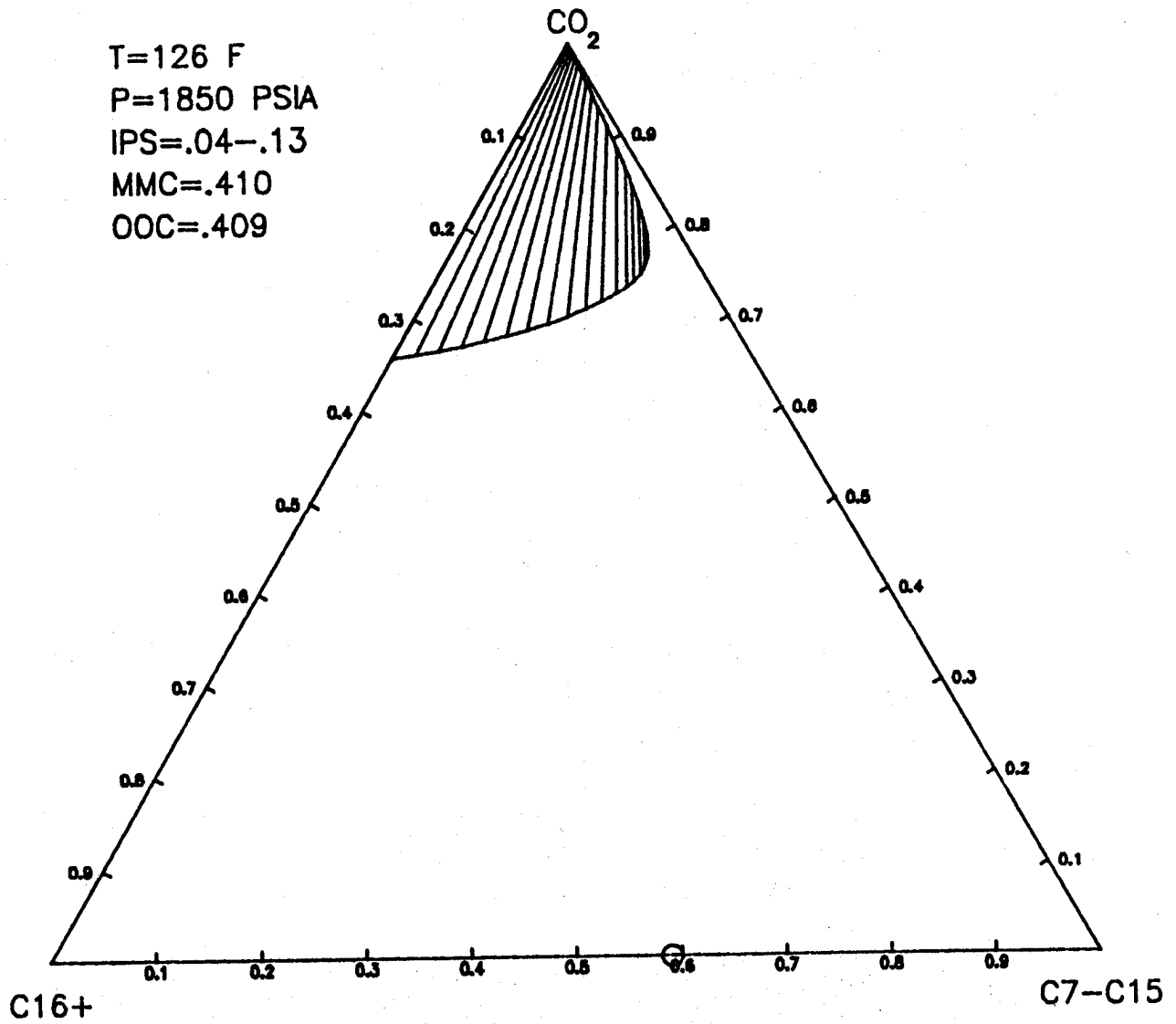


FIGURE 4-17: Calculated Ternary Phase Diagram for Abernathy Collins Crude Oil (IP Range 4-13, P = 1850 psia).

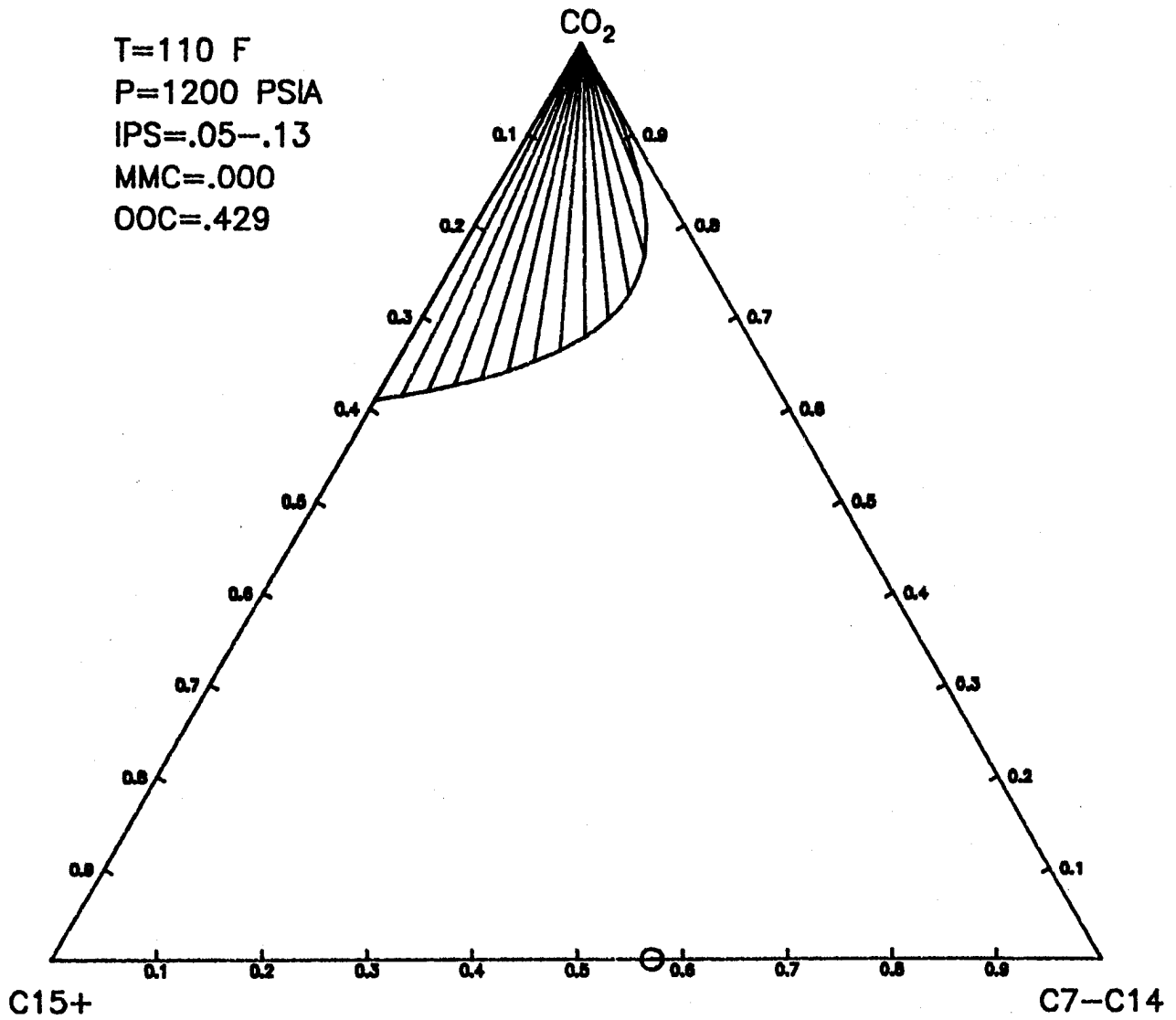


FIGURE 4-18: Calculated Ternary Phase Diagram for Albertson Crude Oil
 (IP Range 5-13, P = 1200 psia).

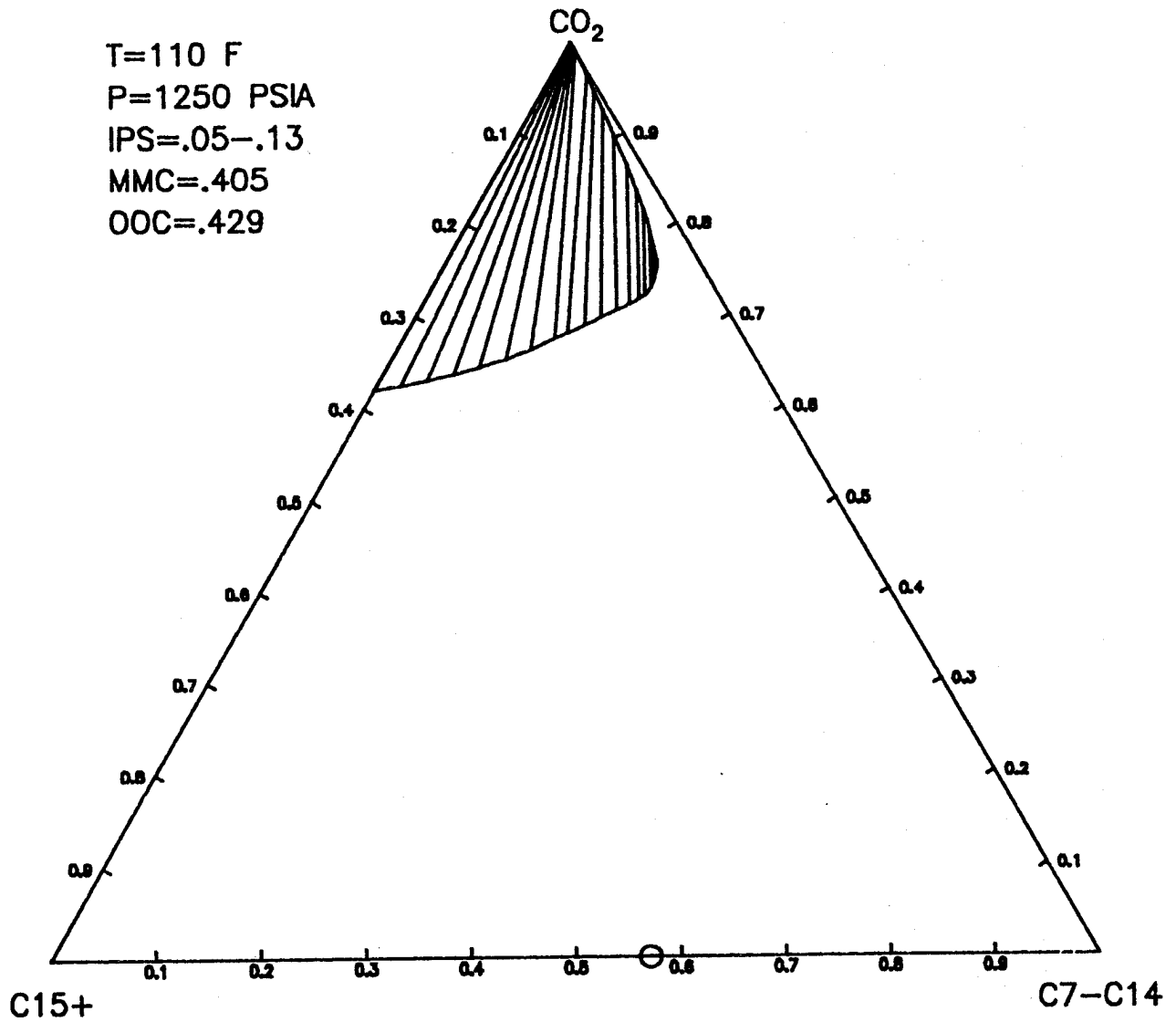


FIGURE 4-19: Calculated Ternary Phase Diagram for Albertson Crude Oil
 (IP Range 5-13, P = 1250 psia).

TABLE 4-13 - Comparison of Calculated* and Measured Miscibility Pressures

Kansas Crude Oils						
Oil	T (°F)	Exper. MMP (psia)	Calc. MMP IP Range = 3-13 (psia)	Calc. MMP IP Range = 4-13 (psia)	Calc. MMP IP Range = 5-13 (psia)	
Abernathy- Collins (ABC)	126	1540		1450	1800-1850	
Johanning B (JOB)	102 115 125	1260 1520 1720	1200 1500 1800	1750 2200 2350		
Albertson (ALB)	110	1260			1250	

* Based on Empirical or Experimental True Boiling-Point Distillation Curve

predict miscibility pressures. Use of the true boiling-point distillation curves, as compared to the ASTM D-86 distillation, allowed prediction of miscibility pressures with larger values of the interaction parameters assigned to the lighter hydrocarbon components.

4.5 Prediction of Miscibility Pressures Using Literature Correlations

Table 4-14 summarizes the miscibility pressures predicted with the various literature correlations. These values are compared with the experimental miscibility pressures for the five oils studied in this project.

The first Holm and Josendal correlation¹⁶, based on temperature and C_5+ molecular weight, consistently overpredicts the MMP. The discrepancy varies from 160 psia on the West Texas oil of Yellig and Metcalfe (150°F), to 410 psia on the ABC oil. This difference is probably related to their experimental MMP definition. They defined the slim-tube MMP based on a final recovery of 94%.

The NPC correlation is clearly unacceptable. The correlation does not predict a smooth increase in MMP with temperature. The NPC method is basically a rough screening guide.

The Yellig and Metcalfe correlation⁴³, based on temperature only, does a good job of predicting the MMP of these five oils. However, this correlation greatly underpredicts the MMP of heavier oils. For example, in this project an MMP of over 2400 psia at 106°F was measured for the SeEVERS oil, also reported in Table 4-14 (See Chapter 3). This oil has an API gravity of 30. The Yellig and Metcalf correlation predicts 1340 psia for this oil, more than 1000 psia lower than the experimental value.

The Johnson-Pollin correlation¹⁹ yields acceptable results at lower temperatures. However, the correlation predicts a change of miscibility pressure with temperature of only 10.5 psi/°F. This appears to be too small a sensitivity to temperature.

The second Holm and Josendal correlation¹⁷ in general does a better job than the initial correlation. This correlation also overpredicts the MMP but the errors are smaller. The largest difference was 210 psia on the ABC oil. This correlation was again based on a final recovery of 94%.

The final correlation is from Alston, et al.². Their experimental MMP definition was based on 90% recovery at CO₂ breakthrough. Their correlation tends to predict values of MMP that are too high. For example, their predicted MMP is 950 psia too high for the ABC oil.

TABLE 4-14 - Summary of Literature MMP Correlation Results
MMP in Psi

<u>Oil</u>	<u>T(F)</u>	<u>MMP</u>	<u>HJ#1</u>	<u>NPC</u>	<u>Y & M</u>	<u>JP</u>	<u>HJ#2</u>	<u>TEX</u>
MJ	90	1050	1350	1200	1100	1100	1250	1110
Y & M	95	1115	1400	1200	1175	1140	1300	1380
	118	1465	1700	1200	1520	1380	1600	1735
	150	1990	2150	1550	2000	1720	2200	2240
JOB	102	1260	1550	1220	1280	1290	1400	1690
	115	1520	1750	1200	1475	1430	1550	1930
	125	1720	1900	1400	1625	1530	1750	2100
ABC	126	1540	1950	1400	1640	1590	1750	2490
ALB	110	1260	1700	1200	1400	1385	1450	1920
SEEVERS	106	>2400			1340			

MJ = Maljamar

Y & M = Yellig & Metcalfe⁴³

JOB = Johanning B

ABC = Abernathy Collins

ALB = Albertson

HJ#1 = Holms & Josendal Correlation 1¹⁶

HJ#2 = Holms & Josendal Correlation 2¹⁷

NPC = National Petroleum Council¹¹

JP = Johnson and Pollin¹⁹

TEX = Alston, et al.²

CHAPTER 5

APPLICATION OF MATHEMATICAL MODELING TO PREDICT DISPLACEMENT PERFORMANCE

5.1 Introduction

Phase behavior studies and application of pseudo-ternary diagrams, as described in earlier chapters, are useful for describing the onset of miscibility conditions. Additionally, when such information is used in conjunction with a mathematical model, it is possible, conceptually, to describe general displacement performance. That is, hydrocarbon recovery can be calculated as a function of the amount of carbon dioxide injected. Also, recovery can be calculated at conditions of immiscible as well as miscible displacement. Thus, the application of mathematical models for performance prediction of the carbon dioxide displacement process was examined.

Two approaches were utilized. The first was based on a compositional simulation which uses a moving-point technique to track movement of the different phases. This approach was not successful in that material balance errors and numerical dispersion exceeded acceptable limits. The model is described in detail by Belden⁶ and will not be discussed further in this report.

The second approach utilized a modified version of the model of Orr, et al.²⁸. This model is not a fully compositional simulator, but relies on the use of ternary or pseudo-ternary diagrams to describe phase behavior. The model, as acquired, assumed carbon dioxide density was a constant and equal in all phases. This was modified, as suggested by Orr³⁰, to account for variation of carbon dioxide density between phases. The model is unsteady state and considers only one space dimension.

In this chapter the model is described briefly. Application of the model to simulate slim-tube displacements performed in this study, as well as results reported in the literature, is also described. Additional details are given by Rocha³⁵.

5.2 Description of the Mathematical Model

5.2.1 Primary Assumptions

The principal assumptions made in the development of the mathematical model are the following:

- a. Flow is in one space dimension.
- b. Four components (or pseudo components) exist and these are distributed in up to three phases. In Orr's model, provision is made for four phases, including one vapor and two liquid hydrocarbon phases. In the present study, the case of more than two

hydrocarbon phases was not considered.

- c. The porous medium has constant porosity and permeability.
- d. Capillary effects are not significant.
- e. Darcy's law describes the flow of each phase.
- f. Flow is horizontal with no gravity effects.
- g. Local thermodynamic equilibrium exists between all phases.
- h. Temperature is constant.
- i. Changes in pressure over the length of a displacement have negligible effect on phase behavior or other physical properties of the fluids.
- j. Solutions are ideal.
- k. The density of each hydrocarbon component is independent of the phase in which it exists.
- l. Carbon dioxide density is a function of the phase in which it exists.
- m. Phase behavior is described using ternary or pseudo-ternary diagrams.
- n. Dispersion is not considered in the derivation of the describing partial differential equations. However, dispersion is included in the finite difference solution of the equations through controlled numerical dispersion (Lantz²³).

5.2.2 Describing Differential Equations

The physical situation considered is displacement in one space dimension of a hydrocarbon phase by carbon dioxide. A material balance on each component, or pseudo component, in a differential element in the porous medium yields the following set of partial differential equations.

$$\frac{\partial}{\partial t} \left[\sum_{j=1}^{n_p} \rho_j S_j X_{ij} \phi \right] = - \frac{\partial}{\partial x} \left[\sum_{j=1}^{n_p} \rho_j X_{ij} V_j \right] ; \quad i = 1, 2 \dots n_c \quad (5-1)$$

where,

n_p = number of phases present

j = index denoting phase

n_c = number of components or pseudo components

i = index denoting component

X_{ij} = composition of i^{th} component in the j^{th} phase

ρ_j = density of the j^{th} phase

S_j = saturation of the j^{th} phase

V_j = velocity of the j^{th} phase

ϕ = porosity

t = time

x = distance

Equation 5-1 is a set of n_c partial differential equations. The set was modified to express flow in terms of fractional flow in each phase. The phase velocity, V_j is expressed as,

$$V_j = f_j q / A \quad (5-2)$$

where

f_j = fractional flow of phase j

q = local volumetric flow rate

A = cross sectional area open to flow

Using Darcy's law, fractional flow in the j^{th} phase is given by

$$f_j = \frac{k_j / \mu_j}{\sum_{j=1}^{n_p} k_j / \mu_j} \quad (5-3)$$

where

k_j = effective or relative permeability of the j^{th} phase

μ_j = viscosity of the j^{th} phase

Equation 5-1 is thus modified to the form

$$\frac{\partial}{\partial t} \left[\sum_{j=1}^{n_p} \rho_j S_j X_{ij} \phi \right] = \frac{-\partial}{\partial x} \left[\sum_{j=1}^{n_p} \rho_j X_{ij} f_j q / A \right] ; \quad i = 1, 2 \dots n_c \quad (5-4)$$

Alternately, a form in terms of dimensionless time and position may be specified as

$$q_{inj} \frac{\partial}{\partial \tau} \left[\sum_{j=1}^{n_p} \rho_j S_j X_{ij} \right] = \frac{-\partial}{\partial \xi} \left[\sum_{j=1}^{n_p} \rho_j X_{ij} f_{jq} \right]; \quad 1, 2 \dots n_c \quad (5-5)$$

where,

$$\tau = q_{inj} t / \phi A L$$

$$\xi = x/L$$

$$q_{inj} = \text{volumetric injection rate at } \xi = 0$$

The initial and boundary conditions are

$$\begin{aligned} Z_i &= Z_{i0} & \tau &= 0 & 0 < \xi <= 1 \\ & & i &= 1, 2 \dots n_c \end{aligned} \quad (5-6)$$

where

$$Z_i = \text{overall composition of component } i$$

$$T = T_0 \text{ (specified temperature)}$$

$$P = P_0 \text{ (specified pressure)}$$

$$\sum_{j=1}^{n_p} \rho_j X_{ij} f_{jq} = \sum_{j=1}^{n_p} \rho_j X_{ij} f_{jq} q_{inj}; \quad i = 1, 2 \dots n_c \quad (5-7)$$

$$\xi = 0 \quad \tau > 0$$

Equations 5-6 and 5-7 state that initial overall compositions of each phase are specified as are the injection rates for each component.

A number of auxilliary equations are required for solution of Equations 5-5. These are as follows:

$$\begin{aligned} \rho_j &= f_1(X_{ij}, P, T) \\ f_j &= f_2(S_j, X_{ij}, P, T) \\ X_{ij} &= f_3(P, T, Z_i) \end{aligned} \quad (5-8)$$

where,

$$f_1, f_2, f_3 = \text{general functional notation}$$

$$P = \text{system temperature}$$

$$T = \text{system pressure}$$

$$Z_i = \text{overall composition of component } i$$

Equation 5-8 implies that an equation of state or other empirical representation of phase behavior exists, and that relative permeability data are available for the porous medium.

5.2.3 Finite-Difference Approximation

Equation 5-5 is expressed in finite difference form as follows:

$$\begin{aligned} & \left[\sum_{j=1}^{n_p} \rho_j S_j X_{ij} \right]_k^{n+1} = \left[\sum_{j=1}^{n_p} \rho_j S_j X_{ij} \right]_k^n \\ & - \frac{\Delta \tau}{q_{inj} \Delta \xi} \left\{ \left[\sum_{j=1}^{n_p} \rho_j X_{ij} f_{jq} \right]_k^n - \left[\sum_{j=1}^{n_p} \rho_j X_{ij} f_{jq} \right]_{k-1}^n \right\}; \quad i = 1, 2, \dots, n_c \end{aligned} \quad (5-9)$$

where

k = index denoting spatial position

n = index denoting time level

Equation 5-9 is an explicit finite difference formulation.

5.2.4 Calculation of Phase Behavior

Phase behavior is described in terms of ternary or pseudo-ternary diagrams as discussed in Chapters 2 and 4. Thus, the model considers the system to be composed of carbon dioxide, two hydrocarbon components (or pseudo components) and water. As discussed in Chapter 2, water does not affect phase behavior other than to solubilize carbon dioxide. For a given fluid system, and for a fixed pressure and temperature, the ternary diagram representation is computed using the Soave-Redlich-Kwong (SRK) equation of state as described in Chapters 2 and 4. The possible co-existence of three hydrocarbon phases was not treated in this work.

The general form of the phase behavior on ternary or pseudo-ternary diagrams is illustrated in Figure 5-1. The system was described mathematically as illustrated in Figure 5-2. (In the figure, the numbers along the binodal curve are those assigned in the model of Orr²⁸). The binodal curve was represented by four quadratic equations. These were applied over the regions 1-3, 3-6, 6-13 and 13-15. Point 13 (8-13 on Figure 5-2) is the critical point. Thus, three quadratic equations were used to describe the bubble-point curve and one equation was used to fit the dew-point curve. The boundaries of each of the regions were extrapolated to common points T_1 , T_2 and T_3 . These points served to define tie lines within each of the three regions. That is, a line from the position of an overall composition to the appropriate intersection point (T_1 , T_2 or T_3) defines the tie line passing through the overall composition point.

The other form of phase behavior illustrated in Figure 5-1 (two pairs of immiscible components) was handled in the same manner except

———— ONE PAIR OF IMMISCIBLE COMPONENTS
- - - - TWO PAIRS OF IMMISCIBLE COMPONENTS

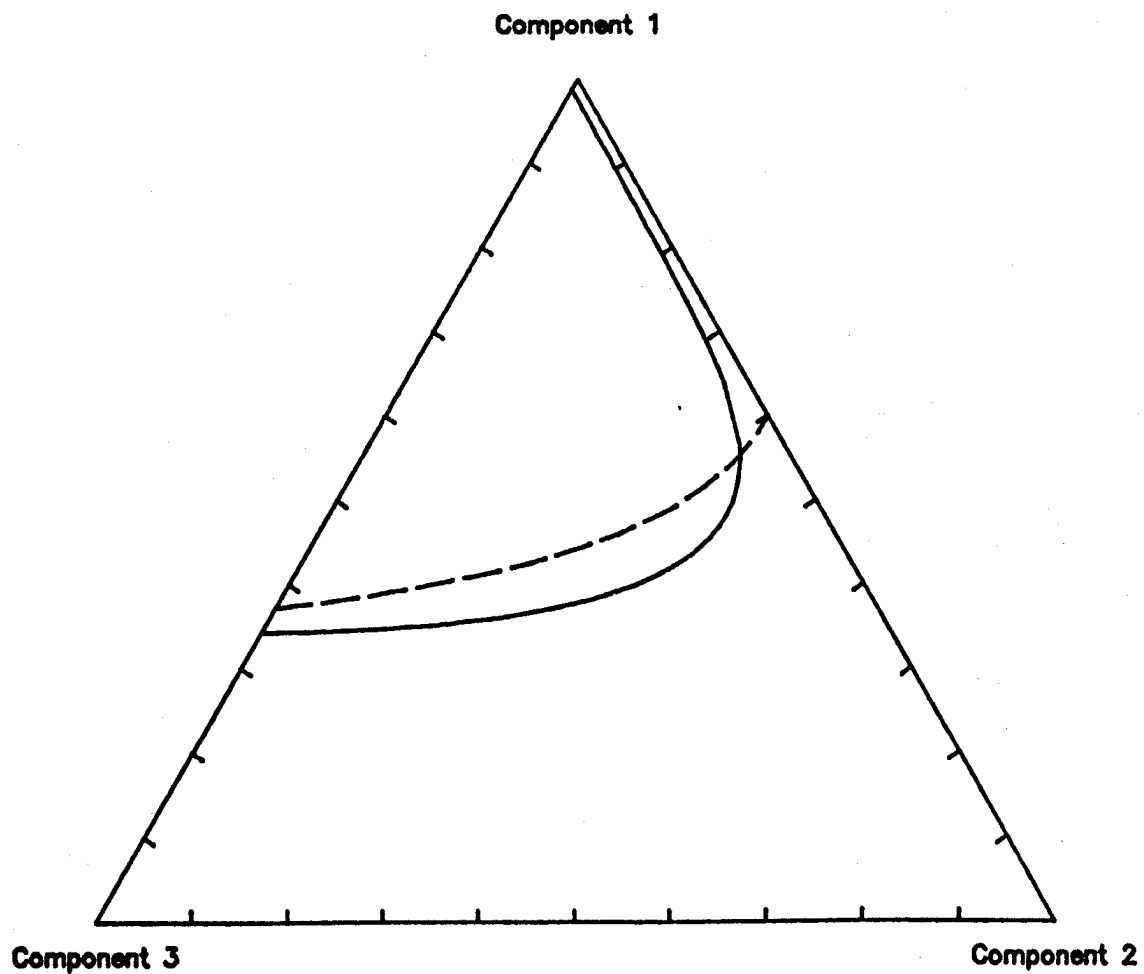


FIGURE 5-1: Phase Behavior Representation on a Ternary Diagram - Types of Phase Behavior Considered

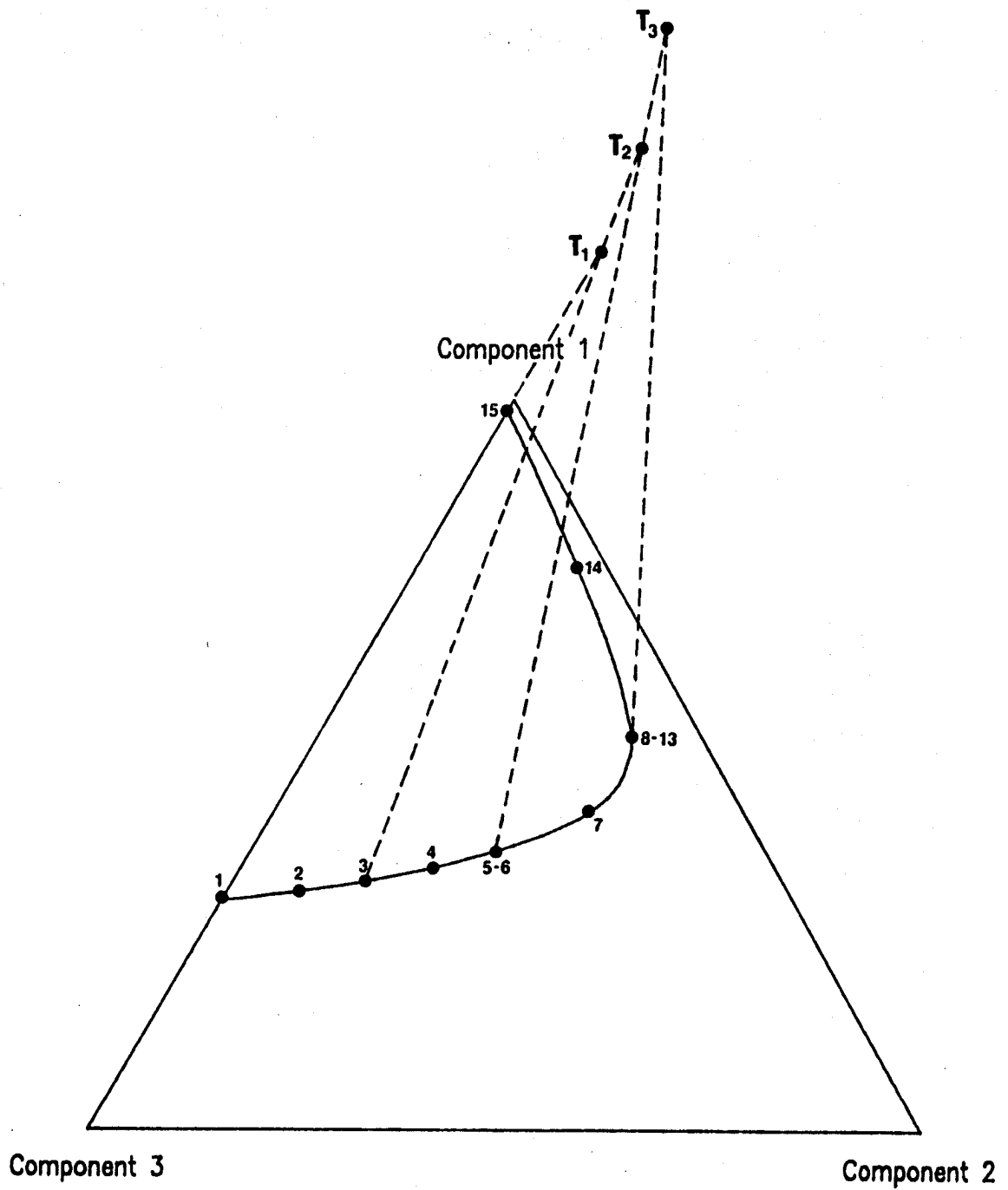


FIGURE 5-2: Representation of Phase Behavior in the Mathematical Model

Specific equations used in the model are given by Rocha³⁵.

5.2.5 Calculation of Physical Properties

Density Model

Under the assumption of ideal behavior of the CO₂-hydrocarbon mixture, the specific molar volume, v^{id} , of a mixture is given by

$$v^{id} = \sum_{i=1}^{n_c} X_i v_i \quad (5-10)$$

where,

v_i = specific molar volume of pure component i

X_i = mole fraction of component i

Considering that the density is equal to the inverse of the specific volume, from Equation 5-10, the phase density is

$$1/\rho_j' = \sum_{i=1}^{n_c} X_i / \rho_i' \quad (5-11)$$

where

ρ_j' = molar density of phase j

ρ_i' = molar density of component i

The mass density is

$$\rho_j = \frac{\sum_{i=1}^{n_c} X_{ij} M_i}{\sum_{i=1}^{n_c} X_{ij} M_i / \rho_i} \quad (5-12)$$

where

M_i = molecular weight of component i

Viscosity Model

The mathematical model used to calculate the viscosity of the mixture is the fourth root mixing rule,²² used extensively in refinery calculations.

$$\mu_j^{1/4} = \left[\sum_{i=1}^{n_c} C_{ij} / \mu_i^{1/4} \right]^{-1} \quad (5-13)$$

where

μ_j = viscosity of phase j

μ_i = viscosity of component i

C_{ij} = volume fraction of component i in phase j

Relative Permeability Model

In calculations performed in this study, only two phases were flowing. Relative permeability expressions applied were the following:

$$k_{rog} = E_{og} \left[\frac{S_l - S_{lc}}{1 - S_{lc}} \right]^{e_{og}} \quad (5-14)$$

$$k_{rg} = E_g \left[\frac{S_g - S_{gc}}{1 - S_{lc} - S_{gc}} \right]^{e_g} \quad (5-15)$$

where

k_{og} = relative permeability of the gas phase

k_{rog} = relative permeability of the oil phase in presence of a gas phase

E_g = value of k_{rg} at minimum liquid saturation (residual water plus residual oil to gas)

E_{og} = end point on the oil relative permeability curve, i.e., the relative oil permeability at zero gas saturation and connate water saturation.

S_l = liquid saturation (oil plus water)

S_g = gas saturation

S_{lc} = minimum liquid saturation (oil and water)

S_{gc} = minimum gas saturation

e_{og}, e_g = empirical curve-fit parameters

Additional details about the relative permeability model are given by Orr²⁸ and Rocha³⁵.

5.2.6 Approximation of Dispersion

Lantz²³ conducted a study of the truncation error associated with the diffusion-convection equation when it is expressed using different numerical techniques. His results are summarized in Table 5-1. The terms in the table are coefficients of the second derivative term which

following manner.

Table 5-1
Summary of Truncation Error Expressions

Difference Form		Error Forms	
Spatial	Time	Miscible	Immiscible
BD	Explicit	$(\Delta\xi - \Delta\tau)/2$	$\frac{df_w}{dS_w} (\Delta\xi - \frac{df_w}{dS_w} \Delta\tau)/2$
CD	Explicit	$\Delta\tau/2$	$-(\frac{df_w}{dS_w})^2 \Delta\tau/2$
BD	Implicit	$(\Delta\xi + \Delta\tau)/2$	$\frac{df_w}{dS_w} (\Delta\xi + \frac{df_w}{dS_w} \Delta\tau)/2$
CD	Implicit	$\Delta\tau/2$	$(\frac{df_w}{dS_w})^2 \Delta\tau/2$

A dispersion term has not been included in the describing partial differential equations (Equation 5-1) or the finite difference equations (Equation 5-9). However, because finite time step (Δt) and spatial increment (Δx) sizes are used, numerical dispersion is introduced through the error term of the finite-difference equation. By selecting appropriate Δt and Δx sizes, numerical dispersion is approximately controlled to be equal to the desired true dispersion.

In the present model, the backward difference (BD) explicit error forms were used to control dispersion.

5.2.7 Summary of Solution Procedure

The numerical procedure is summarized in the following steps. Additional details and a program listing are given by Rocha³⁵.

- The set of Equations 5-6 are solved for the term on the left-hand side for each equation, one grid node at a time. For the first time step, initial conditions are specified ($n = 0$) at all grid points and the term on the left hand side is solved for $n = 1$.
- For the calculation of a), ρ_j , X_{1j} and f_j are calculated based on the known compositions (and saturations) at all grid points.
- The solution of the Equation set 5-6 yields the overall composition at each grid node at time level $n + 1$.
- A phase behavior equilibrium calculation is made to determine the composition and saturation of each phase at each grid node.

- e. Since CO₂ density varies, depending on the phase in which the CO₂ exists, volumetric flow rate, q, varies from node to node. The flow rate is approximated as follows:

$$\Delta W_k = (\rho_a - \rho_b) V_k$$

$$\rho_{Avg_k} = (\rho_a + \rho_b)/2$$

$$\Delta q_k = \Delta W / \rho_{Avg}$$

$$q_k = q_{k-1} - \Delta q$$

where

ΔW = change in calculated mass that exists in the volume associated with grid k as a result of phase equilibrium calculation (constant P)

ρ_a = overall density of fluid in volume associated with grid k after equilibrium

ρ_b = overall density of fluid in volume associated with grid k before equilibrium

ρ_{Avg_k} = average overall density of fluid in volume associated with grid k

Δq_k = change in volumetric flow rate as a result of phase behavior calculation

q_k, q_{k-1} = volumetric flow rate at grid nodes k and k-1

- f. The procedure returns to step "a" and is repeated for the next time level.

5.3 Application of the Model to Describe Linear Displacements in Slim-Tube Apparatus

5.3.1 Introduction

The modified mathematical model of Orr²⁸ described above was used to simulate several of the slim-tube displacements discussed in Chapters 2-4. Systems modeled are listed in Table 5-2, along with displacement pressures and temperatures. The results of the simulations are discussed in what follows. Two types of comparisons are made between calculated and measured displacement performances. In the first, hydrocarbon recovery as a function of pore volumes of CO₂ injected is compared for individual experimental displacement experiments. In the second, final hydrocarbon recovery as a function of displacement

pressure is compared for several displacement experiments. This latter result is the basis for determination of MMP.

In all cases, except for the Maljamar crude oil, the phase behavior representation on ternary or pseudo-ternary diagrams was calculated using the SRK equation of state previously discussed. Interaction coefficients used are indicated in Table 5-2. For the two Kansas oils, the calculations were based on the ASTM D-86 distillation compositions. Thus, the IP ranges which best fit the MMP values were used, as discussed in Chapter 4. For the Maljamar oil, the pseudo ternary diagram reported by Orr³¹ was used.

Preliminary calculations using the model indicated that it was desirable to account for a change in CO₂ density when it was solubilized in the liquid hydrocarbon phase. Accounting for this density difference in the two phases significantly improved the agreement between calculated and experimental displacement results for the systems studied. A limited amount of data was available on apparent CO₂ density in a liquid mixture of butane-decane⁸. Using these data, the estimated apparent liquid CO₂ density was 0.55 g/cm³ at 160°F and 1400 psia. As a frame of reference, pure CO₂ density at 160°F ranges from 0.185 g/cm³ at 1200 psia to 0.277 g/cm³ at 1500 psia. In general, as will be discussed, the apparent CO₂ density in the liquid hydrocarbon phase was used as a history-matching parameter.

For the simulations involving binary hydrocarbon systems, physical properties were obtained from literature sources^{1,10,25,27,32,36,39,41}. Properties used for the crude oils are discussed in Chapter 4.

Additional details of the simulations are given by Rocha³⁵.

5.3.2 Carbon Dioxide Displacing Binary Hydrocarbon Systems 82% n-Butane, 18% n-Decane

The initial system studied was the displacement of an "oil" consisting of 82% n-butane and 18% n-decane as listed in Table 5-2. Single displacements were first simulated using the experimental apparent CO₂ liquid density of 0.55 g/cm³. The calculated recovery curves were significantly below the experimental curves over most of the displacement process. To improve the fit, apparent CO₂ liquid density was reduced, by trial and error, to 0.35 g/cm³. This improved the agreement considerably.

Comparisons between calculations and experimental results are shown in Figures 5-3 and 5-4 for pressures of 1200 and 1400 spsi. A CO₂ apparent liquid density of 0.35 g/cm³ was used for both calculations. As seen, agreement between calculated and experimental results is quite good. Similar comparisons of 1300 and 1500 psi were not as satisfactory but were within experimental error.

Table 5-2
Systems Simulated with the Carbon Dioxide Displacement
Model

Oil (mole%)	P(psi)	T(°F)	Interaction Coefficient
82% n-butane 18% n-decane	1200-1500	160	$K(\text{CO}_2\text{-C}_4) = 0.105$ $K(\text{CO}_2\text{-C}_{10}) = 0.109$ $K(\text{C}_4\text{-C}_{10}) = -0.032$
82% n-butane 18% n-butylbenzene	1100-1500	160	$K(\text{CO}_2\text{-C}_4) = 0.105$ $K(\text{CO}_2\text{-C}_{10}) = 0.090$ $K(\text{C}_4\text{-C}_{10}) = 0.049$
50% n-hexane 50% n-decane	930-1190	100	$K(\text{CO}_2\text{-C}_6) = 0.1306$ $K(\text{CO}_2\text{-C}_{10}) = 0.1100$ $K(\text{C}_6\text{-C}_{10}) = 0$
Maljamar	800-1200	90	Literature Data ³⁰
Yellig and Metcalfe	1150-1550	118	IP Range 6-13
	1650-2100	150	IP Range 6-13
Abernathy-Collins	1325-1650	126	IP Range 4-13
Johanning B	1050-1650	102	ASTM D-86 Composition IP Range 2-13
	1250-2050	125	ASTM D-86 Composition IP Range 2-13 ASTM D-86 Composition

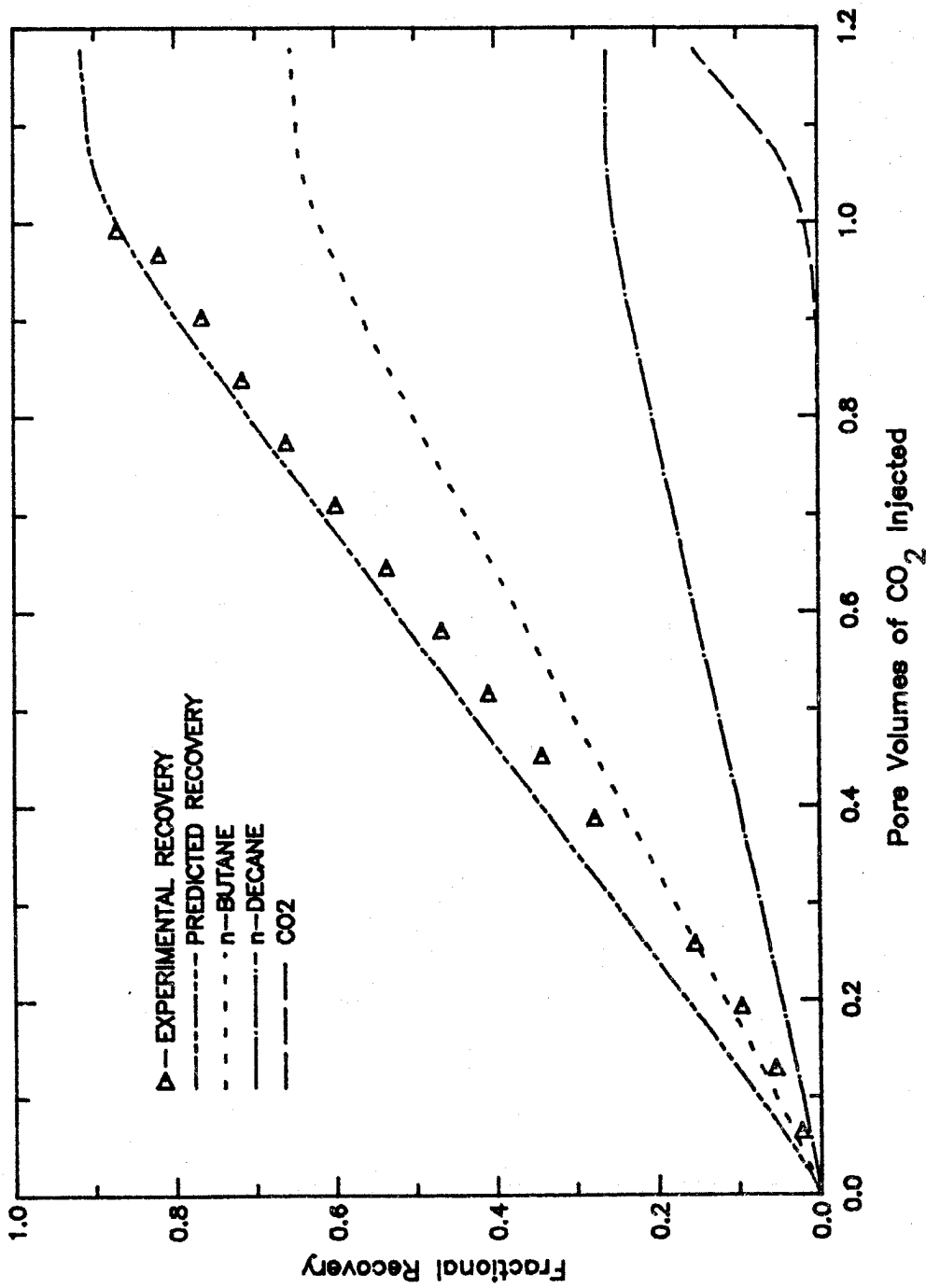


FIGURE 5-3: CO₂ Displacing Butane and Decane (P = 1200 psia, T = 160°F).

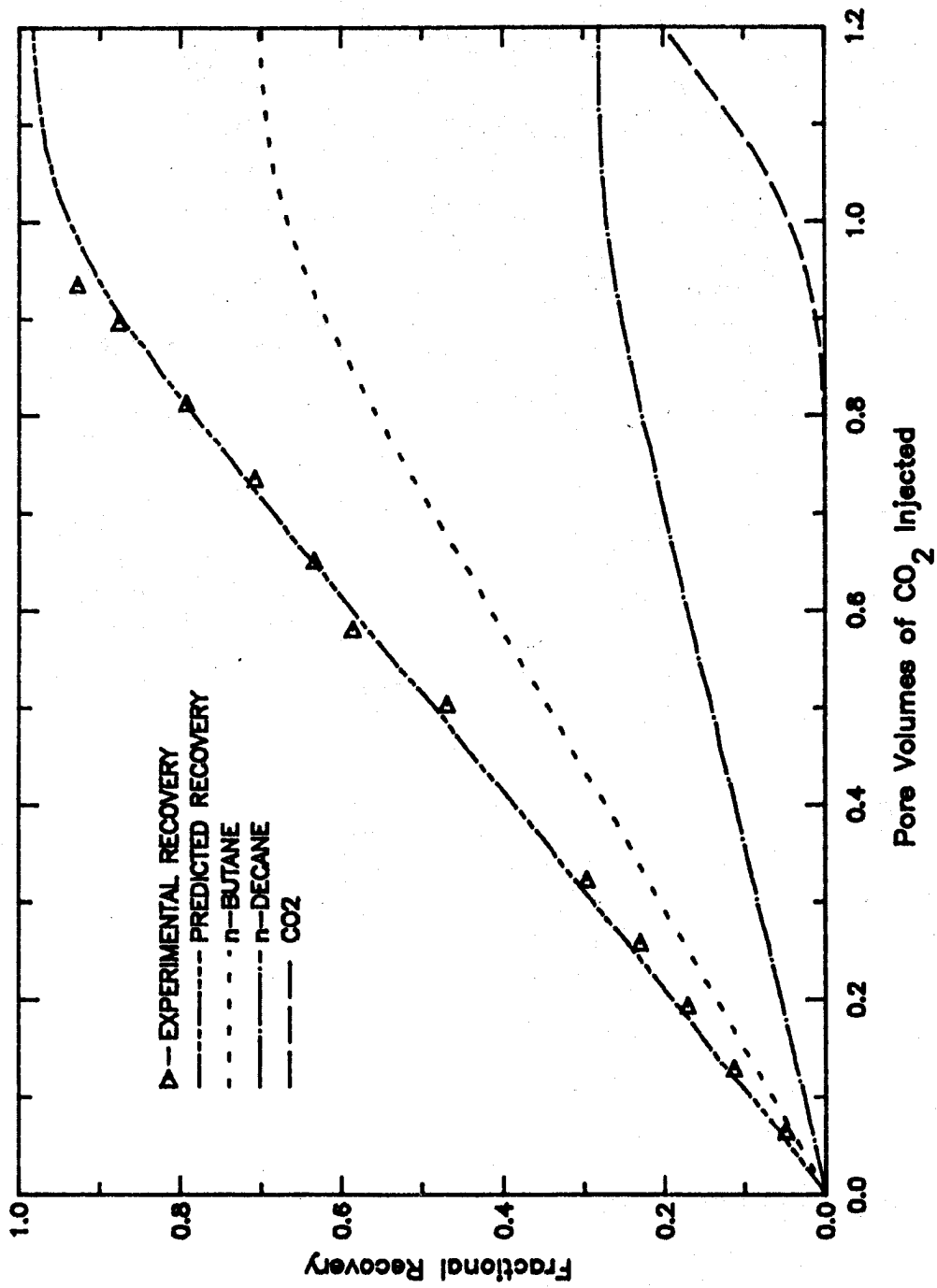


FIGURE 5-4: CO₂ Displacing Butane and Decane (P = 1400 psia, T = 160°F).

The second type of comparison, recovery versus displacement pressure, is shown in Figure 5-5. There is some uncertainty in this comparison for the following reason. Experimental recoveries reported are those at CO₂ breakthrough at the effluent of the slim-tubes. Experimentally, these recoveries were determined by passing the effluent through a solution of calcium chloride and noting the point at which calcium carbonate precipitated. However, this corresponding point is not known precisely for the calculated curve because of uncertainties about the effect of numerical dispersion and low-pressure phase behavior. Thus, two plots of predicted recovery are shown in Figure 5-5. The lower set of points corresponds to recovery at the point at which 1% of a pore volume of CO₂ has been produced. The upper set of points correspond to recovery at 1.0 pore volume of CO₂ injected. In general, agreement is satisfactory. The calculated MMP is approximately 1350 to 1400 psi and is within about 100 psi of the experimental value.

82% n-Butane, 18% n-Butylbenzene

Similar calculations to those described above were made for the hydrocarbon system consisting of 82% n-butane and 18% n-butylbenzene. For displacement pressures between 1100 and 1500 psi, the model predictions of hydrocarbon recovery versus pore volumes of CO₂ injected were in excellent agreement. A value of 0.35 g/cm³ apparent CO₂ liquid density was used as for the butane-decane system. Results are shown in Figures D-1 to D-5 in Appendix D.

Comparisons of breakthrough recoveries as a function of displacement pressure are shown in Figure 5-6. Again, two sets of calculated recovery points are presented. The lower set corresponds to hydrocarbon recovery at a point at which 1% of a pore volume of CO₂ has been produced, while the upper set represents recovery at 1.0 pore volume CO₂ injected. Predicted MMP is approximately 1300 psi, in excellent agreement with the experimental value.

50% n-Hexane, 50% n-Decane

The third binary hydrocarbon system studied was a 50:50 mixture of hexane and decane at 100°F. Pressure varied from 930 to 1110 psia. Through trial and error, an apparent CO₂ liquid density of 0.50 g/cm³ was selected for CO₂ in the liquid hydrocarbon phase.

Again, the comparison between calculated and measured displacement performance was quite good. Results are given as Figures D-6 to D-9.

Fractional recovery as a function of displacement pressure is shown in Figure 5-7. For this system, the fractional recovery reported is ultimate recovery (as opposed to breakthrough recoveries reported for the C₄-C₁₀ systems).

5.3.3 Carbon Dioxide Displacing Maljamar and Yellig and Metcalfe Oils

Properties of the oils and results taken from the literature were discussed in Chapter 4.

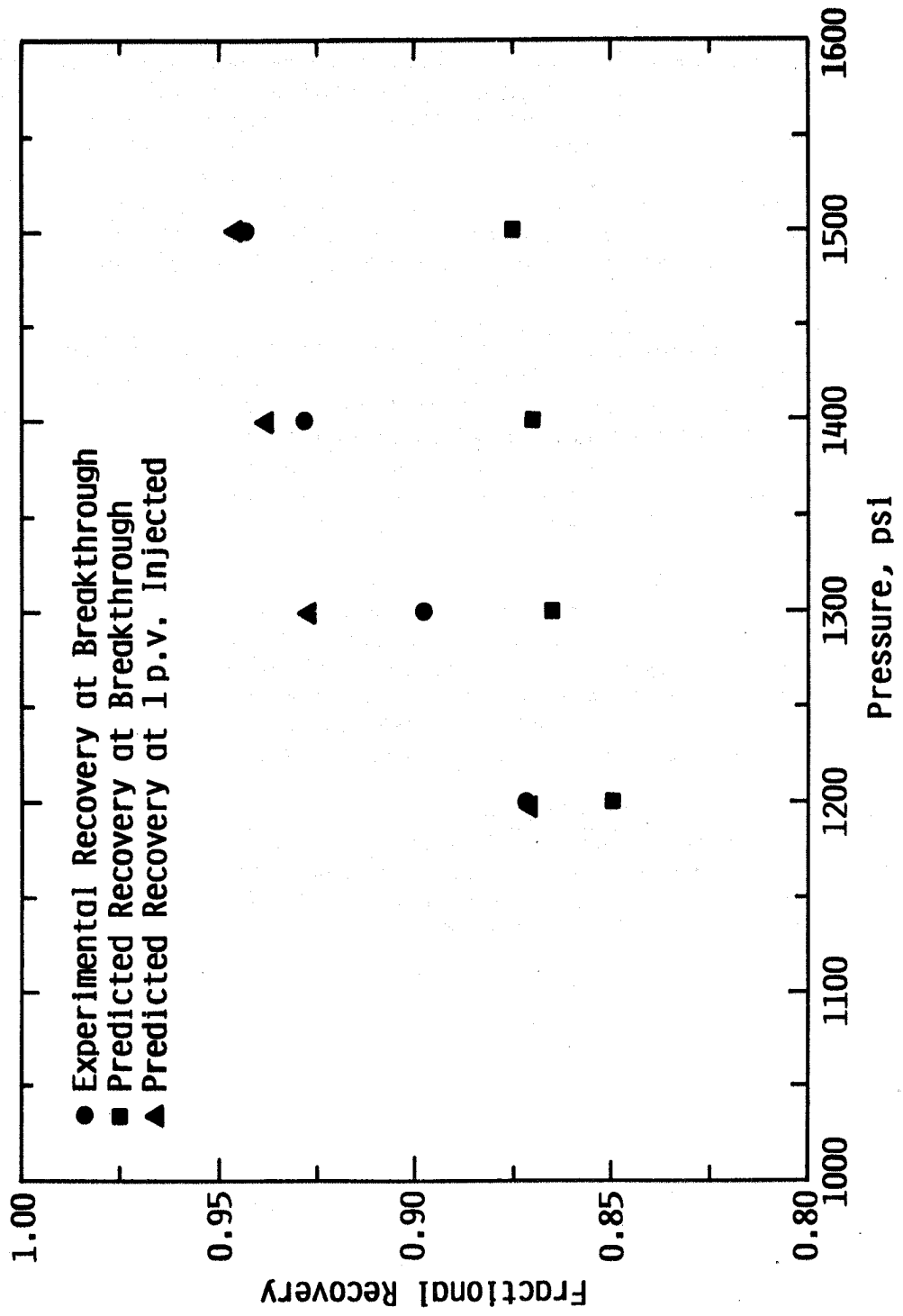


FIGURE 5-5: CO₂ Displacing 82% Butane and 18% Decane at 160°F.

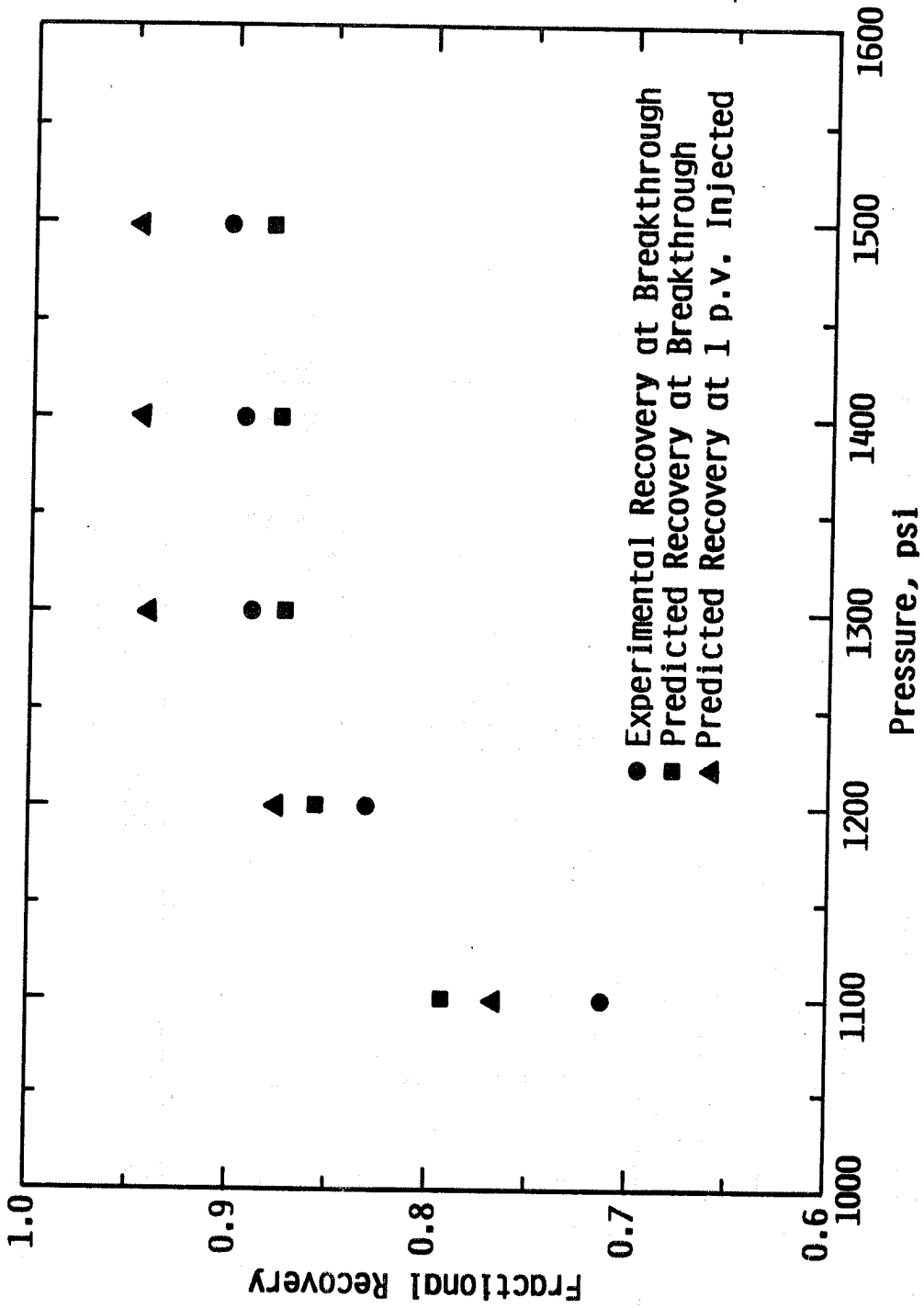


FIGURE 5-6: CO₂ Displacing 82% Butane and 18% Butylbenzene at 160°F).

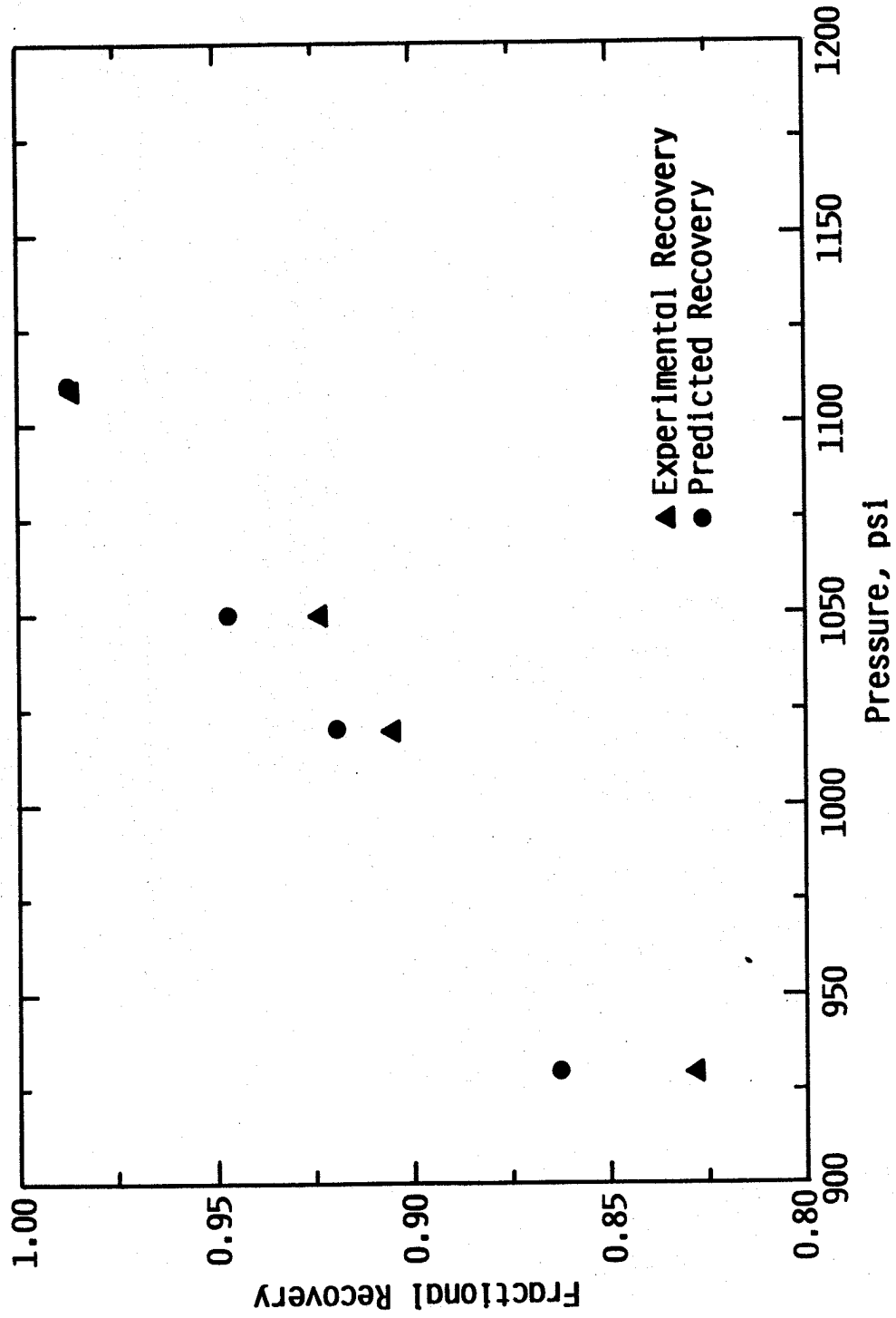


FIGURE 5-7: CO₂ Displacing 50% Hexane and 50% Decane (T = 100°F).

Maljamar Oil

For the Maljamar crude, recoveries versus pore volumes of CO₂ injected were reported at two pressures (800 and 1200 psia).³⁰ Also, a pseudo-ternary diagram for the oil was presented in the literature³¹ and was used in the model (rather than calculate a pseudo-ternary diagram using the SRK equation of state).

Comparisons between calculated and experimental displacement performance at the two pressures are presented in Figure 5-8. Apparent CO₂ liquid densities used were 0.78 g/cm³ at 1200 psia and 0.918 g/cm³ at 800 psia as suggested by Silva³⁷. As seen, the agreement is quite acceptable.

Yellig and Metcalfe Oil

The only displacement data reported for the Yellig and Metcalfe oil⁴³ were final fractional recoveries as a function of displacement pressures. However, results were simulated as for the other systems. Apparent CO₂ liquid density used was 0.7 g/cm³. Calculated ultimate recoveries are compared to experimental data at temperatures of 118°F and 150°F in Figures 5-9 and 5-10. The agreement at a temperature of 118°F is excellent. AT 150°F, agreement is good near and above the apparent MMP of 1850 psi. However, at lower pressures the mathematical model predicts recoveries that are too high.

5.3.4 Carbon Dioxide Displacing Kansas Crude Oils

Displacement calculations were made to simulate performance with two of the Kansas oils studied. As indicated in Table 5-2, these were the Abernathy-Collins and Johanning B crudes. As previously stated, compositions were based on the ASTM D-86 distillations and interaction coefficient ranges were used which yielded MMP values in agreement with experimental data (discussed in Chapter 4). Apparent liquid CO₂ density was set at 0.60 g/cm³. This was set based on a history match of the displacement data.

Abernathy-Collins Oil

Comparisons of calculated and measured displacement results at pressures of 1330 psia and 1670 psia for the Abernathy-Collins oil are shown in Figures 5-11 and 5-12. The agreement at 1330 psia is good. However, at 1670 psia the predicted recovery curve is higher than measured recovery over most of the displacement run. This latter comparison was typical of most of the calculations for both of the Kansas crudes. For these oils, the slim-tube displacements displayed very non-linear increases in recovery as a function of volume of CO₂ injected. The reason for this behavior is not clear and it could not be correctly simulated with the model.

Ultimate fractional recovery as a function of displacement pressure is shown in Figure 5-13 for the Abernathy-Collins crude. The agreement between calculated and measured recoveries is good, however, the predicted recovery is somewhat low at pressures above the MMP. The

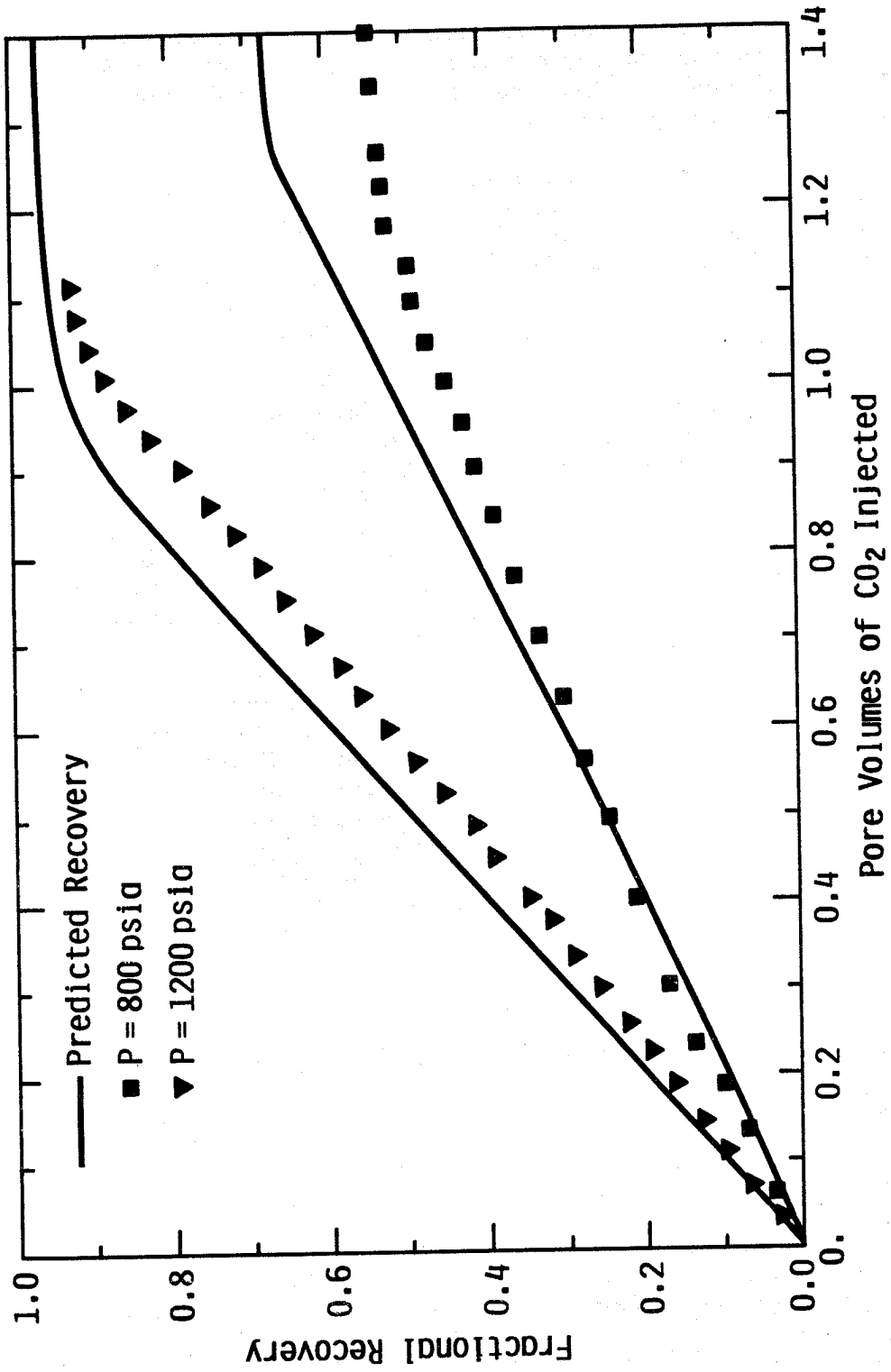


FIGURE 5-8: CO₂ Displacing Maljamar Separator Oil.

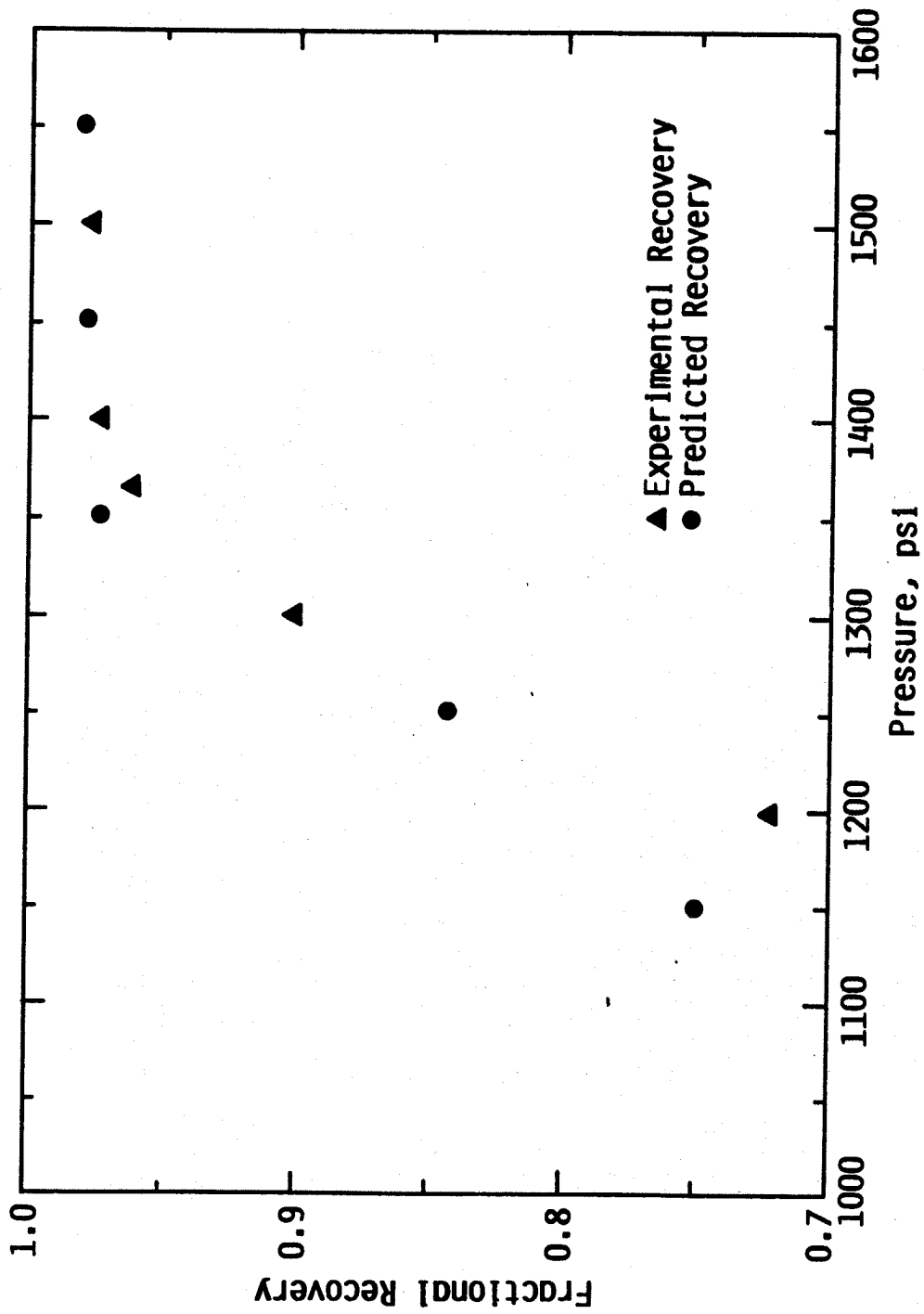


FIGURE 5-9: CO₂ Displacing Yellig and Metcalfe STO (T = 118°F).

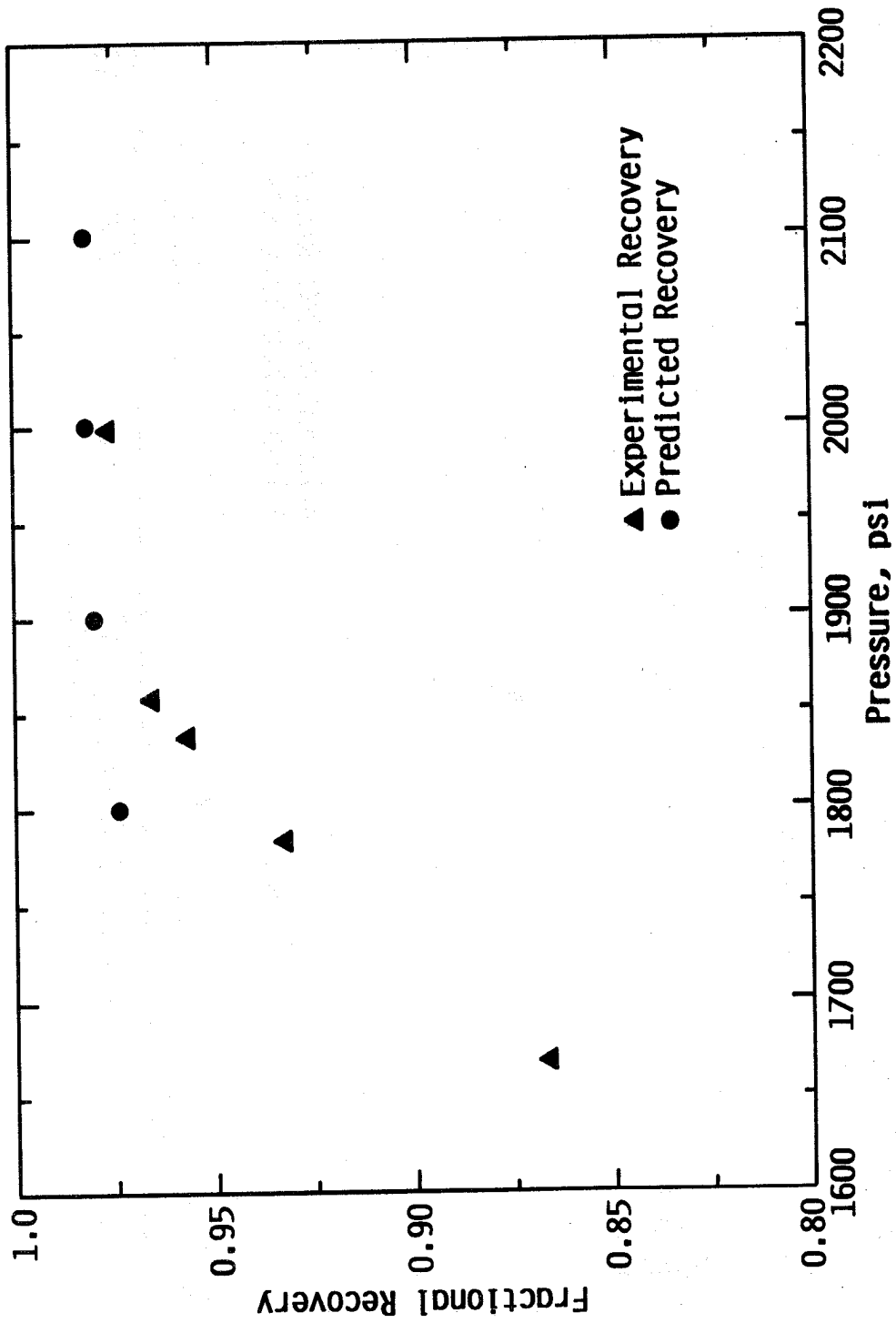


FIGURE 5-10: CO₂ Displacing Yellig and Metcalfe STO (T = 150°F).

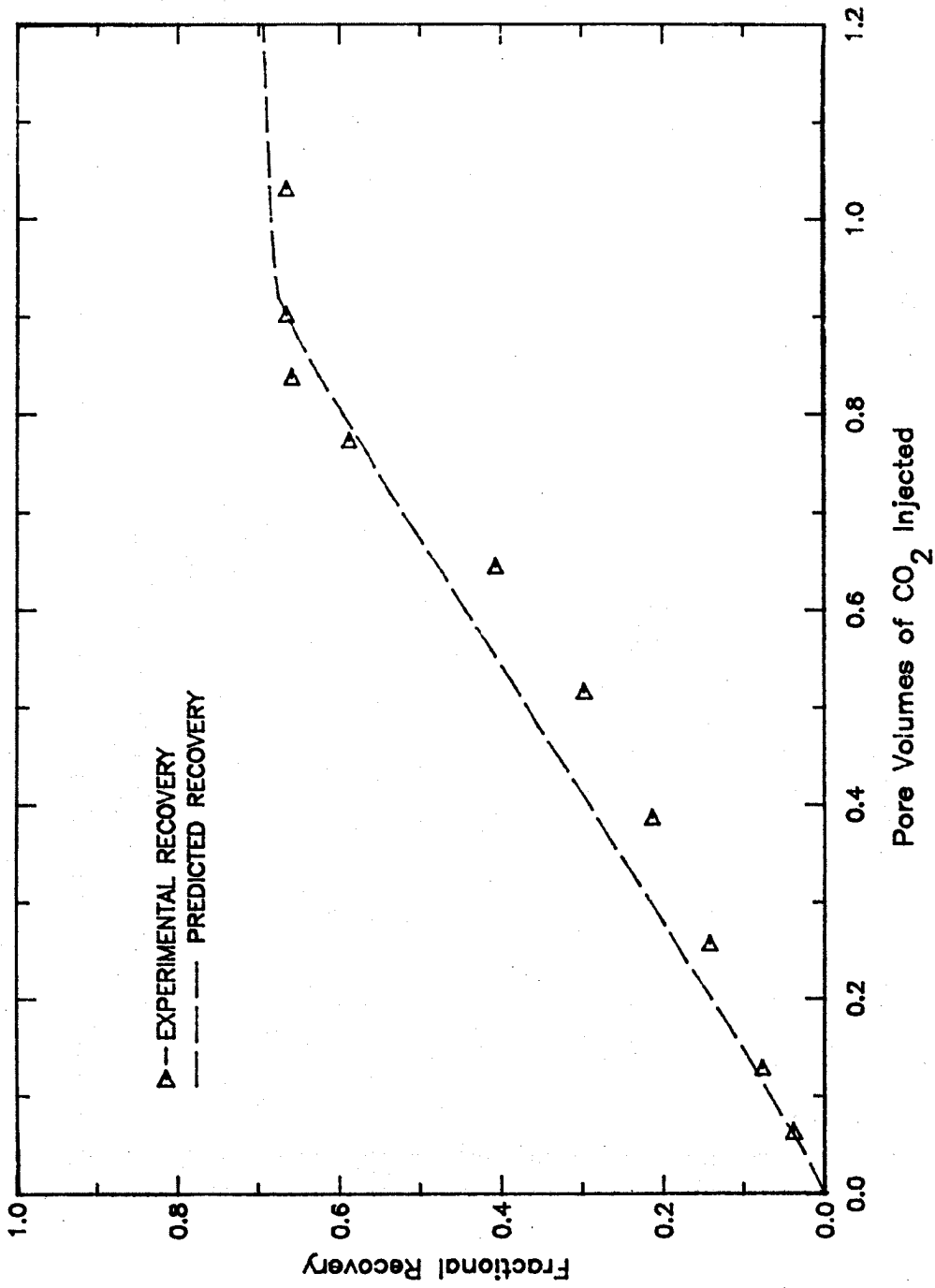


FIGURE 5-11: CO₂ Displacing Abernathy-Collins #1 (P = 1330 psia, T = 126°F).

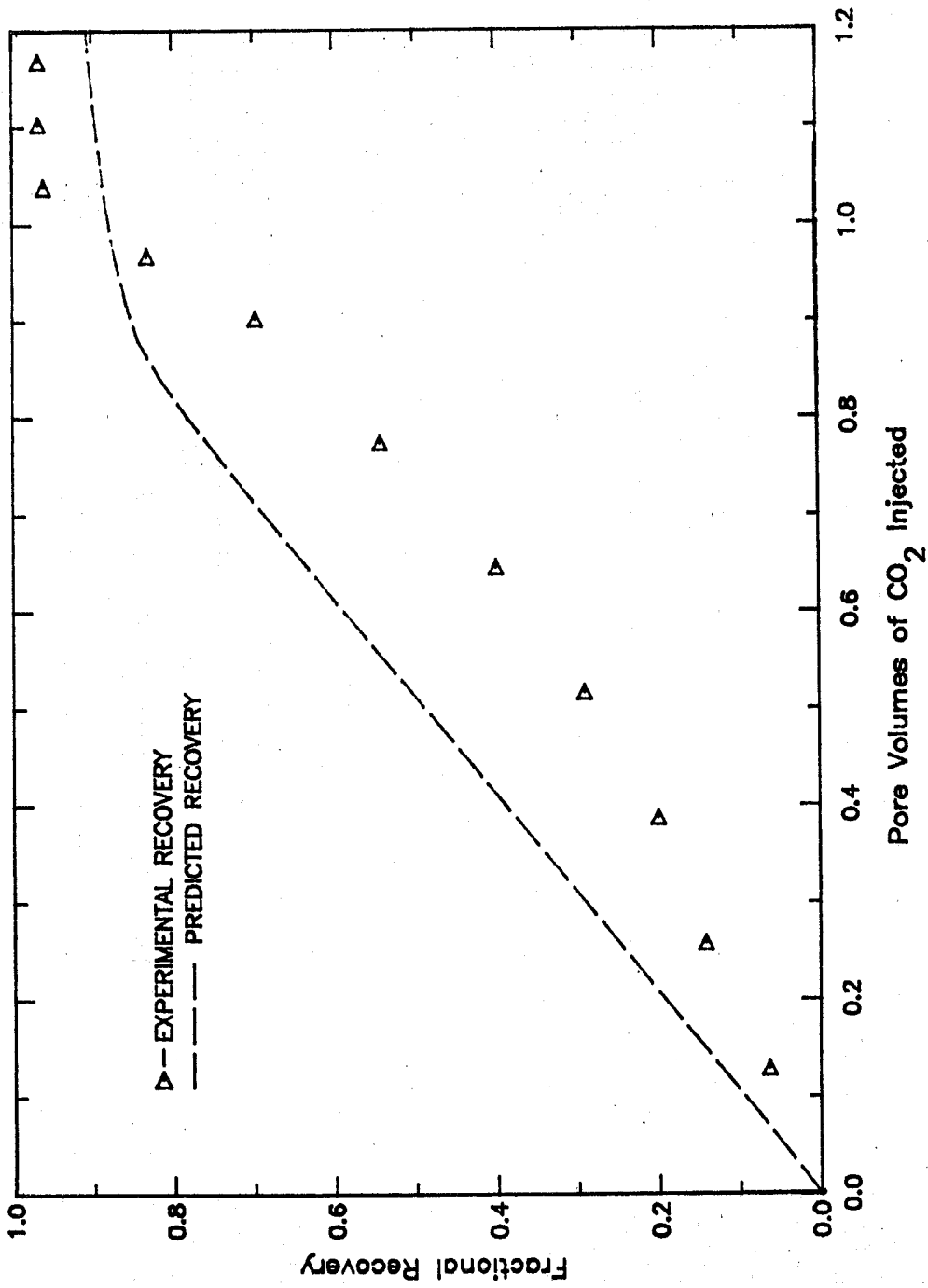


FIGURE 5-12: CO₂ Displacing Abernathy-Collins #1 (P = 1670 psia, T = 126°F).

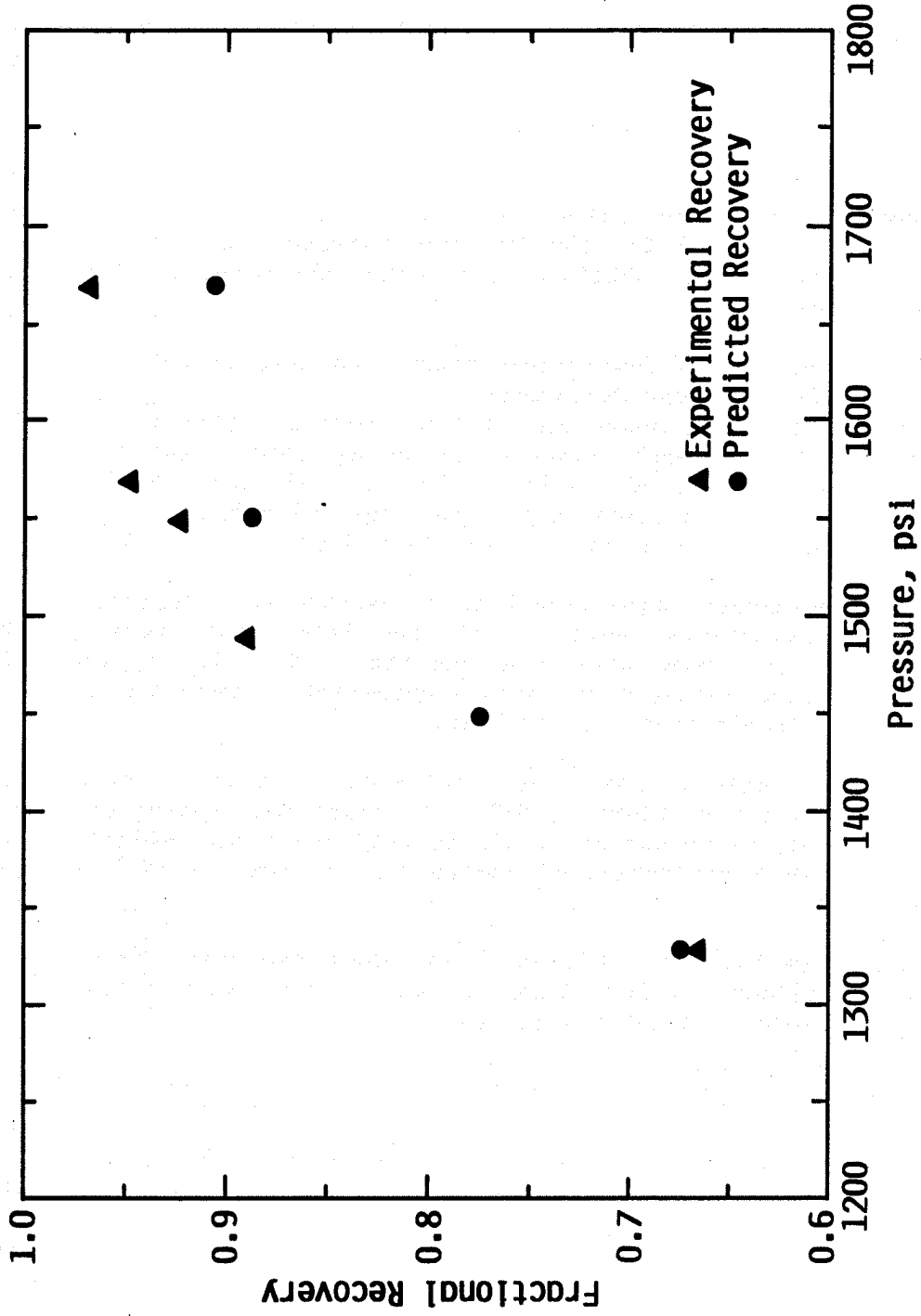


FIGURE 5-13: CO₂ Displacing Abernathy-Collins #1 (T = 126°F).

calculated MMP of 1500-1550 psia does agree with the slim-tube result. This is expected since phase behavior calculations were based on an IP range which yielded a correct MMP (Chapter 4).

Johanning B Oil

The experimental displacements with the Johanning B crude at two temperatures, 102°F and 125°F, were simulated. Typical comparisons with the data are given as Figures D-10 to D-13. For this crude the MMP was much higher than for the Abernathy-Collins and was approximately 1800 psia at 125°F.

Comparisons between calculated and measured recoveries are given in Figures 5-14 and 5-15 for the two temperatures used. Comparisons are comparable to those obtained with the Abernathy-Collins and are generally acceptable.

5.3.5 Summary of Comparisons Between Calculated and Measured Displacement Performance

The mathematical model was used to simulate slim-tube displacement performance for several systems including three binary hydrocarbon mixtures and four crude oils. In general the comparisons were satisfactory. An exception is the poor agreement between predicted and measured recoveries as a function of CO₂ injected for the Kansas crudes.

The experimental data were history matched to a degree. The phase behavior descriptions were based on data both from analytical measurements and from slim-tube results. The CO₂ apparent liquid density was also adjusted to improve agreement between the calculations and measured displacement performance.

The mathematical model does provide an estimate of performance not available from correlations of MMP. The model can predict recoveries at conditions both above and below miscibility pressure. Additionally, the model provides a prediction of recovery as a function of the amount of CO₂ injected.

All comparisons in this work were done for displacements in slim tubes. Complications introduced by use of reservoir cores or actual field conditions were not considered.

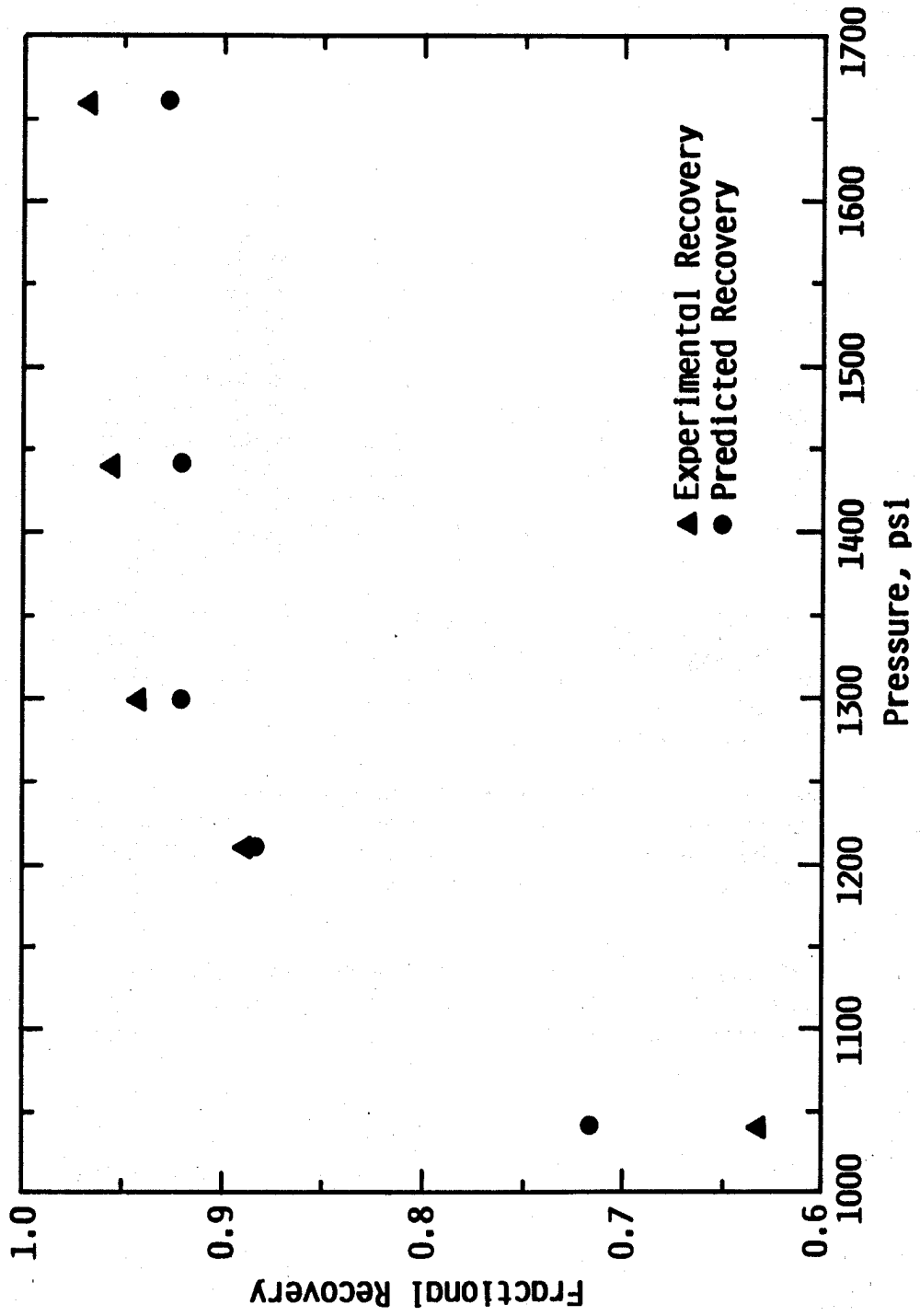


FIGURE 5-14: CO₂ Displacing Johanning B #1 (T = 102°F).

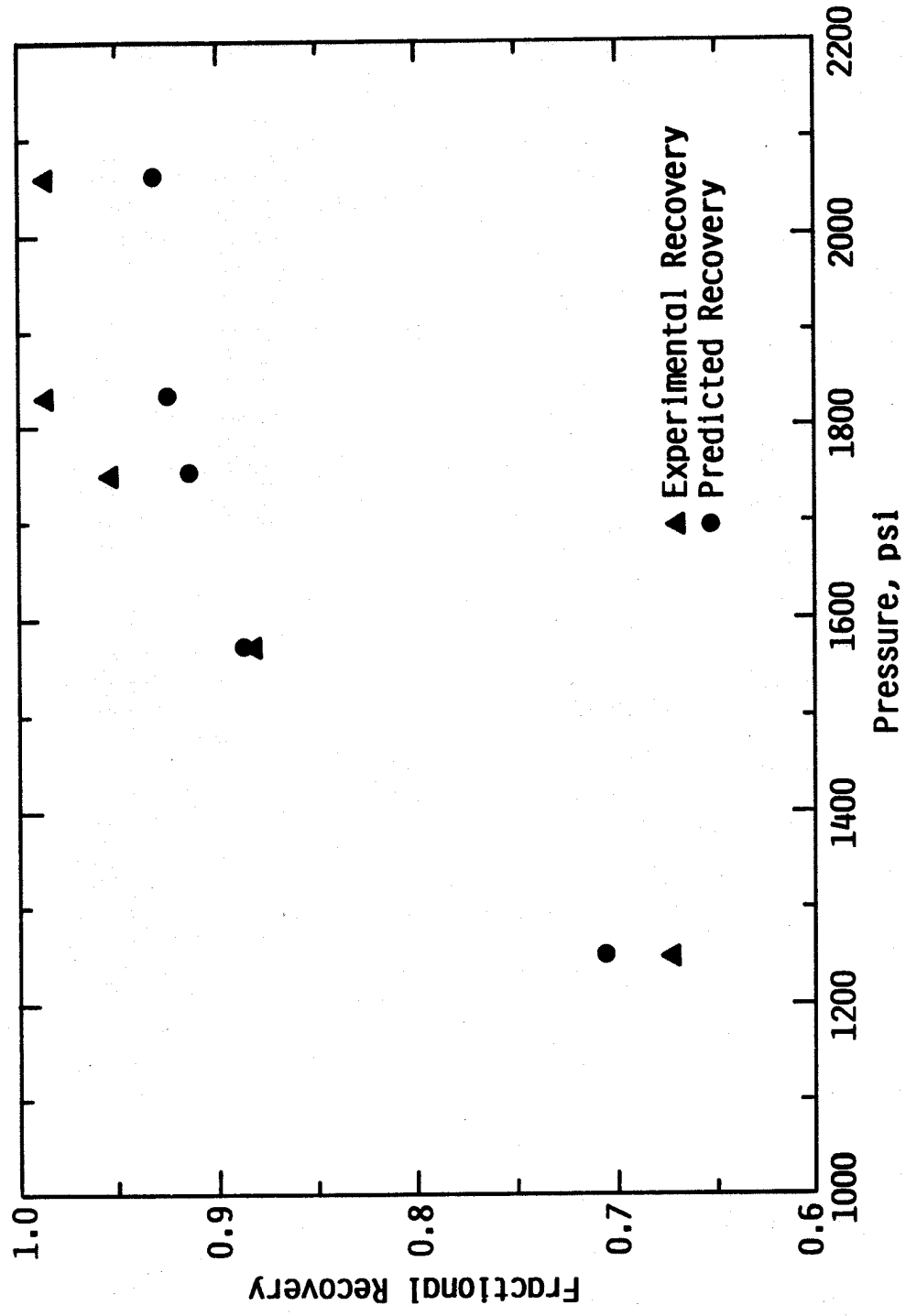


FIGURE 5-15: CO₂ Displacing Johanning B #1 (T = 125°F).

CHAPTER 6

SUMMARY OF MAJOR CONCLUSIONS

Bubble-point phase-behavior data were taken for binary and ternary systems containing carbon dioxide. These data were judged to be reliable based on agreement with similar data reported in the literature. The phase behavior was adequately simulated with the Soave-Redlich-Kwong (SRK) equation of state when suitable interaction coefficients were used. Addition of water to the CO₂-hydrocarbon system reduced the bubble point due to absorption of CO₂ into the water phase. However, when absorption of CO₂ was accounted for, phase behavior on a water-free basis was essentially unchanged from the case when no water was in the system.

Several displacements were conducted in a slim-tube apparatus. For ternary systems (CO₂ plus two hydrocarbon components), measured MMP values were in good agreement with values predicted based on known phase behavior. The presence of immobile water in these displacements had negligible effect on MMP. Miscibility pressures were measured for a number of Kansas crude oils. MMP was a function of API gravity, decreasing as API gravity increased. MMP also increased with temperature and decreased when lower molecular weight hydrocarbons were added to the crude (C₄-C₆).

The SRK equation of state was used to generate pseudo-ternary diagrams for two oils described in the literature and three Kansas crudes. For the literature oils, calculations were based on reported compositions. The Kansas oil compositions were estimated from ASTM D-86 and true boiling-point distillation curves. Literature sources were used in conjunction with the estimated compositions to calculate required physical properties.

The pseudo-ternary diagrams were applied to estimate MMP values obtained from slim-tube displacements. It was determined that the best results were obtained when a linear range of interaction coefficients were used in the SRK equation of state. The smallest coefficient in magnitude was assigned to C₅ and the largest to C₂₅⁺. When a suitable set of interaction coefficients was used in the equation of state, the MMP was correctly predicted for a given crude. The dependence of MMP on temperature was also described satisfactorily. It was not, however, possible to model adequately all of the oils studied with a single set of interaction coefficients. The value of the lowest coefficient (assigned to C₅) had to be adjusted to produce a satisfactory prediction of MMP.

The method was relatively insensitive to the specifications of the pseudo components in the pseudo-ternary representation. Also, the method was not very sensitive to the interaction coefficient value assigned to the heavy component (C₂₅⁺).

Finally, the slim-tube displacement results were simulated mathematically using a modification of a model reported in the literature. The model was based on the use of pseudo-ternary diagrams to describe phase behavior. The model, in general, did a good job of describing displacement performance in a slim-tube apparatus. History matching was required however. Use of the model allows prediction of MMP and displacement performance in an ideal porous media system.

REFERENCES

1. Agaev, N.A. and Golubev, I.F., "The Viscosity of n-Hexane in the Liquid Gaseous State at High Pressures and Different Temperatures", Akademia Nauk USSR, Doklady Physical Chemistry, 151, pp. 635-640.
2. Alston, R.B., Kokolis, G.P. and James, C.F., "CO₂ Minimum Miscibility Pressure: A Correlation for Impure CO₂ Streams and Live Oil Systems", SPE 11959, presented at the SPE 58th Annual Technical Conference and Exhibition, San Francisco, Oct. 5-8, 1983.
3. American Petroleum Institute, Technical Data Book - Petroleum Refining, 4th Ed., Washington, D.C., 1980.
4. Angus, S., Armstrong, B. and deReuck, K. M., International Thermodynamic Tables of the Fluid State, 3. Carbon Dioxide, Pergamon Press, New York (1976).
5. Azadeh, M., "Development of a Method for Evaluating Carbon Dioxide Miscible Flooding Prospects (Sand Packed Slim Tube)", M.S. Thesis, University of Kansas (1981).
6. Belden, K., "A One-Dimensional, Two-Phase Carbon Dioxide Miscible Displacement Model Using a Moving Point Routine", M.S. Thesis, University of Kansas (1984).
7. Benham, A.L., Dowden, W.E. and Kunzman, W.J., "Miscible Fluid Displacement - Prediction of Miscibility", Pet. Trans. AIME, 219, (1960) pp. 229-236.
8. Cramer, H.C., "Bubble Point Pressure Data of the CO₂-n-Butane-n-Decane, CO₂-n-Butane-n-Butylbenzene Systems at 160°F and 1400 psia", M.S. Thesis, University of Kansas (1983).
9. Daub, E., "Prediction of Carbon Dioxide-Stock Tank Oil Minimum Miscibility Pressures with the Soave-Redlich-Kwong Equation of State and A Characterization of the Oil," M.S. Thesis, University of Kansas, (1984).
10. Dolan, J.P., Starling, K.E., Lee, A.L., Eakin, B.E. and Ellington, R.T., "Liquid Fluid Viscosity of n-Butane", J. of Chem. and Engr. Data, 8, No. 3, (July 1963) pp. 396-399.
11. Enhanced Oil Recovery - An Analysis of the Potential for Enhanced Oil Recovery From Known Fields in the United States - 1976 to 2000, National Petroleum Council, Washington, D. C., December 1976.
12. Ezekwe, J.N., "Effect of Paraffinic, Naphthenic and Aromatic Distribution in the Hydrocarbon Mixture and Water on the Phase Equilibria of Carbon Dioxide-Hydrocarbon Systems Over the Temperature Range From 333°K to 366°K", Ph.D. Dissertation, University of Kansas (1982).

13. Forziati, A.F., Willingham, C.B, Mair, B.J. and Rossini, F.D., "Hydrocarbons in the Gasoline Fraction of Seven Representative Crudes, Including All the Distillates to 102°C and the Aromatics to 160°C", Bureau Standards J. Research, 32, No. 1 (1944) p. 11-37.
14. Grabowski, M.S. and Daubert, T.E., "A Modified Soave Equation of State for Phase Equilibrium Calculations. 1. Hydrocarbon Systems", Ind. and Engr. Chem. Proc. Des. Dev., 17, No. 4 (1978) pp. 443-448.
15. Grabowski, M.S. and Daubert, T.E., "A Modified Soave Equation of State for Phase Equilibrium Calculations. 2. Systems Containing CO₂, H₂S, N₂ and CO", Ind. and Engr. Chem. Proc. Des. Dev., 17, No. 4 (1978) pp. 448-454.
16. Holm, L.W. and Josendal, V.A., "Mechanisms of Oil Displacement by Carbon Dioxide", J of Pet. Tech., 26, (1974) pp. 1427-1438.
17. Holm, L.W. and Josendal, V.A., "Effect of Oil Composition on Miscible-Type Displacement by Carbon Dioxide", Soc. of Pet. Engrs. J., 22, No. 1 (1982) pp. 87-98.
18. Howat, C.S. and Swift, G.W., "A Procedure for the Design of Experiments in Fluid Phase Equilibria", Fluid Phase Equilibria, 14, (1983) pp. 289-301.
19. Johnson, J.P. and Pollin, J.S., "Measurement and Correlation of CO₂ Miscibility Pressures", SPE 9790 presented at SPE/DOE Enhanced Oil Recovery Symposium, Tulsa, Oklahoma (April 5-8, 1981).
20. Katz, D.L. and Firoozabadi, A., "Predicting Phase Behavior of Condensate/Crude-Oil Systems Using Methane Interaction Coefficients", J. Pet. Tech. (November 1978), pp. 1649-1655.
21. Kesler, M.G. and Lee, B.I., "Improved Predictions of Enthalpy of Fractions", Hydro. Proc. (March 1977), pp. 153-158.
22. Koval, E.J., "A Method for Predicting the Performance of Unstable Miscible Displacement in Heterogeneous Media", Soc. of Pet. Engr. J., 3 (June 1963), pp. 145-154.
23. Lantz, R.B., "Quantitative Evaluation of Numerical Diffusion (Truncation Error)", Soc. of Pet. Engr. J., (September 1971), pp. 315-320.
24. Laurance, D.R., "Phase Equilibria and PUT Behavior in the Systems : n-Butane, Butene-1, Butadiene-1, 3", Ph.D. Dissertation, University of Kansas (1973).
25. Lee, A.L. and Ellington, R.T., "Viscosity of n-Decane in the Liquid Phase", J. of Chem. and Engr. Data, 10, No. 4 (October 1965), pp. 346-348.

26. Metcalfe, R.S. and Yarborough, L., "Effect of Phase Equilibria on the CO₂ Displacement Mechanism", Soc. Pet. Engr. J., 19, (1979), pp. 242-252.
27. Michels, A., Botzen, A. and Schurman, W., "The Viscosity of Carbon Dioxide Between 0°C and 75°C and at Pressures Up to 2000 Atmospheres", Physica, XXIII, pp. 95-102.
28. Orr, F.M., "Simulation of the One Dimensional Convection of Four-Phase, Four-Component Mixtures", DOE Research Report, DOE/ET/12082-8, (1980).
29. Orr, F.M., Yu, A.D. and Lien, C.L., "Phase Behavior of CO₂ and Crude Oil in Low-Temperature Reservoirs", Soc. Pet. Engr. J., (August 1981), pp. 480-492.
30. Orr, F.M., Silva, M.K. and Lien, C.L., "Equilibrium Phase Compositions of CO₂-Crude Oil Mixtures...Comparison of Continuous Multiple Contact and Slim Tube Displacement Tests", SPE 10725, presented at Tulsa, Oklahoma, (April 4-7, 1982).
31. Orr, R.M. and Taber, J.J., "Displacement of Oil by Carbon Dioxide", DOE Research Report, DOE/BC/10331-4, (April 1982).
32. Reamer, H.H., Sage, B.H. and Lacey, W.N., "Phase Equilibria in Hydrocarbon Systems", Indus. and Engr. Chem., 38, No. 10 (October 1946), pp. 986-989.
33. Reid, R.C., Prausnitz, J.M. and Sherwood, T.K., The Properties of Gases and Liquids, 3rd Ed., McGraw-Hill Book Company, New York (1977), pp. 657-662.
34. Riazi, M.R. and Daubert, T.E., "Simplified Property Predictions", Hydro. Proc., (March 1980), pp. 115-116.
35. Rocha, C., "Simulation of the Carbon Dioxide Miscible Displacement Process", M.S. Thesis, University of Kansas (1985).
36. Sage, B.H., Lavender, H.M. and Lacey, W.N., "Phase Equilibria in Hydrocarbon Systems. Methane-Decane System", Indus. and Engr. Chem., 32, No. 5, (May 1940), pp. 743-747.
37. Silva, M., New Mexico Petroleum Recovery Research Center, Personal Communication.
38. Simon, R. and Graue, D.J., "Generalized Correlations for Predicting Solubility, Swelling and Viscosity Behavior of CO₂-Crude Oil Systems", J. Pet. Tech., (January 1965), pp. 102-106.
39. Stewart, D.E., Sage, B.H. and Lacey, W.N., "Volumetric Behavior of n-Hexane in the Liquid Phase", Indus. and Engr. Chem., 46, No. 12, (December 1954), pp. 2529-2531.

40. Turek, E.A., Metcalfe, R.S., Yarborough, L. and Robinson, R.L., "Phase Equilibria in Carbon Dioxide-Multicomponent Hydrocarbon Systems: Experimental Data and an Improved Prediction Technique", SPE 9231, presented at the 55th Annual Fall Technical Conference and Exhibition, Dallas, Texas (September 21-24, 1980).
41. Vargaftik, N.B., Tables on the Thermophysical Properties of Liquid and Gases, 2nd Ed., John Wiley and Sons, pp. 357.
42. Whitson, C.H., "Effect of Physical Properties Estimation on Equation-of-State Predictions", SPE 11200, presented at the SPE 57th Annual Technical Conference, New Orleans, (September 26-29, 1982).
43. Yellig, W.F. and Metcalfe, R.S., "Determination and Prediction of CO₂ Minimum Miscibility Pressures", J. of Pet. Tech., (January 1980), pp. 160-168.
44. Yellig, W.F., Personal Communication, 1984.

Table A-2

Bubble-point Pressures for CO₂-Ethylbenzene at
140, 170, 200°F

<u>Mixture Mole Fraction, CO₂</u>	<u>Bubble-point Press, kPa*</u>
140°F	
0.315	4592
0.396	5619
0.442	6253
0.521	7302
0.552	7722
0.750	9784
0.885	10914
170°F	
0.329	5399
0.450	7495
0.544	9046
0.638	10563
0.721	11776
0.830	13031
200°F	
0.297	5571
0.398	7563
0.494	9556
0.596	11534
0.694	13293
0.801	14872

* To convert from kPa to psi multiply by 0.14504

Table A-3

Bubble-point Pressures for CO₂-Propylbenzene at
140, 170, 200°F

<u>Mixture Mole Fraction, CO₂</u>	<u>Bubble-point Press, kPa*</u>
140°F	
0.321	4454
0.396	5509
0.507	7102
0.619	8667
0.700	9681
0.810	10721
0.885	11225
170°F	
0.349	5763
0.406	6743
0.506	8549
0.601	10259
0.712	12052
0.863	13858
200°F	
0.345	6405
0.398	7508
0.504	9818
0.582	11527
0.697	13858
0.781	15368

* To convert from kPa to psi multiply by 0.14504

Table A-4

Bubble-point Pressures for CO₂-Cyclopentane at 140, 170, 200°F

<u>Mixture Mole Fraction, CO₂</u>	<u>Bubble-point Press, kPa*</u>
	140°F
0.344	4992
0.398	5592
0.500	6612
0.602	7501
0.703	8315
0.781	8915
	170°F
0.348	5957
0.452	7322
0.547	8480
0.638	9384
0.752	10397
	200°F
0.348	6729
0.398	7529
0.494	8970
0.620	10597
0.673	11238

* To convert from kPa to psi multiply by 0.14504

Table A-5

Bubble-point Pressures for CO₂-Cyclohexane at
140, 170, 200°F

<u>Mixture Mole Fraction, CO₂</u>	<u>Bubble-point Press, kPa*</u>
140°F	
0.300	4757
0.402	6047
0.503	7122
0.605	8019
0.802	9432
170°F	
0.300	5530
0.395	7026
0.504	8542
0.710	10852
0.806	11604
200°F	
0.298	6226
0.400	8081
0.496	9659
0.602	11204

* To convert from kPa to psi multiply by 0.14504

Table A-6

Bubble-point Pressures for CO₂-Methylcyclohexane at
140, 170, 200°F

<u>Mixture Mole Fraction, CO₂</u>	<u>Bubble-point Press, kPa*</u>
140°F	
0.298	4337
0.396	5619
0.499	6846
0.702	8880
0.814	9770
170°F	
0.286	4826
0.399	6585
0.501	8108
0.600	9466
0.690	10542
200°F	
0.267	5054
0.402	7543
0.503	9322
0.608	11080
0.711	12541

* To convert from kPa to psi multiply by 0.14504

Table A-7

Bubble-point Pressure Reduction Due to the Presence of Water

CO₂-n-Butane at 160°F

<u>Mole Frac</u> <u>CO₂</u>	<u>Vol. of Water</u> <u>cm³</u>	<u>% Vol. of Water</u> <u>at Bubble Point</u>	<u>Bubble Point</u> <u>Press. Reduction (kPa)*</u>
0.189	50.13	23.39	144.79
0.249	50.13	27.35	165.47
0.295	28.69	17.02	75.84
0.349	50.13	32.51	227.53
0.401	73.66	42.34	448.16
0.401	134.48	57.34	779.11
0.401	175.32	70.05	1358.27
0.415	30.86	24.06	193.05
0.493	4.87	5.14	27.58
0.493	9.38	9.50	68.95
0.493	32.78	26.95	227.53
0.493	61.10	40.88	406.79
0.493	87.76	49.88	606.74
0.507	28.88	22.73	151.68
0.596	50.13	39.56	351.63
0.607	29.11	22.22	165.47

* To convert from kPa to psi multiply by 0.14504

Table A-8

Bubble-point Pressure Reduction Due to the Presence of Water

CO₂-n-Decane at 160°F

<u>Mole Frac</u> <u>CO₂</u>	<u>Vol. of Water</u> <u>cm³</u>	<u>% Vol. of Water</u> <u>at Bubble Point</u>	<u>Bubble-Point</u> <u>Press. Reduction (kPa)*</u>
0.253	9.285	4.68	48.26
0.298	9.285	5.37	68.95
0.403	9.285	6.92	137.90
0.504	9.285	8.09	186.16
0.599	9.285	9.15	158.58
0.705	9.858	10.00	186.16
0.705	22.815	22.57	386.11
0.705	45.912	37.06	744.63
0.705	69.995	47.33	1192.79
0.705	103.893	57.11	1861.58
0.705	152.343	66.27	2737.22
0.709	9.285	10.23	124.11
0.810	9.285	11.06	96.53

* To convert from kPa to psi multiply by 0.14504

Table A-9

Bubble-point Pressure Due to the Presence of Water

CO₂-Toluene at 160°F

Mole Frac <u>CO₂</u>	Vol. of Water <u>cm³</u>	% Vol. of Water <u>at Bubble Point</u>	Bubble Point <u>Press. Reduction (kPa)*</u>
0.398	9.24	8.92	165.47
0.398	49.61	36.96	689.48
0.398	108.42	56.15	1385.85
0.398	149.37	63.77	1854.69
0.511	28.17	26.65	530.90
0.511	46.64	37.73	786.00

* To convert from kPa to psi multiply by 0.14504

Table A-10

Bubble-point Pressure Reduction Due to the Presence of Water

CO₂-n-Butane at 100°F

<u>Mole Frac</u> <u>CO₂</u>	<u>Vol. of Water</u> <u>cm³</u>	<u>% Vol. of Water</u> <u>at Bubble Point</u>	<u>Bubble-Point</u> <u>Press. Reduction (kPa)*</u>
0.558	11.46	12.43	62.05
0.558	77.62	49.40	413.69
0.558	122.29	60.82	689.48
0.558	151.54	65.92	848.06
0.680	42.19	35.37	186.16
0.680	89.83	54.15	427.47
0.680	83.15	50.00	420.58
0.879	150.79	65.23	827.37

* To convert from kPa to psi multiply by 0.14504

Table A-11

Bubble-point Pressures at 160°F

Data Point	mole fraction					P	Uncert.	Density
Number	<u>x(1)</u>	<u>x(2)</u>	<u>x(3)</u>	<u>x(4)</u>	<u>x(5)</u>	<u>psia</u>	<u>mol. fr.</u>	<u>g/cm³</u>
1	0.670	0.000	0.330			1386	0.003	0.735
2	0.068	0.068	0.258			1415	0.002	0.712
3	0.681	0.138	0.180			1395	0.002	0.695
4	0.712	0.200	0.088			1387	0.002	0.643
5	0.754	0.206	0.040			1399	0.002	0.546
6	0.753	0.207	0.040			1392	0.002	0.548
7	0.580	0.000		0.420		1399	0.010	0.815
8	0.597	0.090		0.313		1399	0.002	0.765
9	0.646	0.186		0.169		1388	0.002	0.709
10	0.702	0.219		0.079		1389	0.002	0.637
11	0.755	0.206		0.039		1413	0.002	0.556
12	0.752	0.208		0.040		1409	0.002	0.556
13	0.637	0.000		0.363		1541	0.007	0.815
14	0.614	0.000			0.386	1420	0.006	0.859
15	0.633	0.108			0.259	1406	0.002	0.791
16	0.667	0.178			0.156	1389	0.002	0.719
17	0.713	0.200			0.087	1404	0.002	0.661
18	0.782	0.192			0.025	1400	0.002	0.501
19	0.786	0.188			0.026	1402	0.002	0.497
20	0.671	0.000			0.329	1554	0.006	0.861
21	0.634	0.184			0.183	1339	0.002	0.737
22	0.754	0.205	0.0207	0.0162	0.0041	1404	0.002	0.558

where

x(1)	Carbon Dioxide
x(2)	n-Butane
x(3)	n-Decane (P)
x(4)	n-Butylcyclohexane (N)
x(5)	n-Butylbenzene (A)

APPENDIX B

ADDITIONAL SLIM-TUBE MISCIBILITY PRESSURE MEASUREMENTS

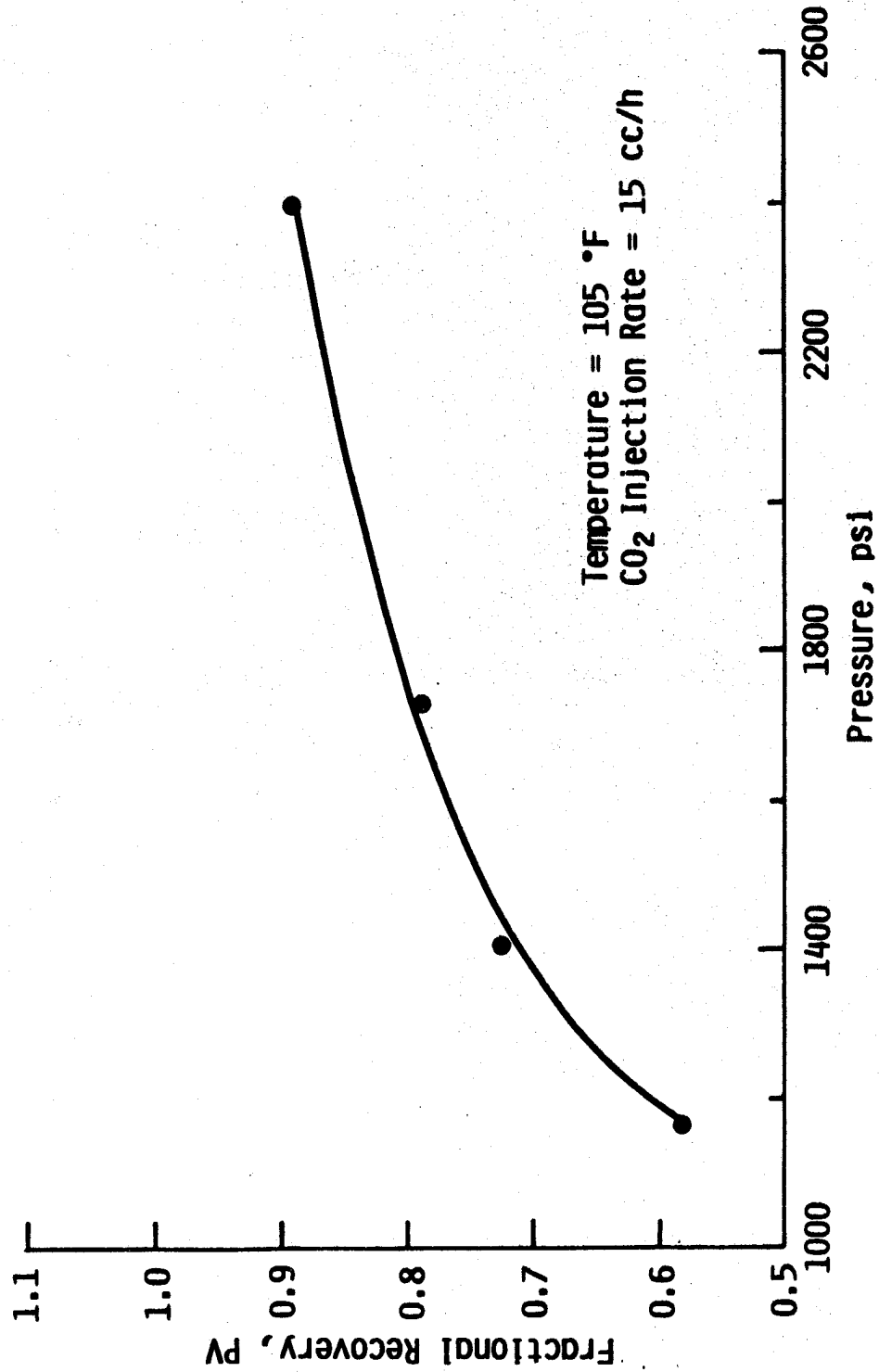


FIGURE B-1: Slim Tube Results - Seevers Crude Oil.

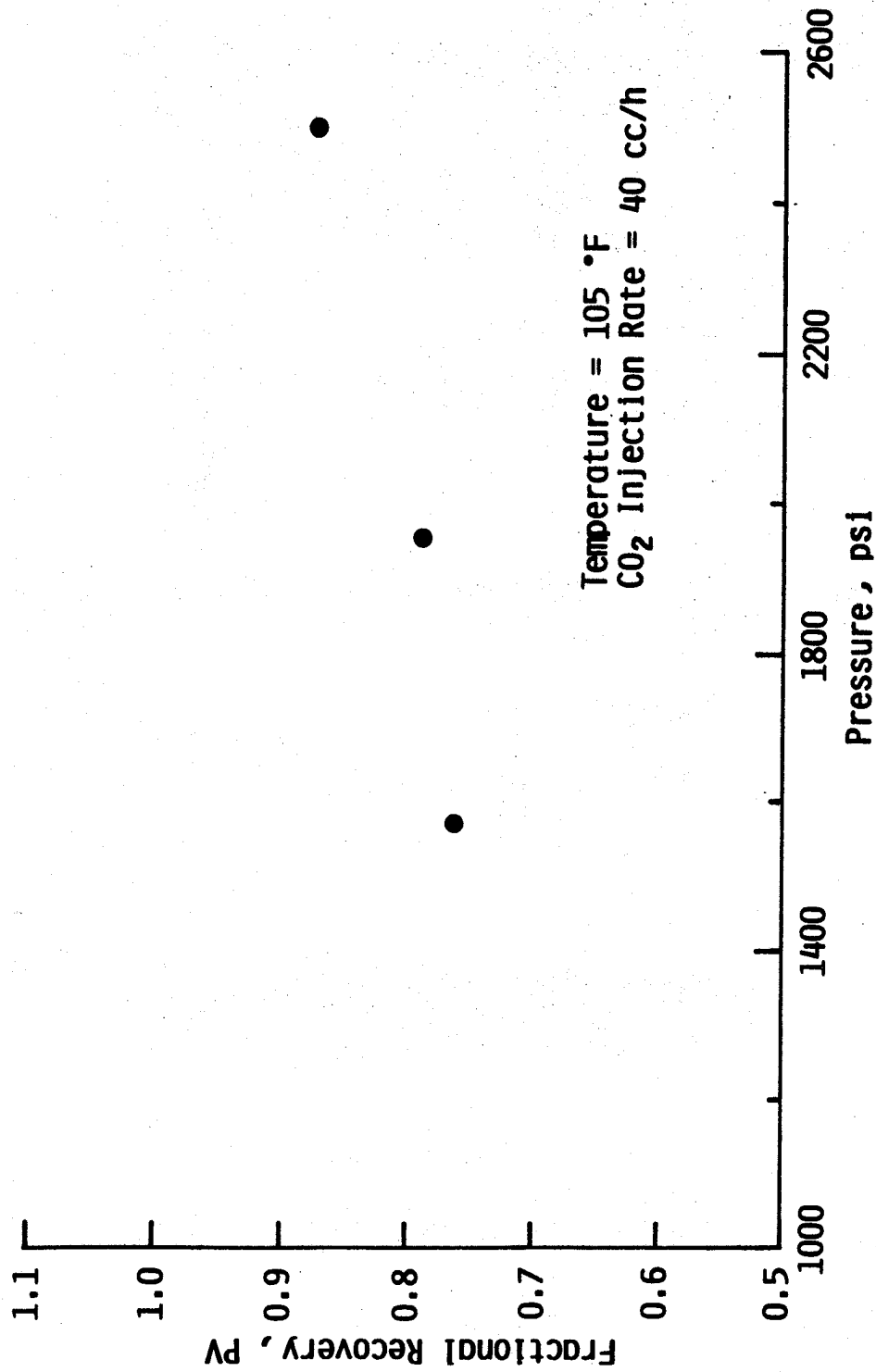


FIGURE B-2: Slim Tube Results - Newcombe Crude Oil.

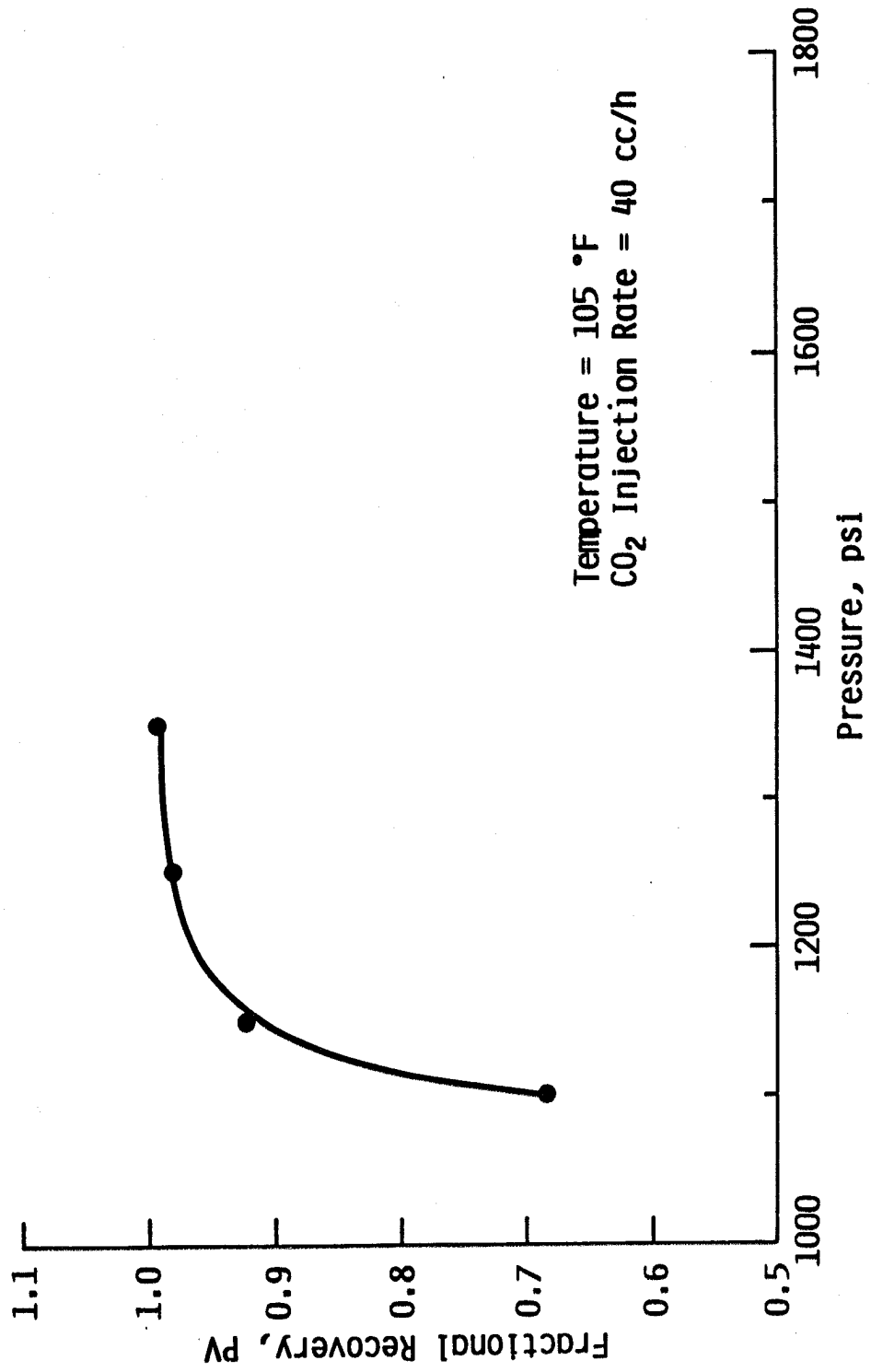


FIGURE B-3: Slim Tube Results - Albertson Crude Oil.

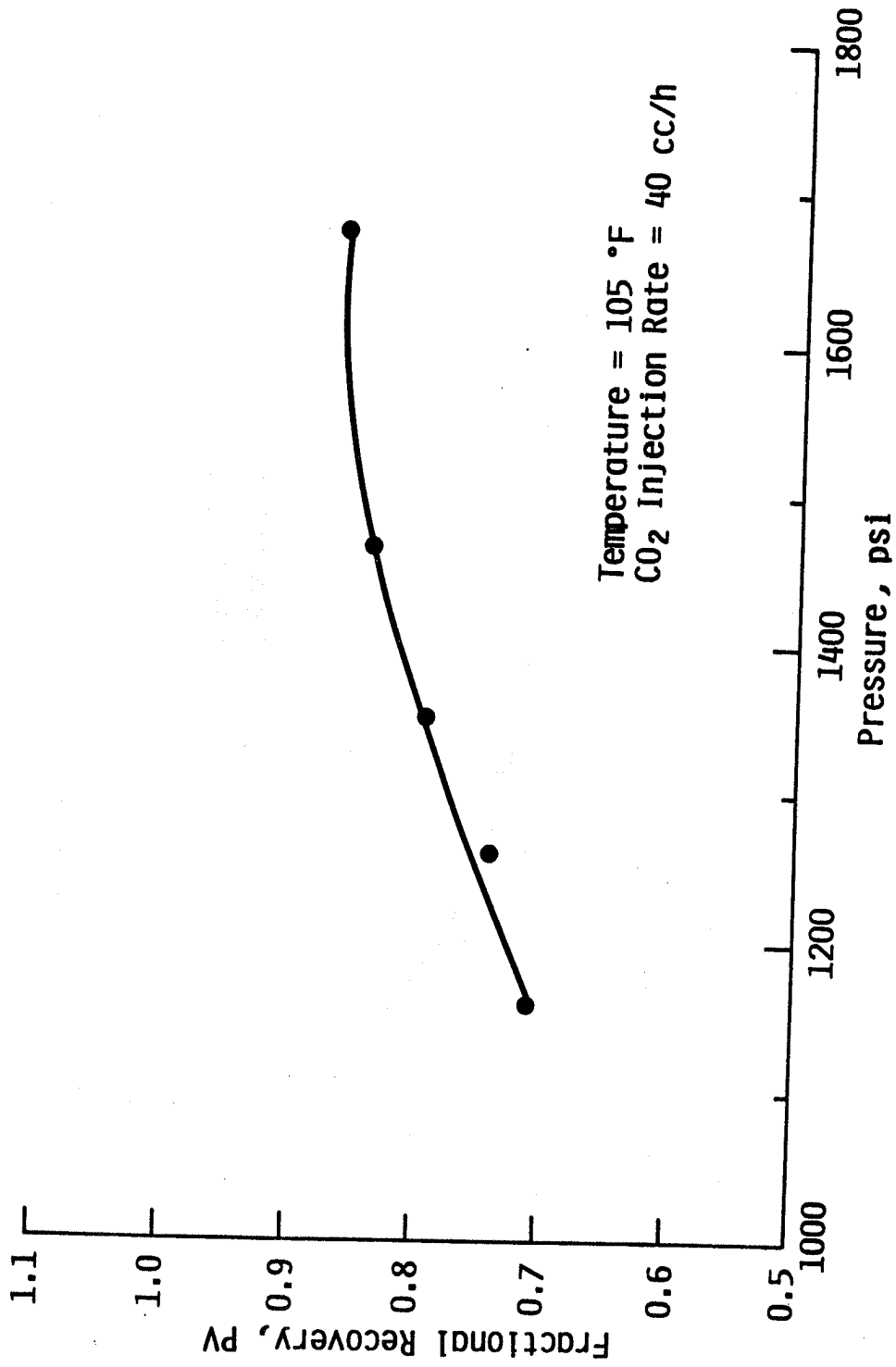


FIGURE B-4: Slim Tube Results - Olson B #6 Crude Oil.

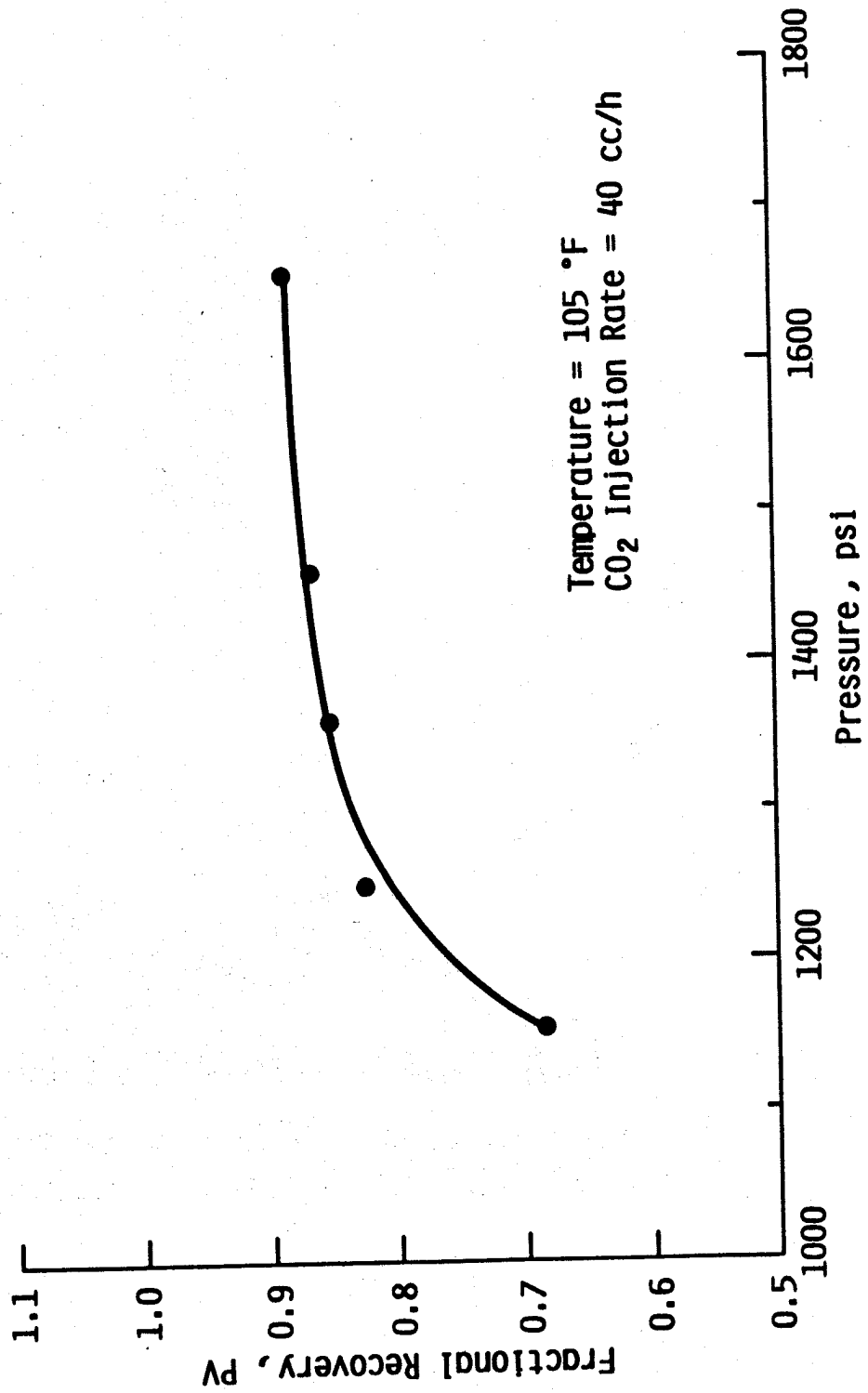


FIGURE B-5: Slim Tube Results - Newcomer #4 Crude Oil.

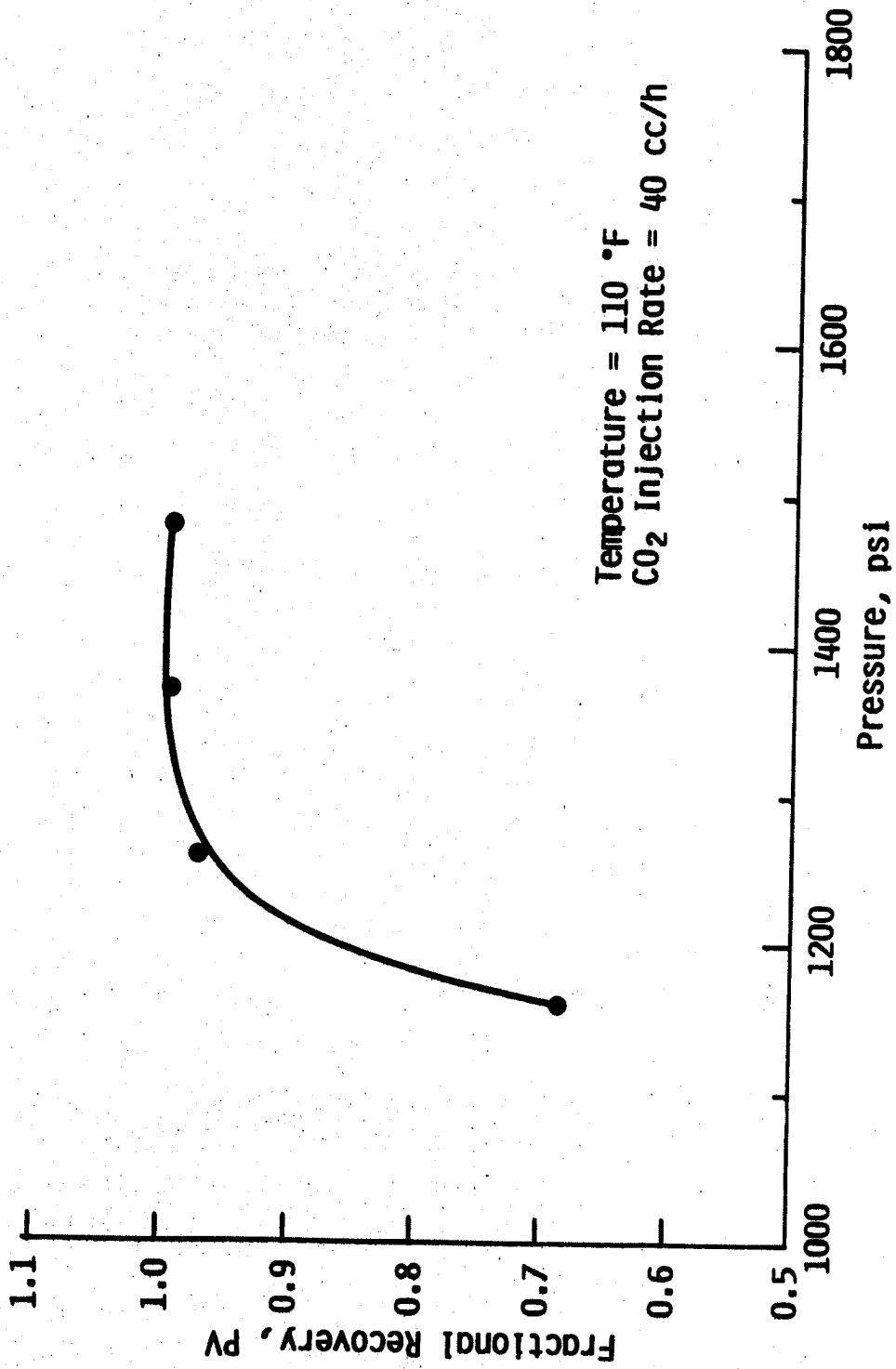


FIGURE B-6: Slim Tube Results - Olive Crude Oil.

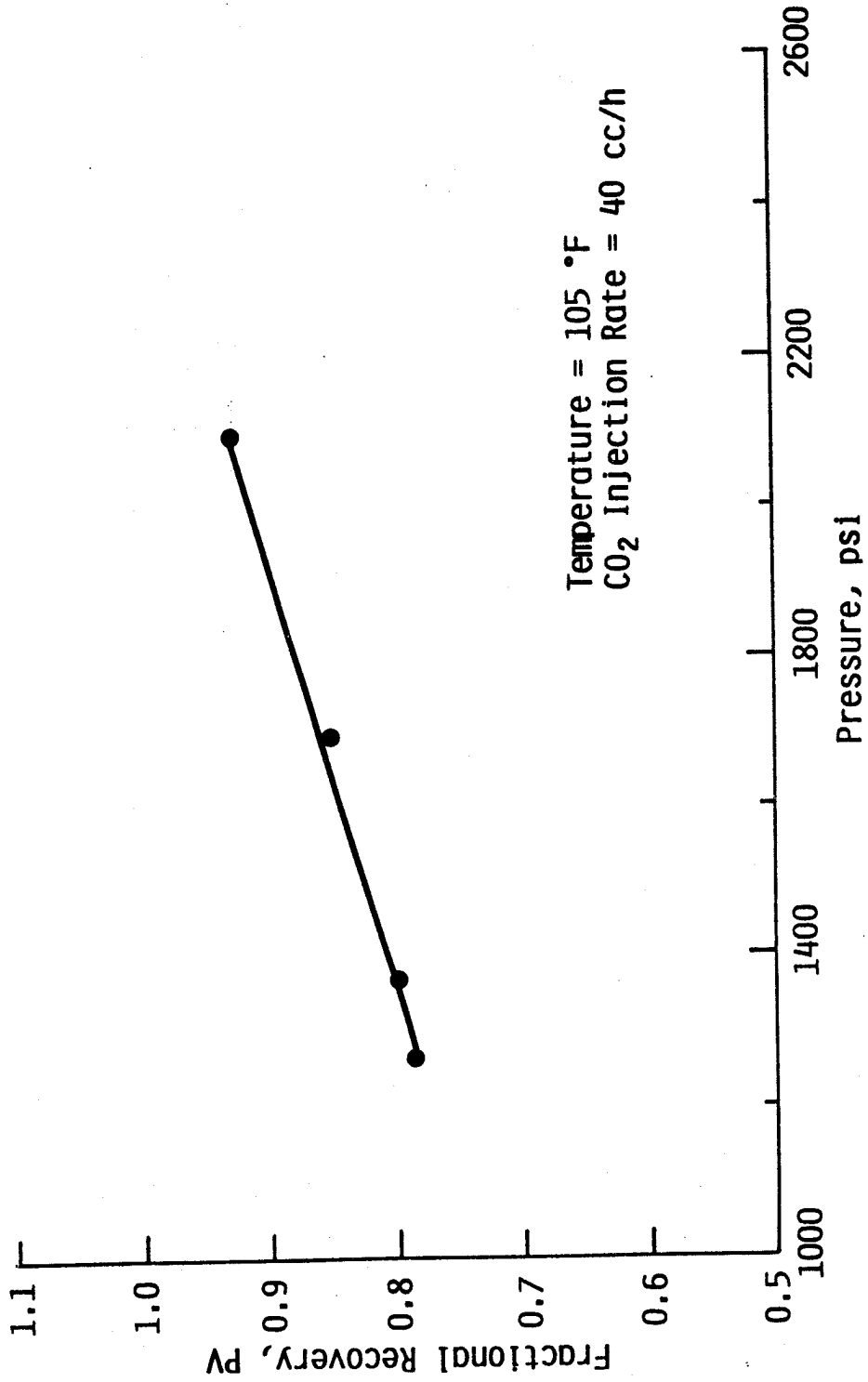


FIGURE B-7: Slim Tube Results - #1 Dieter Crude Oil.

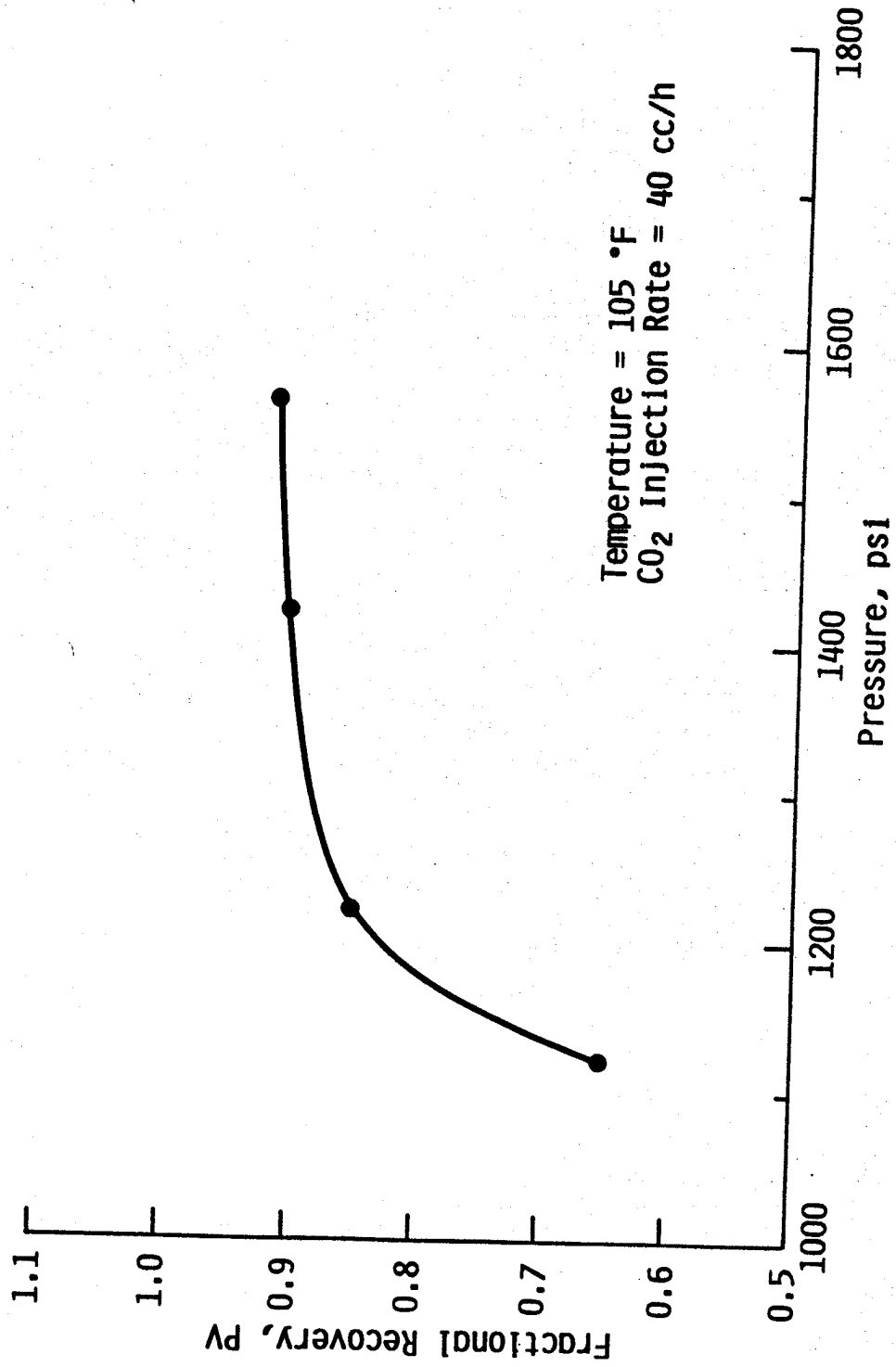


FIGURE B-8: Slim Tube Results - #1 Lofgren Crude Oil.

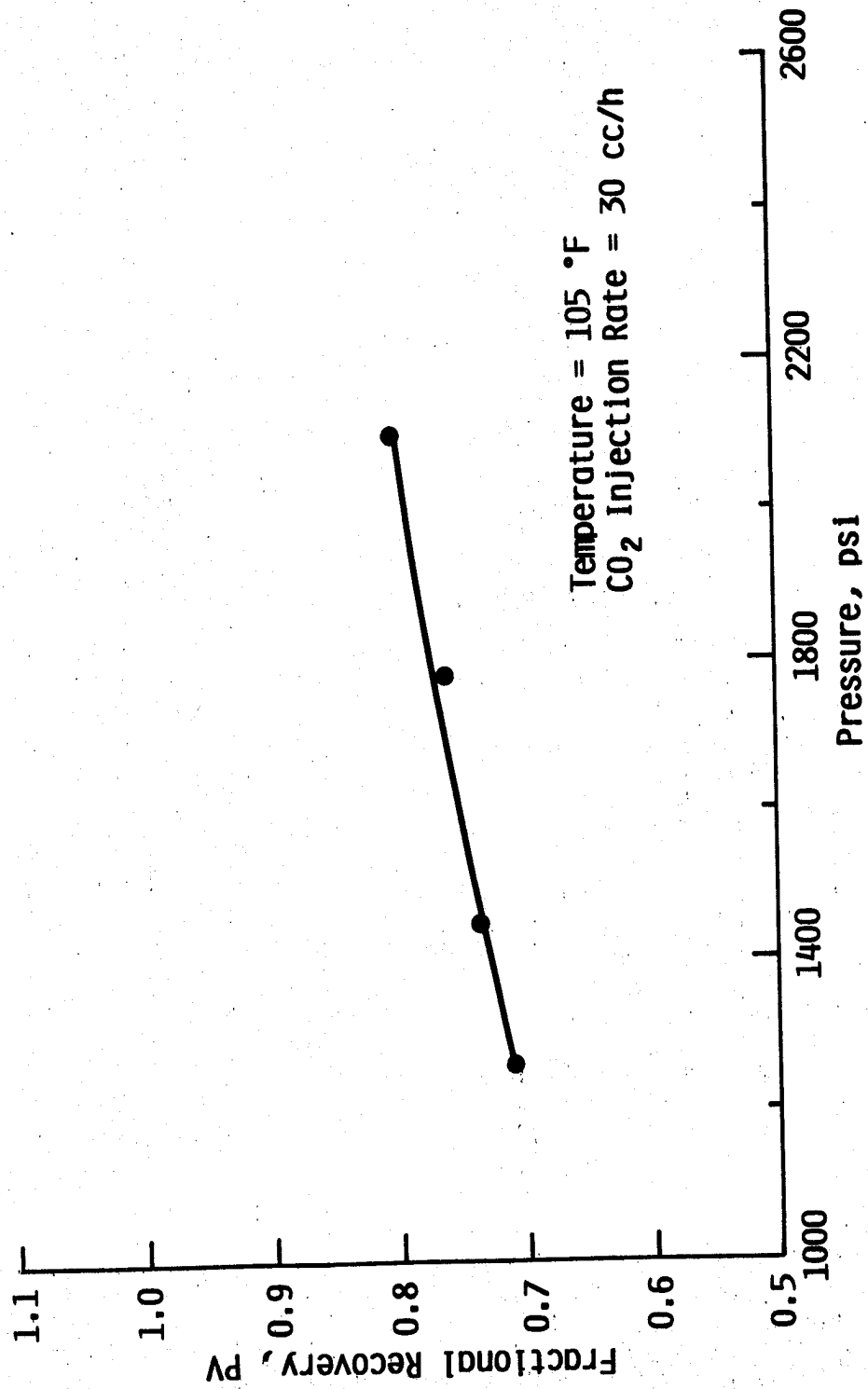


FIGURE B-9: Slim Tube Results - #2 Bishop Crude Oil.

APPENDIX C

SUPPLEMENTAL TABLES AND FIGURES FOR CHAPTER 4

Nomenclature for Appendix C

SG	=	specific gravity
K_w	=	Watson Characterization Factor
SCN	=	Single Carbon Number
M/F	=	weight
WT	=	volume
MW	=	molecular weight
TC	=	critical temperature
PC	=	critical pressure
SG	=	specific gravity
MW	=	molecular weight
W	=	acentric factor
KFW	=	Katz-Firoozabadi-Whitson ²⁰
BP	=	Boiling Point
TB	=	Average Boiling Point

TABLE C-1 - Summary of Generalized Katz-Firoozabadi-Whitson²⁰
Properties

SCN	BP RANGE(F)		TB(F)	SG	MW
6	97.9	156.7	147.	.690	84.
7	156.7	210.1	197.5	.727	96.
8	210.1	259.1	242.	.749	107.
9	259.1	304.4	288.	.768	121.
10	304.4	346.4	330.5	.782	134.
11	346.4	385.5	369.	.793	147.
12	385.5	422.2	407.	.804	161.
13	422.2	456.7	441.	.815	175.
14	456.7	489.2	475.5	.826	190.
15	489.2	520.	511.	.836	206.
16	520.	547.	542.	.843	222.
17	547.	577.	572.	.851	237.
18	577.	603.	595.	.856	251.
19	603.	628.	617.	.861	263.
20	628.	652.	640.5	.866	275.
21	652.	675.	664.	.871	291.
22	675.	696.	686.	.876	300.
23	696.	717.	707.	.881	312.
24	717.	737.	727.	.885	324.
25	737.	756.	747.	.888	337.
26	756.	775.	766.	.892	349.
27	775.	793.	784.	.896	360.
28	793.	810.	802.	.899	372.
29	810.	826.	817.	.902	382.
30	826.	842.	834.	.905	394.
31	842.	857.	850.	.909	404.
32	857.	874.	866.	.912	415.
33	874.	888.	881.	.915	426.
34	888.	901.	895.	.917	437.
35	901.	915.	908.	.920	445.
36	915.	928.	922.	.922	456.
37	928.	941.	934.	.925	464.
38	941.	953.	947.	.927	475.
39	953.	966.	959.	.929	484.
40	966.	978.	972.	.931	495.

TABLE C-2 - Summary of TC, PC, and W Calculations with
Lee-Kesler²¹ Equations for KFW Properties

SCN	TB(°F)	SG	MW	TC(°K)	PC(ATM)	W	K _w
6	147.0	0.690	84.0	507.7	32.4	0.271	12.3
7	197.5	0.727	96.0	542.5	31.1	0.310	12.0
8	242.0	0.749	107.0	570.5	29.1	0.349	11.9
9	288.0	0.768	121.0	598.1	27.0	0.393	11.8
10	330.5	0.782	134.0	622.2	25.0	0.437	11.8
11	369.0	0.793	147.0	643.2	23.2	0.480	11.8
12	407.0	0.804	161.0	663.7	21.7	0.523	11.9
13	441.0	0.815	175.0	682.1	20.5	0.561	11.8
14	475.5	0.826	190.0	700.5	19.4	0.601	11.8
15	511.0	0.836	206.0	718.9	18.2	0.644	11.8
16	542.0	0.843	222.0	734.3	17.2	0.685	11.9
17	572.0	0.851	237.0	749.4	16.3	0.723	11.9
18	595.0	0.856	251.0	760.6	15.6	0.754	11.9
19	617.0	0.861	263.0	771.2	15.0	0.784	11.9
20	640.5	0.866	275.0	782.5	14.4	0.816	11.9
21	664.0	0.871	291.0	793.6	13.8	0.849	11.9
22	686.0	0.876	300.0	804.2	13.3	0.880	11.9
23	707.0	0.881	312.0	814.3	12.8	0.909	11.9
24	727.0	0.885	324.0	823.6	12.4	0.937	12.0
25	747.0	0.888	337.0	832.4	11.9	0.966	12.0
26	766.0	0.892	349.0	841.3	11.5	0.991	12.0
27	784.0	0.896	360.0	849.7	11.1	1.015	12.0
28	802.0	0.899	372.0	857.8	10.7	1.040	12.0
29	817.0	0.902	382.0	864.6	10.5	1.060	12.0
30	834.0	0.905	394.0	872.2	10.1	1.083	12.0
31	850.0	0.909	404.0	879.8	9.9	1.102	12.0
32	866.0	0.912	415.0	887.0	9.6	1.123	12.0
33	881.0	0.915	426.0	893.9	9.4	1.142	12.1
34	895.0	0.917	437.0	899.9	9.1	1.162	12.1
35	908.0	0.920	445.0	905.9	8.9	1.177	12.1
36	922.0	0.922	456.0	911.9	8.7	1.196	12.1
37	934.0	0.925	464.0	917.6	8.5	1.210	12.1
38	947.0	0.927	475.0	923.2	8.3	1.227	12.1
39	959.0	0.929	484.0	928.5	8.1	1.242	12.1
40	972.0	0.931	495.0	934.1	7.9	1.259	12.1

CORE LABORATORIES, INC.
Reservoir Fluid Analysis

August 2, 1983

Page 1 of 2

File RFL 830486

TABLE 5.1

Company The University of Kansas
Center for Research, Inc.
Well Abernathy-Collins No. 1
TORP Account 4390

ASTM D-86 DISTILLATION OF STOCK TANK OIL
IN 50°F. CUT STEPS TO 700°F.

$$K_w = 11.8$$

Gravity, °API @ 60°F. = 33.9
Specific gravity @ 60°/60°F. = 0.8555
Molecular weight = 237

<u>Cut Number</u>	<u>Temperature °F.</u>	<u>Volume Percent</u>	<u>Specific Gravity @ 60°/60°F.</u>
0	176	IBP	
1	223	3.0	0.6849
2	273	10.0	0.7145
3	325	18.0	0.7394
4	375	24.5	0.7609
5	426	28.5	0.7766
6	476 481	34.0	0.7927
7	530 538	40.0	0.8109
8	580 594	45.5	0.8274
9	632 657	52.0	0.8426
10	682 726	59.0	0.8543
	700*	65.0	
11	(700)753	71.0	0.8551
Residue		29.0	0.9759

Residue molecular weight = 576

*Stopped distillation

CORE LABORATORIES, INC.
Reservoir Fluid Analysis

August 2, 1983

Page 2 of 2

File RFL 830486

TABLE 5.9

Company The University of Kansas
Center for Research, Inc.
Well Johanning B No. 1
TORP Account 4390

ASTM D-86 DISTILLATION OF STOCK TANK OIL
IN 50°F. CUT STEPS TO 700°F.

Gravity, °API @ 60°F. = 36.2 $K_w = 11.8$
Specific gravity @ 60°/60°F. = 0.8441
Molecular weight = 216

<u>Cut Number</u>	<u>Temperature °F.</u>	<u>Volume Percent</u>	<u>Specific Gravity @ 60°/60°F.</u>
0	204	IBP	
1	254	3.0	0.7145
2	305	12.0	0.7386
3	354	21.5	0.7576
4	404	28.0	0.7774
5	456	34.0	0.7951
6	507 513	41.0	0.8118
7	557 568	48.0	0.8257
8	607 626	55.5	0.8384
9	658 692	65.0	0.8514
	700*	74.0	
10	(700)753	77.5	0.8566
Residue		22.5	0.9596

Residue molecular weight = 498

*Stopped distillation

CORE LABORATORIES, INC.

James R. Fortner

James R. Fortner
Area Manager
Reservoir Fluid Analysis

JRF:HLS:mc

7 cc: Tertiary Oil Recovery Project (TORP)
Dept. of Chemical and Petroleum Engr.
4008 Learned Hall
University of Kansas
Lawrence, KS 66045
Attn: Mr. Edward Daub

151

CORE LABORATORIES, INC.
Reservoir Fluid Analysis

January 24, 1984

Page 1 of 2

File RFL 830775

TABLE 6.1

Company The University of Kansas Tertiary Oil Recovery Project

Well Albertson Crude

ASTM D-86 DISTILLATION OF STOCK TANK OIL IN 50°F. CUT STEPS TO 700°F.

Gravity, °API @ 60°F. = 35.5
 Specific gravity @ 60°/60°F. = 0.8472 $K_w = 11.7$
 Molecular weight = 222

<u>Cut Number</u>	<u>Temperature °F.</u>	<u>Volume Percent</u>	<u>Specific Gravity @ 60°/60°F.</u>
0	136	IBP	
1	186	3.5	0.6717
2	236	10.0	0.7005
3	285	16.0	0.7298
4	337	22.0	0.7519
5	388	27.5	0.7702
6	438	32.5	0.7879
7	488 493	38.0	0.8038
8	538 547	43.5	0.8193
9	590 606	49.5	0.8328
10	640 668	55.5	0.8452
11	690 738	66.5	0.8556
	700*	70.5	
12	(700) 753	76.5	0.8567
Residue		22.5	1.0012
Loss		1.0	

Residue molecular weight = 605

*Stopped distillation

These analyses, opinions or interpretations are based on observations and material supplied by the client to whom, and for whose exclusive and confidential use, this report is made. The interpretations or opinions expressed represent the best judgement of Core Laboratories, Inc. (all errors and omissions excepted); but Core Laboratories, Inc. and its officers and employees, assume no responsibility and make no warranty or representations as to the productivity, proper operation, or profitability of any oil, gas or other mineral well or sand in connection with which such report is used or relied upon.

CORE LABORATORIES, INC.
Reservoir Fluid Analysis

January 24, 1984

Page 2 of 2

File RFL 830775

Well Albertson Crude

TABLE 6.9
TRUE BOILING POINT DISTILLATION OF STOCK TANK OIL

<u>Cut Number</u>	<u>Temperature, °F.</u>	<u>Recovery, Volume %</u>	<u>Specific Gravity @ 60°/60°F.</u>
0	89	IBP	
1	161	3.98	0.6589
2	210	8.79	0.7170
3	260	14.83	0.7302
4	310	20.60	0.7234
5	362	26.09	0.7714
6	410	30.90	0.7895
7	460	36.39	0.8085
8	510	41.17	0.8191
9	560	46.22	0.8320
10	610	51.33	0.8437
Residue		45.24	0.9462
Loss		3.43	

Residue molecular weight = 537

CORE LABORATORIES, INC.



James R. Fortner
Area Manager
Reservoir Fluid Analysis

JRF:DK:mc

7 cc: Tertiary Oil Recovery Project
4008 Learned Hall
University of Kansas
Lawrence, KS 66045
Attn: Prof. Don W. Green

TABLE C-7 - Comparison of Distillation Curves for the
Abernathy-Collins Crude

ASTM D-86(Experimental)		TBP(Empirical)		EFV(Empirical)	
<u>T(F)</u>	<u>VOL%</u>	<u>T(F)</u>	<u>VOL%</u>	<u>T(F)</u>	<u>VOL%</u>
176	0	101	0		
273	10	239	10	349	10
441	30	429	30	479	30
638	50	653	50	618	50
751	70	776	70	694	70
753	71	780	71		

TABLE C-8 - Calculated Binary Bubble-Point Temperatures Versus ASTM
Cut Temperature

<u>CUT #'s</u>	<u>ASTM D-86</u>	<u>CALC. BPT</u>
1,2	223	229.1
2,3	273	269.9
3,4	325	316.9
4,5	375	364.7
5,6	426	425.8
6,7	481	477.2
7,8	538	530.4
8,9	594	591.3
9,10	657	650.8
10,11	726	714.6

TABLE C-9 - Summary of Additional IP Ranges Utilized in Ternary Analyses

<u>SCN</u>	.02-.13 (2-13)	.03-.13 (3-15)	.04-.13 (4-13)	.06-.13 (6-13)	.03-.15 (3-15)
5	.0200	.030	.0400	.0600	.030
6	.0255	.035	.0445	.0635	.036
7	.0310	.040	.0490	.0670	.042
8	.0365	.045	.0535	.0705	.048
9	.0420	.050	.0580	.0740	.054
10	.0475	.055	.0625	.0775	.060
11	.0530	.060	.0670	.0810	.066
12	.0585	.065	.0715	.0845	.072
13	.0640	.070	.0760	.0880	.078
14	.0695	.075	.0805	.0915	.084
15	.0750	.080	.0850	.0950	.090
16	.0805	.085	.0895	.0985	.096
17	.0860	.090	.0940	.1020	.102
18	.0915	.095	.0985	.1055	.108
19	.0970	.100	.1030	.1090	.114
20	.1025	.105	.1075	.1125	.120
21	.1080	.110	.1120	.1160	.126
22	.1135	.115	.1165	.1195	.132
23	.1190	.120	.1210	.1230	.138
24	.1245	.125	.1255	.1265	.144
25	.1300	.130	.1300	.1300	.150
26+	.1300	.130	.1300	.1300	.150

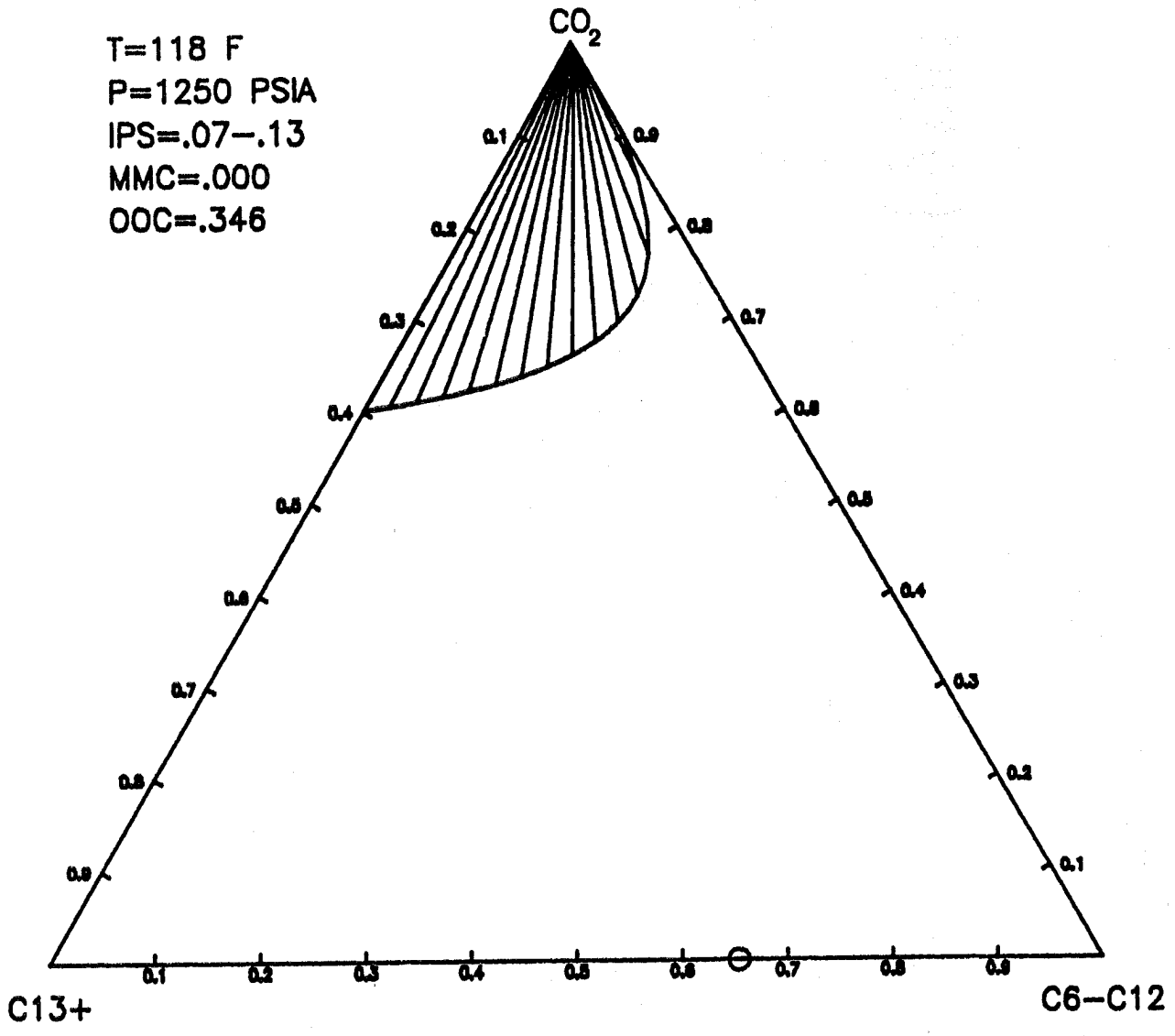


FIGURE C-1: Calculated Ternary Phase Diagram for Yellig and Metcalfe Oil (IP Range 7-13, P = 1250 psia, T = 118°F).

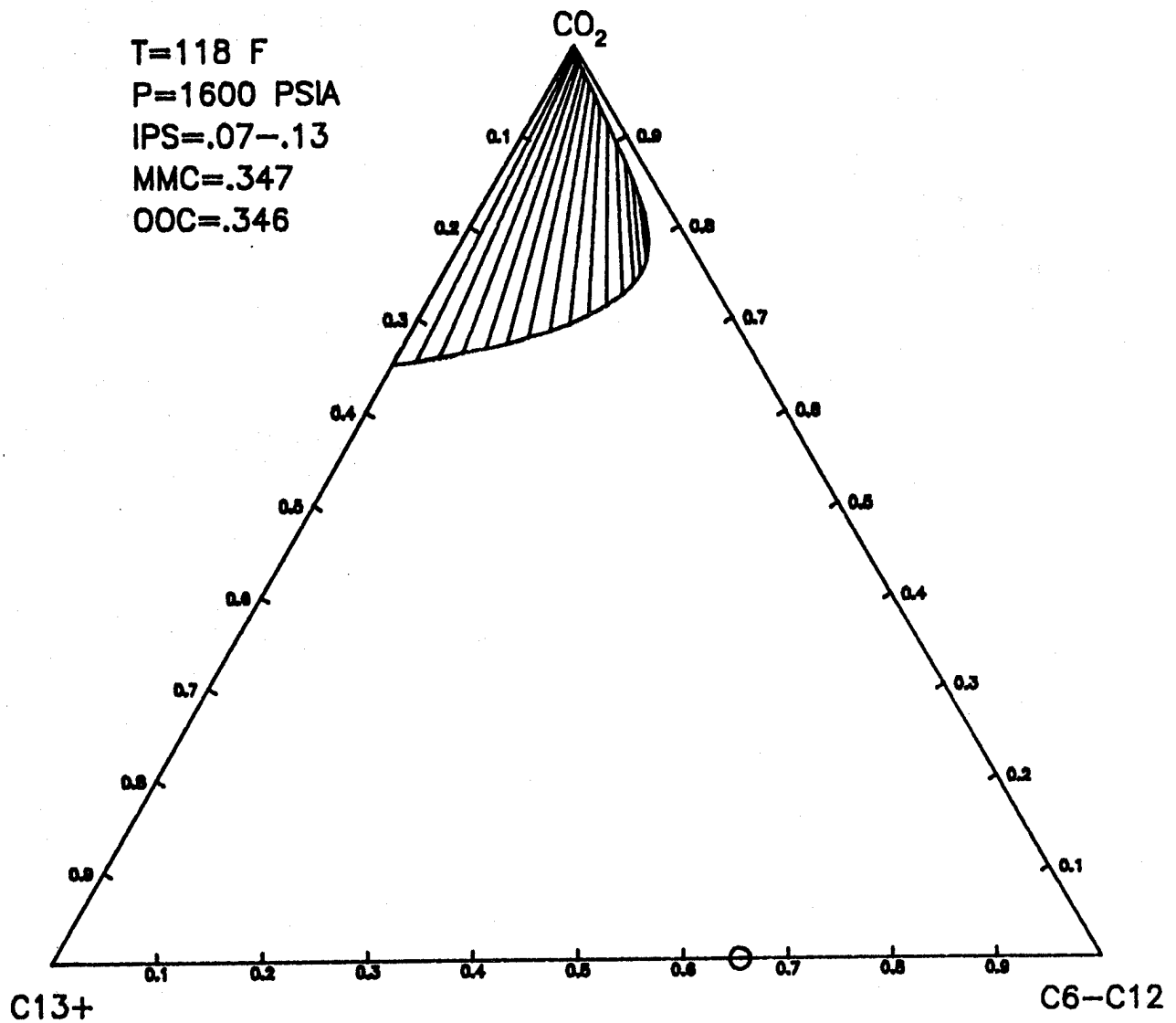


FIGURE C-2: Calculated Ternary Phase Diagram for Yellig and Metcalfe Gil
 (IP Range 7-13, P = 1600 psia, T = 118°F).

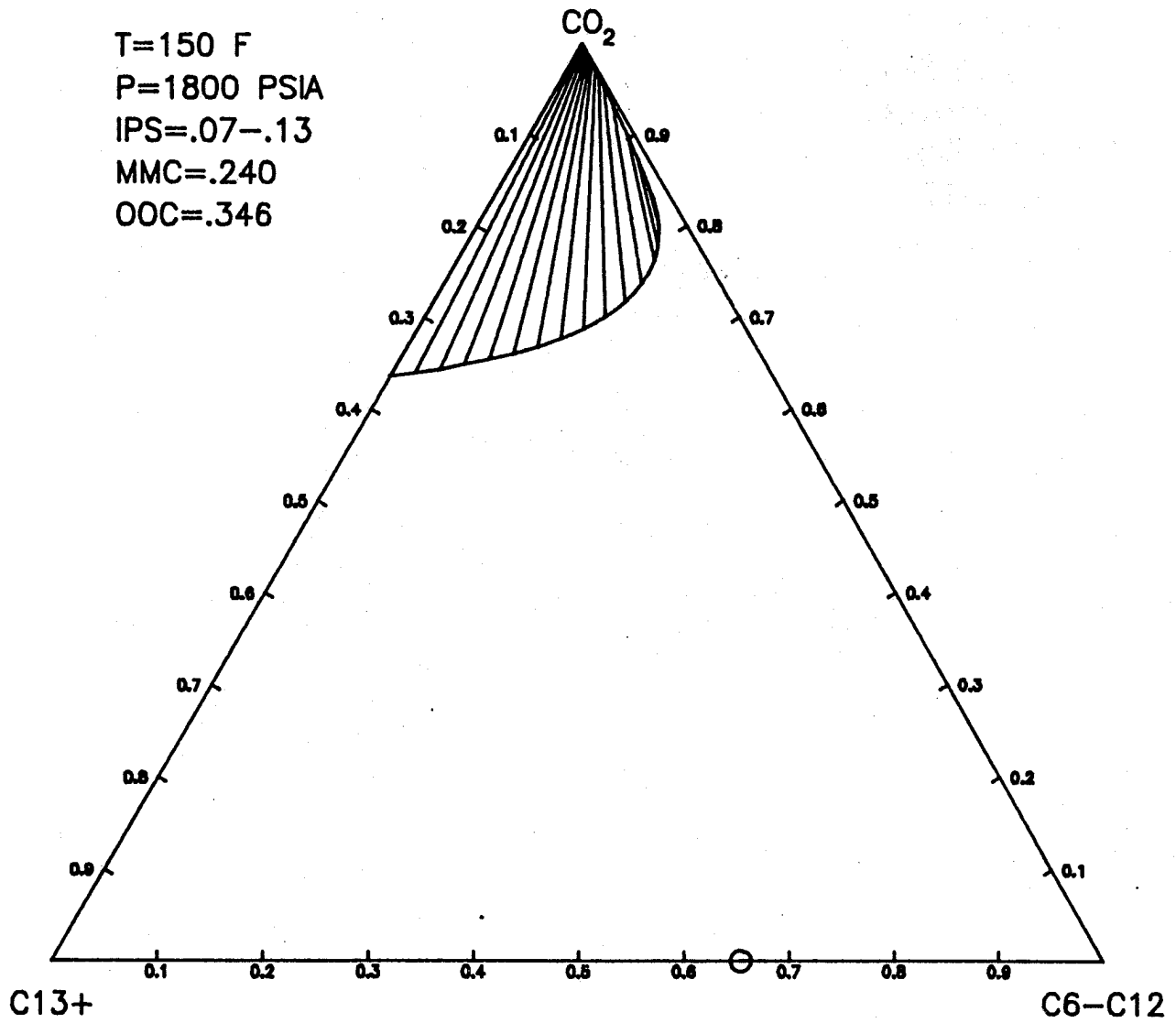


FIGURE C-3: Calculated Ternary Phase Diagram for Yellig and Metcalfe Oil
 (IP Range 7-13, P = 1800 psia, T = 150°F).

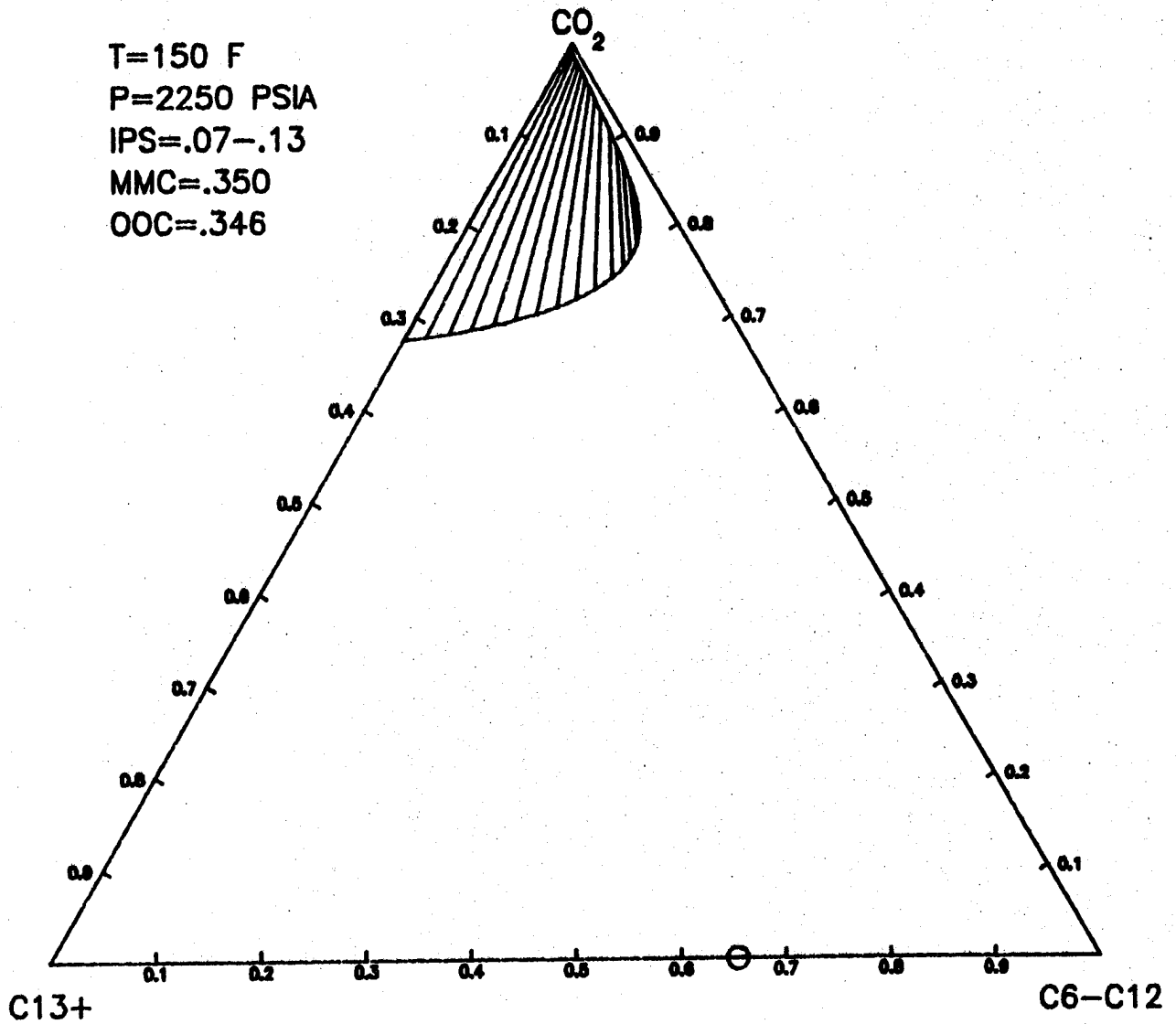


FIGURE C-4: Calculated Ternary Phase Diagram for Yellig and Metcalfe Oil
 (IP Range 7-13, P = 2250 psia, T = 150°F).

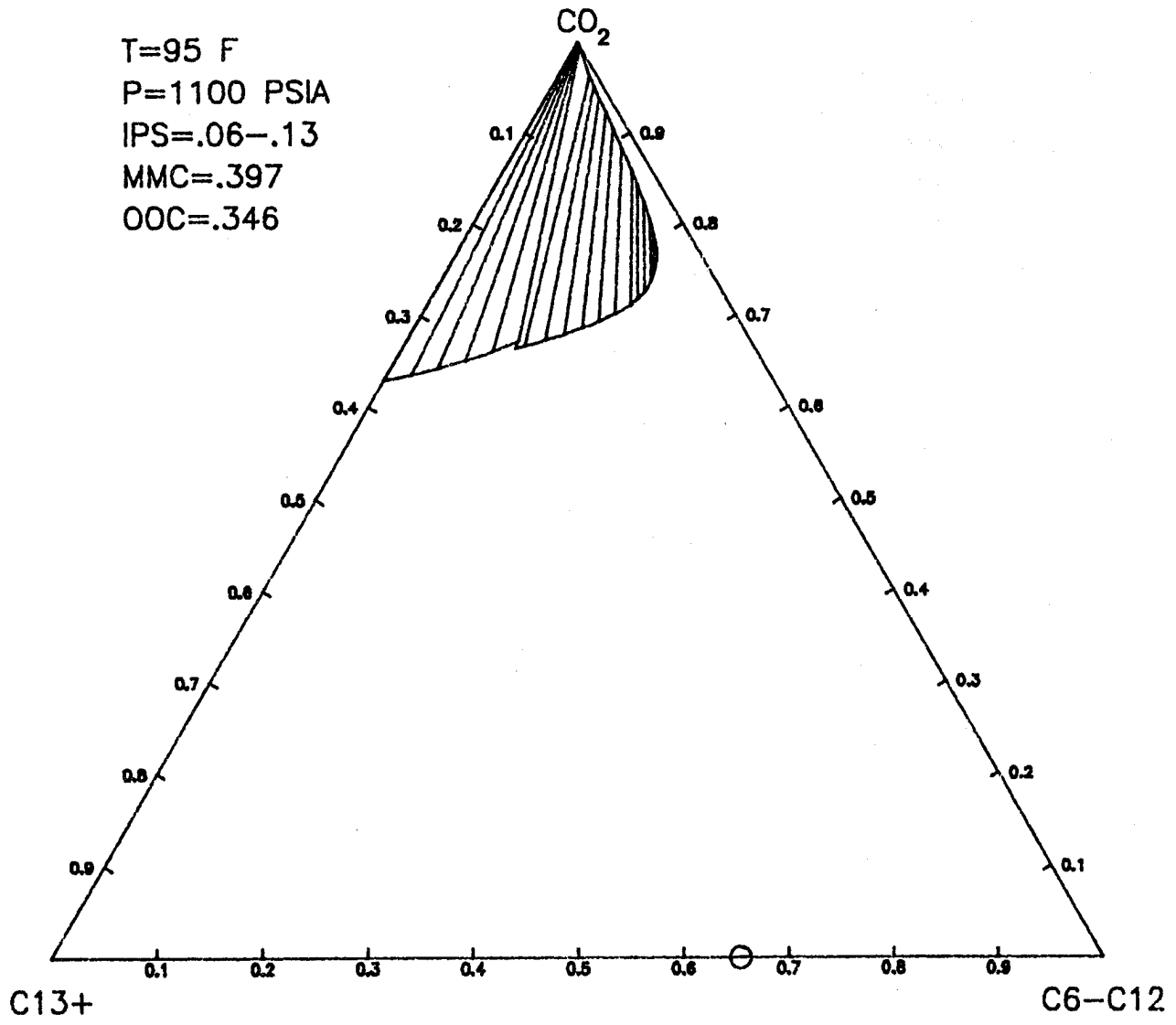


FIGURE C-5: Calculated Ternary Phase Diagram for Yellig and Metcalfe Oil (IP Range 6-13, P = 1100 psia, T = 95°F).

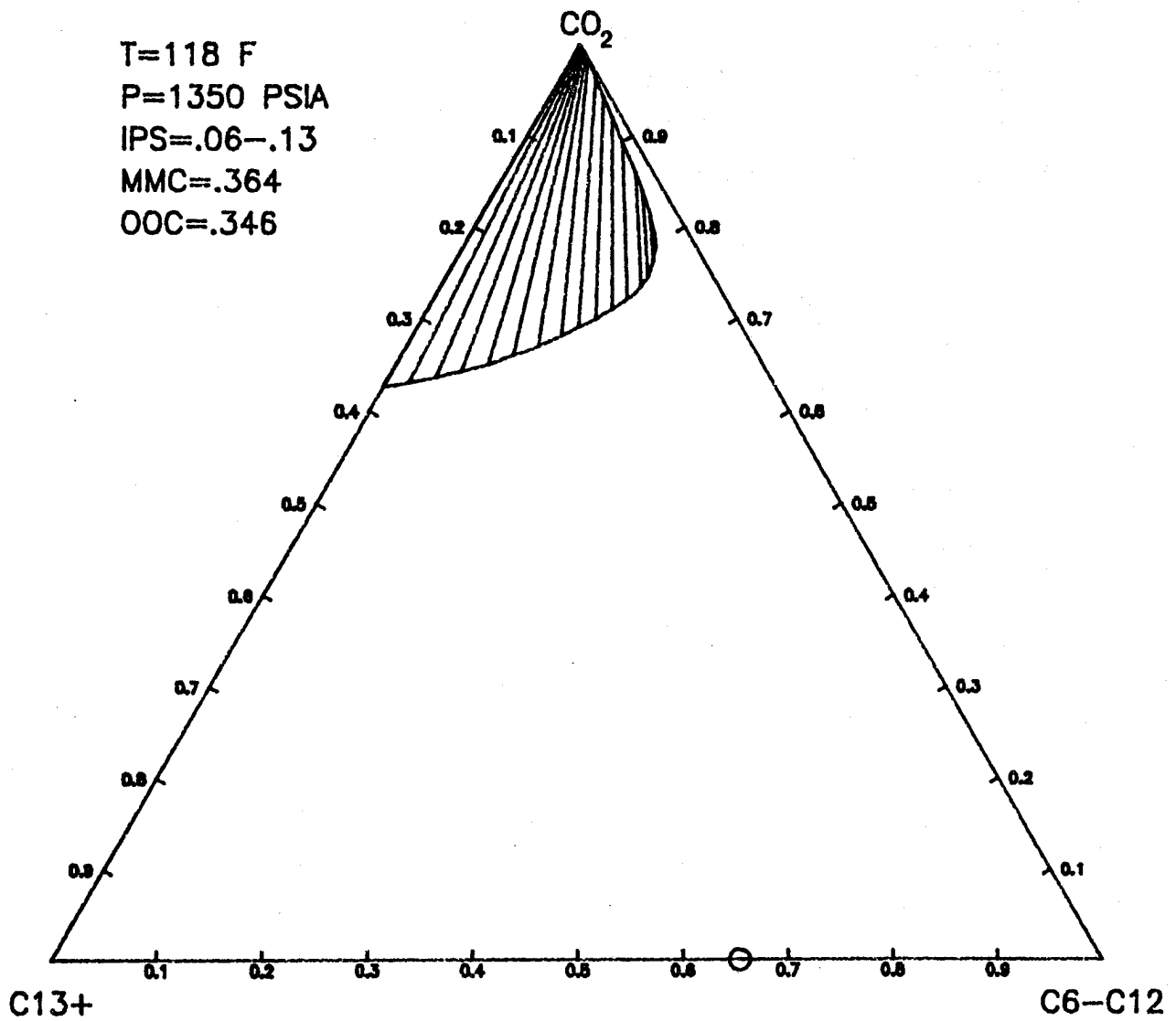


FIGURE C-6: Calculated Ternary Phase Diagram for Yellig and Metcalfe Oil
 (IP Range 6-13, P = 1350 psia, T = 118°F).

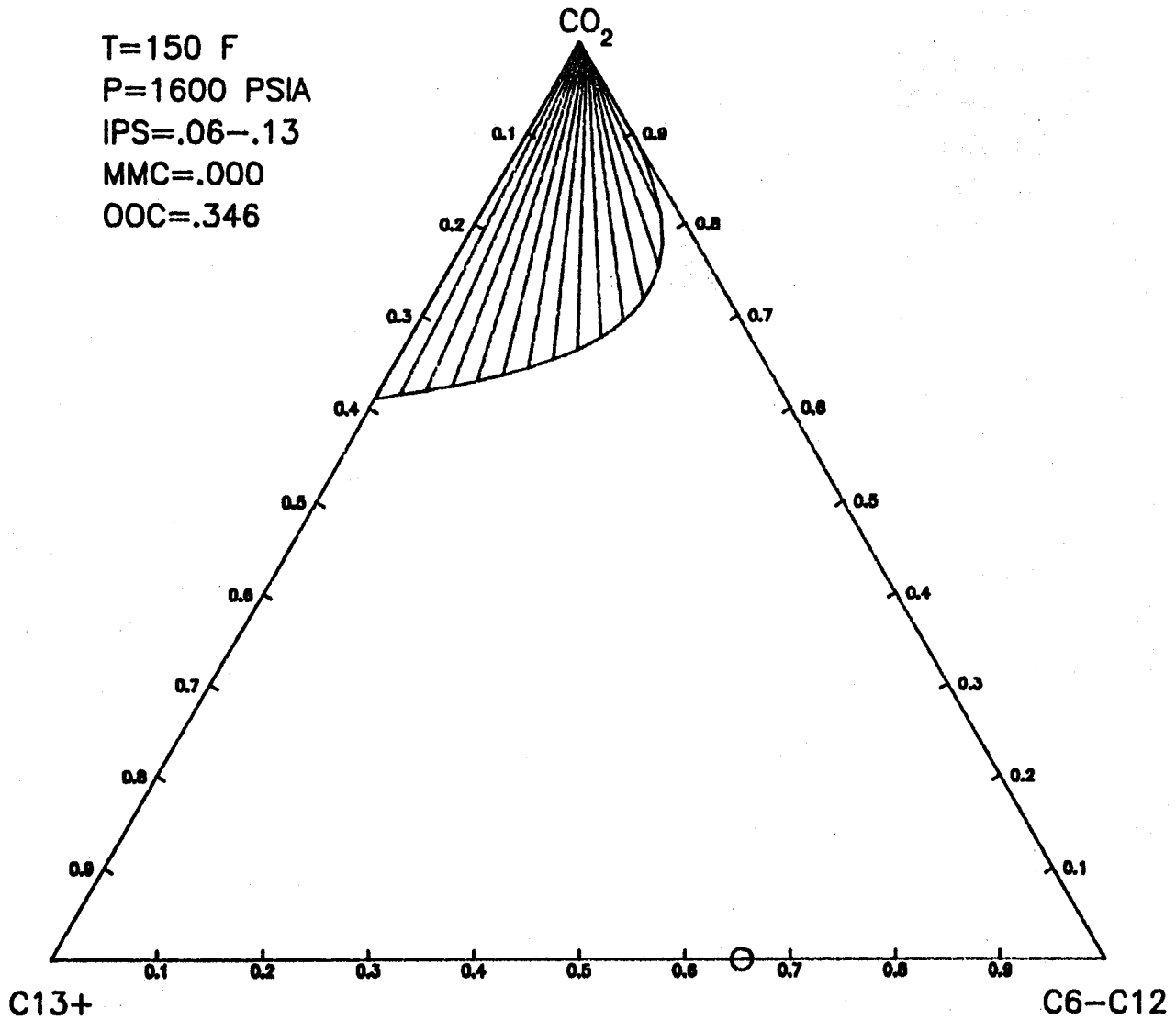


FIGURE C-7: Calculated Ternary Phase Diagram for Yellig and Metcalfe Oil
 (IP Range 6-13, P = 1600 psia, T = 150°F).

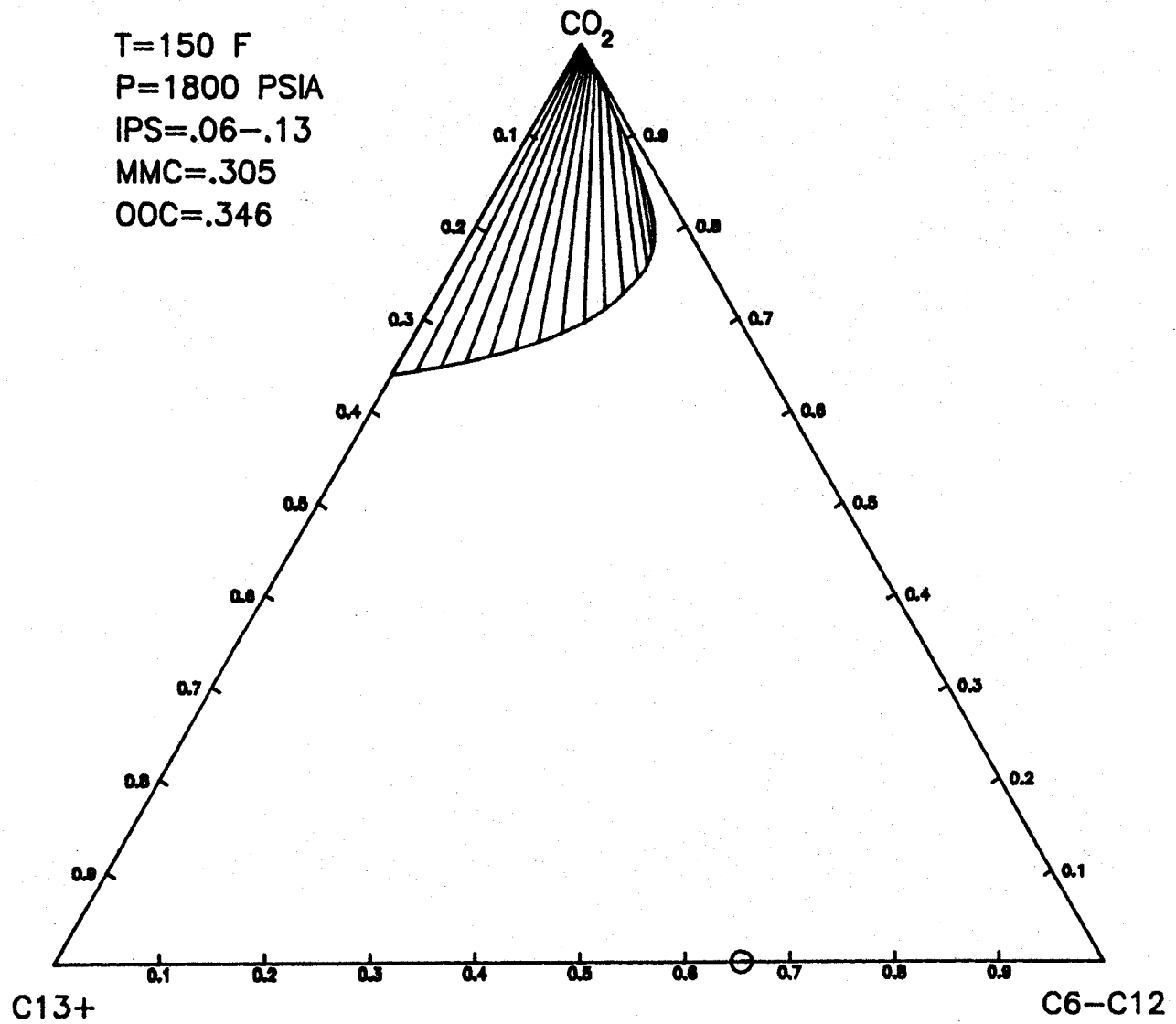


FIGURE C-8: Calculated Ternary Phase Diagram for Yellig and Metcalfe Oil
 (IP Range 6-13, P = 1800 psia, T = 150°F).

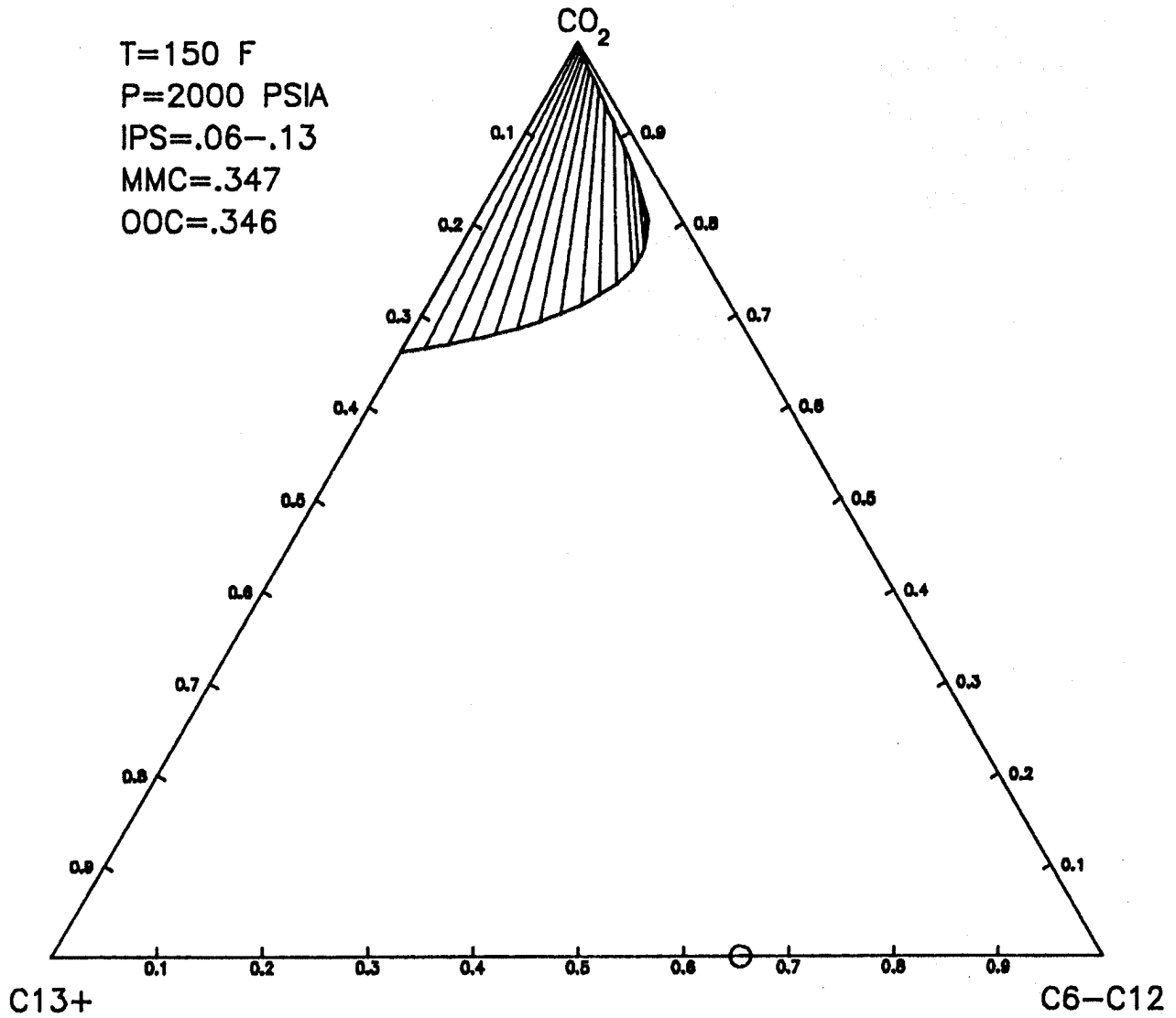


FIGURE C-9: Calculated Ternary Phase Diagram for Yellig and Metcalfe Oil
 (IP Range 6-13, P = 2000 psia, T = 150°F).

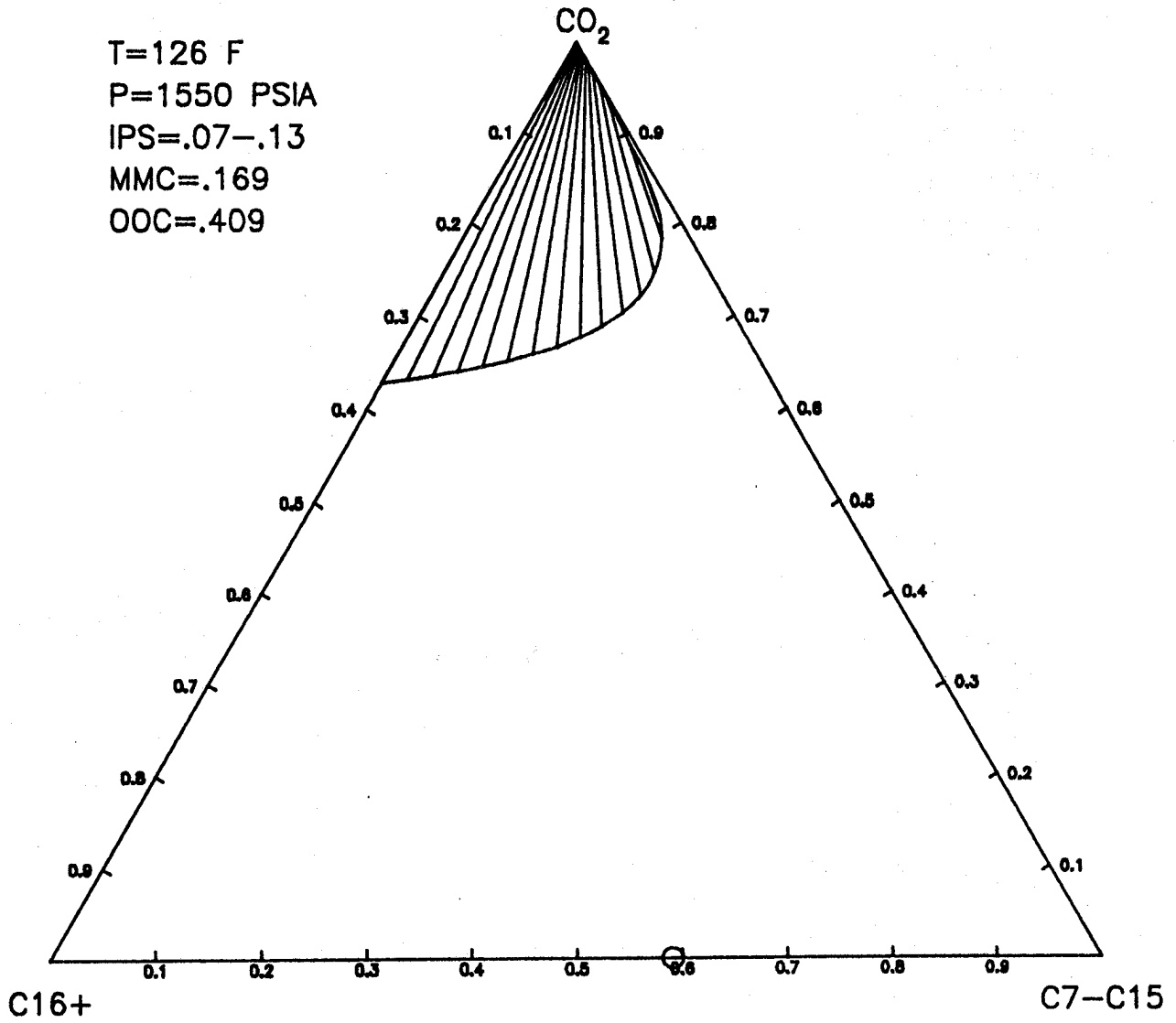


FIGURE C-10: Calculated Ternary Phase Diagram for Abernathy-Collins Crude Oil (IP Range 7-13, P = 1550 psia, T = 126°F).

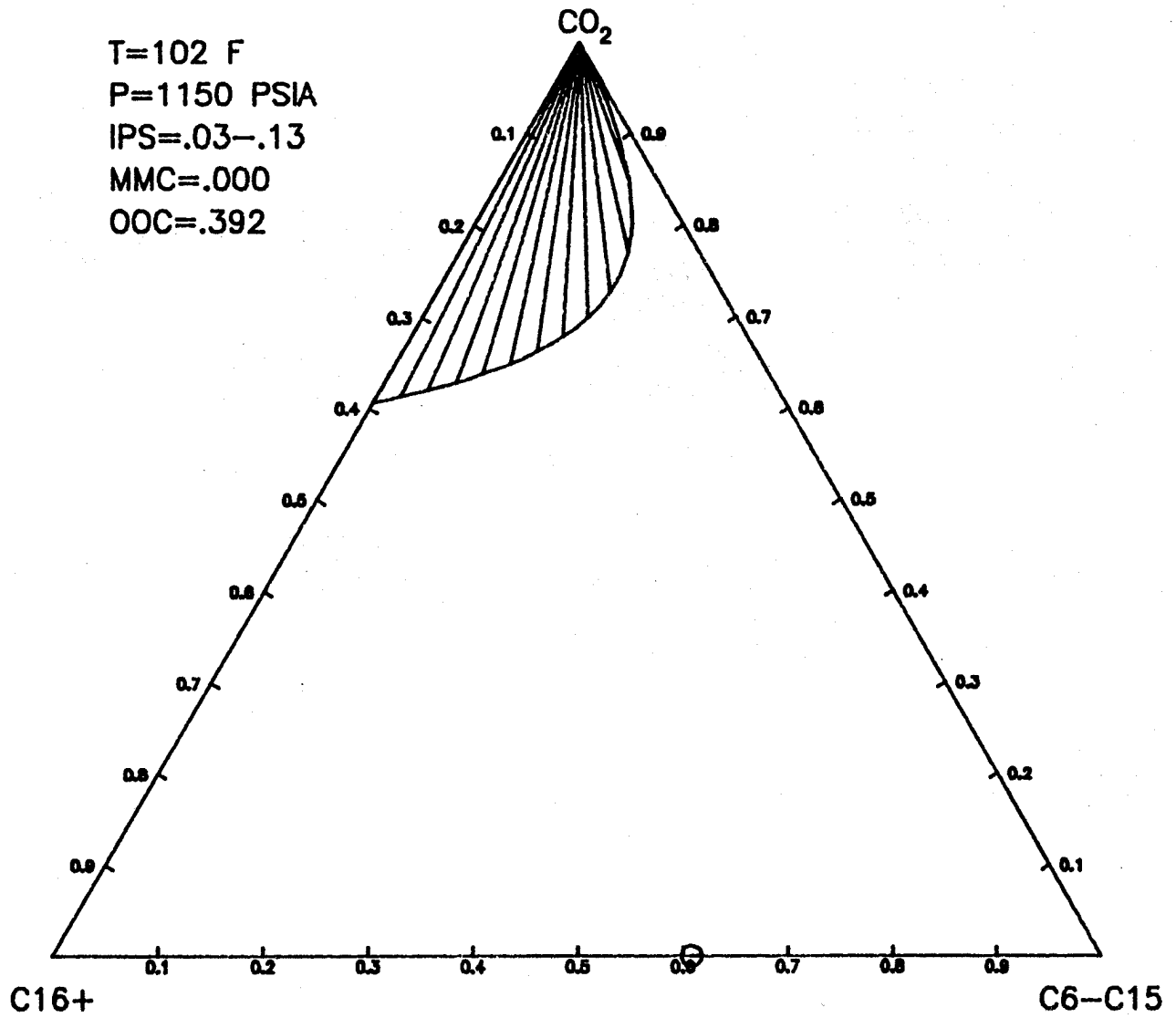


FIGURE C-11: Calculated Ternary Phase Diagram for Johanning B Crude Oil
 (IP Range 3-13, P = 1150 psia, T = 102°F).

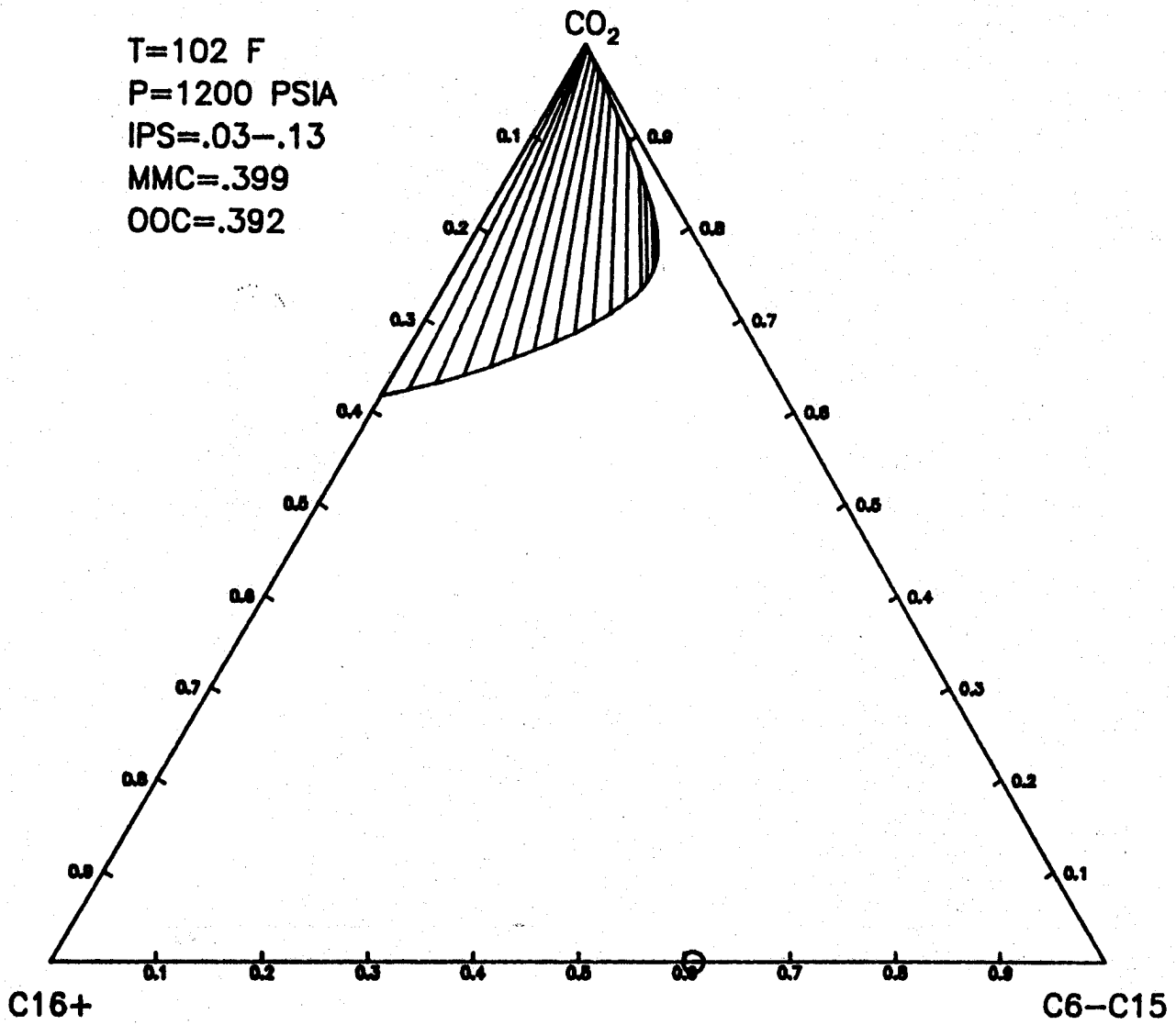


FIGURE C-12: Calculated Ternary Phase Diagram for Johanning B Crude Oil
 (IP Range 3-13, P = 1200 psia, T - 102°F).

APPENDIX D

SUPPLEMENTAL FIGURES FOR CHAPTER 5

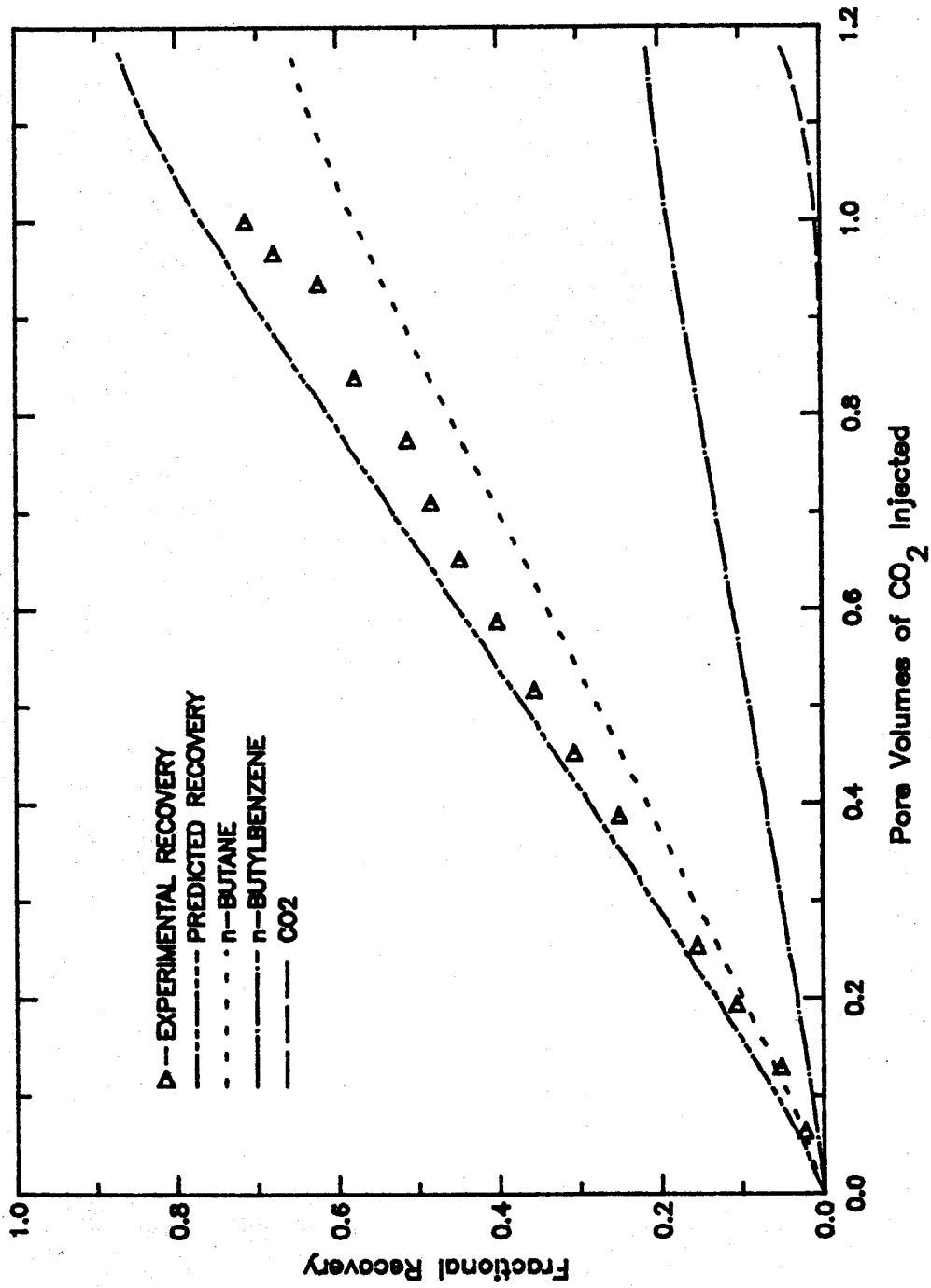


FIGURE D-1: CO₂ Displacing Butane and Butylbenzene (P = 1100 psia, T = 160°F).

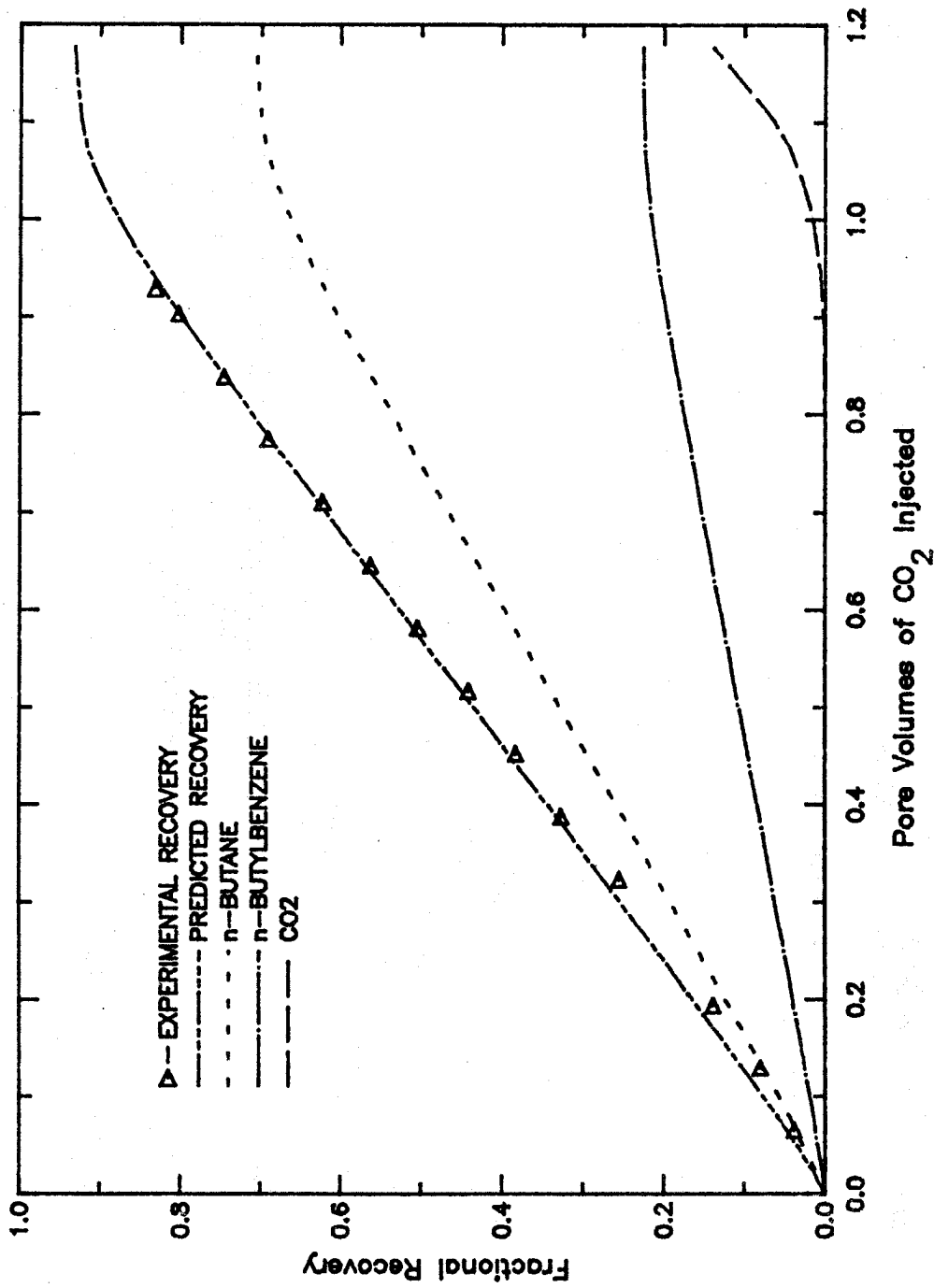


FIGURE D-2: CO₂ Displacing Butane and Butylbenzene (P = 1200 psia, T = 160°F).

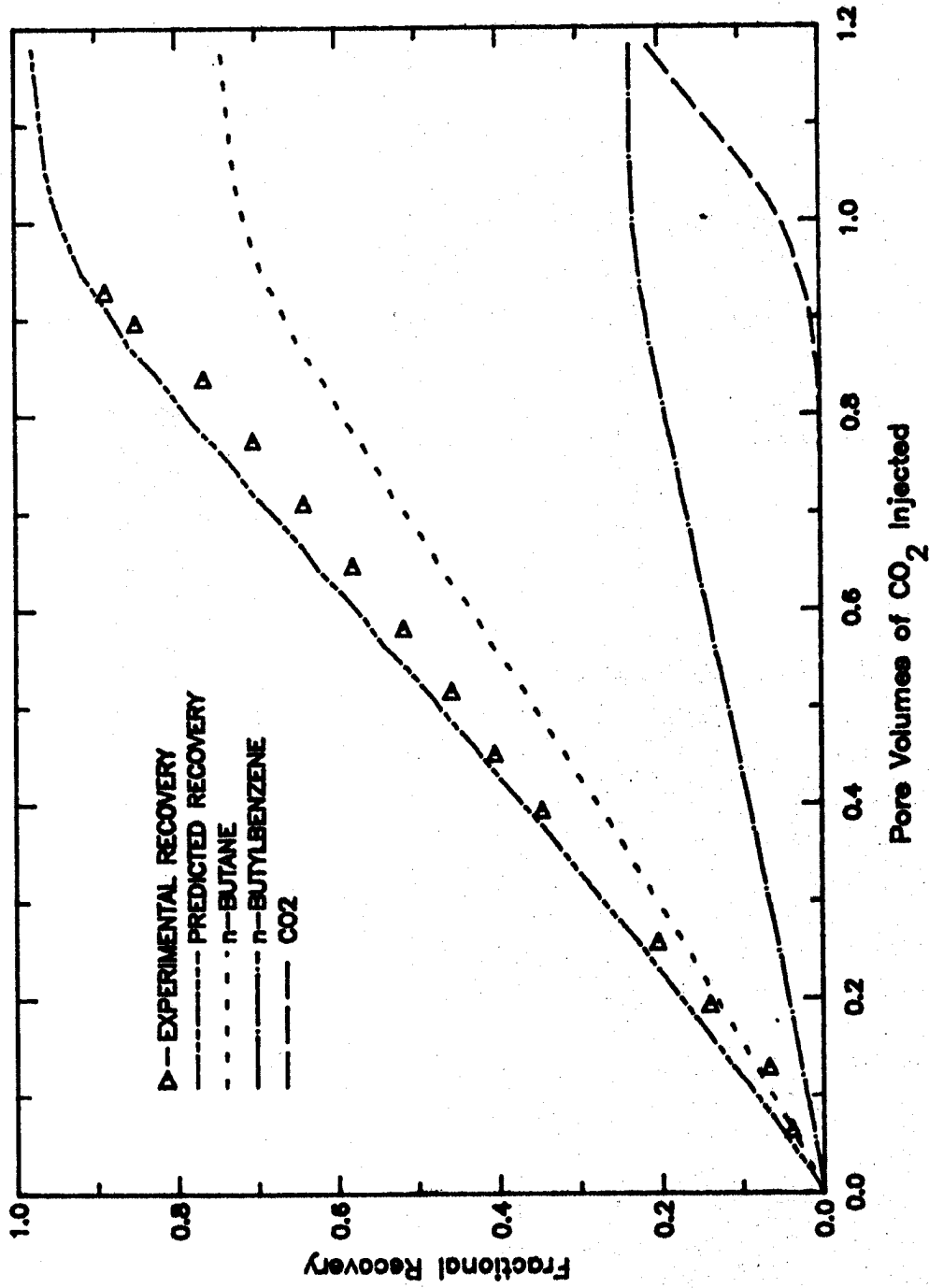


FIGURE D-3: CO₂ Displacing Butane and Butylbenzene (P = 1300 psia, T = 160°F).

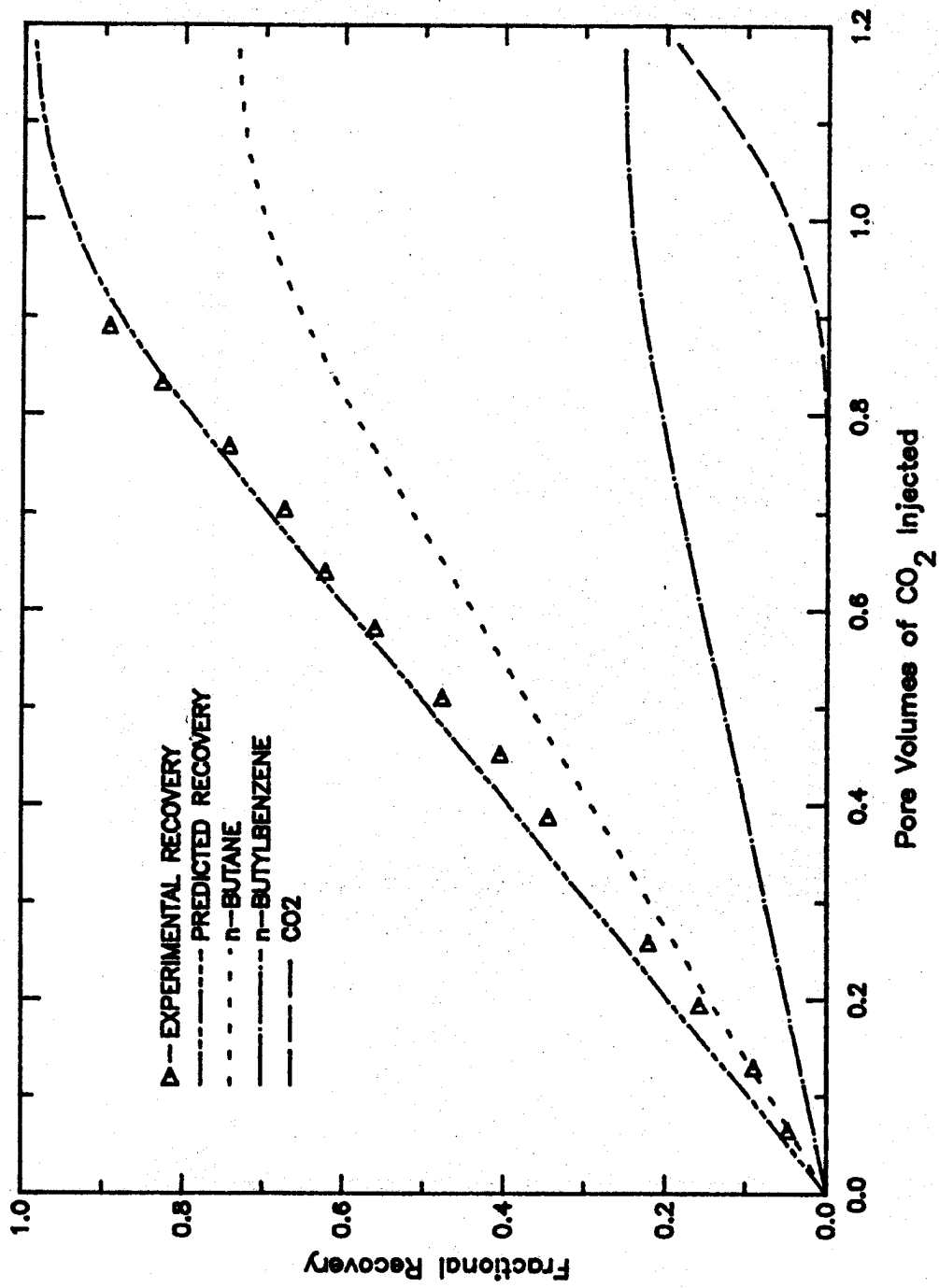


FIGURE D-4: CO₂ Displacing Butane and Butylbenzene (P = 1400 psia, T = 160°F).

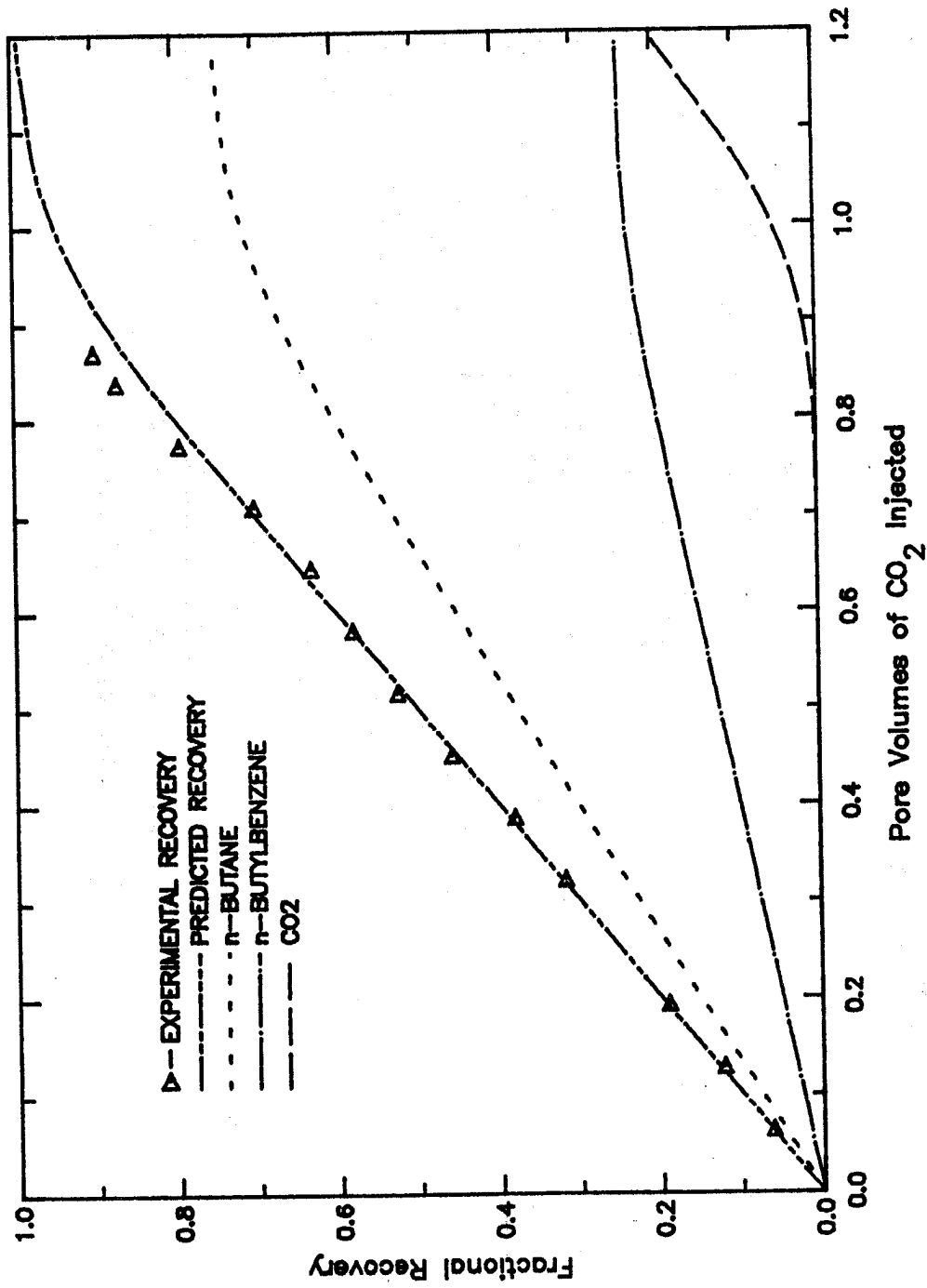


FIGURE D-5: CO₂ Displacing Butane and Butylbenzene (P = 1500 psia, T = 160°F).

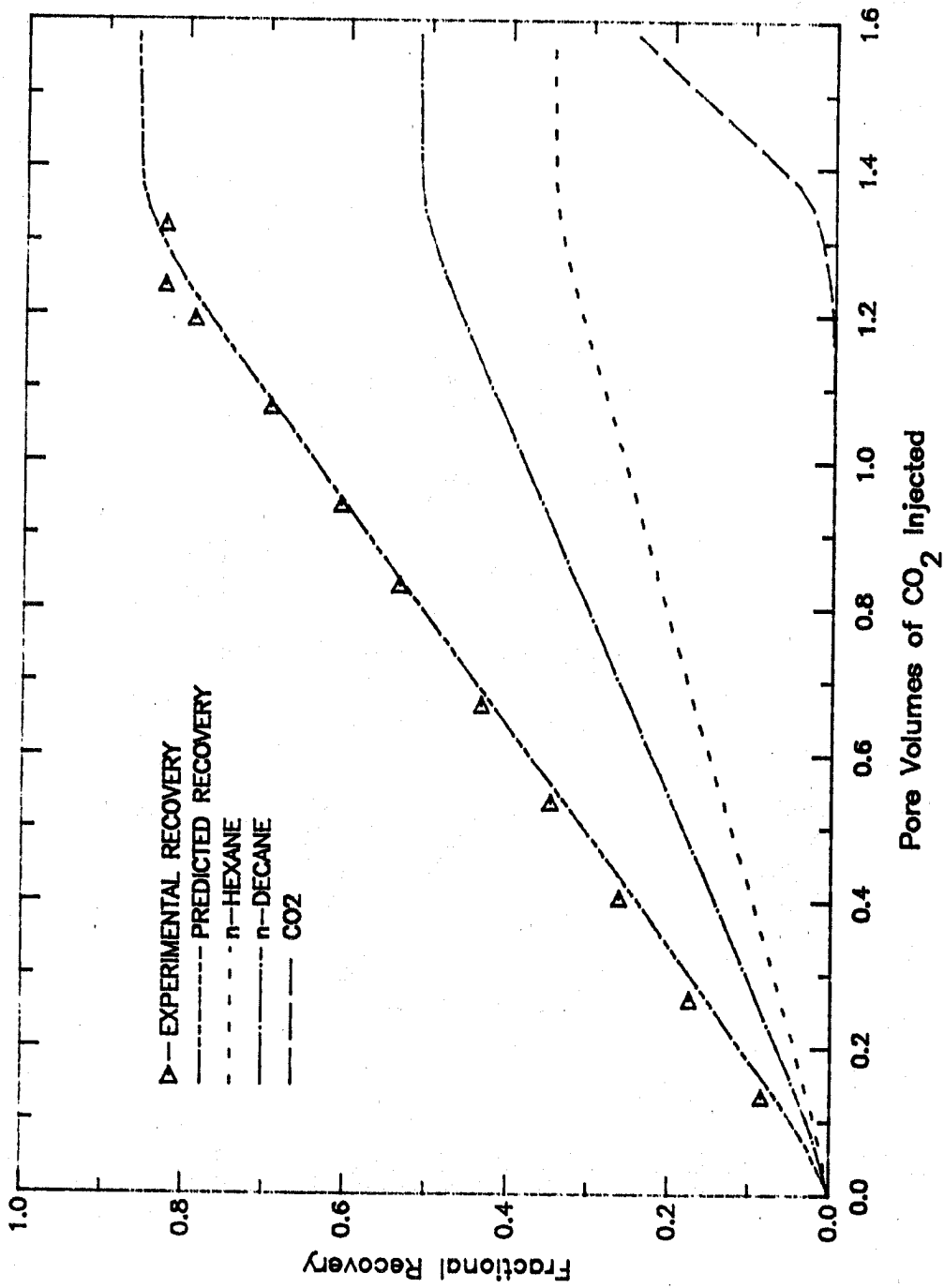


FIGURE D-6: CO₂ Displacing Hexane and Decane (P = 930 psia, T = 100°F).

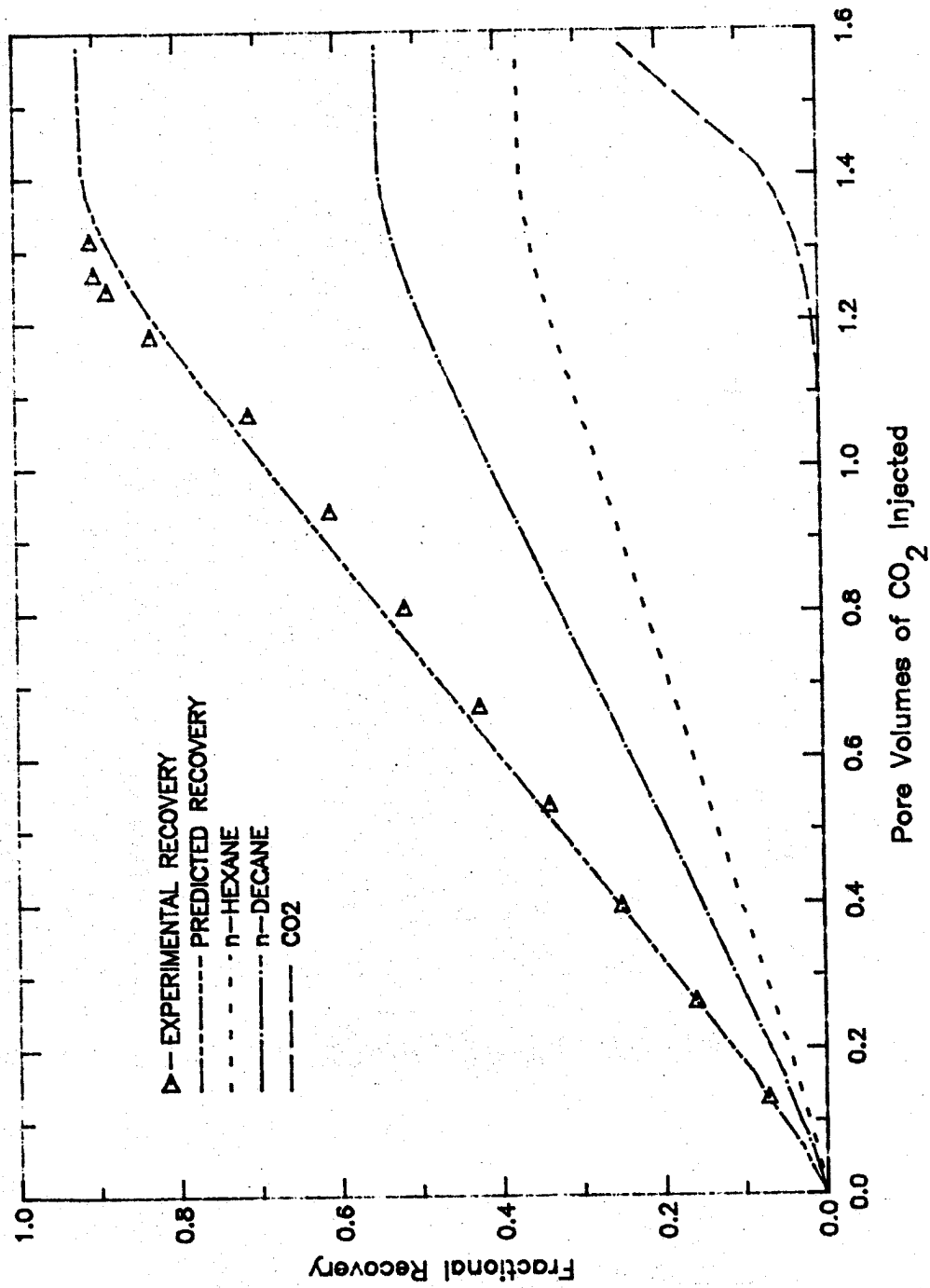


FIGURE D-7: CO₂ Displacing Hexane and Decane (P = 1020 psia, T = 100°F).

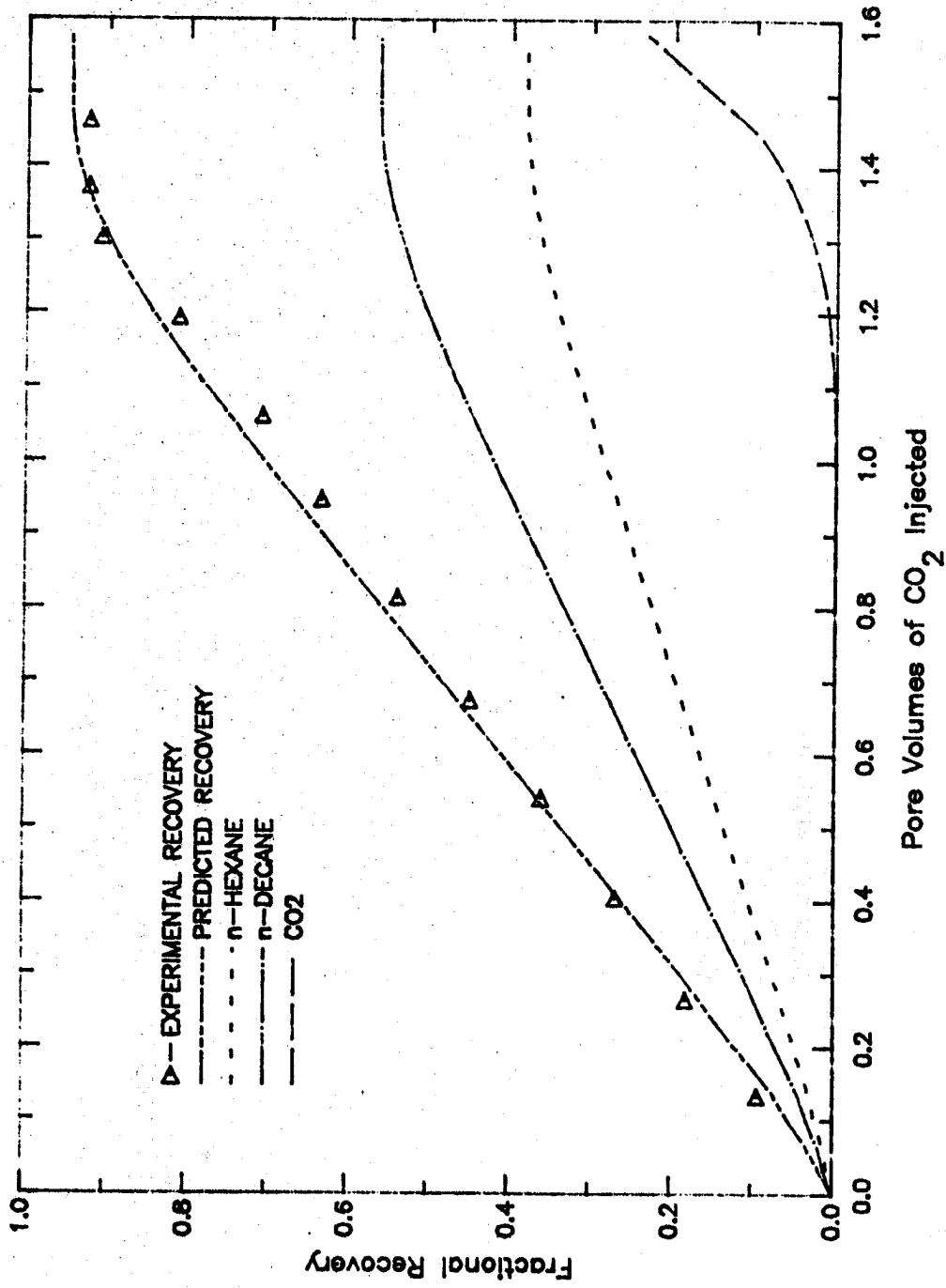


FIGURE D-8: CO₂ Displacing Hexane and Decane (P = 1050 psia, T = 100°F).

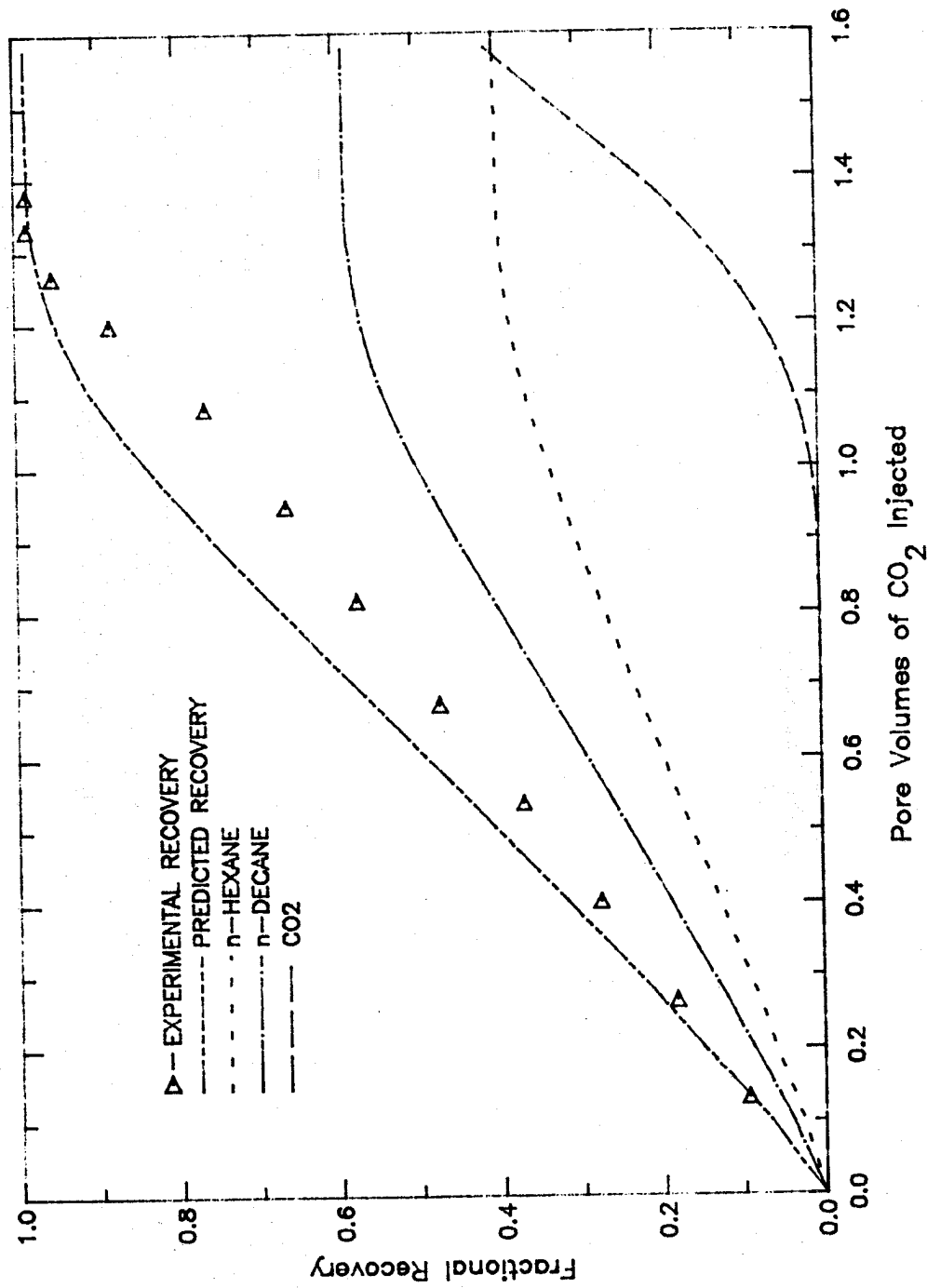


FIGURE D-9: CO₂ Displacing Hexane and Decane (P = 1110 psia, T = 100°F).

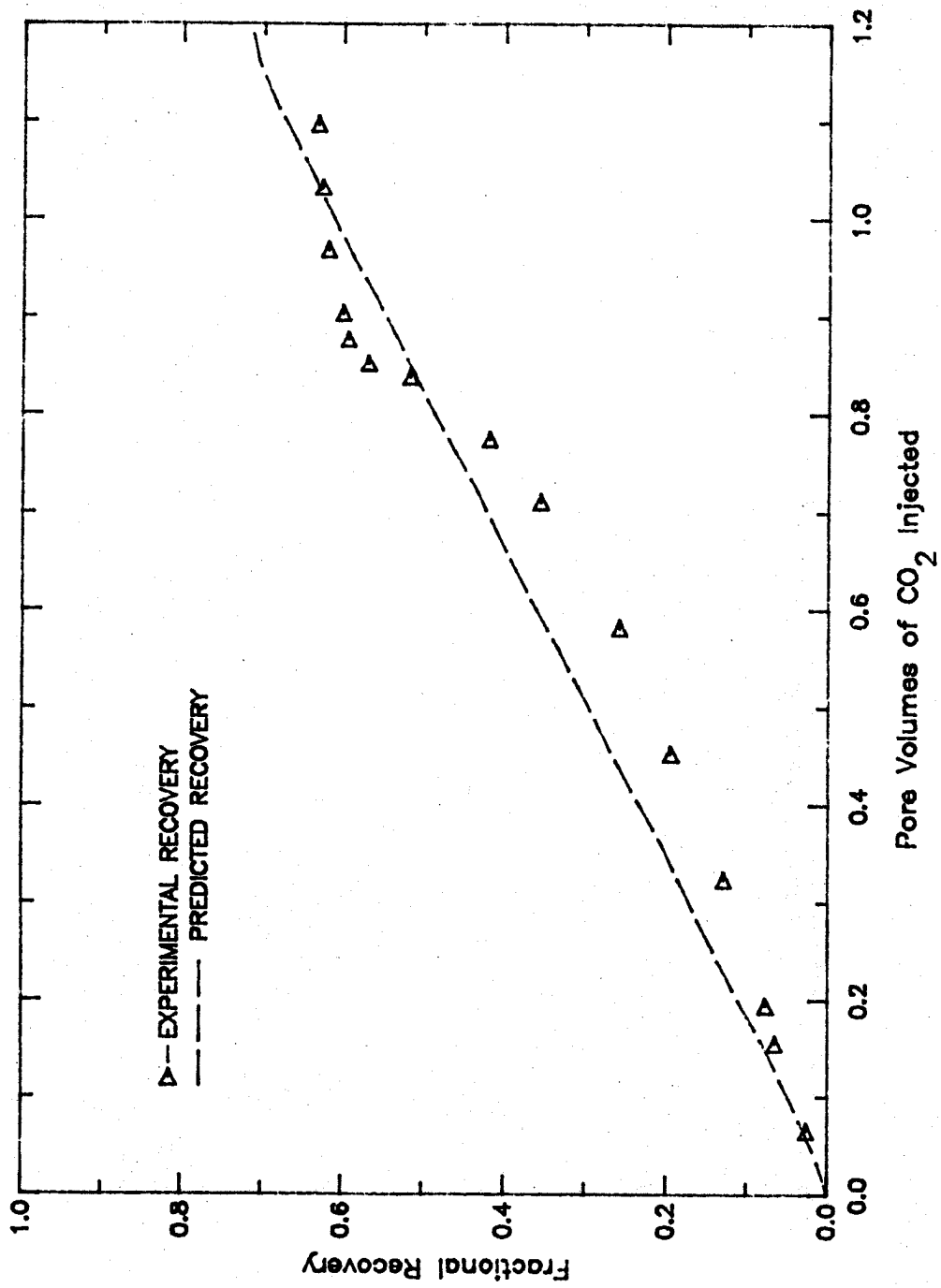


FIGURE D-10: CO₂ Displacing Johanning B #1 (P = 1040 psia, T = 102°F).

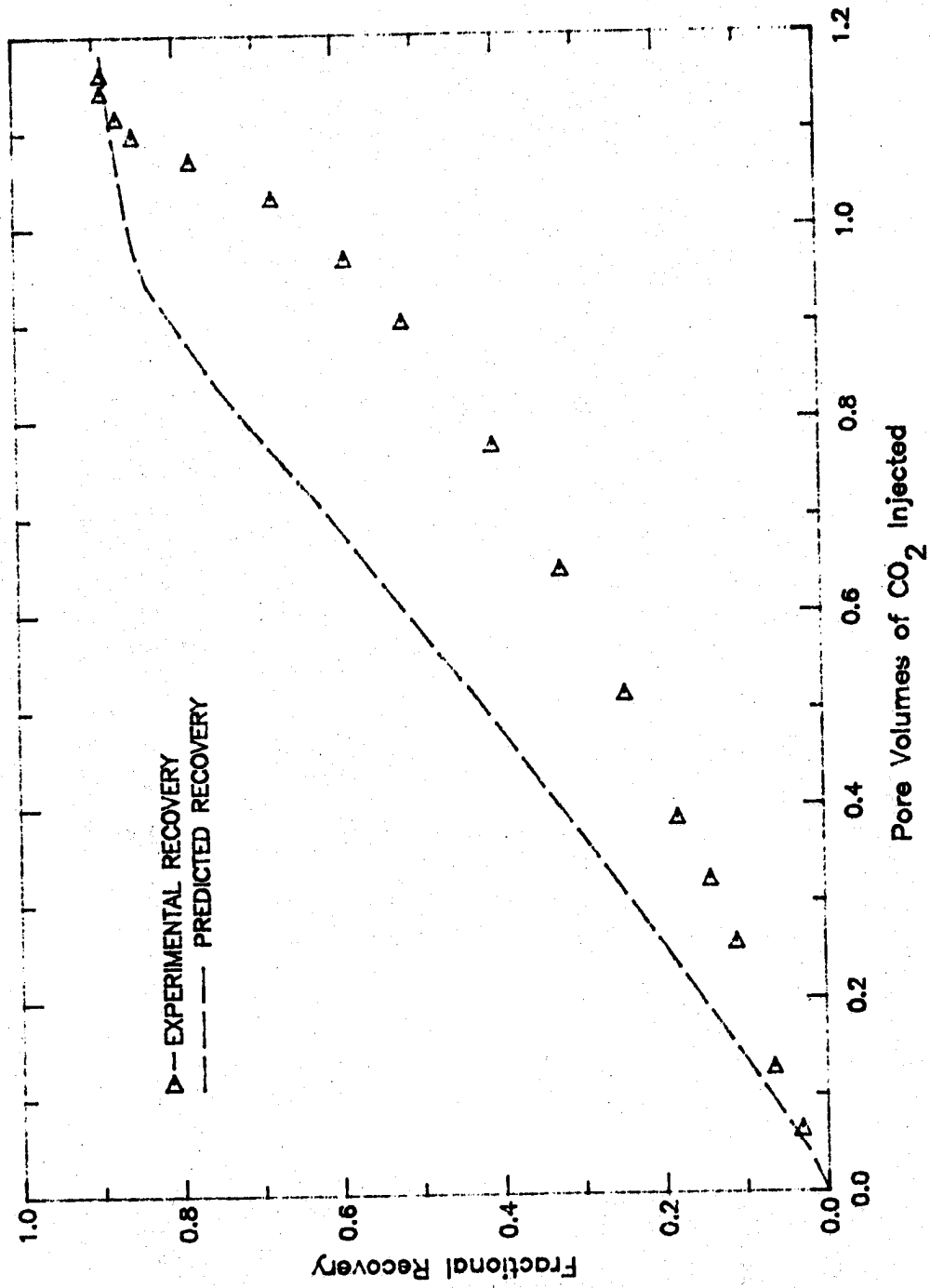


FIGURE D-11: CO₂ Displacing Johannung B #1 (P = 1210 psia, T = 102°F).

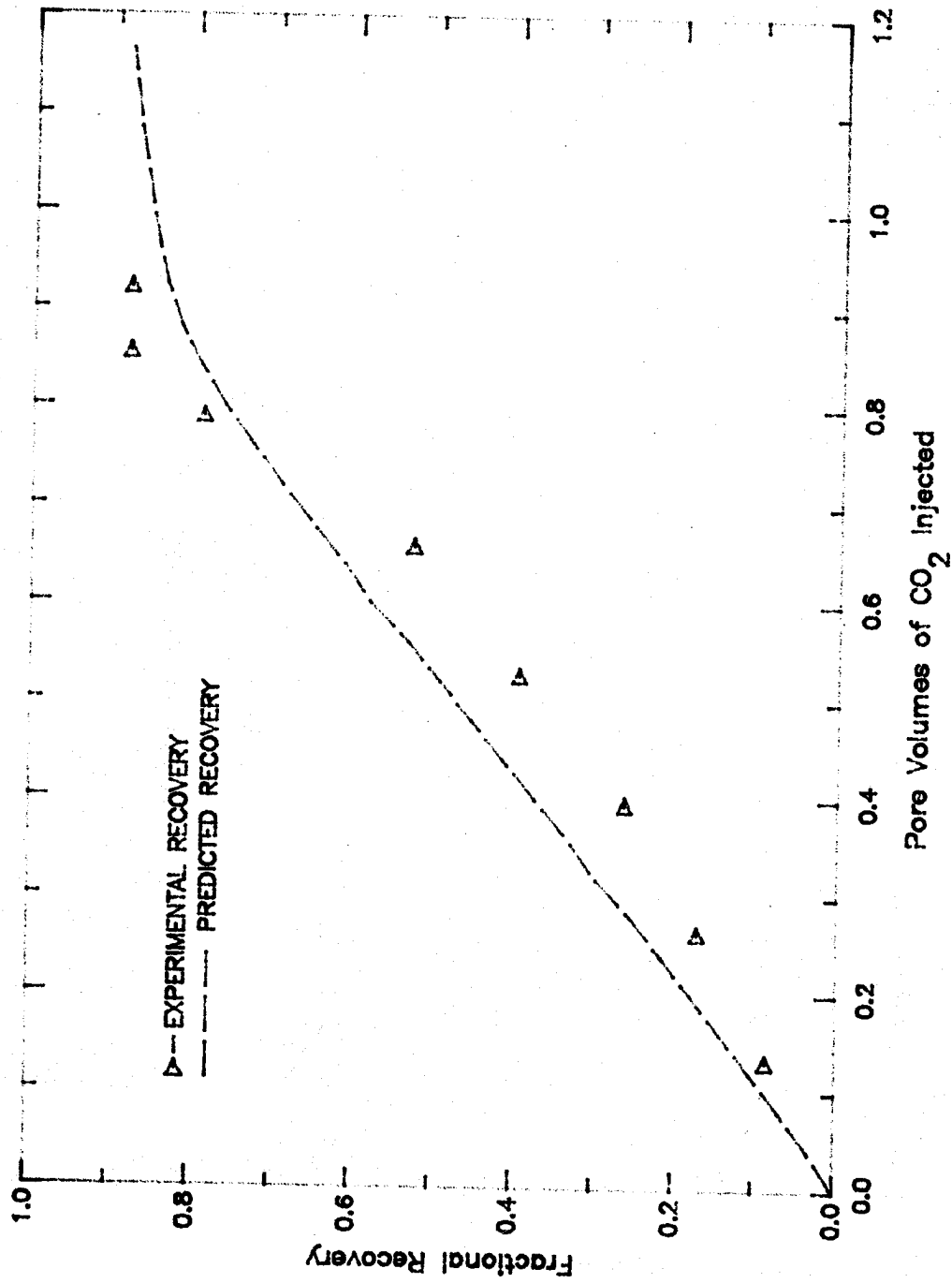


FIGURE D-12: CO₂ Displacing Johanning B #1 (P = 1570 psia, T = 125°F).

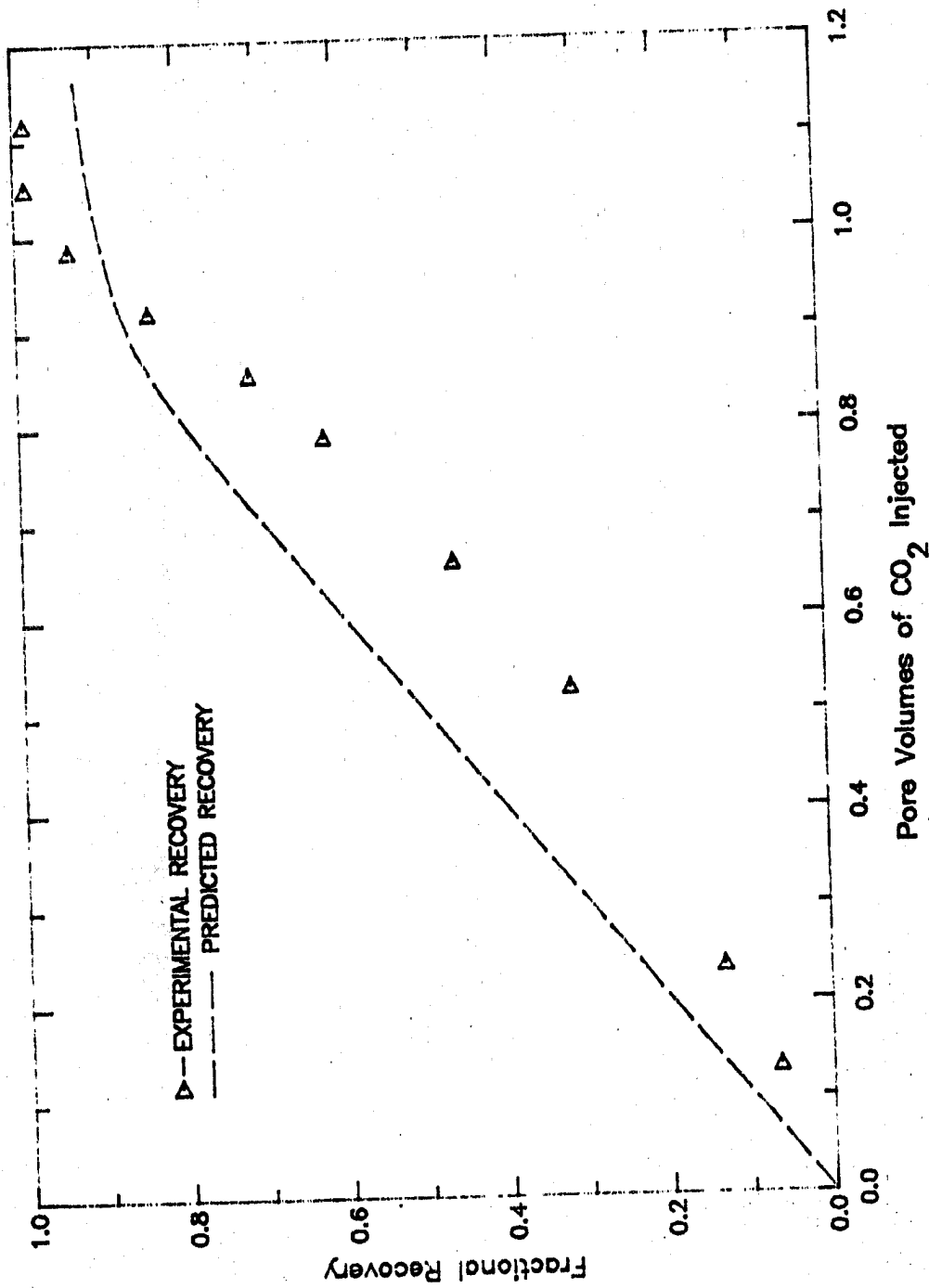


FIGURE D-13: CO₂ Displacing Johanning B #1 (P = 2060 psia, T = 125°F).